DEVELOPMENT OF LAMELLA HEAT EXCHANGER INTAKE CHARGE AIR COOLING USING VEHICLE AIR-CONDITIONING SYSTEM

By

IKHTIAR MUHAMMAD USMAN

Thesis Submitted to the School of Graduate Studies, Universiti Putra Malaysia, in Fulfilment of the Requirements for the Degree of Doctor of Philosophy

September 2023

FK 2023 27

DEDICATION

This thesis is gratefully dedicated to:

My beloved parents for their love, support and encouragement

&

My beloved wife, daughter, son, brothers, and sister.

Abstract of thesis presented to the Senate of Universiti Putra Malaysia in fulfilment of the requirement for the degree of Doctor of Philosophy

DEVELOPMENT OF LAMELLA HEAT EXCHANGER INTAKE CHARGE AIR COOLING USING VEHICLE AIR-CONDITIONING SYSTEM

By

IKHTIAR MUHAMMAD USMAN

September 2023

Chair : Associate Professor Abdul Aziz bin Hairuddin, PhD
Faculty : Engineering

The high intake air temperature for engines, caused by the rise in ambient temperature and through the usage of compression devices, has a detrimental impact on performance parameters (power, torque, fuel consumption, and exhaust emissions) due to less oxygen molecules available in the air-fuel ratio for complete combustion. To rectify this matter, the engine intake charge air cooling (EICAC) technique through intercooler heat exchanger (IHE) is the best solution without modifying the engine itself. Previous studies explained that the traditional intercoolers available in the market are less efficient, non-operational in vehicle slow driving speed or stand-still operation, and incompatible for naturally aspirated engine due to their dependence on ambient conditions. Further the innovative cooling devices has complex designs, required additional cooling circuits, modifications in engine setup, offers shallow thermal capacity compared to design sizes with a high pressure drop in airflow, which is undesirable. Therefore, there is a need of a better IHE to overcome the said limitations in prior art inventions.

In this regard, a new Lamella heat exchanger (LHE) is developed to operate as an intercooler for a 1.5L naturally aspirated Proton-Wira SI-engine (four-stroke, four-cylinder), using stainless steel metal 316L. A coolant source (refrigerant) is utilized from vehicle air conditioning (VAC) system due to its high heat transfer property. Computational fluid dynamics (CFD) simulations through ANSYS FLUENT software are performed to analyze the proposed model of LHE regarding the thermal capacity and pressure drop at various engine speeds (Rpm 1000 to 8000, with an increment of 500) and intake temperatures (40℃, 45℃, 50℃ and 55℃). The admirable amount of heat transfer and temperature drop ranges between 0.42kW to 2.14kW and 15.8℃ to 46℃ respectively, with minimal pressure drop of 0.004 kpa to 0.095 kpa, is recorded, which made LHE is distinctive among the available intercoolers. The experimental investigation is carried out to see the actual influence of LHE on the test vehicle, using the chassis dynamometer test bench. Operating the AC of a test vehicle with ambient air results in high exhaust emissions by 67%, 8%, 21%, and 7% for CO, CO_2, HC and NO_X respectively, increased fuel consumption by 32.3%, loss in engine power and torque by 14% and 13% respectively, compared to the normal stage without AC and LHE. The cold intake air introduced a significant result in terms of reduced exhaust emissions and improved engine power and torque. The amount of lost power and torque due to AC are recovered by 17 % and 24% respectively, by bringing the cold intake air into an engine. Similarly, the increased quantities of exhaust tailpipe emissions specifically due to AC operation is lowered by 43.6%, 39.5%, 47.3%, 64.5% for CO, CO_2, HC and NO_x respectively. In conclusion, LHE has successfully enhanced the performance of test vehicle as EICAC technique.

Keywords: Cold intake air; Internal combustion engine; Lamella heat exchanger; Spark ignition engine; Energy recovery

SDG: Goal 13; Take urgent action to combat climate change and its impacts

Abstrak tesis yang dikemukakan kepada Senat Universiti Putra Malaysia sebagai memenuhi keperluan untuk ijazah Doktor Falsafah

PEMBANGUNAN PENUKAR HABA LAMELLA PENYEJUKAN UDARA AMBILAN MENGGUNAKAN SISTEM PENYAMAN UDARA KENDERAAN

Oleh

IKHTIAR MUHAMMAD USMAN

September 2023

Pengerusi : Profesor Madya Abdul Aziz bin Hairuddin, PhD
Fakulti : Kejuruteraan

Suhu udara ambilan yang tinggi untuk enjin, yang disebabkan oleh kenaikan suhu persekitaran dan melalui penggunaan peranti mampatan, mempunyai kesan buruk pada parameter prestasi (kuasa, daya kilas, penggunaan bahan api dan pelepasan ekzos) kerana molekul oksigen yang kurang tersedia dalam nisbah udara-bahan api untuk pembakaran lengkap. Bagi membetulkan perkara ini, teknik penyejukan udara cas masuk enjin (EICAC) melalui penukar haba penyejuk antara (IHE) adalah penyelesaian terbaik tanpa mengubahsuai enjin itu sendiri. Kajian terdahulu menjelaskan bahawa penyejuk antara tradisional yang terdapat di pasaran adalah kurang cekap, tidak beroperasi dalam kelajuan pemanduan perlahan kenderaan atau operasi pegun, dan tidak serasi untuk enjin sedutan tabii kerana bergantung pada keadaan persekitaran. Tambahan pula, peranti penyejukan yang inovatif mempunyai reka bentuk yang kompleks, memerlukan litar penyejukan tambahan, pengubahsuaian dalam persediaan enjin, menawarkan kapasiti terma cetek berbanding saiz reka bentuk dengan susutan tekanan yang tinggi dalam aliran udara, yang tidak diingini. Oleh itu, terdapat keperluan IHE yang lebih baik untuk mengatasi had tersebut dalam ciptaan seni terdahulu.

Dalam hal ini, penukar haba Lamella (LHE) baharu dibangunkan untuk beroperasi sebagai penyejuk antara bagi enjin SI 1.5L sedutan tabii Proton-Wira (empat lejang, empat silinder), menggunakan logam keluli tahan karat 316L. Sumber penyejuk (bahan penyejuk) digunakan daripada sistem penghawa dingin kenderaan (VAC) kerana sifat pemindahan haba yang tinggi. Simulasi perkomputeran dinamik bendalir (CFD) melalui perisian ANSYS FLUENT dilakukan untuk menganalisis model cadangan LHE berkenaan kapasiti haba dan susutan tekanan pada pelbagai kelajuan enjin (RPM 1000 hingga 8000, dengan kenaikan 500) dan suhu pengambilan (40℃, 45℃, 50℃ dan 55℃). Jumlah pemindahan haba dan susutan suhu yang mengagumkan masing-masing antara 0.42kW hingga 2.14kW dan 15.8℃ hingga 46℃, dengan susutan tekanan minimum 0.004 kPa hingga 0.095 kPa direkodkan, yang menjadikan LHE adalah di antara penyejuk antara yang distingtif. Kajian eksperimen dijalankan untuk melihat kesan sebenar LHE pada kenderaan ujian, menggunakan meja ujian dinamometer

casis. Kendalian AC kenderaan ujian dengan udara persekitaran menghasilkan pelepasan ekzos yang tinggi sebanyak 67%, 8%, 21%, dan 7% masing-masing untuk CO, CO_2, HC dan NO_x, meningkatkan penggunaan bahan api sebanyak 32.3%, kehilangan kuasa enjin dan daya kilas masing-masing sebanyak 14% dan 13%, berbanding peringkat biasa tanpa AC dan LHE. Udara masukan sejuk memperkenalkan hasil yang ketara dari segi pengurangan pelepasan ekzos dan peningkatan kuasa dan daya kilas enjin. Jumlah kuasa dan daya kilas yang hilang akibat AC dipulihkan masing-masing sebanyak 17% dan 24%, dengan membawa udara masukan sejuk ke dalam enjin. Begitu juga, peningkatan kuantiti pelepasan paip ekzos khusus disebabkan oleh operasi AC diturunkan masing-masing sebanyak 43.6%, 39.5%, 47.3%, 64.5% untuk CO, CO_2, HC dan NO_x. Kesimpulannya, LHE telah berjaya meningkatkan prestasi kenderaan ujian sebagai teknik EICAC.

Kata Kunci: Udara ambilan tersejuk; Enjin pembakaran dalaman; Penukar haba lamella; Enjin pencucuhan bunga api; Pemulihan tenaga

SDG: Matlamat 13; Mengambil tindakan segera untuk memerangi perubahan iklim dan kesannya

ACKNOWLEDGEMENTS

I am grateful to Allah S.W.T., the Almighty, for providing me with the fortitude and determination needed to finish the thesis. I would like to take this opportunity to express my gratitude to everyone who has helped me during my doctoral studies.

I would like to take this opportunity to convey my heartfelt gratefulness and appreciation to my principal supervisor, Associate Professor Dr. Abdul Aziz bin Hairuddin, for his time, advice, and support throughout the entirety of my research effort. Additionally, I would like to take this opportunity to express my appreciation to the members of my supervising committee, namely Dr. Azizan As'arry and Dr. Khairil Anas Md Rezali, for their assistance in the form of meaningful contributions to the research work and technical feedback that results in improvements to the thesis and the work that has been published.

I want to express my sincere gratitude to my devoted mother, cherished father, dear wife, wonderful siblings, and sister for their unwavering support, affection, and patience during my academic tenure at Universiti Putra Malaysia. Without them, this accomplishment would have been unattainable. Additionally, I would like to extend my gratitude to the Higher Education Commission of Pakistan for its financial assistance during the course of my doctoral studies.

This thesis was submitted to the Senate of Universiti Putra Malaysia and accepted as a fulfilment of the requirements for the degree of Doctor of Philosophy. The Members of the Supervisory Committee were as follows:

Abdul Aziz bin Hairuddin, PhD
Associate Professor
Faculty of Engineering
Universiti Putra Malaysia
(Chairman)

Azizan bin As'arry, PhD
Senior Lecturer
Faculty of Engineering
Universiti Putra Malaysia
(Member)

Khairil Anas bin Md Rezali, PhD
Senior Lecturer
Faculty of Engineering
Universiti Putra Malaysia
(Member)

ZALILAH MOHD SHARIFF, PhD
Professor and Dean
School of Graduate Studies
Universiti Putra Malaysia

Date: 18 April 2024

TABLE OF CONTENTS

LIST OF TABLES

LIST OF FIGURES

LIST OF ABBREVIATIONS

CAC	Charge air cooling
CFD	Computational Fluid Dynamics
CH_4	Methane
CO	Carbon monoxide
CO_2	Carbon dioxide
COP	Coefficient of performance
DOE	Design of experiment
EICA	Engine intake charge air
EICAC	Engine intake charge air cooling
EIHE	Evaporative intercooler heat exchanger
EPA	Environmental Protection Agency
H_2	Hydrogen
H_2O	Water
HC	Hydrocarbon
HE	Heat exchanger
HEVs	Hybrid electric vehicles
ICE	Internal combustion engine
IEA	International Energy Agency
IHE	Intercooler heat exchanger
IPCC	Intergovernmental Panel on Climate Change
LHE	Lamella heat exchanger
MAE	Mean absolute error
NASA	National Aeronautics and Space Administration
NO_x	Nitrogen oxide

PHEVs	Plug-in hybrid electric vehicles
PM	Particulate matter
R^2	Coefficient of determination
UniKL-MFI	Universiti Kuala Lumpur-Malaysia France Institute
UPM	Universiti Putra Malaysia
VAC	Vehicle air conditioning

CHAPTER 1

INTRODUCTION

1.1 Background

The United Nations (UN) 2030 agenda for sustainable development, with its 17 sustainable development goals (SDGs) and 169 targets, calls for sustainable transformation of societies across the globe. Among them, SDG 13 "take urgent action to combat climate change and its impacts" aims to reduce global emissions, enhance climate resilience and adaptive capacity, and strengthen coordination and cooperation on climate related issues (Nathaniel & Adeleye, 2021). Dagnachew et al. (2021) nominated the transport as one of the vital sector for achieving the SDG 13. To be precise (in transport sector), the passenger car has its own significance, as it supports the achievement of virtually all the goals, including those associated with economic and social development, connecting goods with markets and access to services. Several initiatives are calling for drastic changes, and vehicle electrification is being heavily promoted. Despite the trend of electrification, ICEs will continue to dominate in road transport as well as other transport sectors in the coming decades (Kalghatgi, 2018; Malaquias et al., 2019; Reitz et al., 2020). In 2030, around 60% to 90% of sold light-duty passenger vehicles will be equipped with ICE, including ICEVs, HEVs and PHEVs. In the approach to 2050, the trend of electrification is expected to continue, but the share of ICE equipped vehicles is forecast to remain above 50%. The progress of electrification in the heavy-duty vehicle sector is much slower, with more than 92% vehicles predicted to be powered by ICEs in 2030. Actually, the main barriers of electric vehicles are the battery cost and driving range. The battery cost cannot be reduced in the short term, and in the long run, it will be affected by the relationship between the supply and demand of raw materials (Reitz et al., 2019). However, there will be a sharp increase in costs by adding batteries to increase the driving range without a mature infrastructure. In addition to these limitations, the performance of electric vehicles declines sharply in harsh conditions i.e. extreme winter and summer (Zhao et al., 2020). These limitations of electric vehicle are driving the development of effective, but previously deemed uneconomical, methods to increase the ICEs efficiency with advanced combustion modes, and to further reduce pollutant emissions.

Currently, the global stock of passenger cars is around 1.19 billion, and the number of commercial vehicles totals 249 million, of which almost 99% are powered by ICEs, accounting for 81.3% of the oil demand in the transport sector (Yue & Liu, 2023). Therefore, in addition to mitigating climate change, improving fuel efficiency of passenger cars directly contributes to better access to energy services (SDG 7). Efficiency improvements of cars also contribute to improving local air quality (SDG 11) and reducing human health impacts (SDG 3). It also reduces oil import and consumption (SDG 12), and aids the transition to low-carbon transport. According to United Nations and NASA studies, the use of fossil fuels (especially for transport sector) by humans is blamed for a very fast change in climatic patterns. Burning of fossil fuels result in generation of green-house gases (GHGs) that trap heat and cause global warming. A latest report by World Meteorological Organization (WMO) predicts that global mean temperature during 2023 and 2027 is likely to be between 1.1 and 1.8 °C higher than average over the years 1850–1900 (Nullis, 2023). The sixth assessment report of the intergovernmental panel on climate change (IPCC) identified that the possible range of human-induced alteration in global surface temperature in 2010–2019 relative to 1850–1900 is 0.8 to 1.3°C, with the best estimate of 1.07°C. Since 2012, the global surface temperature has increased significantly, with the most recent five years (2016–2020) being the warmest five-year duration on record between 1850 and 2020 (Masson-Delmotte et al., 2021), shown in Figure 1.1. Most countries suffering from weather temperature increasing are Middle East countries, where a high ambient temperature recorded in summertime (Salimi & Al-Ghamdi, 2020).

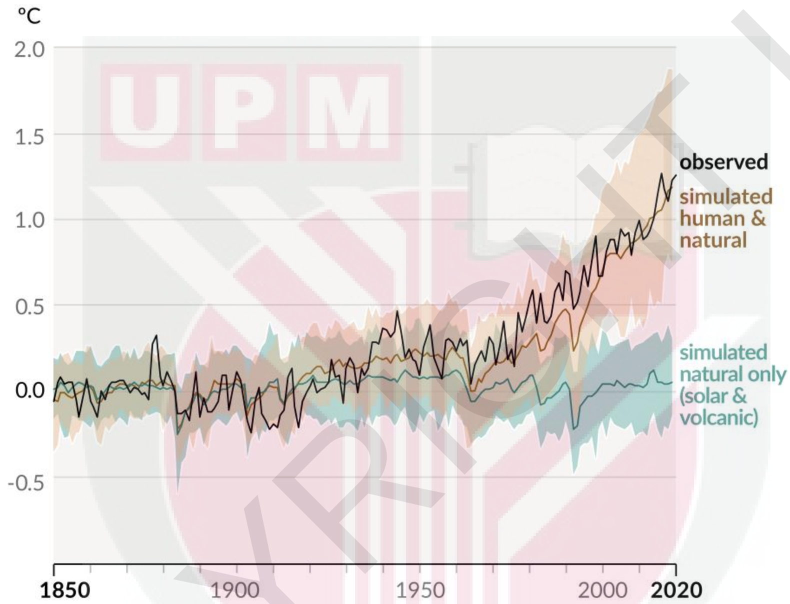

Figure 1.1: Variation in worldwide surface temperature (annual average) as observed and computed using human and natural and only natural factors (both 1850-2020)
(Masson-Delmotte et al., 2021)

The ambient temperature does not affect ICE performance directly, instead, it does have an effect on the air intake temperature before entering the combustion chamber or turbocharger, as well as on the engine cooling system and affects various aspects of engine operation, including air density, combustion process, power output, fuel consumption, and engine efficiency (Geeks, 2023). The specific humidity of the intake air depends on the relative humidity, temperature and pressure of the ambient air (Wimmer & Schnessl, 2006). To operate the engine in an optimal range it would be necessary to adapt the engine control settings to respective ambient conditions. Besides the rise in the ambient air temperature nowadays, usage of compression devices like superchargers and turbochargers also caused an increment in air intake temperature and pressure (José Galindo et al., 2018), which negatively impacts IC engine performance and fuel consumption (Thomaz et al., 2021). Such air property is not appropriate for a complete combustion process (T. Hu et al., 2007), which means air thermal performance has a direct impact on the conversion efficiency and output power of the vehicle engine unit (Huang et al., 2015**;** Aun et al., 2020). Therefore, engine intake charge air (EICA) temperature plays an important role in engine performance (Aun et al., 2020), in terms of combustion performance, exhaust emissions, and fuel consumption (Manmadhachary et al., 2017), as the mixture air density affects by the temperature variation (Irimescu et al., 2017a). Previous studies briefly explained that a reduction in engine intake charge air (EICA) temperature has a significant contribution to improve engine performance (Mamat et al., 2009; Mamat et al., 2013; Teoh et al., 2021). Johnson (2010) described that engine efficiency has a particular advantage of getting cold intake air. As, cold air is denser than hot air (Weinrebe et al., 2022) containing more oxygen, which helps in better combustion, subsequently gaining more power and better fuel economy. Therefore, to introduce cool air to the engine intake, a heat exchanger (T. Alam & Kim, 2018) commonly referred to as an intercooler, is often added to only charged engines (F. Burke, 2018).

1.2 Problem Statement

Most traditional intercoolers use air or water as a coolant source (Pawar, 2016; Kula et al., 2022)**.** However, these designs did not achieve lower than ambient temperature or had no effect at low engine speeds and static vehicle positions. They are only suitable for charged engines due to their dependence on ambient conditions (Elrentisy et al., 2022), consequently useless for naturally aspirated engines, where the intake air conditions are identical to ambient air conditions. Further, there is no proper place for intercooler in naturally aspirated engines. Therefore, researchers have only investigated the effect of cold intake air on naturally aspirated engine without developing intercoolers, and experimentations were performed in laboratory test benches through the application of external cooling sources, as listed in table 1.1 from Sr. No 1-5 along with the reported problems due to high intake air temperature. For charged engines, researchers utilized advanced coolant sources for their newly developed intercoolers to overcome the shortages of traditional intercoolers, listed in table 1.1 from Sr. No 6-10. The limitations related to their studies and developments are truly the driving force for this study.

Table 1.1: Prior art inventions related to cold intake air for naturally aspirated and charged engines

Sr. No	Author/engine type	Problems reported due to high intake air temp.	Applied cooling technique/ source	Limitations
1	(Abbod et al., 2019) Naturally aspirated SI engine	High contents of exhaust emissions and exhaust gas temperature	Using external water source for cooling the intake air	Only studied the effect of cold intake air on engine. Higher range of rpm is overlooked along with the solution to provide cold intake air for real operation.
2	(Raman & Bahari, 2021) Naturally aspirated SI engine	Increases tendency to knock and reduction in engine thermal efficiency	Using external air cooler	The maximum engine speed is taken as 3000 rpm. Study on higher range of rpm is missing. Further, solution to provide cold intake air for real operation is not mentioned.
3	(Nazmi et al., 2021) Naturally aspirated SI engine	Rich fuel air mixture for combustion and reduction in volumetric efficiency	Using external heater and cooler	Experimentation performed using dynamometer test bench. However, only considered the higher side of intake temperature i.e. 35 to 70℃ for experimentation. Real cold temperature range is missing.
4	(Mnati et al., 2022) Naturally aspirated SI engine	Decrement in fuel economy and oxygen molecules in available air	Using external evaporative cooling pad	Only studied higher side of air intake temperature range, between 40 to 58℃. Below ambient temperature range is overlooked.
5	(Kamal et al., 2022) Naturally aspirated SI engine	Increment in brake specific fuel consumption and decrement in brake power and torque	Using external electrical cooler	Selected test conditions/ranges are limited i.e. minimum intake temperature is taken as 25℃ and maximum speed upto 2500 rpm. Moreover, solution to provide cold intake air for real operation is missing.
6	(Novella et al., 2017) Turbocharged engine	High combustion peak temperature	Through absorption chiller ammonia based	Requires waste heat recovery system and high exhaust thermal power for its operation.
7	(Davide Di Battista et al., 2018) Turbocharged engine	High fuel consumption, emissions and shorter combustion duration	Through shell and tube heat exchanger using refrigeration system	Design size of intercooler is not mentioned. Further high pressure losses occurred due to designed intercooler.
8	(S.J. Yang et al., 2019) Turbocharged engine	Shorter combustion duration	Water cooled intercooler system using air conditioning system	Low cooling capacity due to indirect cooling of intake air; from refrigerant to water, and then water to intake air. Also requires modification in engine setup for its operation.
9	(Galindo et al., 2019) Turbocharged engine	Faster burning rate and decrement in engine torque	Using jet ejector cooling system	Requires additional cooling system and high exhaust thermal power. Moreover, very expensive setup and maintenance. Also caused high pressure loss.
10	(Ma'arof et al., 2020) Turbocharged engine	Reduces air-fuel ratio	Using spray of water or suitable chemicals	Requires hydraulic system for pumping and refilling for every next usage. Engendered medium thermal capability.

It may conclude that there is no specific designed intercooler for naturally aspirated engine, which surely point towards the research gap. Further, the available intercoolers for charged engines have limitations in terms of low to medium thermal capability, medium to high pressure loss, complex and large scale design sizes. They also required additional cooling circuits and modifications in engine bays due to its complexity, and could only be installed while designing the new vehicle, as the literature did not cater the consideration of available space in existing vehicle engines to fix the proposed device in existing vehicle engines. As the most effective way to cool the intake charge air of an engine without modifying the engine itself is to improve an external parameter and add-on installation equipment (Zhuang et al., 2020). Besides that, most of the designers investigated their developed intercoolers and systems in laboratories, where available space and size of the intercooler are not an issue, and this method differs from the actual scenario, where the performance of the vehicle needs to be tested in real-time, with the actual installation of intercoolers in existing engine bays. Therefore, a practical solution is required, which involves the new, efficient and compact intercooler, to provide the high thermal cooling performance with minimal pressure loss, while consuming the least amount of space for its installation in naturally aspirated engine, without modifying the engine setup. As a result, vehicle engine performance must be improved on real time basis.

1.3 Objectives

The prime objective of this study is to develop an IHE with minimum pressure drop and maximum cooling capability, that can be utilized by vehicles with SI engine in order to improve their performance. The specific objectives are as follows:

1. To develop an IHE as an engine intake charge air cooling device by utilizing vehicle air conditioning system as a coolant source, through computational fluid dynamics simulations (ANSYS FLUENT).

2. To assess the performance of a fabricated IHE in laboratory conditions, in terms of a temperature drop, pressure drop, heat transfer, and coefficient of performance.

3. To evaluate the real time effectiveness of IHE as well as the impact of cold intake air on the performance of SI engine, in terms of fuel consumption, power, torque and emissions by using chassis dynamometer and vehicle parking test.

1.4 Scope of the study

1. The study specifically aims to examine the impact of cold intake air on vehicle engine power, torque, fuel consumption and emissions. The selected test vehicle for the present study is 1.5L Proton-Wira, four-cylinder four stroke naturally aspirated SI engine, model 2004.

2. A new IHE is developed as charge air cooler through CFD simulations (ANSYS FLUENT) and its design size is depended on the maximum available space in the selected test vehicle engine bay to install it as an aftermarket product on the intake manifold line, without modifying the engine setup.

3. Refrigerant coolant (R134a) is taken from the VAC system as a coolant medium for IHE, the same used for passenger compartment cooling.

4. Maximum allowable pressure drop across IHE for this study is taken as 5%.

5. For numerical and laboratory tests (at UPM thermodynamics laboratory), the intake temperatures of hot/ambient air are taken as 40℃, 45℃, 50℃, and 55℃, against the engine speed range of 1000 rpm-8000 rpm, with an increment of 500. Heat transfer, temperature drop, pressure drop, number of transfer units and logarithmic mean temperature difference are selected as the performance indicators of IHE.

6. The IHE is specially made to function in all vehicle status operations, particularly when cooling performance is difficult while the car is stationary or in a parking spot or at a high rpm. Therefore, the study covered all rpm ranges from minimum 1000 rpm to the maximum allowable operating speed by car manufacturer i.e., 6500 rpm, during its real time testing on the chassis dynamometer bench (MAHA, LPS 3000) at UniKL-MFI, Malaysia.

7. For vehicle static or parking test, the test vehicle is parked for 11 minute in order to provide the sufficient time to IHE to express its cooling capability and also its impact on engine exhaust emissions (CO, CO_2, HC, NO_x) and fuel consumption.

1.5 Significance of study

This study contributes to vehicle engine performance in terms of better power and lower emissions in all vehicle statuses; vehicle static position, at low and high engine speed, through manipulating the temperature parameter of air, by engine intake charge air cooling technique. This technique improved the density of air in response to lower temperature occurred by a newly designed and constructed IHE device that is suitable in size and cooling capacity for selected engine type. Moreover, this study contributes to understand the working and designing of the newly proposed IHE. The proposed intercooler model solved the limitations of the available designs in the market. First in terms of higher cooling capability by offering more surface area per unit volume for heat transfer which subsequently reduces the intake temperature of air by a significant margin. Secondly, through minimal pressure loss from the intercooler to avoid the interruption in airflow to engine intake and able to reduce the intake air temperature at a high engine speed, which is one of the challenges to solve from the current design. Third, by solving size constraint issues for its installation in existing vehicle engine bays through its compactness. Further, the presented IHE can use for both cooling and heating purposes, which offers the flexibility of its use in virial environments. It can also be useful for charged engines. The cleaning service can be very easy to handle and does not need technical experience. The present study is a contribution towards the achievement of SDG 13 by lowering exhaust emissions. It is also a step towards implementing exhaust emissions standards set by regulating authorities for internal combustion engines.

1.6 Thesis layout

This thesis contains five chapters. The introduction section includes the problem statement, aims and objectives, the scope of the work, along with the importance of the research. The second chapter embraces state of the art literature review related to matters appropriate to the present work. It covers an overview of combustion in ICE, emissions due to combustion, ambient temperature influence on ICE, and the impact of intake charge air temperature on the engine. It also contains an introduction to the intercoolers, their conventional and modern types, including advanced research conducted to enhance their performance using different methods and mediums. Moreover, the outline of vehicular air conditioning systems and vehicle performance tests is a part of this chapter.

The third chapter provides a summary of the research's methodology. First, the design criteria of the proposed IHE are elucidated. Afterward, the numerical investigation of the proposed IHE designs is presented using the ANSYS platform. Further, fabrication of the final selected IHE geometry and experimental validation with the numerical results is elaborated using a laboratory setup. Last but not least, installing a newly designed IHE in the test vehicle for the applied vehicle test using a chassis dynamometer test bench to analyze the performance of IHE and the effect of intake temperature on engine performance. The fourth chapter comprises the findings from numerical and experimental studies of the proposed intercooler associated with its performance. Further, the outcomes of the investigation related to the effect of engine intake charge air temperature on engine performance were listed. The results were displayed using tables, graphical representations, and statistical analysis. The fifth chapter presents the conclusions and future recommendations derived from the outcomes of this investigation.

CHAPTER 2

LITERATURE REVIEW

2.1 Introduction

This chapter discusses a detailed literature review regarding the influence of cold intake air on engine performance in terms of exhaust emissions, engine power, and fuel. The theory behind installing intercoolers with engines and broad assessment of the conventionally available intercoolers in the market to attain cold intake air. Further, it also reveals the latest designs and techniques of engine intake charge air cooling systems using vehicular air conditioning units. Finally, the shortcomings and gaps prevailing in the literature archive are presented, which is the primary goal of this chapter. The radial cycle diagram of the literature review is given in Figure 2.1.

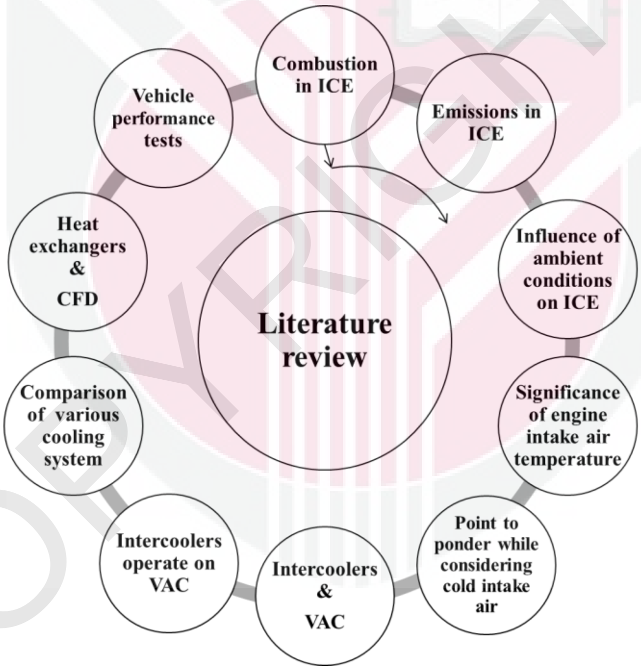

Figure 2.1: Aspects of literature review

2.2 Combustion in ICE

It is preferable to describe the ICE before proceeding to the combustion phenomenon. The ICE is the dominant prime mover technology in several domains. It is the most common mode of transportation in today's culture and will probably stay for decades to come (Sinigaglia et al., 2022; Bhatt and Shrivastava, 2022). By far, the most prevalent type of engine or prime mover is the reciprocating internal combustion four-stroke spark-ignition (SI) and compression-ignition (CI) engines (Ferrari et al., 2022). Most engines get mechanical energy by conversion of thermal energy and are referred to as heat engines (Hall et al., 1982). To be exact, it utilizes a fuel, like gasoline or diesel, and burns it to transform chemical energy into heat energy (Sahu et al., 2022). Combustion is basically a chemical reaction that includes fuel and air, particularly oxygen (O_2), which causes smoke. In ICE, a mixture of air and fuel burns in the combustion chamber (Mokhtari et al., 2017)**.** In a traditional SI engine, the air and fuel are uniformly mixed in the intake system before being introduced into the cylinder through the intake valve, where it blends with leftover gases before being compressed (Narendhiran et al., 2022). An electric discharge through a spark plug initiates combustion at the completion of the compression stage under normal working conditions. (Ge & Zhao, 2019). In SI engines, combustion can be majorly classified into two categories; complete and incomplete combustion (Simanjuntak et al., 2022).

In complete combustion, the gasoline fuel burns completely and have no leftovers. Only carbon dioxide and water are produced (G. Speight, 2020). There must be sufficient availability of oxygen (Ghasemzadeh et al., 2018) for each carbon atom in the chemical compound to find a match or a pair in the ambient air. Whereas, incomplete combustion occurs when insufficient oxygen is present to properly burn the fuel to create carbon dioxide and water (Forde et al., 2014). Pollution and high fuel consumption can result from incomplete combustion. According to Ganesan (2012) incomplete combustion is caused by poor mixing of combustible material and flame quenching. If certain fuel particles do not locate a molecule of oxygen to ignite, this is referred to as poor or improper mixing (Caillat & Vakkilainen, 2013). This results in high exhaust emissions (Kolakoti et al., 2022).

2.3 Emissions in ICE

Generally, perfect combustion rarely happens, even when the air and fuel mixture entering an engine are at the optimal stoichiometric condition. The incomplete combustion of the air-fuel combination in the combustion chamber produces undesirable pollutants and emissions. Carbon monoxide (CO), carbon dioxide (CO_2), nitrogen oxides (NO_x), particulates (PM), and hydrocarbons (HC) are the most common emissions from ICE (Wang et al., 2020; Adithya et al., 2021; Sun et al., 2022). These emissions/fumes/exhaust gases/toxins from ICEs are the primary subject of concern for the world, owing to their detrimental influence on air quality (Anenberg et al., 2017), human health, and global warming. As a result, most countries are working together to manage this particular concern. ICEs emit nearly half of the NO_x, CO, and HC pollutants in the environment, making them a substantial source of atmospheric air pollution and a severe danger to human health and climate (Su et al., 2021). Emissions from the road transportation sector are primarily influenced by vehicle technology (engine capacity, power, and sizes), fuel type (diesel/gasoline /gas), and vehicle age (Matti Maricq, 2007; Jaiprakash and Habib, 2018). According to Alves et al. (2015) exhaust emissions are also influenced by vehicle speed and acceleration/deceleration.

2.3.1 Formation of emissions

In the combustion process, nitrogen oxide (NO) and nitrogen dioxide (NO_2) are collectively known as nitrogen oxides (NO_x) and are commonly produced at high temperatures (R. M. Harrison, 2005; George D Thurston, 2017). Many additional oxides, such as N_2O_4, N_2O, N_2O_3, and N_2O_5, are produced in small amounts but disintegrate spontaneously in the ambient situation of NO_2. Nitrogen oxides are primarily generated from N_2 and O_2 during the high-temperature combustion of fuel in vehicles. Behind the flame, at high combustion temperatures, the following chemical processes occur (Brusseau et al., 2019):

$$\boldsymbol{N_2 + O_2 \Rightarrow 2NO} \tag{2.1}$$

$$\boldsymbol{N_2 + 2H_2O \Rightarrow 2NO + 2H_2} \tag{2.2}$$

The chemical equilibrium equation indicates that a considerable quantity of NO will be produced towards the conclusion of combustion. Furthermore, due to the low temperature of the exhaust, the bulk of NO produced will disintegrate. However, some of the NO produced stays in the exhaust because of the poor reaction rate at exhaust temperatures. The primary player here is atmospheric ozone, which oxidizes NO to the substantially deadlier NO_2 via the following reaction (C. H. Wu et al., 1973):

$$\boldsymbol{NO + O_3 \Rightarrow NO_2 + O_2} \tag{2.3}$$

Therefore, the highest concentration of NO_2 relies on the local meditation of ozone. It must be noted that NO emissions to the environment are one of the causes threatening the Earth's ozone layer (Pronobis, 2020). CO is a transitional product during combustion, and if the conversion of CO to CO_2 is not complete, then it stays in the exhaust system (Vakkilainen, 2017) and is also entitled as silent killer (Byard, 2019; Can et al., 2019). If the air-fuel ratio is set to 15, theoretically, it is possible to say that exhaust of a combustion engine is free of carbon monoxides. CO is usually produced from an engine that has a rich fuel-air ratio. As the quantity of CO produced surges, the mixture becomes increasingly rich in fuel (V. Rapp et al., 2016). Even if the fuel mixture is slightly lean, a small quantity of CO will pass through the exhaust. This is owing to the fact that balance is not engendered when the products reach the exhaust. The products generated during combustion at high temperatures are non-sustainable, and the following processes occur before the balance is restored (Heywood, 1988).

$$\boldsymbol{2H_2O + O_2 \Rightarrow 2(1-y)H_2O + 2yH_2 + yO_2} \tag{2.4}$$

$$\boldsymbol{C + O_2 \Rightarrow CO_2 \Rightarrow (1-x)CO_2 + xCO + \frac{x}{2}O_2} \tag{2.5}$$

When the products turn cool to exhaust temperature, a large portion of the CO interacts with oxygen to create CO_2. However, just a little quantity of CO will be left in the exhaust. HC is emitted as a result of incomplete combustion (Hu and Ladommatos, 1996; Laskowski et al., 2019) caused by inefficient engine design, poor fuel quality, or control system failure. Design parameters, combustion chamber design, and operational variables such as air-fuel ratio, speed, load, and mode of operation (idling, running, or accelerating), all influence the quantity of hydrocarbon emitted. HC in spark-ignition engines derive from numerous sources, which include flame quenching at the walls of the combustion chamber and at the entry of crevice volumes, immersion, and dispersion of fuel vapor into oil layers on the wall of the cylinder, misfiring and incomplete burning (Tavakoli et al., 2021).

2.3.2 Emission control parameter

Different techniques have been used to reduce the emissions from SI engines, including improved combustion conditions (Buruiana et al., 2021) and catalytic after-treatment (Koltsakis and Stamatelos, 1997; Dey and Mehta, 2020). In addition, the utilization of technology innovations in fuel injectors, oxygen sensors, and onboard computers in vehicle engines has provided better control and subsequently optimized the engine combustion process, leading to better and improved combustion. In addition, the combustion conditions are improved by increasing fluid turbulence and fuel mixing in the cylinder, modifying the size and position of the intake valve and utilizing direct fuel injection in the cylinder (Alkidas, 2007). Since any engine that uses internal combustion fuel requires air to function (Balmer, 2011). This is because, without air, particularly oxygen, fuels cannot burn and supply the combustion force to operate the engine. The oxygen shortage while operating the engine results in a rich mixture that contributes to the higher unburned gaseous fuel, owing to a faster burning rate and shorter ignition delay. Too much oxygen results in a lean mixture that lead to unstable combustion and misfire (Abdelaal et al., 2013). To attain complete combustion, it is necessary to ensure that charged air entering the combustion chamber contains enough oxygen. As the number of oxygen molecules in the air increases with the decrease in temperature of air and vice versa, justified by ideal gas law (Alao & Babatunde, 2020).

$$\boldsymbol{\rho = PR^{-1}T^{-1}} \tag{2.6}$$

The above equation proved that air temperature is an important phenomenon in the combustion process. It is also verified from the basic equations of the thermal efficiency (air-standard efficiency) of the Otto cycle (V. Ganesan, 2012):

$$\eta_{th} = \frac{W_{net}}{Q_{in}} = \frac{Q_{net}}{Q_{in}} \tag{2.7}$$

$$Q_{net} = \dot{m}.c_v.(T_3 - T_2) - \dot{m}.c_v.(T_4 - T_1) \tag{2.8}$$

$$Q_{in} = \dot{m}.c_v.(T_3 - T_2) \tag{2.9}$$

Thus

$$\eta_{th} = \frac{\dot{m}.c_v.(T_3 - T_2) - \dot{m}.c_v.(T_4 - T_1)}{\dot{m}.c_v.(T_3 - T_2)} \tag{2.10}$$

$$\eta_{th} = 1 - \frac{(T_4 - T_1)}{(T_3 - T_2)} = 1 - \frac{T_1(\frac{T_4}{T_1 - 1})}{T_2(\frac{T_3}{T_2 - 1})} \qquad 2.11$$

For processes (1-2) and (3-4) isotropic on the (P-V) diagram, the thermal efficiency can be simplified as (Hiereth & Prenninger, 2007):

$$\eta_{th} = 1 - \frac{T_1}{T_2} = 1 - \left[\frac{V_2}{V_1}\right]^{k-1} = 1 - \left[\frac{1}{r}\right]^{k-1} \qquad 2.12$$

Where r = compression ratio, k = C_p/C_v

Observing equation (2-12), the temperature of the engine's intake and combustion is the most important factor when it comes to its thermal performance. For naturally aspirated engines, the inlet temperature relies on the outside (ambient) temperature (Chhalotre et al., 2018), while for charged engines, it depends on how well the IHE works (Engkuah et al., 2016). However, combustion temperature depends on burning combustion and heat release, which vary with the fuel/air ratio. Theoretically, the engine's thermal efficiency increases as the inlet temperature decreases (Z. Zhang et al., 2022), which is the main focus of this study.

2.4 Influence of ambient conditions on ICE

The ambient conditions have an impact on engine combustion (Cui et al., 2021; Shahridzuan et al., 2021). The air humidity and temperature are the most significant ambient variables that impact the performance of ICE (Lindhjem et al., 2004; Chang et al., 2017), as the amount of humidity in the air affects combustion. With an increment in air humidity, it slows down the combustion process and lowers the maximum combustion temperature. On one side, this will have a good impact on the knock margin and NO_x emissions, but it will have a detrimental impact on the engine's efficiency. The other parameter temperature, is one of the fundamental thermodynamic properties (Childs et al., 2000), that may be detected with thermometers (thermocouples) (Rossouw, 2016). Ambient temperature referred towards the temperature of the surrounding environment (Epstein & Moran, 2019), influences the energy usage of ICE cars (Taggart, 2017). The temperature of an ICE is critical for combusting the fuel and powering the engine (Musgrove et al., 2018). In an ICE, high temperatures, often known as heat, are required to burn the fuel. However, the temperature must be kept under control to ensure safe operation (Morad & Alrajhi, 2014). The engine cylinders, pistons, and other components may be damaged if the temperature of the engine reaches unacceptable levels. For that matter, it is necessary to have a method of heat removal that will keep the engine operating safely and it majorly depends on ambient temperature (Safakish, 2012). However, ambient air temperature and air inlet or intake temperature have distinct meanings. According to Andrews et al. (2004) ambient air temperature is the temperature outside the engine compartment, whereas air intake temperature is the temperature recorded at the turbocharger's inlet. The ambient temperature does not affect engine performance directly, instead, it does have an effect on the air intake temperature before entering the combustion chamber or turbocharger, as well as on the engine cooling system. In this study, the intake air temperature will be considered a topic concerning ICE performance.

2.5 Significance of engine intake air temperature

The charged air property of temperature and pressure is influenced by the environmental status of weather and by the exciting components integrated into the engine intake charge air (EICA) system as a compression system (Chan et al., 2013). The EICA temperature parameter plays a vital role in engine combustion performance as the air density is affected by the temperature variation (Irimescu et al., 2017b). According to Mattson (2019) raising the mixture's input temperature surges the temperature at the end of compression, which raises the temperature of the final portion of the charge to ignite, thus reducing the delay period and increasing the chances of knock (Yue & Som, 2021). Earlier studies (Douaud & Eyzat, 1978) also brief that propensity for knock to occur is a function of, among other factors, cylinder end gas temperature and pressure. As a result, at a given engine load, a lower intake air temperature minimizes the knock propensity. This would enable an earlier center of heat release, reducing both exhaust temperatures and BSFC directly. At high engine loads, a decrease in intake temperature results in a decrease in exhaust temperature, even at a particular center of heat release (Kadunic et al., 2014). As a result, it's best to keep the intake temperature as low as possible but not too low in order to avoid fuel vaporization. Alam et al. (2005) studied the effect of inlet air temperature on direct injection diesel engine performance and emissions. They concluded that with the increase in inlet air temperature, average cylinder temperature and specific fuel consumption increase, and a decrease in AF ratio and thermal efficiency is observed.

Acquiring cold intake air provides a special benefit for engine performance since it is denser than hot air and contains more oxygen, which promotes greater combustion, higher power, and improved fuel economy (Johnson, 2010). The impact of charge air cooling on the engine's overall performance has been investigated in the literature archive (Ni et al., 2014) and has witnessed substantial improvement in engine performance and reductions in engine emissions. Lowering the temperature of intake air causes a reduction of thermal losses and stresses, thus contributing to an adiabatic engine with higher indicated efficiency. It is beneficial not only for vehicle engines but also for increasing the performance of power plants (Baakeem et al., 2017; Pradeep Varma and Srinivas, 2015). The same cooling-related potential benefits are evident when water is injected into the intake line: as a result of water droplets evaporating, a significantly lower air temperature is attained, resulting in a mixture (air and steam) that enhances indicated mean effective pressure and knock resistance (Mingrui et al., 2017; Soysal et al., 2022). This particular intake air cooling method is discovered to be superior than the cooled EGR method (Bozza et al., 2016). Some of the key advantages of cold intake air are discussed in the following sub-section:

2.5.1 Impact of EICA temperature on emissions

Owing to the high temperature of combustion, vehicles produce more HC, PM, CO, non-methane volatile organic carbon (NMVOC) (Sadavarte & Venkataraman, 2014). High operational temperature also results in higher NO_x exhaust emissions (Torregrosa et al., 2008; Andrews et al., 2007). This is most likely owing to enhanced thermal NO production by means of the Zeldovich mechanism (Hamrock et al., 2004). Therefore, mitigating the negative impacts of high combustion temperature is valuable (Pinilla Fernandez et al., 2021). To compensate for cylinder-to-cylinder differences or variations, Haraldsson et al. (2004) found the inlet temperature of the air as a useful technique and observed the maximum brake efficiency and minimum NO_x exhaust emissions in comparison to balance the cylinders with equal inlet temperature or with the quantity of fuel. Sarjovaara et al. (2015) reported that reducing air temperature before inducting to the engine can reduce the NO_x emission and exhaust temperature of diesel engine. Cesur et al. (2013) injected steam in the intake line of gasoline engine to introduce cooling effect and reported reduction in fuel consumption by 6.44%, NO_x emissions by 40%, and HC by 31.5%. Cinar et al. (2015) examined the effect of high EICA temperature on a single-cylinder, four-stroke HCCI gasoline engine operating at 1200 rpm. Their results showed an increase in in-cylinder pressure with increasing charge temperature and noted advance and period decrease in combustion. Moreover, the fuel consumption along with engine emissions were escalated.

Premkartikkumar et al. (2014) investigated the influence of EICA temperature on a DI diesel engine exhaust emission by reducing the charge air temperature from 300°C to 25°C. The results show a significant fuel economy enhancement, and engine exhaust emissions were generally decreased except for the NO_x emission increase. In a gasoline engine, Abdullah et al. (2015) investigated the influence of EICA temperature variation on the fuel consumption and exhaust emission of a 1.6L gasoline engine. The results showed that the influence of high EICA temperature increased the fuel consumption and CO emissions and advanced with shorter combustion duration. While their study shows a higher oxygen concentration at lower EICA temperature tests, resulted in reduction of BSFC, UHC and CO emissions. Cipollone et al. (2017) investigated the influence of low EICA temperature on a turbocharged diesel engine (F1C 3L) using a coupled IHE chiller unit to cool the charge air. Their results showed a significant reduction in net fuel consumption by up to 6%, 8% saving on CO_2 emissions, and a reduction of 4.5% in NO_x and 12.1% in CO emissions.

2.5.2 Impact of EICA temperature on power

A cooler intake is one of the simplest and most cost effective performance components that can add to any vehicle, whether it's a street vehicle, a racer, or even a tow truck. The entire goal of a cold air intake is to obtain colder air, which really is denser and contains more oxygen per volume. The colder it is, the better. In a power plant, intake air cooling methods such as absorption chiller, high pressure fogging, and evaporative cooling provide 1–15% more output than without cooling of the inlet air (Liu et al., 2019; Şen et al., 2018; Al-Ibrahim and Varnham, 2010). Vehicle air conditioning of a normal car consumes roughly 5 to 8 hp, which Herbert Joyner (1963) tried to recapture the bulk of this normally lost power by utilizing cold refrigerated air output of the air conditioning system. Sugiura (1987) presented the gain in engine power by utilizing cold intake air presented in Figure 2.2**.**

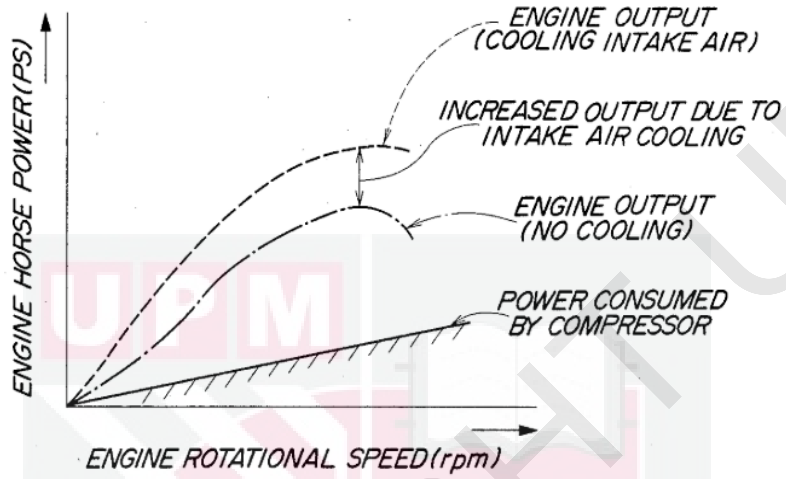

Figure 2.2: Difference in power with and without cold intake air
(Sugiura, 1987)

Nazmi et al. (2021) conducted experiments using Perodua Myvi 1.3L with different air intake temperatures, which were 35°C to 70°C with an increment of 5°C, to discover the effect of different intake temperatures on engine power and torque. The results concluded that with the increased intake air temperature, the engine shows a reduction in power and torque. Similarly, Fathi et al. (2020) investigated the influence of EICA temperature on a novel two-stage direct injection homogeneous charge compression ignition (DI-HCCI) combustion engine model using the multi-zone approach. Their results indicated that with the increase in intake air temperature, engine power decreases. In other words, the colder the intake, the better engine performance. Kadunic et al. (2014) measured the impact of cold air introduced in turbocharged 1.4L SI-engine experimentally to prove the concept of better engine performance through charge air cooling using a modified air condition system. The results recorded that maximum torque was increased by up to 12.5%. Arif et al. (2021) proved in their studies, that cold intake air helps to enhance the engine power. Aftermarket cold air intake systems are marketed with claims of increased engine efficiency and performance. However, there is no thumb rule or any formula that indicates the magnitude of the power gain associated with a particular temperature drop. Numerous factors exist. Jonathan Fiello, vice president of product development and engineering at K&N Engineering in Riverside, Calif said; "There is no conventional scale that we can use which indicates that a reduction in temperature by X amount results in a gain in horsepower of Y amount. In terms of temperature, you're going to see substantial advantages down low and substantial losses up high; however, the kind of gasoline consumed, the displacement of the engine, and the type of induction, whether forced induction or naturally aspirated, all have a significant effect" (Becker, 2019).

2.6 Point to ponder while considering cold intake air system

Engine performance is sensitive to induction depression, especially for IC engines running without a turbocharger or supercharger. Managing air supply to the combustion chamber is a key component of modern vehicle engines since it may significantly impact performance, emissions, and fuel efficiency. To improve an engine's performance and, therefore, the vehicle's performance, the supply of air-fuel mixture into the combustion chamber should be managed both qualitatively and quantitatively (Kaul et al., 2021). The inlet manifold is the duct that connects the intake system to the engine's inlet valve through which the air-fuel mixture enters the engine and has pronounced significance in determining the engine's efficiency (Jemni et al., 2021). The schematics of the air intake system are presented in Figure 2.3.

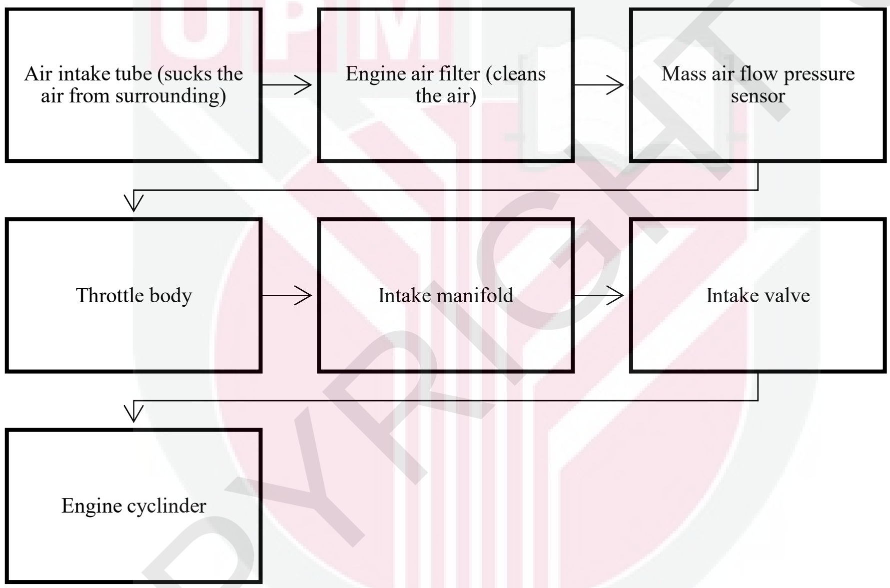

Figure 2.3: Block diagram of the air intake system
(Raman & Bahari, 2021)

One of the most significant factors affecting performance in ICE is the intake manifold (Lim et al., 2020). All of the advantages of lower air intake temperatures can be nullified by a cold-air intake system that limits airflow or causes high pressure drop when matched to a stock system. A system must guarantee that the amount of cold air flowing in is equivalent to or better than the amount of air receiving with the stock system in order to be successful. It is well established that the pressure drop that occurs throughout the air intake system has a substantial impact on the power of the ICE (Mamat et al., 2009). An intake manifold having a low-pressure drop is very important to maximize the mass of the drawn air into the cylinder (Gocmen & Soyhan, 2020). The performance of an engine is subject to induction depression, particularly for ICEs that do not use turbochargers or superchargers, and the pressure drop is caused by the suction induced while the piston is in descending position. According to Daniel Marty, engineering manager for TMG

Performance Products, parent company for Corsa Performance and Volant Performance in Berea, Ohio; “If you want to improve your engine's output, the best way to do so is by minimizing blockages to obtain laminar airflow and maximizing the amount of air entering the engine. This will use more fuel to get surplus power. For subsonic applications, laminar airflow is the most efficient. The mathematics for air flow is way easier and the gain in power is high. If, for instance, there’s a restriction in your intake that’s causing, let’s say even just a 5% increase in pressure drop through that intake system, and you could get that down to 1% pressure drop, that pressure drop, you are not talking about a square root function now. You are talking about a ratio. So, you get more power proportionally from a relatively small change in the restriction than you get from a relatively small change in temperature” (Becker, 2019).

2.7 Intercoolers

Heat exchangers, also known as intercoolers, are typically installed to supercharged and turbocharged engines to provide cold air to the engine intake (Fredrico Burke, 2018), due to their beneficial impact on engine output and fuel economy (Sergienko et al., 2021; Yu et al., 2019). Unlike a radiator, a turbo intercooler cools the air supplied into the engine instead of cooling the engine. The intercooler's job is to cool the input gas and densify the air needed for optimal combustion (Yum et al., 2017). The Ideal Gas Law, describes the physics of air and necessitates the installation of an intercooler. Explaining the ideal gas law as fundamental is important since pressure and temperature are directly related, and increasing pressure using a turbocharger or supercharger results in increased heat production. Hot air density is lower than cold air, and as a result, it contains fewer oxygen molecules per unit volume (Ravindra & R. R. Arakerimath, 2017). This implies that the engine receives less air in a given stroke (in case of hot air), thus resulting in less power engendered. Hot air further raises the temperature of the combustion chamber, which may assist in the pre-detonation of the combustion cycle, which can result in detonation (Z. Wang et al., 2017). Intercoolers improve induction system performance by eliminating induction air heat generated by the supercharger or turbocharger (Prabhu, 2015; Handibag et al., 2020; Mifdal et al., 2015) and encouraging more complete combustion. This actually reduces the heat of compression, which is the rise in induction air temperature that happens in any gas when its pressure is upraised and increases the induction air density (Cash et al., 2016). Generally, an IHE is often divided into four categories based on the medium utilized as a coolant, which includes liquid and gas, described in the following sub-section.

2.7.1 Air to air

The configuration of this type of intercooler (air to air) is that the charged air is blown or forced to be chilled by ambient air flowing through cooling pins placed integrally on multiple tubes as it travels through the several numbers of tubes (S.J. Yang et al., 2019). Earlier, Sankar and Kishore (2016) explained the position and functioning of the charge air cooler as presented in Figure 2.4. It is commonly installed between the compressor and the intake manifold. The ambient air is drawn into the compressor via an air filter, in which it is compressed to an elevated temperature. Hot compressed air exits the compressor and passes through a charge air cooler, discards its heat into the ambient air flowing outside, and cools down. A cool charge from the intercooler is then allowed to enter the engine's intake system through the intake manifold.

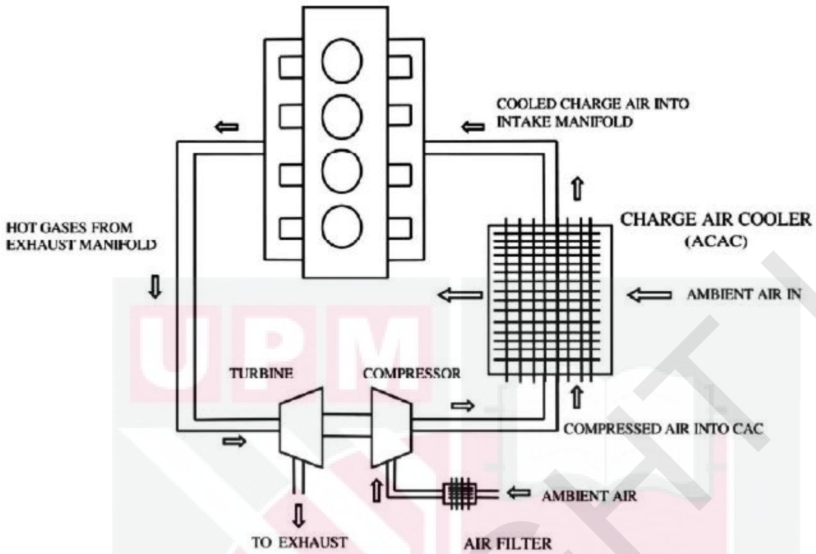

Figure 2.4: Air-to-air charge cooler circuit
(Sankar & Kishore, 2016)

2.7.1.1 Advantages and disadvantages

The advantages of the air-to-air intercooler are many, including a simpler construction, fewer components, less weight, and no need for a hydraulic setup as is the case with an air-to-water intercooler. One of the disadvantages of having this system is that since it is air-cooled, it has to be placed at the front of the car (Puetzer, 2015). This means that the piping required to connect the components and the route taken by the air from the turbocharger to the intercooler and then to the engine is a bit longer. Cooling capacity depends on outside ambient temperatures and humidity. Non-suitable for low-speed or parking operations (Curran & Irick, 2009).

2.7.2 Air to liquid

The water-cooled intercooler, on the other hand, is built in an improved package (Mezher et al., 2013), that the charged/compressed air is compelled to be cooled by a coolant flow circuit in contact with the tube (Engkuah et al., 2016; Ma'arof et al,. 2019). A radiator plus a pump make up this circuit presented in Figure 2.5. After flowing through a radiator, the water is sent to a water-charged air cooler, which is used to chill the air and remove heat. The engine must incorporate an entire hydraulic system for the said intercooler. At the front of the engine, there is an additional heat exchanger. The actual/real intercooler is installed inside the intake manifold or somewhere near the engine. Still, the system operates within the same thermal range of air-air type intercooler as the cooling method depends on the external atmospheric air condition.

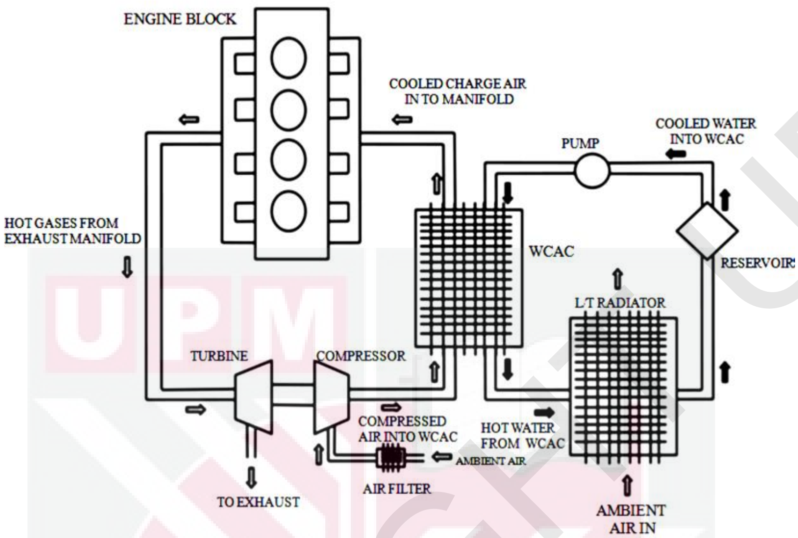

Figure 2.5: Water-cooled air charge cooler
(Sankar & Kishore, 2016)

2.7.2.1 Advantages and disadvantages

An air-to-water intercooler has a faster response time from the engine, which is very important when trying to get the maximum performance out of your vehicle comparable to air to air intercooler due to the high specific heat of water (Arif et al., 2021). The disadvantage of this system is that it involves many components like the heat exchanger, pump, reservoir, and much more (H. Nasution et al., 2015), and there is also the danger of the coolant leaking.

2.7.3 Air – solid surface intercooler

The phenomena of electric current passing through connection junctions of two different materials create cooling and heating results at both sides of the intersection, which was discovered by Jean Charles Athanase Peltier in 1834 (Nikam & Hole, 2014). These thermoelectric effects were improved by Abram Ioffe in 1950 when they found semiconductors had a higher thermoelectric effect than other materials (metals or insulators). He suggested refrigeration could be accomplished using a multi semiconductor array to create a wide solid thermal surface. Figure 2.6 illustrates the thermoelectric semiconductor working method and an IHE device designed by (Jia-Wei & Hsueh, 2013).

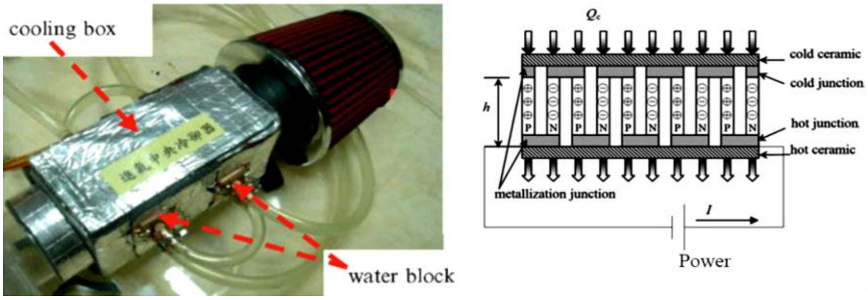

Figure 2.6: Air intake cooling box and scheme of thermo-electric module construction
(Jia-Wei & Hsueh, 2013)

The thermoelectric technology can be utilized as IHE in the automobile field and for other purposes such as a fridge, electronic heatsinks, and fuel coolers. This new technology introduced a significant super-cooling reaching frozen temperature. Still, the area consumed by the semiconductors is small and needs to combine more extra thermoelectric parts to create a larger surface area, which makes it expensive and requires an electronic computer controller for power distribution. Therefore, this technology is used in small-scale cooling capacity filed like microchips and computers CPU cooling heatsinks (Wiriyasart et al., 2019; Cuce et al., 2020).

2.7.4 Air - gas intercooler

The revolution of intercooler performance enhancement continues to search for better coolant mediums that offer higher thermal capacity. The pressurized gas successfully achieved higher thermal performance (Nader et al., 2019). Generally, the pressurized gas cycle system consists of two types, depending on the coolant source.

2.7.4.1 One-shot IHE

This system uses the pressurized (CO_2 or N_2) gas or any other gases with high thermal evaporative properties to cool down the IHE by releasing the gas in one direction and expanding inside the cooling domain shown in Figure 2.7. The process ends with consuming all pressurized gas sources evaporated inside the cooling area. This kind of intercooler is not suited for daily driven cars but rather for use in drag race vehicles because of the excellent cooling capacity (Ravindra & R. R. Arakerimath, 2017). The limitation of this system is the duration of use depending on the gas source tank, and operation is costly and needs to refile for the next use.

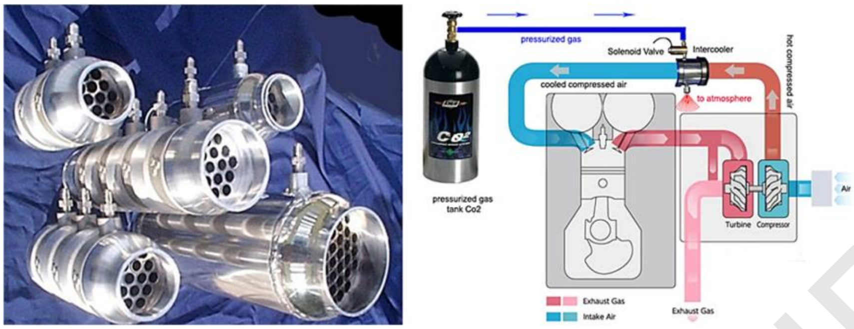

Figure 2.7: One-shot pressurized CO_2 gas within an intercooler heat exchanger
(Aaron, 2011)

2.7.4.2 Intercooler sprayer

Basically, an intercooler sprayer is just a collection of water jets that may be used to wet down an intercooler, as illustrated in Figure 2.8. That technique effectively lowers the temperature of an intercooler below that of the surrounding air. Cooling the charge will not only enable to get more power from the engine, but it will also help keep the engine cool if the intercooler is placed in front of the radiator. This is among the most essential aspects of installing a high-efficiency intercooler sprayer. Not only water is effective as a spray fluid, but also certain chemicals that evaporate more quickly than water can be used for even greater efficiency, which will allow to extract much more heat from the intercooler. However, the process ends with consuming all pressurized gas sources sprayed on the cooling surface area.

Figure 2.8: Intercooler sprayer system
(Choo, 2005)

2.8 Advanced technologies to obtain cold intake air

A relatively new approach utilizes water to cool the intake air (Harada et al., 2016) through a low temperature coolant loop in a dual-temperature engine cooling configuration (R. Cipollone et al., 2013). This approach improves the overall thermal management of the vehicle (allowing for a redesign of the cooling channels within the engine block and head) (R. Cipollone et al., 2012) and also reduces engine warm-up time by up to 30% in automobiles(R. Cipollone et al., 2013). Recent studies have concentrated on the heat recovery from exhaust gases to feed cooling-dedicated components, such as jet ejector cooling devices, to obtain air cooling below ambient temperature (Zegenhagen and Ziegler, 2015a; Zegenhagen and Ziegler, 2015b). Galindo et al. (2019) also conducted a thermodynamic analysis of the jet ejector refrigeration cycle and claimed that 0℃ intake temperature could be attained for those engines whose exhaust thermal power is sufficient to drive the jet ejector refrigeration system. The schematic diagram of the jet ejector refrigeration attached to the engine is shown in Figure 2.9.

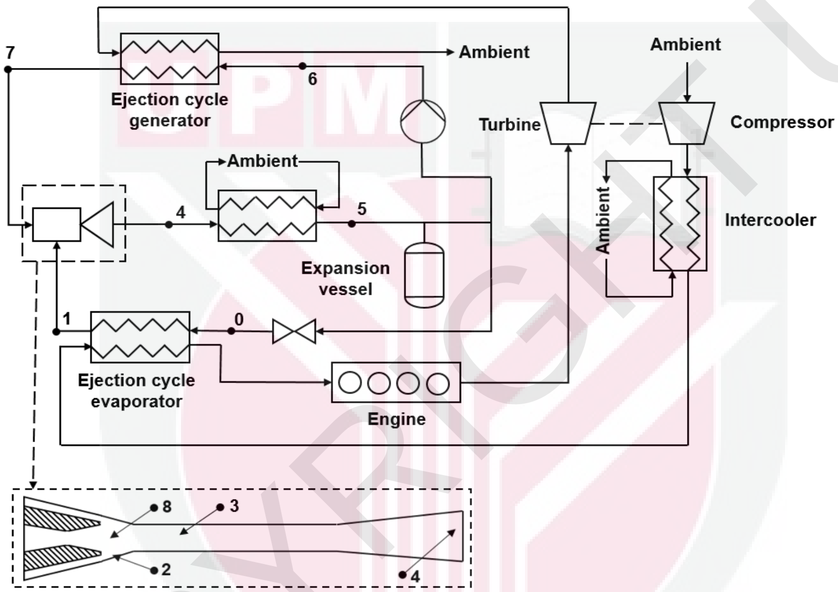

Figure 2.9: Ejection cycle arrangement intended to cool down engine intake
(J. Galindo et al., 2019)

The advantages linked to waste heat recovery must be weighed against the negative effects of a higher induced engine backpressure (D. Di-Battista et al., 2015), while also taking into account the additional fuel used to drive a compression chiller that does not necessarily require. Other strategies focus on the possible improvement that can be attained by charge cooling using a heat pump or a mechanically driven compression chiller; the viability of these strategies should be evaluated in light of the present trend toward engine downsizing. Among alternate theories for additional charge cooling, sorption-based theories are particularly intriguing. An absorption refrigeration system connected to the intake air-line has been reported to boost engine efficiency by up to 4% (Novella et al., 2017); in particular, the adsorption system can be powered by exhaust energy, as long as the pressure drop on the exhaust is kept to a minimum (Manzela et al., 2010). It can accommodate the cooling requirement of a coach vehicle (Jianbo Li, 2013). Although controlling the adsorption system has proven to be quite challenging, Rêgo et al. (2014) found it simple to manage in a range of high engine operating points. The weight increase caused by these technologies is unquestionably a negative outcome that decreases propulsion power (D. Di-Battista et al., 2015). Further cooling improvements have been done using a VAC unit on the intake pipe, discussed in section 2.10.

2.9 Vehicle Air Conditioning (VAC) system

VAC is virtually ubiquitous and is included as standard equipment in almost every newly manufactured vehicle (Hundy et al., 2016). The use of VAC in passenger cabins for thermal comfort (Ketwong et al., 2021) is increasingly considered a need rather than a leisure, and cooling is particularly important while traveling during the summers or over the year in nations with a hot and humid environment (Qi et al., 2017), as it decreases driver tiredness (Mebarki et al., 2013), and increases road safety with the comfort of the driver (M. Y. Lee, 2017). The VAC is usually subjected to highly variable environmental conditions, necessitating extensive efforts to assess its overall effectiveness (Piao et al., 2021). The conditions entail inlet circumstances, which decide the temperatures of the air entering the evaporator and condenser; consumer selections, which define the volume flow rate of the evaporator and the ventilation manner; driving styles, which dictate the speed of the compressor and the velocity of the condenser face; and compartment material, number of occupants, and weather patterns, which ascertain the external and internal thermal loads (Gado et al., 2008).

2.9.1 Major components and working of VAC System

The parts of a VAC system are nearly identical to those of a room's air conditioning system, but there have been numerous modifications crafted to a VAC system to make it more compact and to fit in with the components of an engine. The air conditioning system in cars is comprised of the following components: the compressor, the condenser, the condenser fan, the expansion valve, the receiver drier/air conditioner accumulator, the evaporator, and the evaporator fan (Bentrcia et al., 2017). Most of the VAC system operates with the vapor compression refrigeration cycle (X. Yang et al., 2017) to maintain thermal comfort within the compartment. Figure 2.10 presents the typical VAC system cycle.

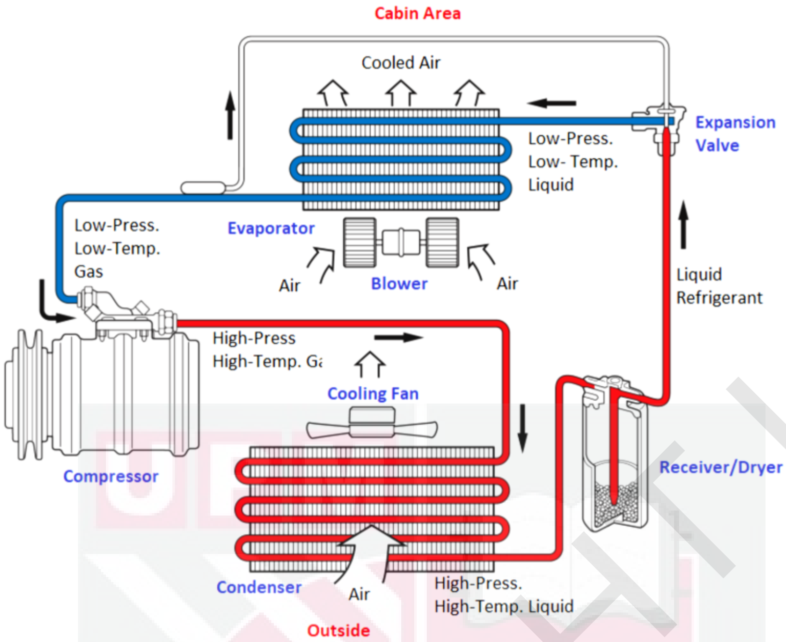

Figure 2.10: VAC schematic arrangement
(A. Bhatia, 2018)

The evaporator, which is another kind of heat exchanger utilized in the air conditioning system, absorbs heat from the compartment of a passenger and transfers it to the liquid refrigerant circulating in the evaporator, which turns into vapor form, which then cools the compartment with the assistance of the blower fan (Stubblefield & Haynes, 2000). Once the high-temperature, low-pressure vapor is sent to the compressor (Nimkar et al., 2021), the increased pressure over the vapors causes it to condense and transform into liquid refrigerant. At that stage, the refrigerant is in a liquid form under high temperature and at high pressure. Once in the condenser, the high-pressure, high-temperature liquid refrigerant is cooled by forced convection supplied by the radiator fan or by a distinct fan (Subiantoro et al., 2014). Although the temperature of the refrigerant has dropped, however, the pressure of the refrigerant has remained almost constant. It is then transported to the expansion valve, where the high pressure and low temperature refrigerant are released, and the refrigerant is returned to its natural condition (T. Lee et al., 2021). After that, the refrigerant is returned to the evaporator for the next cycle to take place. A receiver dryer is installed between the evaporator and the compressor to transform the leftover refrigerant in the liquid state received from the evaporator into vapors before it is sent to the compressor.

2.9.2 Impacts of VAC on engine performance

According to Yeh et al. (2009**),** Khayyam et al. (2011) and Chen et al. (2022), a VAC system can be considered the primary accessory that extracts the greatest amount of power when it is in operation, making it a critical issue due to increasing concerns about energy costs, emissions of greenhouse gases, thermal comfort and automobile performance (Sukri et al., 2016). In most automobiles, the compressor is directly linked to the engine crankshaft, as shown in figure 2.11, its speed is similar to the engine speed, which cannot be regulated, and at the same time, cooling capacity fluctuates (Dahlan et al., 2014). It may take up to 5 to 6 kW of power from the car's engine at peak load (Fayazbakhsh & Bahrami, 2013) or 7.5 kW at 6000 rpm according to (Soo et al., 2021), which is roughly equal to a vehicle traveling at 56 km/hr. Although the cost of installing an air conditioning system is usually economical, the additional weight that is added as well as the functioning of the system, both cause the increment in the consumption of fuel (Q. Zhang et al., 2015). Extra fuel consumption by the mobile air conditioning system results in less fuel economy as well as more emissions of greenhouse gases. According to research by S. S. Bhatti et al. (2021) usage of air conditioner decreases the fuel efficiency by about 15-20% and enhances NO_x and CO_2 emissions by approximately 80% and 70%, respectively, however, the exact figures depend on the particular driving parameters (Rugh et al., 2001).

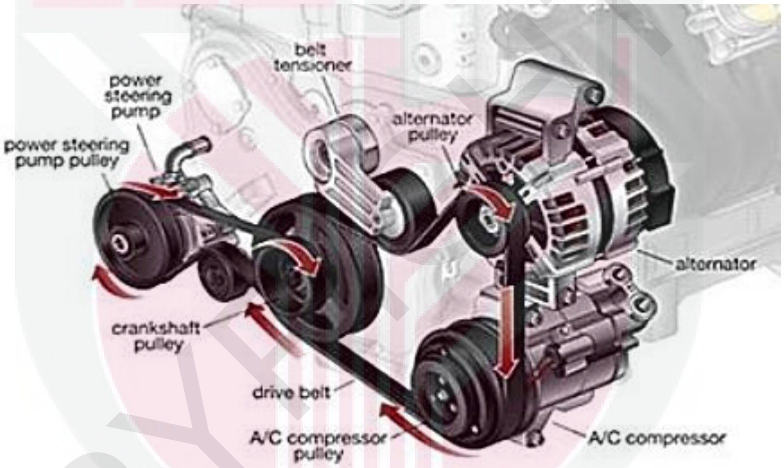

Figure 2.11: Belt driven compressor connection with the engine
(Heard, 2018)

2.10 IHE operates on VAC system

As described in the previous section about the capability of VAC system, R. Cipollone et al. (2017) highlighted in their research that, in modern vehicles, there is potential to use the on-board air conditioning unit for intake air cooling because it is generally over-sized and under-utilized for cabin heating and cooling. Moreover, it can also be integrated into a double circuit cooling system (R. Cipollone et al., 2013), achieving improved cooling performances if a water cooled condenser is utilized (Davide Di Battista & Cipollone, 2016). This possibility would result in an improved engine functioning with no extra onboard devices, i.e., no complexity and weight increase in the engine layout. Figure 2.12 illustrates the general model of the engine layout for intake air cooling from the VAC unit. Further, in response to that opportunity, a cold intake air system using the refrigeration cycle of automotive air conditioning has been investigated and patented by several investigators, presented in Table 2.1.

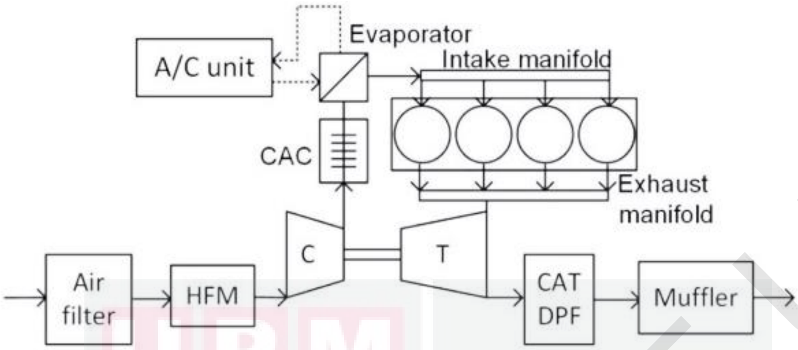

Figure 2.12: Engine layout for intake air cooling
(D. Di-Battista et al., 2018)

Table 2.1: Devices and methods of obtaining cold intake air using VAC

Patent title	Patent number and engine type	Inventions
Refrigerant cooled intercooler. (Alexander H. King, 1951)	US2571256 Aircraft engine.	Utilized a portion of the engine power mechanically to refrigerate the intercooler. The amount of horsepower used to operate the refrigerating machine is less than the loss heretofore incurred in air-cooled intercoolers by their high head resistance.
Utilizing vehicle air conditioning system for internal combustion engine. (Herbert Joyner, 1963)	US3071934A Naturally aspirated engine.	Utilized a portion of the cold refrigerated air flowing to the passenger cabin of the vehicle through duct and mixed it with intake air stream flowing to the carburetor to lower the temperature of the incoming air.
Method and apparatus for refrigerating combustion air for internal combustion engines. (Crooks, 1964)	US3141293A Turbocharged engine.	Utilized exhaust gases of an engine to provide improved technique and equipment for cooling the combustion air of an ICE to near-freezing temperatures in order to enhance not only thermal efficiency but also brake mean effective pressures.
Reciprocating machine with refrigerated cooling of intake air. (Welch & Fish, 1979)	US4169436 A barrel type Reciprocating machine.	Coolant tubes placed inside intake manifold allowing the intake air to be cooled. A suitable refrigerant is circulated through the coolant tubes to cool the intake air and the cylinder itself.
Air conditioner for automotive vehicles capable of cooling intake air supplied to an internal combustion engine. (Sugiura, 1987)	US4683725 Turbocharged engine.	Introduced the method for two evaporators for an automobile air conditioning system, which is linked to the compressor's intake during the cooling cycle. The first evaporator is used to cool the air that is forced into the vehicle's passenger compartment, while the second evaporator, located in the engine's intake system, cools the air that is taken into the engine.
Engine charge air cooler (Hudelson, 2002)	US6394076B1 Supercharged and turbocharged engines.	Presented new device comprises a number of fins located in air passage such that the charge air passes between the fins. A refrigerant tube placed in the housing, passes through each of the fins, removing heat from incoming hot air.
Intercooler system for internal combustion engine. (Klem, 2002)	US20020116927A1 Supercharged engine	Introduced air conditioner evaporator coil refrigeration device to cool air flowing there through prior to engine intake air cooling, cooling performance cannot reach very low temperatures due to small contact surface area of cooling coil.
Charge air management system for an automotive engine. (Sealy et al., 2003)	US6561169B2 Turbo-super charged	Introduced liquid-liquid cooled intercooler for removing heat from hot air. The refrigerated fluid, which chills the liquid coolant in the said intercooler, comprises refrigerant fluid flowing in a VAC system.
Charge air intercooler having a fluid loop integrated with the vehicle air conditioning system (Bucknell & Marc Musial, 2004)	US6796134B1 Turbocharged engine	Presented an intercooler includes: a charge air cooler loop that is diligently connected to the turbocharger to cool pressurized heated air received from the turbocharger before it moves into the car's engine; and a bypass circuit which is connected to the charge air cooler loop and the vehicle's air conditioning unit bypass loop.
Charge air cooler having refrigerant coils and method for cooling charge air. (Yi, 2008)	US7341050B2 Turbo-super charged engine	Invented a device and a technique for cooling charged air. The device consists of multiple tubes, in which tubes on the front side portion contain refrigerant medium extracted from the vehicle's air conditioning unit and tubes on the back side contain pressurized hot air. The ambient air cools down after passing through the frontal refrigerant tubes, and then the cool ambient air passes through charged tubes and removes the heat, so that cool pressurized air will be available at the engine intake.

Table 2.1: Continued

Intake air cooling device for internal combustion engine and automobile using the same. (Noyama et al., 2010)	US7779821B2 Supercharged engine	Introduced an evaporator to cool down the air temperature with the help of vehicle refrigeration unit. Cooling device also hold a knocking sensor, which can control the opening and closing of refrigeration supply in evaporator, according to the requirement.
Engine air intake and fuel chilling system and method. (Johnson, 2010)	US7658183B1 Naturally aspirated engine	Tubular duct through which hot air flows to engine is covered with a helical coil, having refrigerant from vehicle air conditioning system, to reduce the temperature of air. Temperature of the engine fuel is also reduced by the addition of dry ice system, which further cool down the air fuel mixture.
Air intake device. (Ino et al., 2015)	US8955497B2 Turbocharged engine.	Presented an intake chilling device which is coupled with cylinder head, containing cooler and a surge tank. The cooler contain two passages; one is for refrigerant and other is for air flow. The cooler cools the intake air with the help of vehicle refrigerant.
Water cooled intercooler system using air conditioning system and control method thereof. (S.-J. Yang et al., 2019)	US10240514B2 Turbocharged engine	Introduced water cooled IHE system. The cold water used to cool the hot intake air is obtained from vehicle air conditioning system.

2.11 Comparison of various cooling system

The comparison of available intercooler systems in the literature is listed in table 2.2, in the form of their distinct features and limitations. Further, in view of table 2.2, the evaluation is made based on multi-weight scoring model, to appraise the impactful intercooler system, based on weight, cooling capability, market availability, price, maintenance and operation during vehicle static and moving position, presented in table 2.3. For that matter, equal weight was assigned to each particular i.e. 1. Moreover, scores were assigned to each criterion of all intercooler system (0 to 10, low to high) based on their ratings and importance. The weights and scores were multiplied to get a total weighted score for the project. Using these multiple screening criteria, it is observed that the intercooler operating on vehicle refrigeration system has a way highest weighted score, in contrast to other available intercooler systems.

Table 2.2: Distinct features and limitation associated to various intercooler systems

Cooling system	Distinct features	Limitations
Air to air (S.J. Yang et al., 2019) (Puetzer, 2015) (Sankar & Kishore, 2016)	i. simpler in construction ii. fewer components iii. less weight iv. no need for a hydraulic setup	i. cooling capacity depends on outside ambient temperature and vehicle speed ii. placed only at front of car iii. exposed to external damage and road debris
Air to liquid (Engkuah et al., 2016) (Arif et al., 2021) (H. Nasution et al., 2015)	i. efficiency can be exaggerated by using ice, or other chemicals ii. high specific heat of water compare to air type iii. smaller in size	i. cooling capacity depends on outside ambient temperature ii. require additional hydraulic system iii. small coolant leaks into intake air passages can cause misfires and other combustion issues iv. involvement of several components
Thermoelectric (Nikam & Hole, 2014) (Riffat & Ma, 2003) (Cuce et al., 2020)	i. small size ii. light weight iii. no moving mechanical part iv. zero noise v. good cooling capability	i. expensive ii. require electronic computer controller iii. suitable for electronic devices/chips
Pressurized gas **(CO_2 or N_2)** (Nader et al., 2019) (Ravindra & R. R. Arakerimath, 2017)	i. excellent cooling capability ii. instant cooling iii. available in bottles and small containers iv. can place anywhere in car	i. requires refilling for every next usage ii. short time duration iii. expensive iv. non-suitable for daily driven cars
Sprayer (gas) (Ma'arof et al., 2020)	i. able to enhance the cooling capacity of air to air cooling system ii. any suitable chemical can be used iii. bottle/tank can place anywhere in car	i. requires refilling for every next usage ii. short time duration iii. requires hydraulic system for pumping
Jet ejector (Galindo et al., 2019) (Konar, 2015)	i. super cooling capacity in case of high exhaust thermal power ii. high COP	i. expensive ii. complex setup iii. requires high exhaust thermal power iv. nozzle maintenance cost v. requires additional cooling system vi. involvement of several components
Absorption chiller (ammonia based) (Novella et al., 2017) (Lima et al., 2021)	i. super cooling capacity ii. high COP	i. requires waste heat recovery system ii. expensive iii. complex setup iv. requires high exhaust thermal power v. requires extra space for installation vi. involvement of several components vii. high maintenance cost viii. large size and high weight

Table 2.2: Continued

Vehicle refrigeration (S.J. Yang et al., 2019) (Roberto Cipollone et al., 2017a) (Ino et al., 2015)	i. super cooling capacity ii. high COP iii. performs at all engine speed iv. can install anywhere in engine bay v. simple installation vi. no additional cooling/hydraulic circuit requires vii. no additional weight	i. small refrigerant leak into intake air passages can cause misfires

Table 2.3: Mutlti-weight scoring model for evaluation of various intercooler systems

		Score: 0 to 10 (Low to high)							
Particulars	**Weight**	**Air to air**	**Air to liquid**	**Thermoelectric**	**One shot**	**Sprayer**	**Jet ejector**	**Absorption chiller**	**Vehicle refrigeration**
Installation	1	8	4	5	6	6	3	3	7
Market availability	1	10	6	4	7	7	2	2	3
Price	1	8	8	3	2	2	2	2	6
Cooling range	1	4	4	6	6	6	8	8	10
Instant cooling	1	0	0	8	8	8	7	8	10
Maintenance	1	8	8	3	2	2	3	2	7
System reversibility	1	0	0	0	0	0	0	7	10
Weight	1	6	7	8	6	6	5	3	8
Operation during static position	1	0	0	8	3	3	7	7	10
Operation during moving position	1	8	8	10	8	8	9	9	10
		52	**45**	**55**	**48**	**48**	**46**	**51**	**81**

Clearly, the intercoolers operating on vehicle refrigeration system scored the highest number (81), in comparison to various other listed intercoolers, based on the required features from an intercooler. Moreover, table 2.2 demonstrates its maximum distinctive features in contrast to various cooling systems. Therefore, intercoolers operating on vehicle refrigeration system is found to be best. However, the design of intercoolers utilized for that cooling system could be challengeable in various aspects based on table 1.1 and 2.1. The size of the proposed devices or systems isn't taken into account in the literature. IHEs should be small and lightweight enough to deliver the required thermal cooling while occupying the least amount of space. Moreover, despite the fact that adding a new device to the intake line can result in a pressure loss in the airflow passage that surely impact engine performance. The available designs suffer from medium to high pressure Similarly, in terms of their design sizes, the thermal capacity of the proposed devices or systems were also inadequate. In addition to that, those designs require modification in engine bays and need additional cooling circuit for their installation, which is an inappropriate. Therefore, the current study aims to present new IHE, for obtaining cold-intake air utilizing a vehicle's air conditioning system to eradicate the above cited limitations and to offer practical solution.

2.12 Heat exchangers

Irrespective of the category or design/scheme, all heat exchangers work according to the same basic principles namely, the zeroth, first, and second laws of thermodynamics which explain and govern the transfer of heat from one fluid to another (Huilgol, 2021). The design of heat exchanger is based on operating requirements and other variables depends on the requirement of work to be done. The prevailing concern of HE’s designs is to ensure maximum heat transfer while maintaining size to a minimum (Biçer et al., 2020). The material requirement should have excellent heat transfer performance, specific design factors such as package size, price, weight, available space in the vehicle engine bay, and the appropriate cooling medium selected (Xu and Grönstedt, 2010; Sedef and Bilen, 2018). Figure 2.13 illustrates the general types of HE classification according to its construction type (Bhavsar et al., 2013).

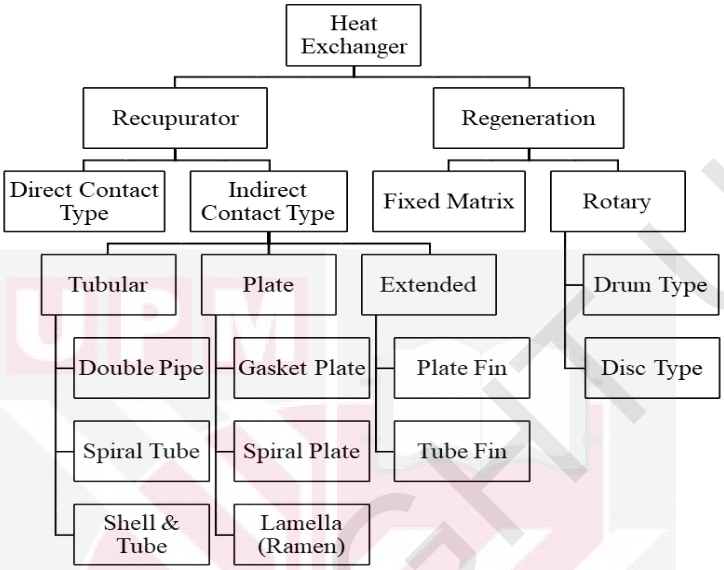

Figure 2.13: Types of heat exchanger according to construction style
(Bhavsar et al., 2013)

2.12.1 Heat exchangers utilized for cold intake air in literature

As stated earlier, about the devices and methods adopted for cold intake air systems. Most of the inventors have utilized tubular type heat exchanger designs with VAC systems in their studies, as listed in Table 2.4.

Table 2.4: Selected heat exchanger design in literature archive

Inventors / Selected heat exchanger design	Figures
(Hudelson, 2002) Tubes enclosed in housing shell. Charge air flows through the housing shell, while refrigerant flows in tube.	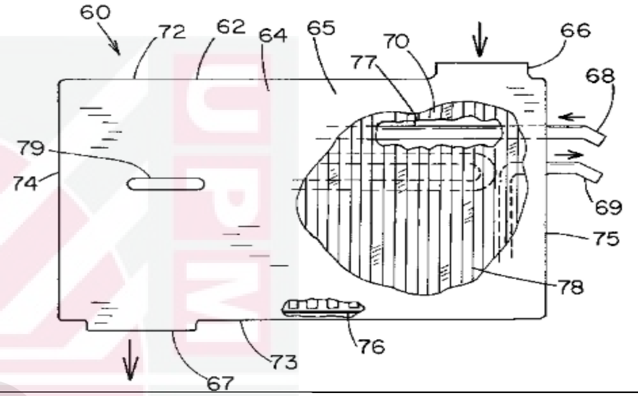
(Yi, 2008) The device consists of multiple tubes, in which tubes on the front side portion contain refrigerant medium extracted from the VAC unit and tubes on the back side contain pressurized hot air.	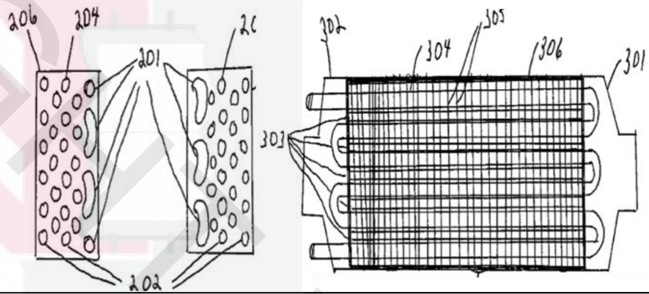

Table 2.4: Continued

(Johnson, 2010) Tubular intake air cooling duct is surrounded by an induction coil which is in contact with the air duct. The refrigerant from the VAC unit flows inside the induction coil.	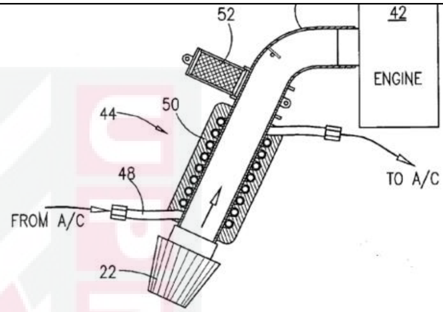
(R. Cipollone et al., 2017a) Shell and tube heat exchanger, in which charge air flows in the tubes while the refrigerant is within the shell.	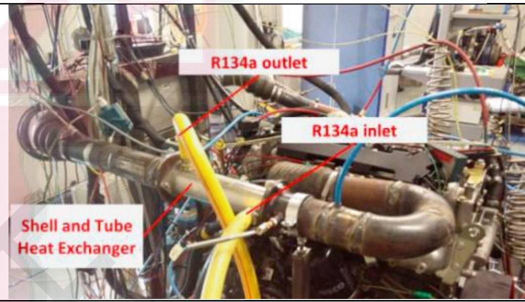
(Pshtiwan M. Sharif et al., 2019) Shell-and-tube heat exchanger with 60 tubes, counter flow, in which air flows in the tubes while the refrigerant is within the shell.	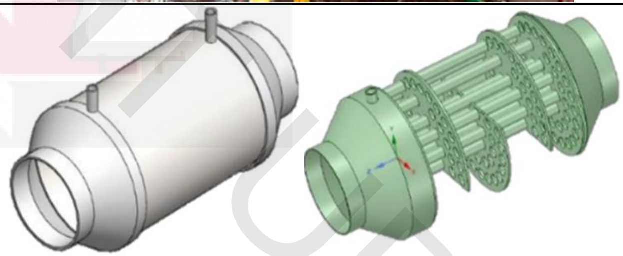

However, compared to shell-and-tube designs, plate heat exchangers (PHE) are up to five times more efficient. Because the plates provide a surface area that is significantly bigger than shell-and-tube designs that would fit in the same space, allowing for exceptionally efficient heat transfer. In addition, shell-and-tube design needs more floor space than plate heat exchangers, as the volume occupied or size of the heat exchanger is crucial for applications with limited floor space (particularly for the present study). Good quality plate-and-frame heat exchangers can work effectively without maintenance for many years and can make capacity adjustment quite simple. It is simple to add, remove, and access plates. Shell and tube units, on the other hand, have a fixed capacity at the time of installation. The least expensive option is a PHE since it has the lowest surface area and the most effective heat transfer due to its high heat transfer coefficients and pure countercurrent flow. Small size and compact designs of PHE are crucial for applications that require limited space (Alfa-Laval, 2022).

2.12.2 Lamella heat exchanger (LHE)

LHE is a kind of heat exchanger that is both compact and efficient. Typically, it is composed of a cylindrical shell enclosing a number of heat-transfer components on the inside (Shah & Sekulic, 2003). These components referred to as lamellas. The design is similar to that of a tube heat exchanger, but with thin and broad channels (lamellas) shaped like flat tubes (pairs of thin dimpled plates that have been edge welded together to form rectangular channels with a high aspect ratio), in lieu of the round tubes used in shell and tube heat exchanger (Thulukkanam, 2013), as shown in Figure 2.14.

Figure 2.14: Rectangular channels of LHE
(Kakaç et al., 2020)

The lamella's interior opening is between 3 to 10 mm (0.1 to 0.4 in.), while its wall thickness is between 1.5 to 2 mm (0.06 to 0.08 in.). On the shell side, lamellas are tightly packed to create narrow passages. To prevent leaking from the shell to the tube side or the other way around, lamellas with gaskets are placed in the end fittings. Both sides of the lamella bunch are fused with the cover of the channel, which is then welded to the inlet and outlet of nozzles from the outer ends. Thus, welding fully sealed the lamella side (Kamaruddin, 2010). In a smaller exchanger, the width of the lamellas increases from either end to the middle of the shell in order to fully consume the offered space, as shown in Figure 2.15.

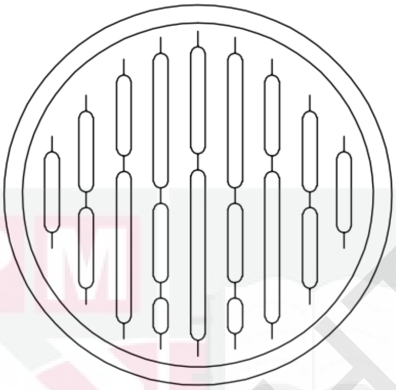

Figure 2.15: Width adjustments of lamellas
(Thulukkanam, 2013)

Baffles are not part of this heat exchanger, so one fluid (flat tube fluid) circulates inside the lamellas, while the other (shell fluid) circulates longitudinally in the gaps between them, as shown in Figure 2.16. Thus, the exchanger has just one pass, and the flow direction is usually counter-flow (Walker, 1983; Hewitt, Shires, and Bott, 1994). To accommodate thermal expansion, one end of the lamella bunch is fixed while the other is floating. Thus, this exchanger has a modified floating head. The walls of a flat tube may contain dimples where adjacent tubes have been spot-welded together. Small hydraulic diameters and the absence of leakage or bypass streams, as in a traditional shell-and-tube exchanger, are generally responsible for high heat transfer coefficients. As with corrugated plate channels, suitable point dimples boost thermal efficiency and pressure drop (H. Wu et al., 2020). Plate spacing ensures it to handle a wide range of fluids, including fibrous slurries. For same duty work, a Lamella heat exchanger weighs less than a conventional shell-and-tube heat exchanger (Kakaç et al., 2020).

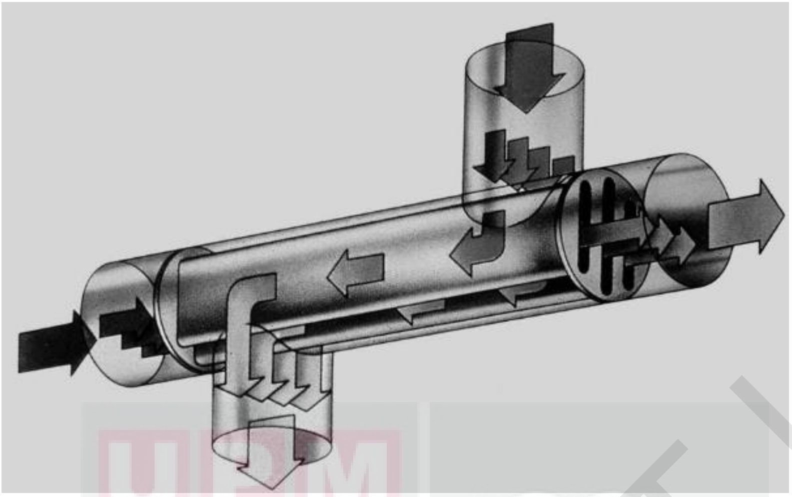

Figure 2.16: Fluid flow characterization in LHE
(Kumareswaran, 2014)

Coefficients of heat transfer for shell and tube heat exchangers are very high but are less than those of PHEs. Due to the fact that the lamella form exhibits more surface for heat transfer per unit volume than the tube shape, therefore LHEs are often more compact than conventional Shell and Tube Heat Exchangers, even when the surface area is the same (Larowski & Taylor, 1983). In contrast with the shell-and-tube exchanger, such type of exchanger is utilized for heat recovery in the chemical processing industry, paper and pulp industry, as well as other commercial applications (Ola, 2011).

2.12.3 Potential benefits of upgrading IHE

The potential benefits of upgrading the IHE are listed by several researchers (Sergienko et al., 2021; Yu et al., 2019; Z. Wang et al., 2017).

1. It helps the engine to respond more quickly to throttle input due to high denser air. This means that the car feels more responsive and lively, making it more enjoyable to drive.

2. It helps to ensure consistent performance, especially in hot weather or during extended periods of high-speed driving, due to the improved capability to handle the heat generated by the engine.

3. It helps to reduce the exhaust emissions more effectively, which ultimately is a step towards emission regulations/policy, leading to friendly and sustainable environment.

4. It helps to reduce the engines operating temperature more conclusively due to high cooling ability, which definitely extends the life of other engine

components. In other words, it improves the engine's reliability by reducing the amount of thermal stress put on various components.

5. It helps to improve the vehicle power to weight ratio, through the compact and light weight design compared to conventional heavy and bulky designs.

6. It helps to allow for a more precise control of the air-fuel ratio, promoting optimal combustion.

7. It helps to minimize the detonation and knock phenomenon more comprehensively, to enhance engine performance.

2.13 Computational fluid dynamics (CFD)

CFD can be defined as the collection of techniques that aid the computer in simulating fluid flows numerically (M. K. M. Nasution et al., 2022). The three fundamental principles that can govern the physical characteristics of any fluid are i) conservation of energy, ii) Newton's second law, and iii) conservation of mass. These fundamental laws may be used to describe any flow issue (M. M. Bhatti et al., 2020). Mathematical equations depicted the fluid behavior in the flow domain, typically in the form of partial differential equations. It is effective in examining the system's performance indicators, whether for the purpose of generating larger profit margins or boosting operational safety and in a number of other helpful characteristics (Joel H. Ferziger et al., 2020). Nowadays, CFD approaches are frequently used in various industries, including the design of cars, turbomachinery, ships, and aircraft (Zakaria et al., 2018; Mader et al., 2020). The commercially accessible CFD codes (ANSYS FLUENT, ANSYS CFX, CFD++, and STAR-CCM+) in the market are currently being used by a number of industries, engineering, and consulting firms worldwide for the simulation of fluid flow solution, heat and mass transfer problems, and combustion in aerospace applications (Sundén & Fu, 2017). The software platform codes in CFD are based on the method of finite volume discretization (Nishikawa, 2019).

2.13.1 CFD study while designing HEs

HEs are typically constructed with a variety of customizable adjustments to produce ideal heat load. Geometric characteristics (e.g., diameter, length, number of tubes, etc.) can be changed to enhance heat transfer surface area, however fluid flow has a substantial impact on performance parameters such as heat transfer rate and efficacy (Jadhav & Koli, 2014). The use of experimental and analytical approaches such as the Bell-Delaware, Logarithmic Mean Temperature Difference (LMTD), and Number of Transfer Units (NTU) method alone in the design of heat exchangers is highly complex, time-consuming, and prohibitively expensive. These techniques can be simplified by resolving the physical system to computer simulations and models, as using CFD software like ANSYS (Bhutta et al., 2012). With CFD simulations, engineers may evaluate heat exchanger systems virtually and with high-quality results without having to invest the real time, money, or resources (Skočilas & Palaziuk, 2015). Therefore, simulation offers a platform for the creation and testing of new equipment at a reasonable cost, and the quality of the findings produced by CFD is credible (Jayakumar et al., 2008).

Taylor & Sundén (2011) have enumerated a number of potential models that could be applied to the CFD analysis and have run simulations on a PHE with various corrugations to demonstrate the potential for using CFD to address a range of heat exchanger-related issues. Counter flow in a tube-in-tube helical heat exchanger was simulated by V. Kumar et al. (2006). The flow through both tubes was studied using the control volume finite difference method for a variety of known cross-sections. Gan et al. (2000) performed a CFD simulation on the tubes of a heat exchanger used in closed-wet cooling towers. It was discovered that the water to air ratio and tube configurations affected the pressure drop. Christian et al. (2019) in their publication, introduced a significant understanding of the usefulness of using a simulation platform to solve corrosion issues in a shell-and-tube heat exchanger for pre-detecting of corrosion. Christian et al. (2019) analyzed the heat transfer and flowed characteristic flow behavior for a double helical tube heat exchanger utilizing nano-fluids. The visualizing results helped to approach a better understanding of the under consideration heat exchanger. Cruz et al. (2022) conducted numerical analysis of the thermal and flow behavior of CuO-water nanofluid under turbulent regions in a shell and tube heat exchanger using ANSYS Fluent.

2.13.2 CFD process while designing PHE

Numerical studies usually begin with determining the calculation domain upon which the numerical study will be based. Selecting the calculation domain for a numerical study can occasionally result in limitations with regard to other processes that need to be selected (Y. Zhang et al., 2016). After the selection of the domain, the computational grid (Mesh) that is created for any given geometric shape depends on a number of factors, including the shape's geometry, the surrounding environment, and the computer's capabilities. In CFD solvers, there are generally four ways to form the Mesh: Automatic, Tetrahedrons, Hex Dominant, Sweep, and Multi-Zone. Most researchers have used the unstructured tetrahedron mesh due to the complex geometry of flow channels within PHEs and the presence of narrow, sloping, and curved pathways. However, some researchers like Doo et al. (2012) and Patil et al. (2013) chose to generate the mesh as a structured hexahedral grid due to the issues with mesh quality that occur when creating the computational grid at the PHE plate contact points. Vankov et al. (2016) proposed a new method for improving mesh quality by allowing a reasonable clearance between the two plates at the contact points. Furthermore, to verify the independence of the numerical study's results from the computational grid, a so-called Mesh test is usually performed, which may involve several forms. Some researchers monitored the fluids' average outlet temperature (Tiwari et al., 2014) or the heat transfer rate (zahrani et al., 2019; Gürel et al., 2020) with the grid size change. Some tracked other parameters, such as pressure drop (Jonghyeok Lee & Lee, 2015). Others tracked the change of Nusselt number (or heat transfer coefficient) and the coefficient of friction with the change in the size of the grid (Y. Zhang et al., 2016).

In the numerical analysis, the selection of boundary conditions that are applied to the calculation domain is crucial. The results are logical and credible to the extent that the conditions used are real or nearly real. Typically, flow turbulence in PHEs happens at relatively low Reynolds numbers (Re > 400) (Gherasim et al., 2011). In general, there are three fundamental ways to analyze turbulent flow using CFD solvers: DNS (Direct Numerical Simulation), LES (Large Eddy Simulation), RANS (Reynolds Averaged Navier- Stokes Simulation). While the third method (RANS) was adopted in many of the numerical studies of the PHE, for example, the turbulence model SST k–ω was used by Y. Zhang et al. (2016), W. Han et al. (2011) and Aboul Khail & Erişen (2022). The realizable k–ε model with scalable wall function was adopted by Al zahrani et al. (2020), and the standard k–ε turbulence standard wall function was adopted by Tiwari et al. (2014). Several algorithms are provided by CFD solvers to solve these partial differential equations. "SIMPLE" (Semi-Implicit Method for Pressure-Linked Equations) is one of them. For the spatial discretization, this algorithm was used to solve the pressure-velocity coupling with the second-order upwind scheme (Al zahrani et al., 2020). While C. Zhang et al. (2017) used the standard method for pressure and the second-order upwind schemes for the momentum and energy equations for spatial discretization. The issue of verifying the results is one of the most significant tasks in the numerical investigation, and it is regarded as a fundamental criterion for its success or failure. Analytical or experimental methods are generally used to validate the outcomes of numerical investigations. It is also feasible to validate the results of the numerical research by comparing them to the results of an experimental or numerical study published in the literature of the geometrical model corresponding to the geometrical model analyzed in the numerical study. Doo et al. (2012) investigated the effect of longitudinal heat conduction in PHEs quantitatively, and to verify the findings, they compared the numerical results (friction coefficient and Colburn factor) with the comparable results from previously published studies (Focke et al., 1985). Dora et al. (2020) endorsed the outcomes of his numerical analysis by comparing it (heat transfer amount) with the findings of an experimental study in the literature (Khairul et al., 2014). Aboul Khail & Erişen (2021) validated the results of a numerical research (Nusselt Number) for flow in a PHE with new plate geometry using a novel analytical method. This method is based on both LMTD and ε-NTU heat exchangers analysis methods.

2.14 Vehicle performance test

Presently, the chassis dynamometer bench seen in Figure 2.17 is almost universally used for road vehicle testing, although there are units intended specifically for forklifts and articulated off-road vehicles.

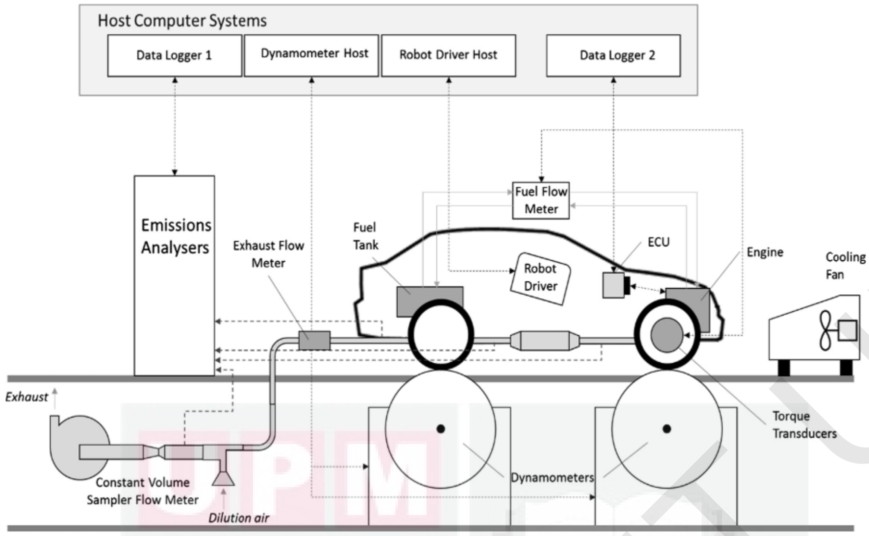

Figure 2.17: Typical Chassis dynamometer layout
(R. D. Burke et al., 2018)

The benefits of having such capabilities available to the designer and test engineer are evident; essentially, they permit the static observation and measurement of the performance of the entire vehicle while it is functioning within its full power range and, in most respects, in motion (Czaban and Szpica, 2013; Yang et al., 2018). A proper chassis dynamometer must provide a level of resistance to the torque applied to the vehicle's drive wheels in order to replicate real world driving conditions (A. J. Martyr & Plint, 2012). The three most important parameters of engine testing are described in subsections:

2.14.1 Emissions

Automobile exhaust gas regulations are becoming stricter with increasing issues of air pollution and global warming caused by traffic (Jo et al., 2019). The monitoring of exhaust emissions is a core part of vehicle-type approval (Borucka et al., 2021). Primarily, the chassis dynamometer test is usually used to measure exhaust emissions (Alcan et al., 2019; Bagheri et al., 2020). The issue with this approach is that the emission levels recorded using the specified driving mode and the emission levels measured on an actual road differ dramatically (Pelkmans and Debal, 2006; Degraeuwe and Weiss, 2017). Still, the chassis dynamometer test is used nowadays by several researchers to find exhaust emissions (Atzler et al., 2021; Gis and Taubert, 2021).

2.14.2 Engine Torque & Power

The vehicle chassis dynamometer measurement and control system refers to the measurement of the speed and torque of the driving wheels of the vehicle (X. Zhang & Zhou, 2020). The output torque is the engine rotating force delivered from the engine's crankshaft to the transmission, subsequently driving the wheels (N. N. Trushin et al., 2019). Basically, torque is a measure of the ability of an engine to do work, whereas power is the rate at which work is done (Atkins, 2009). Therefore, evaluating power and torque is a significant factor in vehicle testing. In SI units, the relationship between torque and power is (Bonnick, 2008):

$$\mathbf{P(kW) = \boldsymbol{\tau}\,(Nm) * \frac{\boldsymbol{\omega}(rpm)}{9549}} \tag{2.13}$$

Where

P = power; τ = torque; and ω = rotational velocity

2.14.3 Fuel performance

Researchers are motivated to create more efficient automobiles by the continuously rising demand for better fuel economy and consumers' concerns about the fuel consumption of their cars (Pavlovic et al., 2021). In addition, the primary auxiliary load of automobiles, which consists of air-conditioning and refrigeration systems, can use up to 25% of the total gasoline or even more in long-haul service vehicles. Therefore, measuring fuel performance is also an important factor in vehicle testing. The consumed fuel by vehicle engines may be expressed in two forms, i) fuel economy; it is the measured distance of a vehicle driving within a controlled capacity of fuel, ii) fuel consumption; it is the measured amount of fuel used to drive the vehicle within a controlled distance.

2.15 Summary

Prior research has shown that reducing air intake temperature dramatically increases combustion stability and efficiency while also lowering exhaust pollutants. Heat exchangers, often known as intercoolers, are frequently installed in supercharged and turbocharged engines to supply cool air to the engine intake. The literature database contains a lot of information about obtaining cold intake air through various mediums and techniques; nonetheless, a few gaps have been identified:

1. Conventional intercoolers (air to air or air to water) are the most widely used intercoolers only for charged engines, where very high temperature and pressure operate, and their performance is dependent on ambient conditions (temperature and humidity of the air). Eventually, they cannot reduce the intake temperature below ambient conditions and performs very deprived at low engine speed and vehicle static position due to less amount of ambient air

passing through intercooler. In the case of naturally aspirated engines, they were found to be non-functional, where ambient conditions are directly related to air intake charge.

2. In order to meet the gap mentioned above, inventors operated their designed intercoolers with the VAC system due to its higher cooling capacity. However, their designs are mostly for charged engines, and their devices and method require modification in engine bays and can only be installed while designing new vehicles, where the availability of space in the engine is not an issue to install the new intercooler and method. The reason behind this argument is that they did not consider the available space in existing vehicle engine bays to install it as an after-market product by neglecting their design sizes. In terms of size, the volume occupied by each component is critical in automotive design. Intercooler heat exchangers should be lightweight and compact enough to provide the necessary thermal cooling while consuming the least space.

3. The available designs in the literature engenders medium to high pressure loss in air flow passage, due to the addition of a new device on the intake line, which surely can affect the engine performance. Further few inventors did not consider this parameter while designing their cooling devices.

4. The thermal capability compared to their design sizes is also questionable (low to medium). Moreover, only few investigators have considered the engine speed in their studies, and the selected range was 1000 to 3000 rpm. The higher range of rpm was also overlooked in the literature.

5. Last but not least, most of the experiments were performed in labs on test beds, with their designed intercoolers, where available space and size of the intercooler are not an issue. However, this method differs from the actual scenario, where the performance of the vehicle needs to be tested in real-time, with the actual installation of intercoolers in existing engine bays.

So there is a need to develop a new IHE that would be suitable and qualified for working with much possible amount of existing engines while considering the above-stated neglected parameters.

CHAPTER 3

METHODOLOGY

3.1 Introduction

This chapter discusses the details of the methodology that provided a way to systematically solve the research problem and describes the various steps adopted along with the logic behind them to fulfill the aims and objectives of the present study. This research work concerned about designing and fabricating a novel IHE device and a technique that can provide cold intake air utilizing the vehicle air conditioning system as a coolant medium. The IHE was developed for a particular test vehicle (Proton–Wira) 1.5L SI-engine four-stroke gasoline-fueled, by keeping in mind the actual installation of fabricated IHE model in test vehicle for the experimental purpose to discover the performance of newly designed IHE as well as the impact of cold intake air on the test vehicle engine. The methodology employed for the said work was divided into three sections.

The first section involved a numerical investigation of the initially proposed/selected designs of the Lamella heat exchanger for the present study, based on the minimum inside openings of the lamellas. The outer dimensions of the LHE were adopted from the previous in-house designed EIHE (Pshtiwan M. Sharif et al., 2019), having the same purpose and boundary conditions. That technique not only helped to understand the behavior response of LHE geometry but also to compare it with the already existing competitive model of the same size. Afterward, according to the actual space available on the intake manifold in the test vehicle, the outer dimensions of LHE were finalized, and the best-suited internal geometry was adopted based on the initial numerical investigation. The final selected size and geometry were again numerically investigated to check its thermal performance. The following section involved a fabrication of the LHE, followed by the leakage tests to find any minute leakage in a fabricated model, as both fluids involved in heat transfer were gases (air & refrigerant). Further, the laboratory testing was executed at UPM thermodynamics laboratory, for verification and validation purposes with the numerical results before proceeding to installation in a test vehicle. The last section involved the installation of LHE in the test vehicle with the VAC system. Applied vehicle tests based on the vehicle status (running or static) were conducted at UniKL MFI, with the help of a chassis dynamometer test bench to observe the performance of LHE and the influence of cold air on engine performance (power, torque, fuel consumption, emissions). Three stages of the test (Normal, AC, LHE+AC) helped to understand the engine response in different scenarios. The overall research methodology in this study is simplified, as shown in Figure 3.1.

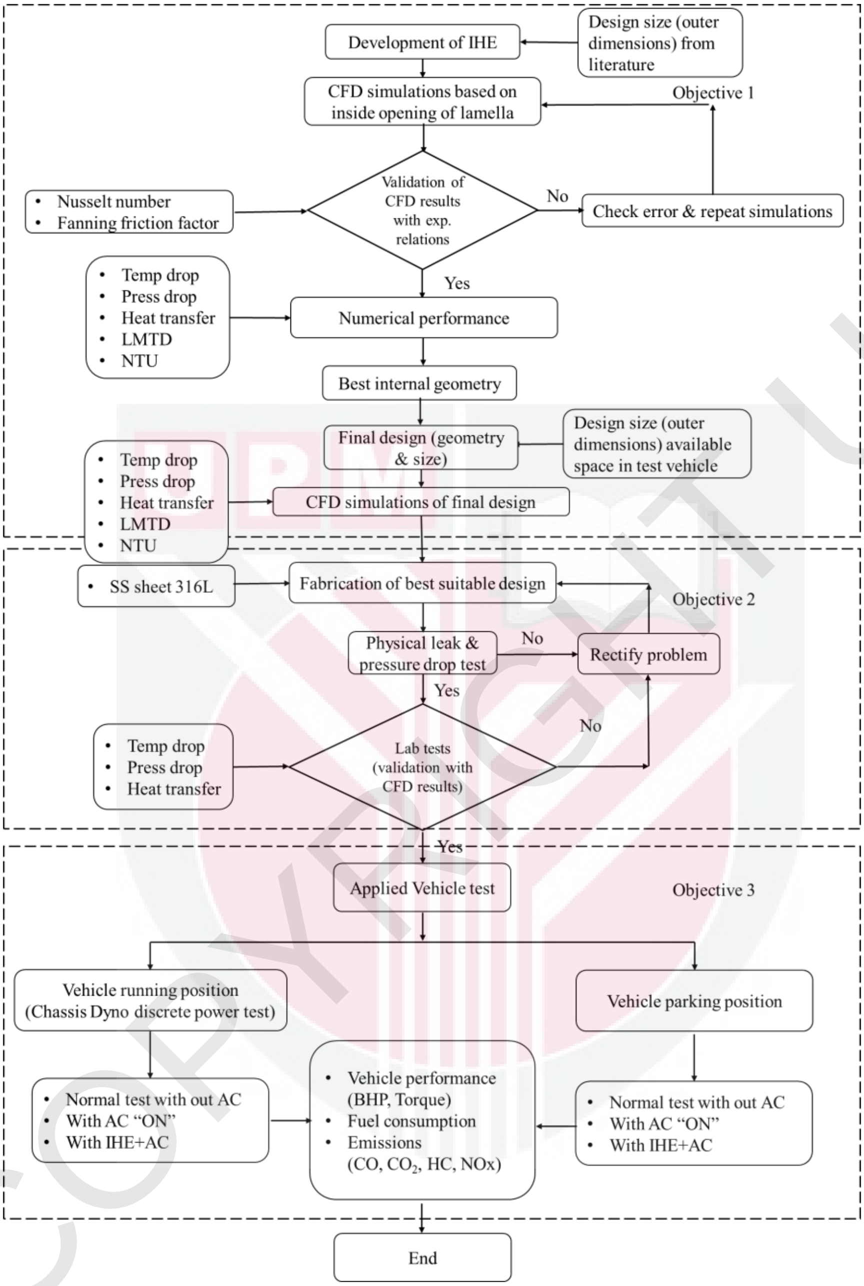

Figure 3.1: Overall schematic flowchart of the methodology with objectives

3.2 Design control parameters

This section defines the design criteria of the Lamella heat exchanger. On what basis the size of geometry was designed, and why? Millions of vehicles have been manufactured till now, and the volume of vehicle production and sales is continuously rising, and forecasts confirm this trend for the next several years (Schenk & Clausen, 2021). It is due to an increase in urbanization (Nithya & Miniyadan, 2021). As it is already briefed in the previous chapter that road transport was a significant source of air pollution and greenhouse gas emissions (Seo et al., 2020). Modern and new vehicles are trying to follow the restrictions applied by authorities on emissions. However, what about the bunch of already existing vehicles on the roads? There is a need to control their emissions as well. In this regard, a lamella heat exchanger was designed for existing vehicles that could be installed as an aftermarket product. It could also be designed for new vehicles as well, but for the present study, it was limited to the existing vehicle.

3.2.1 For existing vehicles

As LHE in this study operates as an intercooler which is usually mounted on the air intake line. For charged engines, there is a proper place for an intercooler, as an intercooler is a necessary part of charged engines and is usually placed in front of the car radiator, as shown in Figure 3.2. However, for naturally aspirated engines, the intercooler is less common and doesn't have any proper place for it, and this study has been done over a naturally aspirated engine. Thus, only some extra space available in the engine bay, as shown in Figure 3.3, was the design size control parameter of LHE. That space availability was directly related to the size of the intercooler (dimensions of shell box).

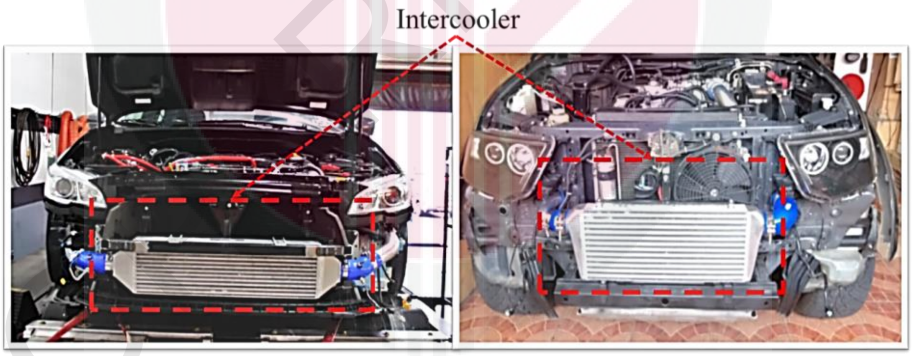

Figure 3.2: Placement of conventional intercooler in vehicle

Available space

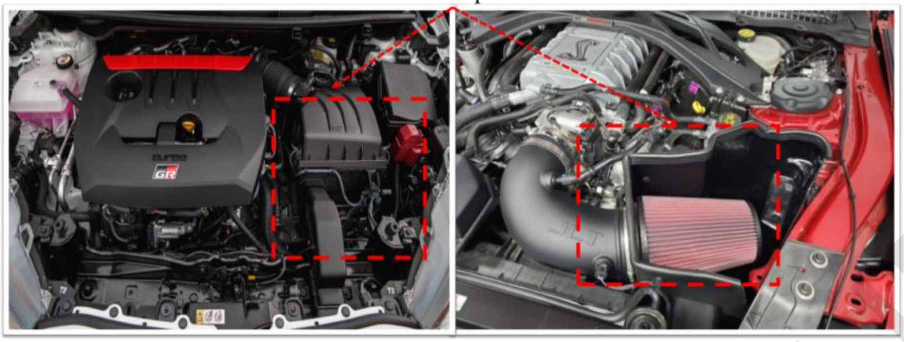

Figure 3.3: Possible space available for intercooler installation

3.2.2 For new vehicles

The volume occupied by any component in engine bays is a very critical aspect. However, any component can be added or removed easily while designing and manufacturing new vehicles. The design criteria for the new vehicles is the thermal (cooling) performance required to perform by the intercooler can be utilized for free LHE size using heat transfer and NTU pressure drop method, where the LHE scale size can be affordable with no attention to vehicle engine bay available space. The same procedure for design control parameters of IHE was also summarized by Pshtiwan M. Sharif et al., (2019) in his study, presented in Figure 3.4. The framework design demonstrates that designers have multiple options available to them for selecting the most effective IHE design approach, and also introduce the fastest way to select the correct option for the IHE design, suitable and affordable for any selected vehicle.

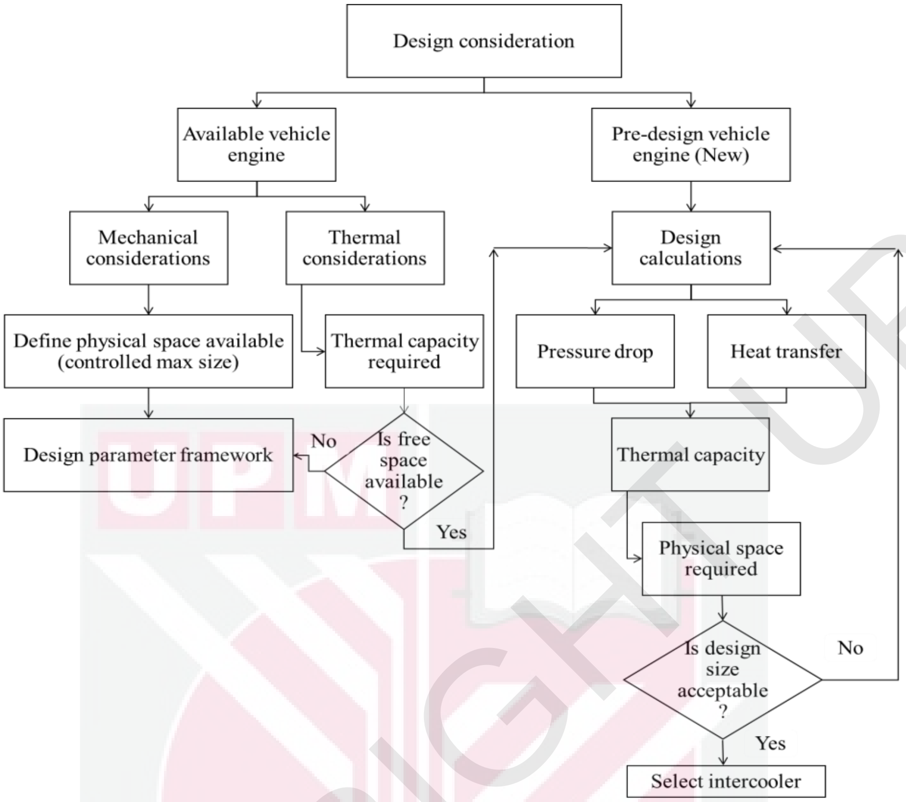

Figure 3.4: Design control parameters of IHE for new and existing vehicles (Pshtiwan M. Sharif et al., 2019)

3.3 Design of LHE

The design of LHE for the present study was dependent on the available space in existing engine bay, as it was directly related to the size of the shell box together with fitting covers. By omitting the fitting covers, the length of the shell box determined the length of the lamella, as both were equal in dimensions. In contrast, the shell box's width regulated the header plate's width, and the inside opening of lamellas decided the number of lamella channels inside the shell box. Similarly, the height and width of the shell box determined the size of the header plate, and the height of the header plates decided the height of lamella (h_l) by excluding the parting height (b). Further, the diameter of the intake manifold decided the opening diameter of fitting covers. Figure 3.5 shows the schematics of the LHE model along with their dimensions.

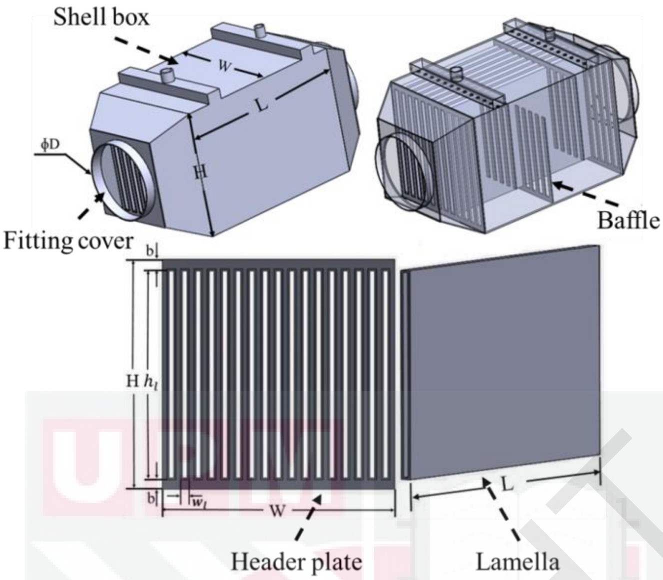

Figure 3.5: Design configuration of LHE

In addition to the conventional LHE, three equally spaced baffle plates having 25% baffle cut, were provided to serve two purposes: support the lamellas for structural rigidity and divert the flow across heat transfer components to obtain a high heat transfer coefficient. The coolant medium's main inlet and outlet points were further divided into multiple inlet and outlet openings to distribute the refrigerant between lamellas equally. The rectangular tube side was selected for chilling the air, as shown in Figure 3.6, referring toward future technical maintenance issues, ease of fouling tube surface cleaning, and lower influence of pressure drop as compared to the shell domain.

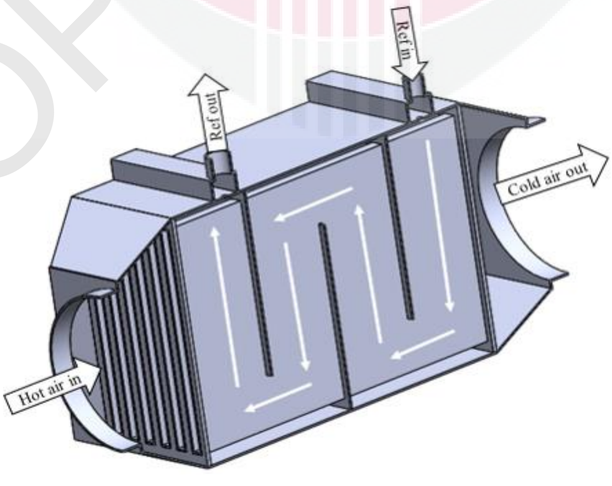

Figure 3.6: Flow arrangement in LHE

Nevertheless, the maximum allowable pressure drop inside LHE should not exceed 5% (Pshtiwan Mohammad Sharif, 2021), as all the benefit of getting cold intake air can mitigate due to high pressure loss by restricting airflow (Mamat et al., 2009). Therefore, a cooling system having a low-pressure drop is very important to maximize the mass of the drawn air into the cylinder (Gocmen & Soyhan, 2020). Further, the inside openings/width of lamella were assumed to be based on the possible range elucidated by Kamaruddin, (2010) and Thulukkanam, (2013) for lamella i.e. 3mm to 10mm, as the width of the lamella plates is an important factor in determining the overall heat transfer area and, consequently, the efficiency of the heat exchanger. Therefore, the inside openings were typically engineered to meet the unique requirement of the heat exchanger (for the present study) i.e. augmentation of heat transfer and reduction in pressure drop. The selection of LHE internal geometry was summarized in Figure 3.7.

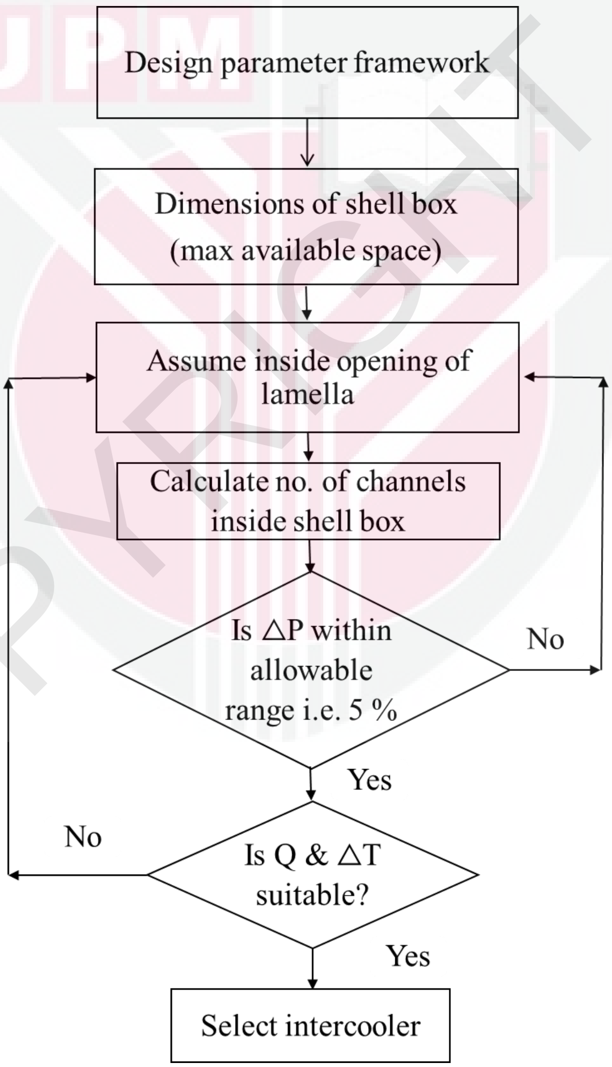

Figure 3.7: Assortment of LHE internal geometry

3.4 Computational fluid dynamics (CFD)

The intention of adopting the CFD technique while designing the LHE for this study was that; during the design phase, CFD provides a cost-effective alternative to trial-and-error methods and allows designers to examine "what-if" possibilities. It also has a great potential to save time and measure all desired quantities at once in the design process and is, therefore, cheaper and faster compared to conventional testing for data acquisition (Jayanti, 2018). ANSYS FLUENT was adopted for numerical inquiry in the present work since Fluent software has the extensive physical modeling capabilities required to model flow, turbulence, heat exchange, and processes for industrial applications. Fluent provides highly scalable high-performance computing (HPC) to assist complex and large-model CFD simulations expeditiously and cost-effectively.

3.4.1 Governing Equations

The CFD method is a numerical solution platform based on the mathematical fundamental governing equations in fluid dynamics analysis, namely used with the continuity, momentum, energy, turbulence model and state equations (Ikhtiar et al., 2016; Arani and Moradi, 2019), are listed related to present study as:

Incompressible steady-state continuity equation (F. Torabi, 2022).

$$\frac{\partial u}{\partial x}+\frac{\partial v}{\partial y}+\frac{\partial w}{\partial z}=0 \quad 3.1$$

X,Y,Z-momentum equations (Jain et al., 2017) respectively.

$$\frac{\partial u}{\partial t}+u\frac{\partial u}{\partial x}+v\frac{\partial u}{\partial y}+w\frac{\partial u}{\partial z}=-\frac{1}{\rho}\frac{\partial p}{\partial x}+v\left(\frac{\partial^2 u}{\partial x^2}+\frac{\partial^2 u}{\partial y^2}+\frac{\partial^2 u}{\partial z^2}\right)+f_x \quad 3.2$$

$$\frac{\partial v}{\partial t}+u\frac{\partial v}{\partial x}+v\frac{\partial v}{\partial y}+w\frac{\partial v}{\partial z}=-\frac{1}{\rho}\frac{\partial p}{\partial x}+v\left(\frac{\partial^2 v}{\partial x^2}+\frac{\partial^2 v}{\partial y^2}+\frac{\partial^2 v}{\partial z^2}\right)+f_y \quad 3.3$$

$$\frac{\partial w}{\partial t}+u\frac{\partial w}{\partial x}+v\frac{\partial w}{\partial y}+w\frac{\partial w}{\partial z}=-\frac{1}{\rho}\frac{\partial p}{\partial z}+v\left(\frac{\partial^2 w}{\partial x^2}+\frac{\partial^2 w}{\partial y^2}+\frac{\partial^2 w}{\partial z^2}\right)+f_z \quad 3.4$$

Energy Conservation equation (Miansari et al., 2020).

$$\rho C_p\left(\frac{\partial T}{\partial t}+u\frac{\partial T}{\partial x}+v\frac{\partial T}{\partial y}+w\frac{\partial T}{\partial z}\right)=k\left(\frac{\partial^2 T}{\partial x^2}+\frac{\partial^2 T}{\partial y^2}+\frac{\partial^2 T}{\partial z^2}\right)+\phi \quad 3.5$$

Turbulent kinetic energy (k) (J. Blazek, 2015).

$$\frac{\partial}{\partial t}(\rho k)+\frac{\partial}{\partial x_i}(\rho k u_i)=\frac{\partial}{\partial x_j}\left[\left(\mu+\frac{\mu_t}{\sigma_k}\right)\frac{\partial k}{\partial x_j}\right]+G_k+G_b-\rho\epsilon-Y_M+S_k \qquad 3.6$$

Rate of dissipation (ε) (Kalkan, 2014).

$$\frac{\partial}{\partial t}(\rho\epsilon)+\frac{\partial}{\partial x_i}(\rho\epsilon u_i)=\frac{\partial}{\partial x_j}\left[\left(\mu+\frac{\mu_t}{\sigma_\epsilon}\right)\frac{\partial \epsilon}{\partial x_j}\right]+C_{1\epsilon}\frac{\epsilon}{k}(G_k+C_{3\epsilon}G_b)-C_{2\epsilon}\rho\frac{\epsilon^2}{k}+S_\epsilon \qquad 3.7$$

Where; ϕ is the dissipation function of the energy equation, $C_{1\epsilon}$, $C_{2\epsilon}$, $C_{3\epsilon}$ are constants, $\sigma_k$and σ_ϵ are turbulent Prandtl numbers, G_k and G_b represents the generation of turbulence kinetic energy due mean velocity gradient and buoyancy respectively.

Equation of state (Cushman-Roisin & Beckers, 2011).

$$P=P(\rho,T) \text{ and } i=i(\rho,T) \qquad 3.8$$

$$P=\rho RT \text{ and } \text{i}=C_V T \qquad 3.9$$

The aforementioned equations are based on conservation laws (the mother of all the problems in fluid dynamics), which are precisely defined by Sharma (2021) in Figure 3.8 for a fixed elemental control volume-based Eulerian technique in fluid dynamics, assuming that the work done is equal to zero.

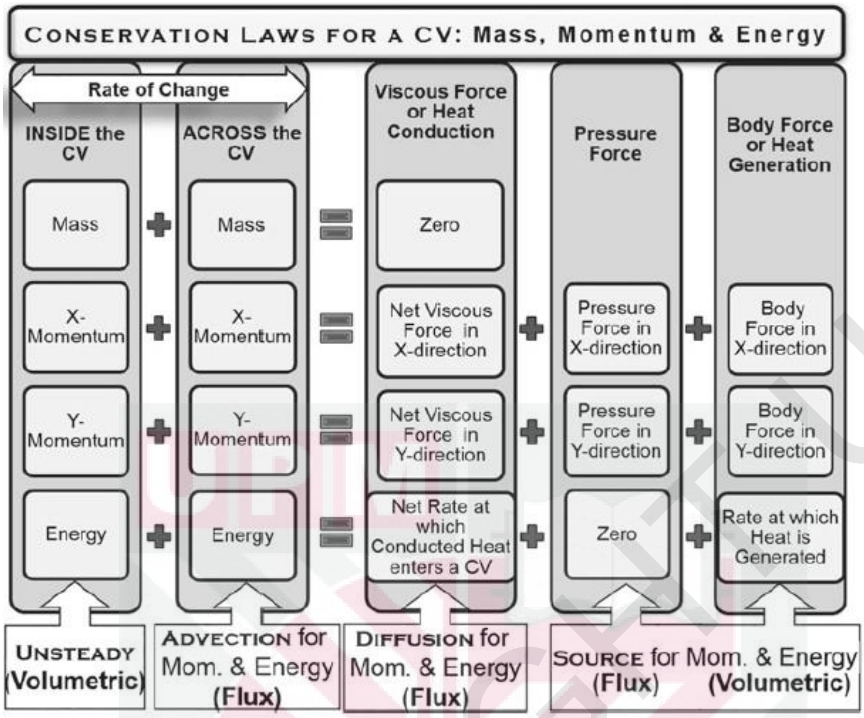

Figure 3.8: A schematic representation of conservation laws, used in fluid dynamics as well as heat transfer, customized for CFD
(Sharma, 2021)

3.4.2 Initial proposed designs for CFD

As the present study is for an existing vehicle i.e., 1.5L naturally aspirated engine, therefore only some extra space available in the engine bay was the design size control parameter of LHE. Pshtiwan M. Sharif et al. (2019), presented an evaporative intercooler heat exchanger (EIHE) operated with a VAC system for a 1.5L naturally aspirated engine while considering the space available in engine bays for its installation. Shell and tube heat exchanger was proposed as EIHE, with multi-tube straight one pass, counter flow. CFD simulations were performed to check the temperature drop by the proposed design at low rpm ranging from 500 to 2000. A selected design geometry of 60 bunches of tubes with a 7.53 mm inner diameter and 150 mm long were placed in the 120 mm diameter of the shell. The total length, excluding fitting covers, was 170 mm, as shown in Figure 3.9.

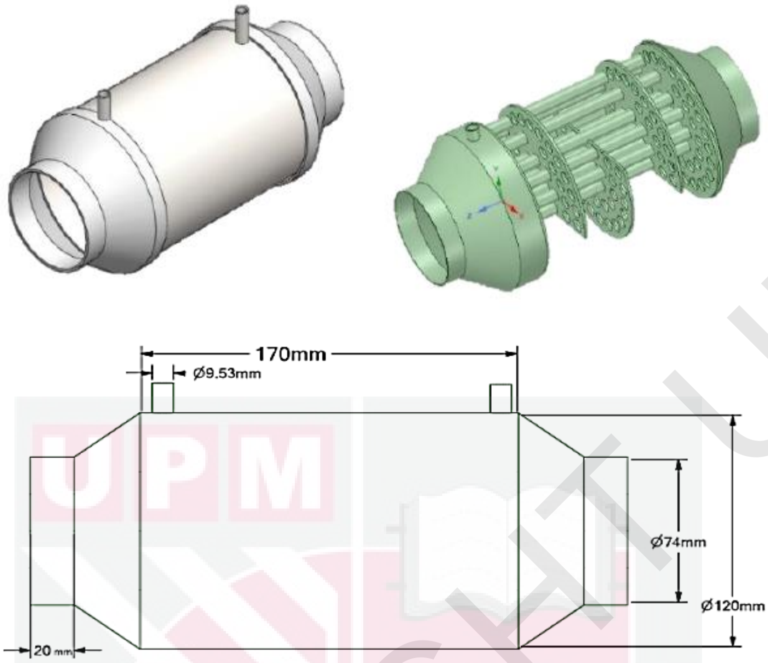

Figure 3.9: Geometry and dimensions of shell and tube heat exchanger
(Pshtiwan M. Sharif et al., 2019)

Initially, the same geometry scale size (dimensions of shell box i.e. H*W*L) was picked for the proposed designs of LHE, as of (Pshtiwan M. Sharif et al., 2019) shown in Figure 3.10, and adopted the shell and tube model as a reference model due to having the same boundary conditions. This helped to check and compare the performance of different LHE geometries along with the reference model.

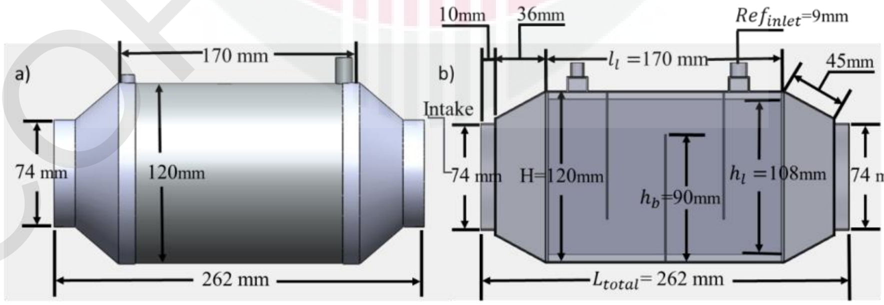

Figure 3.10: Dimensions of shell box a) reference model (Pshtiwan M. Sharif et al., 2019), and b) initially proposed models

Table 3.1 provides the details of the initially proposed geometries. At first, four models of LHE were proposed based on the minimum inside opening/width of lamellas defined by Kakaç et al. (2020), and accordingly, the number of lamellas inside the shell box was calculated from Equation 3.10.

$$N_p = \frac{W}{t + w} \qquad 3.10$$

Where, W; width of shell box, w; width of lamella, t; thickness of lamella material. The reason behind the selection of the minimum (smaller) inside opening/width of lamellas was that the heat transfer increases with the increment in heat transfer components (tube or lamella) in shell box (Merdan & Kadhim, 2021). The lesser the width of lamella, the more number of lamellas can accommodate in confined shell box space, according to equation 3.10. This ultimately increases the heat transfer surface area, which is directly proportional to the rate of heat transfer (Pant et al., 2021). Further, the minimum inside opening of lamella tends to increase the velocity of air inside lamella to meet the required quantum of air for engine, which subsequently leads to higher heat transfer rate and mitigation of the fouling phenomenon. The aspect ratio of each model was calculated between height to width of the lamella (Thulukkanam, 2013). Stainless steel (316L) metal of 1mm thickness, was selected as a material for LHE.

Table 3.1: Details of initially proposed designs

Models	Shell box H * W * L (mm)	Lamella h_l * w_l * l_l (mm)	No. of lamellas for airflow	Aspect ratio h_l /w_l
Model A	120 * 125 * 170	108 * 5 * 170	10	21.6
Model B	120 * 124 * 170	108 * 4 * 170	12	27
Model C	120 * 123 * 170	108 * 3 * 170	15	36
Model D	120 * 121.5 * 170	108 * 2.5* 170	17	43.2

3.4.3 CFD process of initial prosed designs

For simulations, three different engine speeds were selected, i.e., RPM 4000, 5000 & 6000, as the amount of intake air required by the engine (first entered the LHE for the cooling process) was dependent on engine speed (RPM) and calculated using the mass flow rate equation (I. Tosun, 2007) according to the respective volume flow rate (Murad, 2009).

$$\dot{m}_a = \rho_a \,.\, Q_a \qquad 3.11$$

$$Q_a = \frac{0.5\, RPM \,.\, V \,.\, \eta_v}{60000} \qquad 3.12$$

Where,

V; engine size in liters

η_v; volumetric efficiency i.e., 0.8 for naturally aspirated engine

RPM; engine speed

ρ_a; density of air in kg/m^3

The temperature of the intake air was taken as 45℃ (318.15 K), as the standard intake air temperature ranges from 30-70℃, depending on external air conditions, vehicle speed, engine load, and dedicated radiator location in the engine compartment (Davide Di Battista et al., 2018). The demonstration of the simulation structure is presented in Figure 3.11.

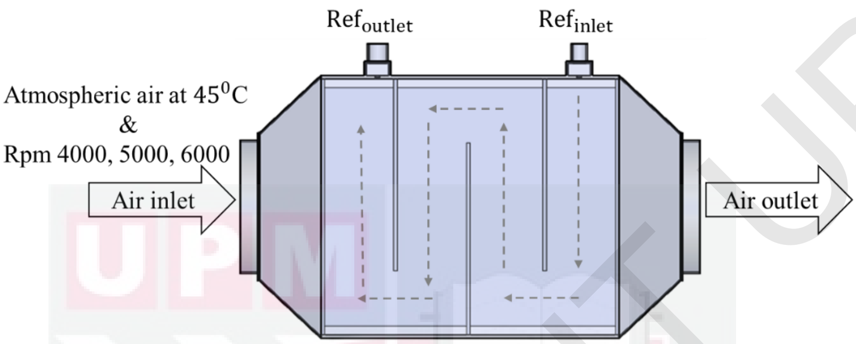

Figure 3.11: Physical appearance of the simulations

CFD process overall is a three (3) step process (Roychowdhury, 2020).

1. Pre-Processing

This step further consists/comprises of three sections, which include a) modeling of geometry to specify the domain of interest, b) mesh generation, and c) setting the boundary conditions.

a) Modelling of geometry

Geometries of LHE (model A, B, C, and D), as shown in Figure 3.12, were drawn using the ANSYS (SCDM), as it is a new way to manipulate CAD models. The model becomes entirely dynamic as a result, enabling the user to move, stretch, add, and remove objects using mouse motions. Additionally, the CAD model is updated in real-time on the screen, giving designers immediate feedback (Adair et al., 2014). This was the reason to utilize this particular tool for geometry creation. An important thing to mention here was that the portion of geometry in which lamellas interacted with refrigerant was selected for numerical study, excluding fitting cups, to save simulation time. Therefore, that particular portion was generated using ANSYS (SCDM). Another design tool offered by ANSYS was named as ANSYS Design Modeler, principally designed to provide powerful CAD-neutral capabilities to users of the entire suite of ANSYS (Ilnicki & Rzasa, 2018).

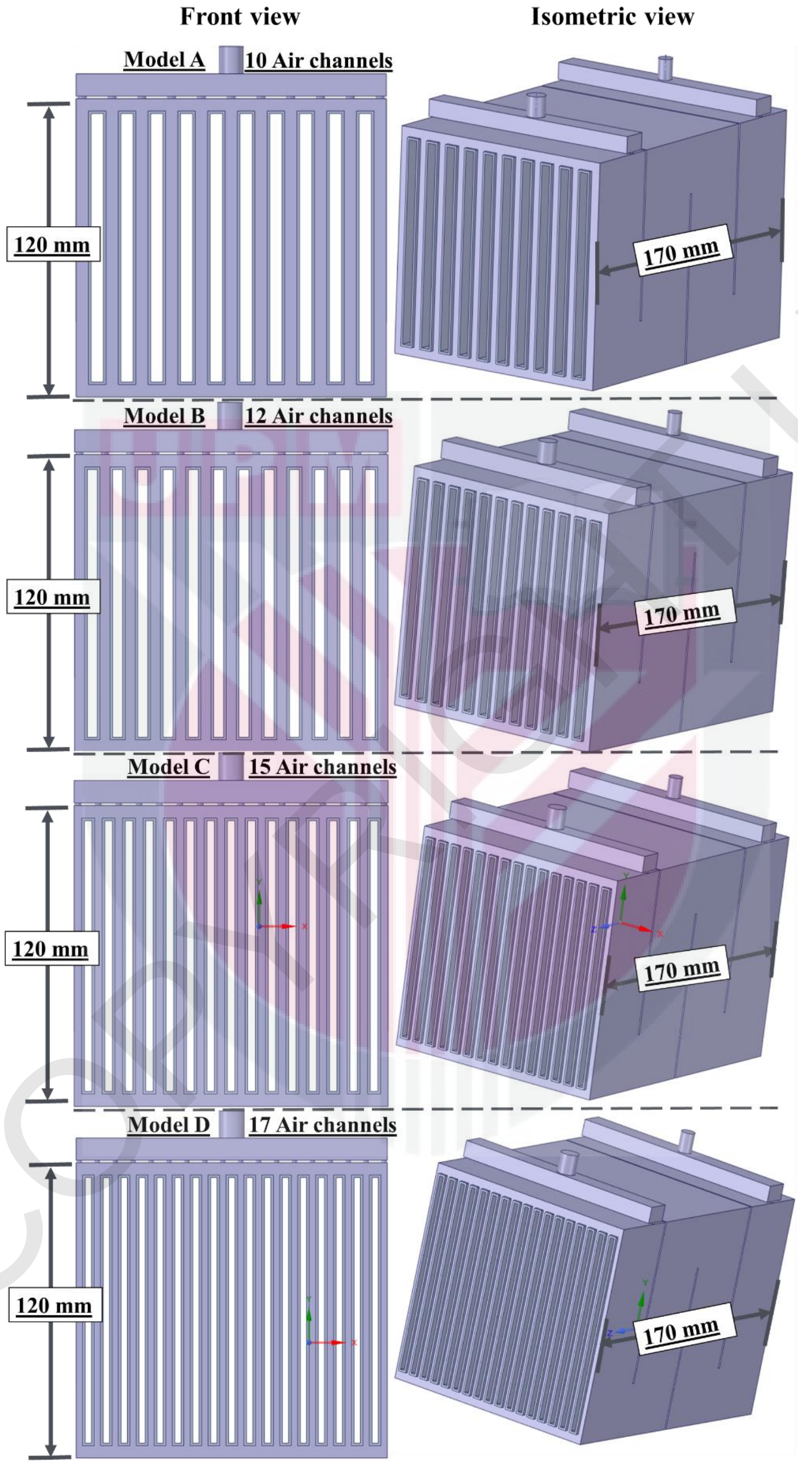

Figure 3.12: Formation of LHE models using ANSYS SCDM

b) Mesh generation

The latest advanced ANSYS platform software version models introduced significant enhancement in the meshing process for better quality and accuracy in the solution process by reducing the size of volume control size and shape using a better volume size technique by the platform application (Nakasone et al., 2006). The geometry of LHE consisted of two domains. One was for the refrigerant flow domain, and the other was for the air flow domain. For the present study, air cooling inside lamella flat tubes was the focus area; thus airflow domain needed finer and denser mesh to capture the heat transfer. Therefore, a structured mesh was implemented in a way to provide finer node distribution within lamellas. However, the unstructured mesh was generated for the refrigerant flow domain due to some complex geometry configuration, as shown in Figure 3.13. The minimum cell size, number of nodes, number of elements, average skewness, average aspect ratio, and average orthogonal quality of the respective models are given in Table 3.2.

Table 3.2: Mesh details of the initially proposed geometries and reference model

Models	Minimum cell size (mm)	No. of nodes	No. of elements	Avg. skewness	Avg. aspect ratio	Avg. orthogonal quality
Model A	1	1,999,890	1,727,943	0.062	1.22	0.93
Model B	1	2,147,590	1,789,239	0.108	1.26	0.92
Model C	1	2,398,910	1,925,956	0.069	1.24	0.93
Model D	1	2,725,358	2,214,827	0.075	1.34	0.92
Ref Model	2	1,468,658	5,399,148	0.21	1.85	0.80

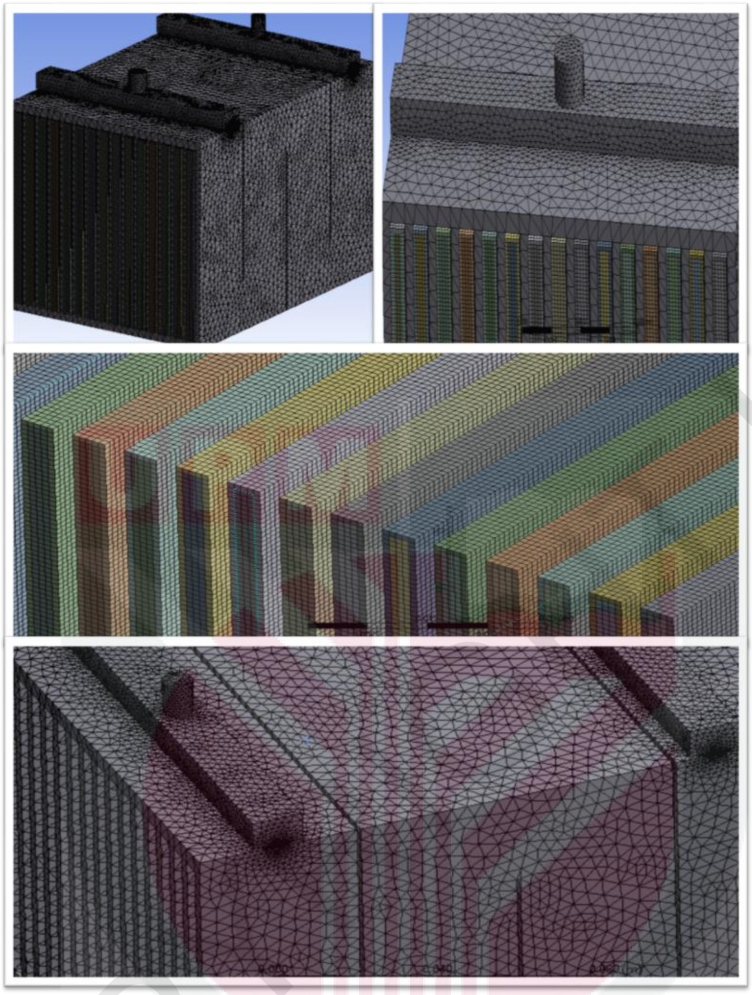

Figure 3.13: Mesh overview

c) Boundary Conditions

After mesh generation, boundary conditions are the most critical step in the CFD process. It is only possible to get the right solution once the settlement of the accurate boundary conditions (Hinch, 2020)**,** which should resemble the most realistic scenario. As fluid flow was involved in this research work, there was a need to define the proper inlet and outlet sections of air and refrigerant. According to the problem under consideration, four boundary conditions presented in Figure 3.14 was applied to geometry i.e.

- Air inlet: from where hot air enters the LHE
- Air outlet: from where cold air leaves the LHE

- Ref inlet: from where refrigerant enters the shell side of LHE
- Ref outlet: from where refrigerant leaves the shell side of LHE

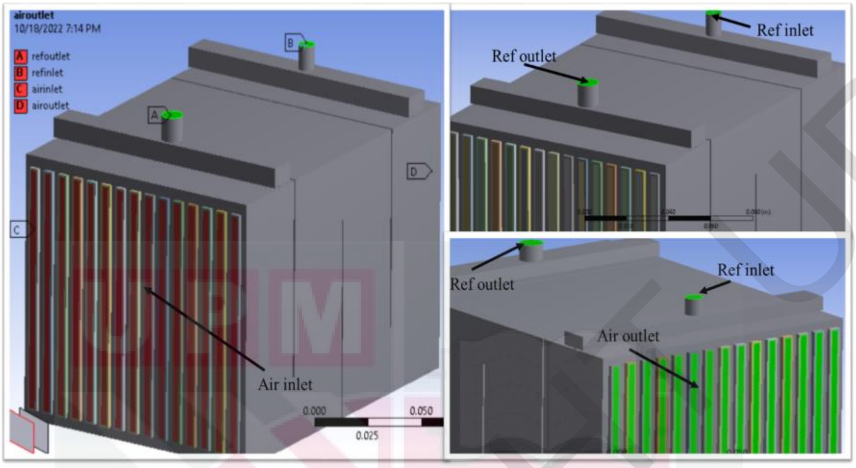

Figure 3.14: Boundary conditions

2. Solver:

Once the problem was set up (defining the boundary conditions), a solver was required to find the solution. Star-CD and Star CCM+ (CD-Adapco), FLUENT and CFX (ANSYS, Inc), GASP (Aerosoft, Inc), CFD++ (Metacomp Technologies), etc. are some of the widely used commercial software as a solver. Solving the equations at each probe point defined during the mesh generation process is possible with such software, and additional models can be added if necessary by the physics. The numerical approaches are also defined at this stage. The solver settings made in this study were as follows by adopting ANSYS FLUENT:

- The three-dimensional, transient, incompressible, and turbulent flow was assumed. Although the air was a compressible fluid, the velocities of air inside lamellas were low; subsequently, the Mach number was less than 0.3 for all the cases under consideration. Therefore, the compressibility effects were negligible, and the variation of the gas density with pressure could safely be ignored in flow modeling (Ansys, 2009) and assumed as incompressible flow.
- Pressure-based segregated solvers were employed to solve single-phase forced convection heat transfer.
- Energy equation was "ON" due to heat transfer involved in the problem.
- Standard k-ε turbulence with a standard wall function model was used as the turbulence model.

- Mass flow inlet type condition selected for Air inlet boundary condition.

- Pressure outlet was selected for both air and refrigerant outlet boundary condition.

- Both gases (air and refrigerant) involved in the problem were considered ideal gases.

- The specific heat capacity of gases was a function of temperature.

- Interfaces of hot and cold sides were thermally coupled.

- No slip boundary condition was used inside lamella walls.

- The Navier–Stokes, and energy equations were solved using the semi-implicit method for pressure-linked equations (SIMPLE) for given boundary conditions.

- A second-order upwind scheme was used for momentum and energy equations.

- For x, y, z velocity components, continuity, k, epsilon, and energy equations, the residual monitors were set to 10^{-6}.

- For airflow inside lamellas, the reference pressure was considered 1×10^{5} Pa.

- "Least squares cell based" was selected as Gradient.

- "First order implicit" was selected as a transient formulation.

- Time step size was taken as 0.5s.

3. Post-processing:

The results from CFD were visualized through post-processing software, i.e., ANSYS CFD-Post, closely related to pre-processing and simulation software (Berger & Cristie, 2015). It was a vital step to accurately derive the correct conclusions from the models under consideration. Tecplot 360, EnSight, FieldView, and ParaView software's can also be utilized for post-processing. The above-stated CFD process has been summarized in Figure 3.15 using Ansys Fluent.

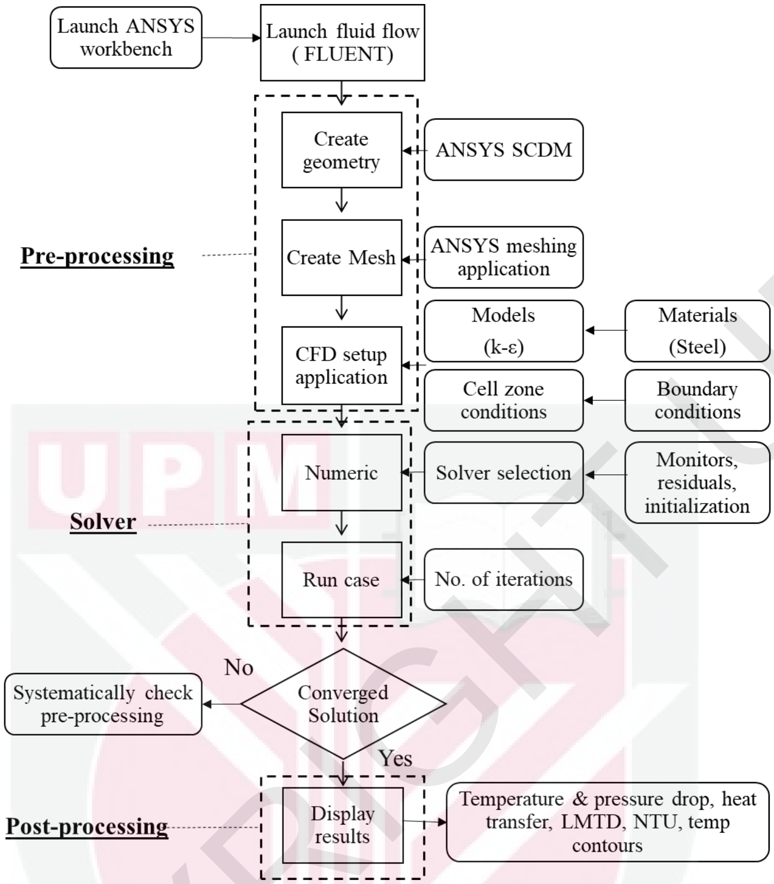

Figure 3.15: Summary of CFD process

3.4.4 Final design size and geometry

As described earlier, the main parameter that controlled the size of LHE was the available space to install the newly designed intercooler with the engine intake air manifold line in the existing vehicle engine bay. The selected test vehicle specification for the present study is given in Table 3.3. The available space in the selected test vehicle engine bay was directly related to finalizing the outer dimensions of the shell box (LHE). Subsequently, the dimension of the shell box was the controlled parameter that organized the number of rectangular channels/lamellas and their length. In this regard, the maximum space available in the selected test vehicle engine bay was measured, as shown in Figure 3.16, and accordingly, the outer size of LHE was finalized.

Table 3.3: Test vehicle mechanical specifications

Parameters	Specifications
Vehicle Model	2004, Proton Wira CE
Bodyweight	1080 kg
Engine size	1.5 liter, 1468 cm3
Engine cylinders	4 in-line
Compression ratio	9.2:1
Power Torque	126 Nm (93 ft·lb)(12.8 kg.m) at 3000 RPM
Maximum power	89 PS (88 bhp) (66 kW) at 6000 RPM
Fuel system	MPFi
Fuel consumption	(5.5 - 7.2) L/100 km
Drive wheels - Traction - Drivetrain	FWD
Transmission type	Auto
Engine manufacturer	Mitsubishi
BMEP (brake mean effective pressure)	1078.6 kPa (156.4 psi)

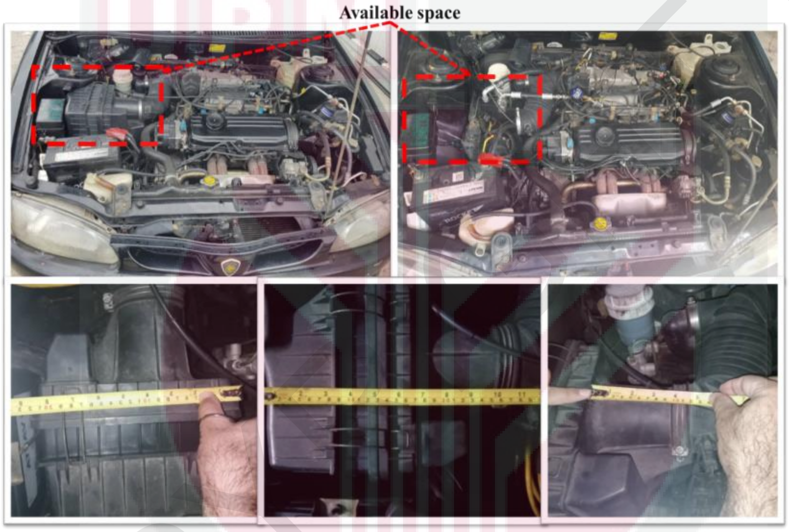

Figure 3.16: Available space in the test vehicle

The measured space available for installation of LHE was 0.007 m^3, which offered a larger space for LHE than the initial design size used for CFD simulations. Therefore, to utilize the maximum available space, the selected final design size was a little bit larger in terms of the height and width of the shell box; however, the length of the shell box remained the same. Subsequently, by increasing the shell box size, the overall surface area of LHE was increased, which means more heat transfer was expected for that selected size compared to the previous size used for initial CFD simulations. However, the best-suited internal geometry for lamella was selected based on simulation results. The final design size and geometry are shown in Figure 3.17.

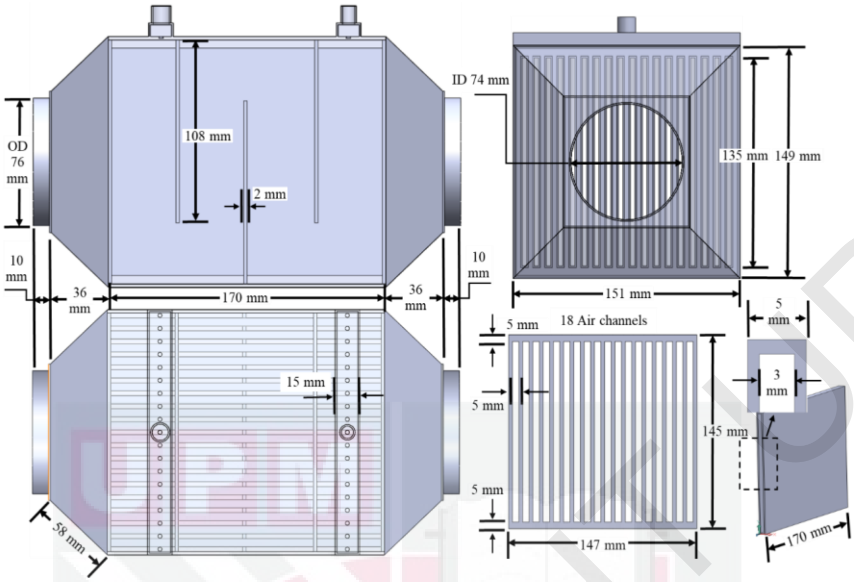

Figure 3.17: Final design size and geometry selected for fabrication

3.4.5 CFD Process of finalized design

The size of the final selected design was enhanced due to the available space in the specified test vehicle engine bay. Therefore, once again, a numerical investigation of the final selected size of LHE was performed on the same pattern and boundary conditions as it was done earlier for four models. Table 3.4 provides the details of the CFD simulations.

Table 3.4: Particulars adopted for numerical simulations

RPM	Intake air temperature ℃
1000	
1500	40
2000	
2500	
3000	
3500	45
4000	
4500	
5000	
5500	50
6000	
6500	
7000	
7500	55
8000	

3.4.6 Grid independence study (GIS)

The GIS was conducted on the final selected LHE geometry for the mesh to determine the appropriate influence number of nodes and elements to provide an accurate result with minimized simulation time. Five different cases of meshing size were selected to conduct the GIS, as shown in Table 3.5. The GIS of the five cases was achieved by comparing the results of pressure drops inside the LHE at RPM 8000. Accordingly, case 2 was adopted as the reference number of mesh for other parametric simulations.

Table 3.5: Number of nodes and elements along with mesh quality, used for GIS

Cases	Element size (mm)	Elements	Nodes	Avg. Skewness	Avg. Aspect ratio	Avg. Orthogonality	Pressure drop (Pa)
Case 1	0.00125	1615496	2002987	0.12082	1.4723	0.9035	82.677
Case 2	0.00150	1283030	1408774	0.20311	1.5790	0.8407	82.246
Case 3	0.00175	1093492	1077715	0.21839	1.7192	0.8211	80.001
Case 4	0.00200	981100	871477	0.23357	1.9071	0.7987	75.231
Cass 5	0.00300	696820	406989	0.29941	2.0737	0.7236	64.782

3.4.7 Verification of CFD simulations

The credibility of simulations was achieved through verification to estimate the degree of accuracy to which the model represents the real phenomenon, and it involves extensive comparisons with experiments. For the present study, the experimental correlation of the nusselt number and fanning friction factor, for fully developed turbulent flow in smooth tubes (Yunus A. Cengel, 2002) was utilized to verify the CFD simulations, to build confidence that the governing equations were solved with certain accuracy, and that the results obtained by solving the right model equations. The relation utilized to find the Nusselt number was introduced by Gnielinski (1976), mentioned at equation 3-13, demonstrating which mode of heat transfer is dominant, whether convection or conduction.

$$\boldsymbol{Nu = \frac{h_a D_h}{k_a} = \frac{\left(\frac{f}{2}\right)(Re - 1000)Pr_a}{1 + 12.7\,(f/2)^{0.5}(Pr_a^{\frac{2}{3}} - 1)} \quad (3 \times 10^3 < Re < 5 \times 10^6)} \qquad 3.13$$

The relations utilized for fanning friction factor (Chit et al., 2019)**,** Reynolds number (B. E. Rapp, 2017) and its corresponding velocity (L.Y. Chen et al., 2022), for airflow inside lamellas was given in Equation 3.14, 3.15, and 3.16 respectively.

$$\boldsymbol{f = (1.58.\ln(Re) - 3.28)^{-2} = \frac{f_{darcy}}{4}} \qquad 3.14$$

$$\boldsymbol{Re = \frac{\rho v D_h}{\mu}} \qquad 3.15$$

$$v_a = \frac{\dot{m}_a}{A_{c,lamella} \cdot \rho_a \cdot N_a} \quad 3.16$$

3.5 Post-processing parameters

3.5.1 Temperature drop

It was the most important factor in this study, as the hot air was indirectly contacted with a coolant medium and definitely lost its temperature. This temperature difference between the air inlet and air outlet section of LHE was observed numerically using ANSYS Fluent at different rpm ranges. Basically, it shows the capability of LHE to attain cold air for engine intake and helps to identify which geometry model is efficient in terms of losing more temperature from the models under consideration. In this regard, temperature drop has its own standing in this research.

3.5.2 Pressure drop

This is an essential factor that was neglected in literature studies, as the pressure drop on the intake line limits the airflow to the engine and causes a decrement in its efficiency (Chiba et al., 2011). Also, the design of LHE was based on the maximum allowable pressure drop, i.e., 5%, so it was necessary to check the pressure drop across lamellas. In general, a pressure drop is an irreversible loss that takes place when the fluid flowing through a tube encounters frictional forces due to the resistance to flow (Li et al., 2020).

3.5.3 Heat transfer

The general function of all heat exchangers is to transfer heat from one fluid to another fluid (H.Forsberg, 2021b). Therefore, the magnitude of heat transfers between the hot air and cold refrigerant was presented in the result section. Heat transmission in a heat exchanger is typically accomplished through convection in each fluid and conduction through the wall that separates the two fluids (Couper et al., 2005). For the present study, the heat transfer rate from energy heat balance theory is the amount of sensible heat transfer rate from the hot air by convection through the tube wall by conduction to latent heat coolant medium by convection are equals (Dincer, 2017).

$$Q_t = Q_{ref} = Q_a \quad 3.17$$

Total heat transfer rate can be expressed (Qiao, 2018) as:

$$Q_t = UA \triangle T_{lm} \quad 3\text{-}18$$

Where,

U; overall heat transfer coefficient
A; surface area of lamellas
$\triangle T_{lm}$; logarithmic mean temperature difference

Heat transfer through refrigerant (Melo et al., 2000).

$$\boldsymbol{Q_{ref} = \dot{m}_{ref}\,(h_{ref,i} - h_{ref,o})} \tag{3.19}$$

Where,

m_{ref}; mass flow rate of refrigerant
$h_{ref,i}$; enthalpy of refrigerant at inlet
$h_{ref,o}$; enthalpy of refrigerant at outlet

Heat transfer through the air (Kaviany, 2014).

$$\boldsymbol{Q_a = \dot{m}_a C_{p,a}\,(T_{a,i} - T_{a,o})} \tag{3.20}$$

Where,

m_a; mass flow rate of air inside lamella
$T_{a,i}$; temperature of air at inlet
$T_{a,o}$; temperature of air at outlet

3.5.4 Logarithmic Mean Temperature Difference (LMTD)

It is normally convenient to deal with the LMTD when investigating heat exchangers since it represents the equivalent mean temperature difference between the two fluids throughout the entire heat exchanger (Jeter, 2006). The logarithmic average of the temperature difference between the hot air and cold refrigerant was measured for all the cases under consideration. LMTD was considered because of temperature change that occurs across the heat exchanger from the entrance to the exit was not linear (X. Cui et al., 2014). It truly reflected the exponential decay of the local temperature difference. The relation of LMTD for manual calculation is given by Nitsche & Gbadamosi (2016).

$$\boldsymbol{\triangle T_{ln} = \frac{(\triangle T_1 - \triangle T_2)}{\ln\left(\frac{\triangle T_1}{\triangle T_2}\right)}} \tag{3.21}$$

3.5.5 NTU

Number of transfer units of the proposed models of LHE was noted. As in heat exchanger design, a number of transfer units (NTU) have a significant role. The performances of a heat exchanger can be easily assessed if the number of transfer units is known

(H.Forsberg, 2021a). The number of transfer units is an amalgamation of overall heat transfer coefficients, transfer area, fluid flow rate, and heat capability. It combines all of these dimensional variables into a single dimensionless parameter (Sinaga et al., 2021) also given by A. Pandey & Dubey (2021).

$$\boldsymbol{NTU = \frac{UA}{C_{min}}} \tag{3.22}$$

3.6 Fabrication of LHE

Once the numerical investigation was done, the LHE fabrication came into a process to make it possible to install in the test vehicle, and its actual performance can be measured. The fabrication was done by keeping in mind the reliability of the final product (selection of the material and welding process). Manufacturing of the LHE, as shown in Figure 3.18, comprises of eighteen airflow channels (lamellas), three baffle plates, two header plates, two fitting covers, and a shell box, according to the dimensions given in Figure 3.17. All the above-stated parts were joined by the Tungsten Inert Gas (TIG) welding, due to its ability to weld thin metals and to provide strong, durable and clean joints without slag and splatter. Stainless steel 316 L was utilized in the manufacturing of LHE, readily available in any market or country and have following advantages, described by Lauren Forth (2021) and Thirumalai et al. (2021), that it has an outstanding weld ability, machinability, and toughness even at cryogenic temperatures. It is also well resistant to corrosion, pitting, potable water, chloride, and corrosive chemicals. Further, the fitting covers were joined with the screw to provide facility to remove from the shell box on the requirement for cleaning purposes of airflow channels (lamellas). Extra fittings at the top of the LHE model shown in the figure were attached additionally to accord it with the air conditioning system used in the lab for experimental testing. Further pictures during fabrication was given in appendix B.

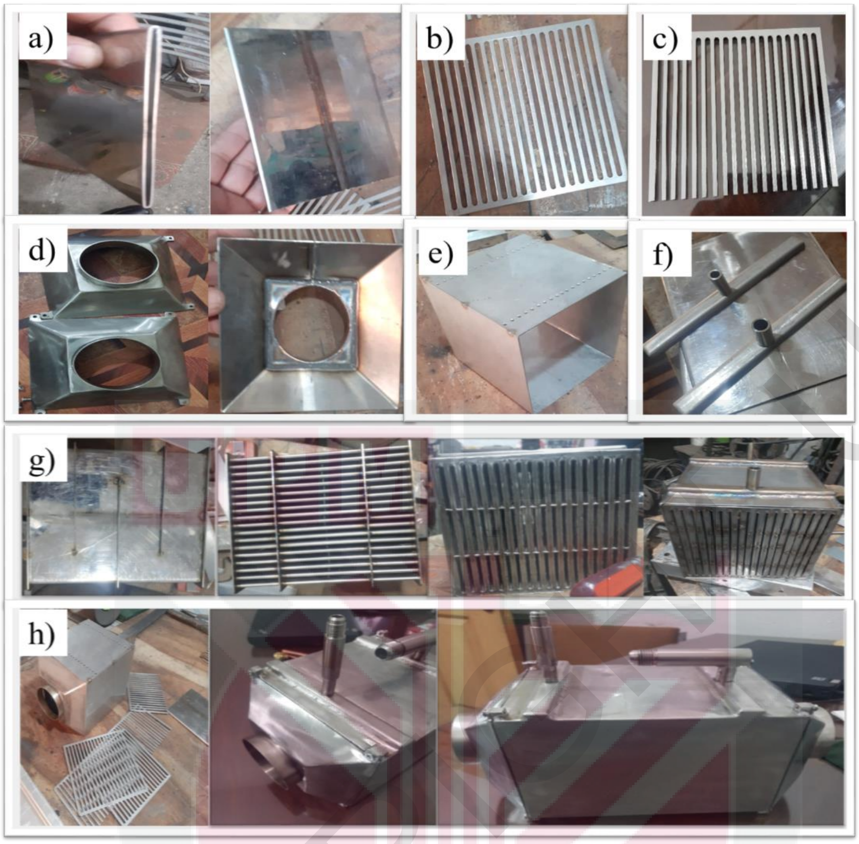

Figure 3.18: Fabrication of LHE, a) Lamella channel, b) header plate, c) baffle plate, d) fitting covers, e) shell box, f) inlet and outlet of referigerant, g) fitting and welding of lamellas in header and baffle plates, and h) final product (LHE) alongwith fittings for experimentation

3.7 Leakage tests of LHE

Leakage tests were performed to find any leakage in the newly constructed LHE. As the refrigerant flow involves in it, any leakage of refrigerant through welding joints will result in harmful effects presented in Figure 3.19. So, this test was valid to prevent any loss of the refrigerant during operation.

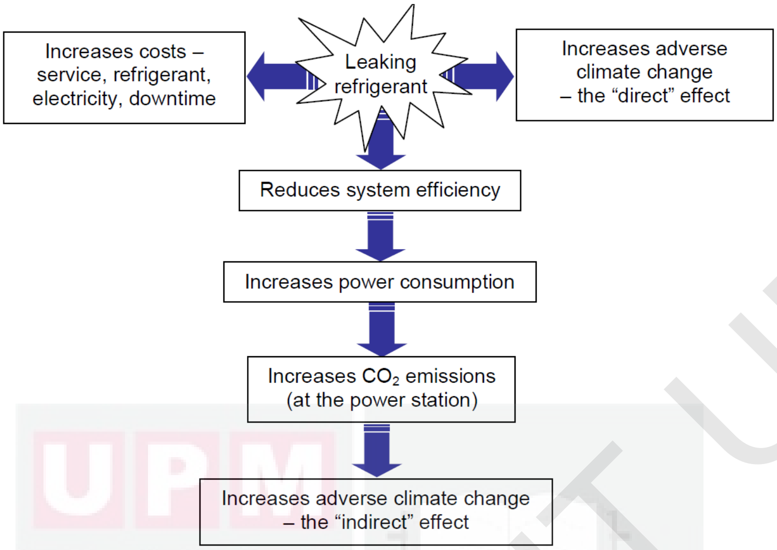

Figure 3.19: Detrimental effects due to leakage of refrigerant
(Refrigeration, 2011)

The goals of the tests were to check the following:

- a pressure drop caused by an unintended poor welding joint, crack or hole
- improvement of seals
- identify the weak spot of a pressure component
- defining the product specifications

Generally, there are many types and procedures for performing leakage tests, but for this study, three types have been adopted (Sarkar, 2017). All the tests were performed by applying high pressure of 11 bar with the help of a compressor, and a pressure gauge was connected to monitor pressure readings.

3.7.1 Pressure Drop Method

This method is simple to implement. It is suitable for determining gross leaks and can be improved using differential pressure gauges. The test object "LHE" was filled with a gas (air) until the testing pressure (11 bar) was achieved with the help of a compressor. The test pressure was then held by shutting off the supply valve for a specified time (15 min) and observing any pressure drop in pressure, as shown in Figure 3.20. Precision gauges were used to detect a possible pressure drop during the testing period.

Figure 3.20: Pressure drop test method using a compressor

3.7.2 Local Leak Detection with a soap solution

This test was performed by applying soap solution on LHE, as shown in Figure 3.21. Further, a high pressure state was maintained in LHE so that possible leaks could be located by watching bubbles forming in the leak area due to the soap solution. Suitable for pinpointing leaks and allowed under the F gas regulations.

Figure 3.21: Leak detection using soap solution

3.7.3 Leak detection using water

This method was adopted to check any minute leakage from LHE. This test was also conducted in a pressurized state. The LHE was immersed in water for 10 minutes. Any possible minute leakage from LHE will exhibit in the form of bubbles and can see with the naked eye, as presented in Figure 3.22.

Figure 3.22: Leak detection using water

3.8 Laboratory experimental tests

After performing the leakage test of the LHE, a model was installed on an experimental testbed setup in the UPM thermodynamics laboratory for experimental investigation and design validation with numerical analysis. The testbed was designed to be suitable in fitting with the selected LHE. The experimental testbed was constructed and created from available local materials. It consists of four major parts: the EICA simulator, ambient simulator, vehicle air-conditioning simulator, and control panel. Particulars of each part was given appendix C. Other components consist of measurement tools and sensors given in appendixes and the (PVC) ducting tubes.

3.8.1 Composition of testbed

The schematic of the testbed is shown in Figure 3.23.

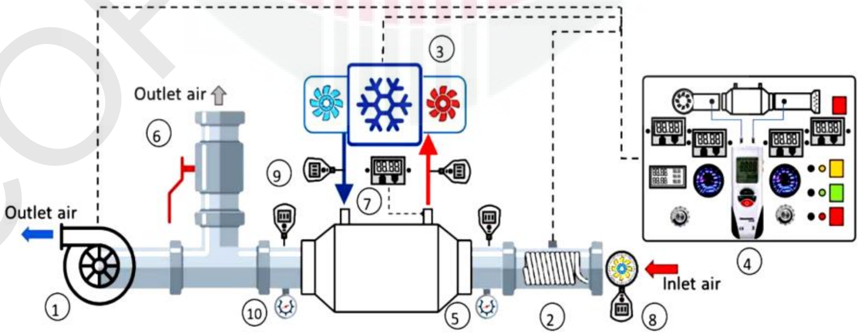

1	Vacuum fan	6	Air flow neutralizer
2	Heater	7	Temperature control
3	Air Conditioner	8	Anemometer gauge
4	Control Panel	9	Thermometer
5	LHE	10	Pressure gauge

Figure 3.23: Configuration of testbed

The heater was installed at the inlet section of air to provide heat to ambient air to gain the desired temperature for test purposes. The same tests were performed as mentioned in Table 3.4 for numerical investigation, so that numerical results were validated against the fabricated model. The air will be sucked through the inlet section with the help of a vacuum fan installed at the outlet section. The amount of air was calculated from the mass flow rate equation (3-11) for different RPM ranges. An anemometer gauge was provided at the inlet section to measure the exact amount of air or velocity required against RPM. Four thermometers were installed at the inlet and outlet sections to measure the temperature drop of air and refrigerant. Similarly, pressure gauges were installed to check the pressure drop across the heat exchanger. The air-conditioning system of 1hp was used in lab tests employing the refrigerant type (R22) attached to the LHE. Figure 3.24 displays the schematics of the attachment of the LHE with the air conditioning system, and Figure 3.25 depicts the actual installation of LHE on the test bed. Before filling the refrigerant gas, air was removed from the system because any moisture inside the system will damage the AC system, especially the compressor. The refrigerant gas was then filled through the suction line till the pressure reached 60-70 Psi on the pressure gauge set.

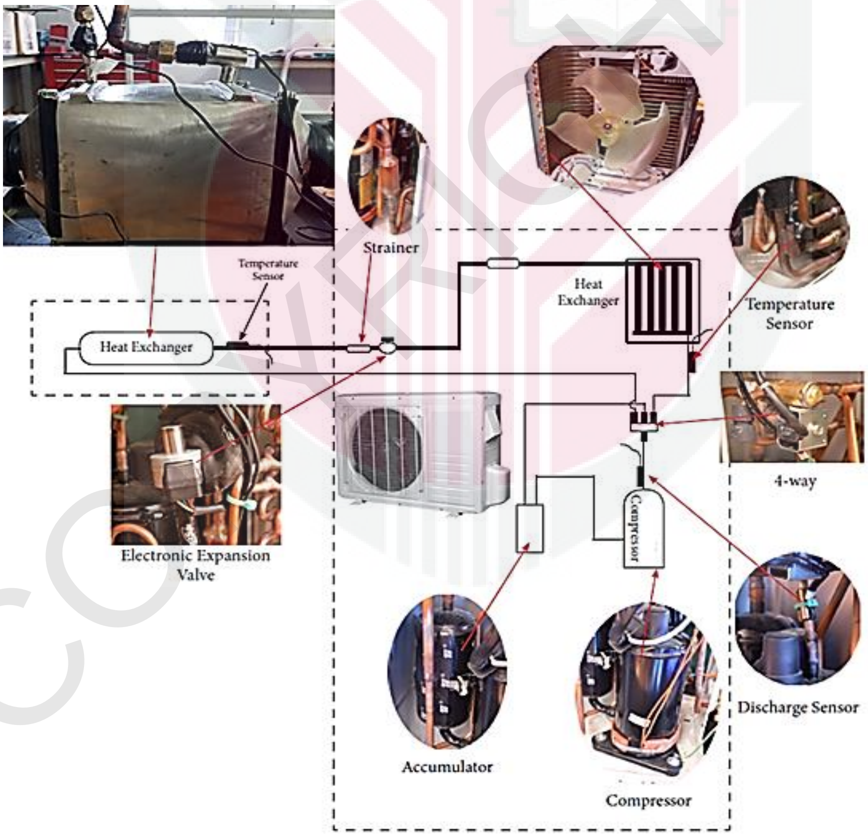

Figure 3.24: Attachment of LHE with air conditioning system in the lab

Figure 3.25: Actual installation of LHE on lab testbed

3.8.2 Design validation

The tests performed in lab were first compared with the results (temperature drop and heat transfer) obtained from numerical simulations in the form of mean absolute percentage error and coefficient of determination.

3.8.2.1 Mean absolute percentage error (MAPE)

A useful statistical evaluation of the performance of the predictive LHE models is helpful in identifying the relative differences between data results obtained numerically and experimentally (S. Kim & Kim, 2016).

$$\boldsymbol{MAPE} = \frac{\mathbf{1}}{\boldsymbol{n}}\sum_{\boldsymbol{i=0}}^{\boldsymbol{n}}\left|\frac{\boldsymbol{y_i} - \boldsymbol{\hat{y}_i}}{\boldsymbol{y_i}}\right| \qquad 3.23$$

3.8.2.2 The Coefficient of Determination (R^2)

The coefficient of determination (R^2) is a statistical measure of how close the data are to the fitted regression line (S. M. Ross, 2010).

$$R^2 = 1 - \frac{\sum_{i=1}^{n}(y_i - \hat{y}_i)^2}{\sum_{i=1}^{n}(y_i - \bar{\hat{y}}_i)^2} \quad 3.24$$

Where; y_i is actual value, $\hat{y}_i$ Predicted value and $\bar{\hat{y}}_i$ the average of the actual values, and n is the number of data samples. The amount of R^2 varies between zero and one ($0 \leq R^2 \leq 1$). A better sensitivity R^2 range presented between 0.8 – 0.99, lower value ranges could be satisfactory in some applications.

3.8.3 Temperature drop test of LHE

The purpose of the newly designed LHE in this research is to lower the intake temperature of the air, induced by an engine to have better combustion conditions and less exhaust emissions, as the intake temperature of the air has a direct influence on both of them (Pan et al., 2015; Teoh et al., 2021). The temperature drop test was the most important one in this study because it defines the thermal performance of lamella tubes, which means how capable the LHE is for lowering the temperature of hot ambient air and heat transfer. Therefore, temperature sensors were installed on the testbed to measure the temperature at the inlet and exit point of LHE and calculated the temperature drop of air through Equation 3.25.

$$T_{drop} = T_{air\_inlet} - T_{air\_outlet} \quad 3.25$$

3.8.4 Heat transfer through LHE

Through the temperature drop test, the amount of heat transfer for the air domain was then calculated using the heat transfer equation 3.20.

3.8.5 Pressure drop test of LHE

The LHE design depended on pressure drop criteria across the airflow domain because the pressure drop across the air intake system is known to significantly influence the indicated power of the IC engine (Heywood, 2018). Since the intercooler is usually mounted on the air intake line of an engine, any obstruction, restriction, or roughness in the system will cause resistance to airflow and cause a pressure drop. The differential pressure gauge was installed on the testbed to measure the pressure drop in the airflow. The factors involved in the pressure drop can be elucidated using Darcy–Weisbach equation (Huo et al., 2019).

$$\Delta P = \frac{f\, l\, \rho\, v^2}{2D_h} \qquad 3.26$$

Where,

ΔP;	Pressure loss due to friction (Pa)
f;	Darcy friction factor (unitless)
D_h;	Hydraulic diameter of the lamella(m)
v^2;	Fluid flow average velocity (m/s)

3.8.6 Coefficient of performance

In the laboratory setup, LHE was connected with a split type air conditioning unit to check its thermal performance. Another factor named COP (Espinel-Blanco et al., 2020) was calculated to witness system effectiveness, defined as the efficiency ratio of the amount of cooling provided by the cooling unit (LHE) to the energy consumed by the system (compressor) (Shaik et al., 2021). The higher the COP, the more efficient the system (Hundy et al., 2008). The air conditioning refrigerant cycle, shown in Figure 3.26, provided a clear idea about the performance calculation of the system i.e. heat absorbed Q_E by LHE (Seyam, 2019), work done by compressor W_{comp} (Nandanwar et al., 2023) and COP (A. K. Coker, 2015).

$$Q_E = \dot{m}_{ref}(h_1 - h_4) \qquad 3.27$$

$$W_{comp} = \dot{m}_{ref}(h_2 - h_1) \qquad 3.28$$

$$COP = \frac{Q_E}{W_{comp}} = \frac{h_1 - h_4}{h_2 - h_1} \qquad 3.29$$

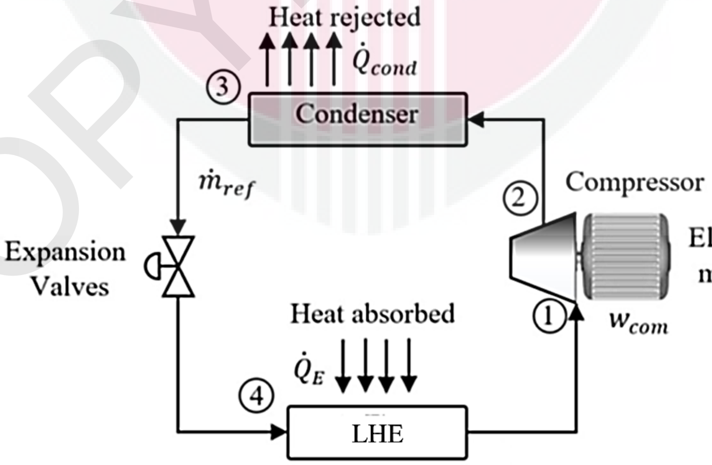

Figure 3.26: Air conditioning refrigerant cycle

3.9 Installation of LHE in testing vehicle

After the completion of laboratory tests at the UPM thermodynamics lab, the final stage of experimental testing was conducted to check the influence of LHE on vehicle performance by installing it in the test vehicle engine bay. Generally, in cars, the air must be filtered before introducing to the air intake system, followed by the combustion chamber (Sutton, 2010). Pollution in the intake of air can decrease the amount of oxygen available for combustion and can change the composition of vehicle emissions (Anthony J. Martyr & Rogers, 2021). Therefore, the LHE was installed after the air filter on the intake manifold line. The schematic diagram of the placement of the intercooler is presented in Figure 3.27.

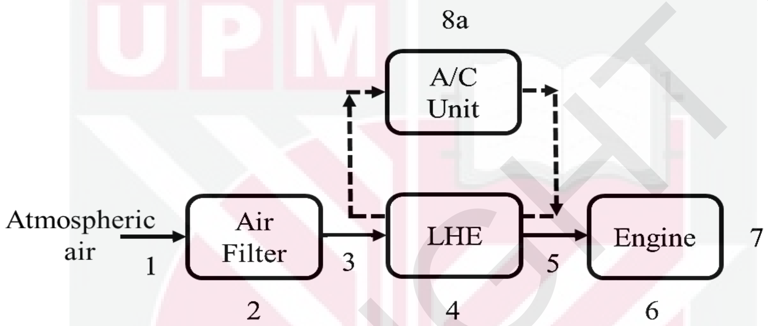

Figure 3.27: Position of the intercooler (LHE) in engine bay

The amount of air (1) required by the engine first passes through air filter (2) to remove impurities. Purified air (3) was then allowed to enter into the Lamella heat exchanger to reduce its temperature with the help of automobile refrigeration system (8a). Ambient air, after the reduction in its temperature (5), may be entered into the engine. The purpose of this placement of the intercooler refers to future technical maintenance so that only purified air can enter into LHE and eliminates any possibility of blockages in lamella channels. The other benefit of this placement of the intercooler was that there was a very short distance remaining between the LHE outlet and the engine inlet; resultantly, there was less chance of again getting some temperature from the engine heat. Further exploring the basic refrigeration system (8a) installed in the vehicle is presented in Figure 3.28a, comprising a compressor, condenser, receiver dryer, expansion valve, and evaporator. The working of the cycle is already explained in chapter 2. By the addition of LHE in basic refrigeration cycle, the system is now presented in Figure 3.28b, clearly depicting the way LHE was installed in the existing standard AC system.

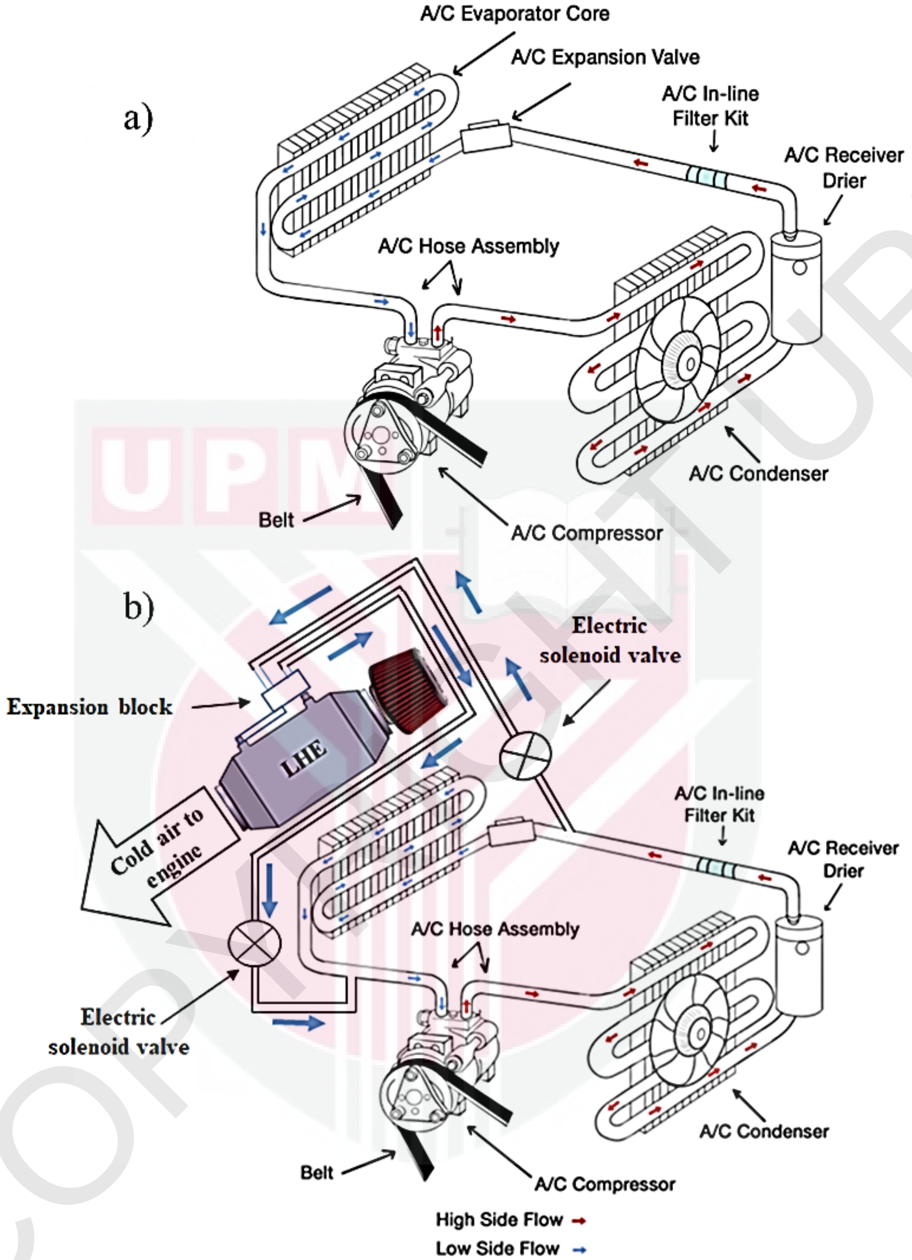

Figure 3.28: Refrigeration system, a) standard AC system, and b) with attachment of LHE

The system was now operated with dual evaporators. The first evaporator was utilized for the cabin cooling process, and the second evaporator (LHE) was used for cold intake air. The additional evaporator was added to the automotive air conditioning cycle by adding a bypass line after the condenser to feed the refrigerant to LHE. A separate expansion valve was added for the second evaporator. Two Electric solenoid valves were added to the bypass loop to control the refrigerant operation and cycle in LHE. Refrigerants, after leaving from both evaporators, again combined at a point for a single entry into the compressor inlet. Figure 3.29 depicts the actual installation of LHE in the vehicle bay.

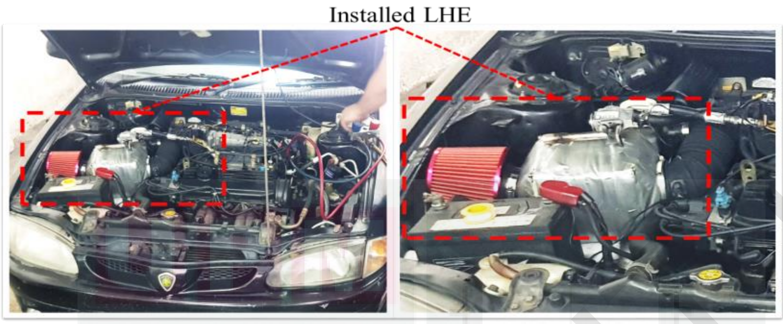

Figure 3.29: LHE fitted in test vehicle engine bay

Moreover, the LHE was fully wrapped with thermally isolated tape from the outer surface to protect it from the engine's heat and other thermal heat produced under the hood. The operation starting of the EICAC cycle was controlled by the main power switch installed in vehicle cabin, and an electric thermostat controlled the cycle operation by controlling the power source of the electric solenoid valves. The refrigerant in the car AC system was charged by operating both the evaporators (for cabin cooling and for the cold intake air) at the same time. The refrigerant continued to charge until the operational pressures (low side 35psig - 40psig and high side175psig - 225psig) were attained (Shana, 2021). This was an important step to follow, as the performance of LHE is ultimately based on refrigerant charge/pressure. In case of high or low refrigerant charge than the required amount or different operating pressures (high and low side) than the required operating pressure for R134a, the VAC system will not work properly/efficiently and couldn't be able to provide required cabin cooling (Yun & Chang, 2021). Subsequently the performance of LHE will also be effected, due to its attachment in the same circuit. Therefore, the performance of LHE is directly related to the efficiency of VAC system, regardless of the engine size and model year. If the VAC system works properly, the gain in engine performance by utilizing LHE (percentage wise) would be the same for any old and new car, relative to the engine performance without using LHE. The detailed installation of LHE in the test vehicle is given in appendix D.

3.10 Applied vehicle test

After the installation of LHE in the engine bay, the next step was to check the response of LHE on engine performance since the development of the vehicle industry and its products is inseparable from vehicle test research (Casadei & Maggioni, 2016). For the applied vehicle test, two types of vehicle status were considered:

1. Vehicle running or moving position: As the name interpret, it represents the state of vehicle in which it was moving.

2. Vehicle parking or static position: It represents the state of the vehicle in which the vehicle was ON but remained standstill for waiting of someone, stuck in a traffic jam or waiting for a traffic signal. This test helped to check the performance and reign of LHE over the conventional intercoolers, which lack to perform in this particular state.

Three stages of tests for both vehicle status (running and static) has covered in this testing, which helped to discover the influence of cold intake air on the engine compared to normal hot intake air, as:

1. Normal stage: this stage represents the state of the vehicle without the use of a standard VAC system. LHE was also not operational at this stage. This stage expressed the behavior of the engine without a VAC system and LHE.

2. AC stage: this stage symbolized that vehicle was using only its standard air conditioning system and helped to identify the effect of the automotive AC unit on the engine performance.

3. LHE+AC: this stage indicated that LHE was operational (ON) along with the standard VAC system and helped to identify the effect of cold air on the engine with respect to ambient air temperature conditions.

Each stage comprises of three repeated tests, to ensure the accurate data reading. The précised form of the applied vehicle tests as described above, is displayed in Figure 3.30.

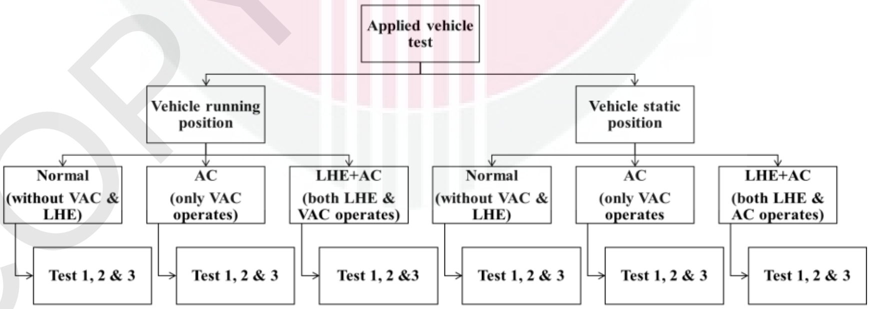

Figure 3.30: Pattern of applied vehicle test

3.10.1 Vehicle running position (Chassis dynamometer test)

For vehicle running position, chassis dynamometer test (Moskalik et al., 2015) was conducted at Universiti Kuala Lumpur-Malaysia France Institute (UniKL-MFI). The testing on a chassis dynamometer is a standard practice with a high degree of precision that may be used to compare the performance of various vehicles, products, or circumstances. It is also comparatively faster and less expensive than on-road testing (Z. Yang et al., 2018). This was accomplished by driving the vehicle in controlled and repeatable conditions while experiencing resistance at the wheels that produce, with appropriate accuracy, that would be encountered on the road in real life (A. J. Martyr & Plint, 2007). The schematic diagram of the chassis dynamometer setup is shown in Figure 3.31. The chassis dynamometer model used was (MAHA Dyno – LPS3000 PKW). Figure 3.32 shows the actual installation of test vehicle on chassis dynamometer test bench.

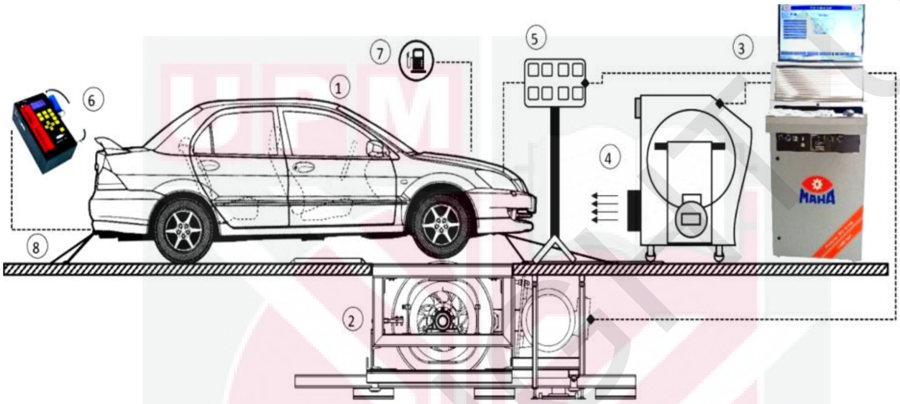

1) Test vehicle	2) Single roller Eddy current	3) Communication Desk
4) Air cooler blower	5) Interface box	6) Exhaust gas analyzer
7) Fuel meter	8) Vehicle secure belts	

Figure 3.31: Chassis dynamometer schematic connection and installation

Figure 3.32: Chassis dynamometer bench test

The chassis dynamometer was tuned with vehicle data information and adjusted to be ready for the test start. The dyno records data when the vehicle is accelerated at full throttle to speed up from 50km/h up to the maximum speed of 180km/h in order to ensure the rpm of the engine should not have exceeded the maximum permissible range, i.e. 6500 rpm for a safe engine operation test. The measuring power accuracy by the system is ±2% (MAHA Standard Operating instructions and User's Manual). The dyno operation program menu-oriented is available in Appendix E.

3.10.2 Vehicle parking position

For vehicle parking or static position test, the test vehicle was parked in the daytime and sunny area for an actual representation of the real-life situation i.e. traffic jam, waiting at a signal or waiting for someone. All three stage tests were performed to evaluate the impact of LHE on the vehicle static position. For each stage test, the vehicle was parked for 11 minute in order to attain improved results and could provide a better understanding of the influence of engine intake charge cooling. The AC of the test vehicle was turned ON right after the 11 minutes' test of the normal stage, and similarly, the LHE was allowed to operate right after the AC stage test. This helped to understand the effect of each stage on others or previous stages.

3.11 Performance parameters observed during applied vehicle test

Based on the objectives of this study, engine power, torque, exhaust emissions and fuel consumption are selected as the performance parameters, to evaluate the impact of cold intake air on engine response. The details of inspection and equipment's used for measuring performance parameters are discussed in sub-section. However, the summarized form of the performance parameters dignified for both vehicle statuses (running and static) is presented in Figure 3.33; for the vehicle running position and Figure 3.34; for the vehicle static position. Further, the way results of performance parameters reported in chapter 4, are summarized in Figure 3.35.

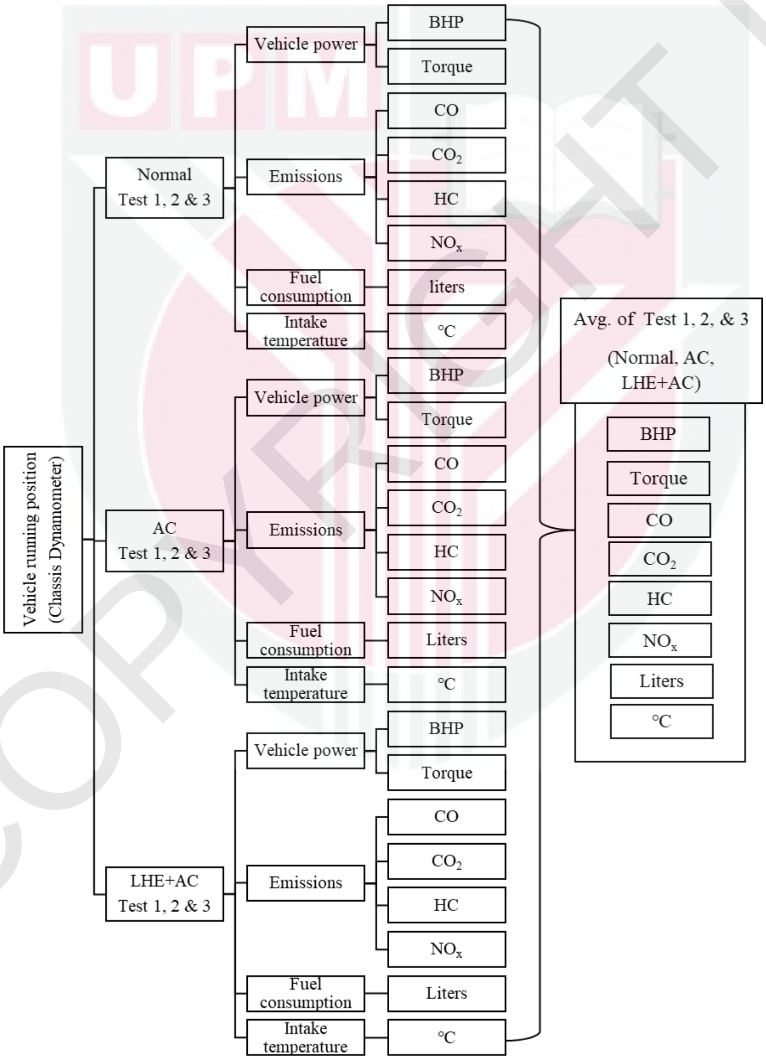

Figure 3.33: Summarized form of tests and their performance parameters related to vehicle running position test

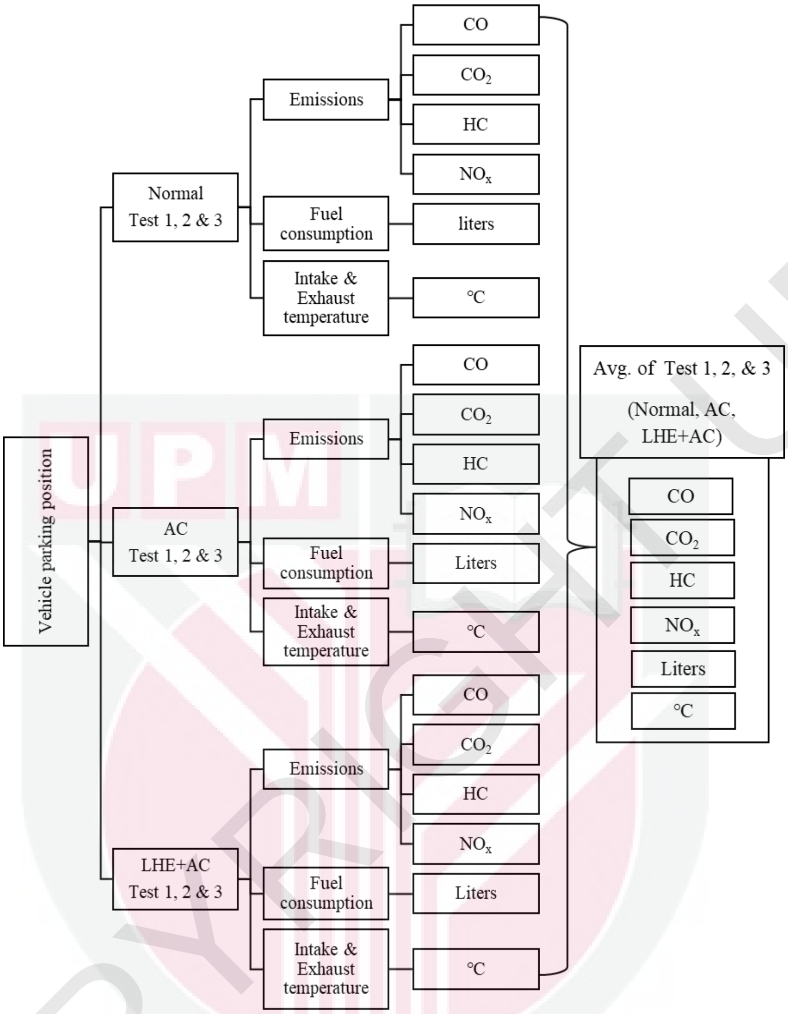

Figure 3.34: Summarized form of tests and their performance parameters related to vehicle parking/static position test

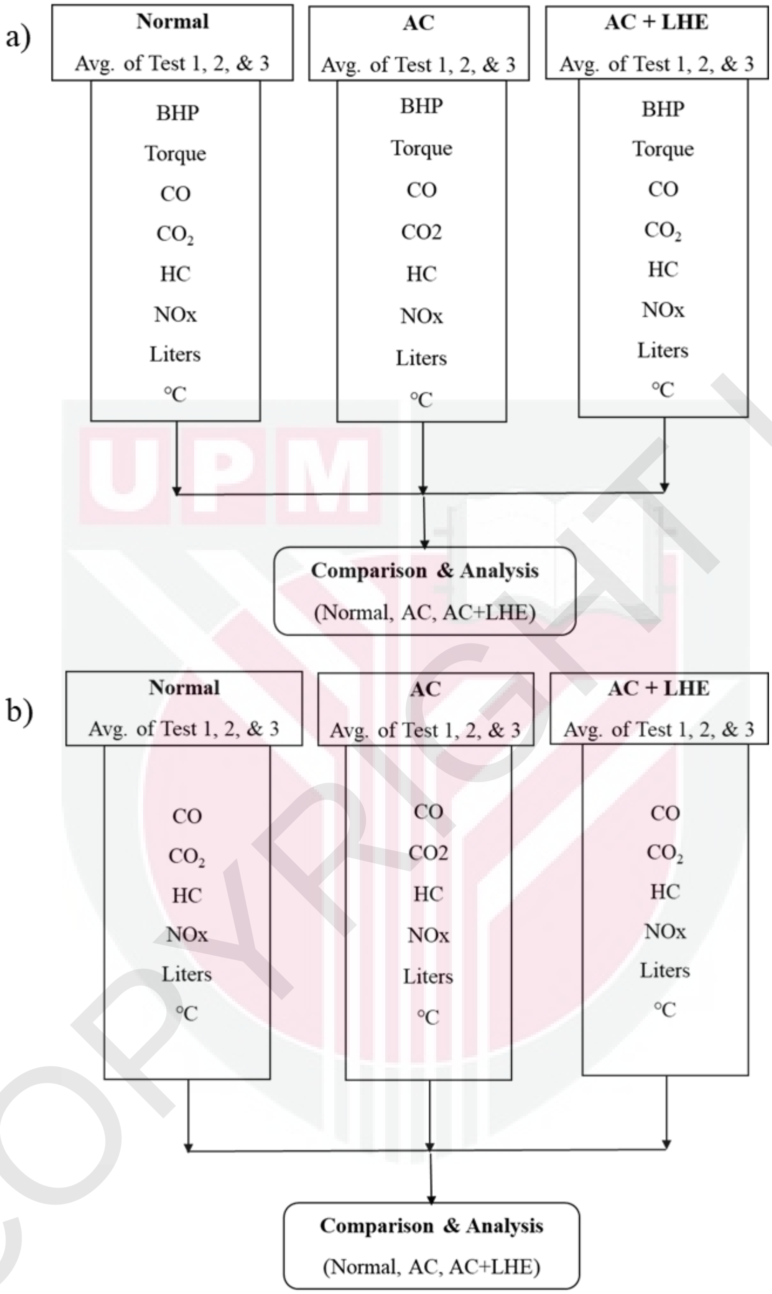

Figure 3.35: Summarized form of results related to performance parameters, presented in chapter 4, a) vehicle running test, and b) vehicle static/parking test

3.11.1 Engine Torque & Power

A. Vehicle running position

The power and torque of the test vehicle was recorded for all three stage tests in order to compare the engine performance, with or without cold intake air. The roller measures the total front-wheel power under steady state operation with acceleration in engine speed by converting the eddy current resistance created power into mechanical power by the software calculation.

B. **Vehicle parking position**

Not feasible and promising to record, as the vehicle is parked in an open sunny area for an actual representation of a real scenario.

3.11.2 Fuel Consumption

Figure 3.36 shows the fuel sensor flow meter model (AICHI Gear flowmeter model OF05ZAT with ±2% error) used for fuel measuring, connected to a digital (LCD) monitor and controller (ZJLCD-M) installed on the vehicle fuel line system. Moreover, the schematics of the flow meter sensor installed on the test vehicle fuel system are shown in Figure 3.37. The sensor (A) records the fuel flow supply entering the fuel injectors. The second sensor was installed on the fuel return line to record the return fuel amount by the LCD meter. The differential number of records represents the fuel consumed by the engine.

Figure 3.36: Fuel meters and measurement devices used to measure the fuel consumption

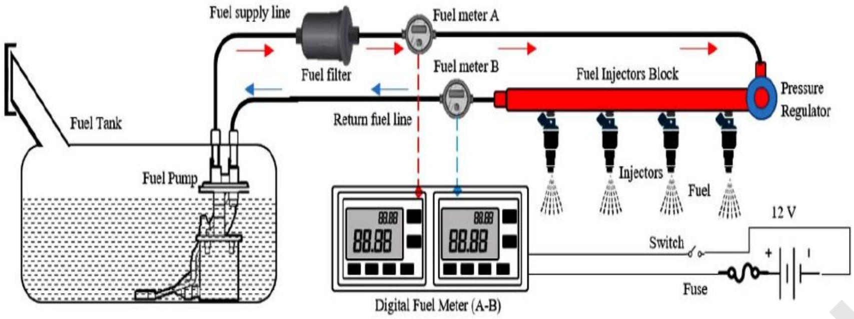

Figure 3.37: Schematic of vehicle fuel system meter and sensors installation with digital LCD flow monitoring

A. Vehicle running position

The total fuel consumed to perform each stage tests were recorded in liters (liters/test). Comparison has been made for all three stages (Normal, AC, LHE+AC) to express the effect of VAC system and cold intake air on fuel consumption.

B. Vehicle parking position

The total fuel consumed in liters for 11 min for each stage was measured for evaluation between different stages.

3.11.3 Emissions

The test vehicle engine emission was measured experimentally by using the emission gas analyzer model (Portable Emission and gas analyzer Enerac 700AV) made by USA Enerac company, as shown in Figure 3.38. The connectivity and opeation guide of gas analyzer was available in appendix F. The device has an automagical internal recalibrating system within $\pm 1\%$ error. The intensity of the following toxic exhaust components was measured:

- carbon monoxide CO (% of gas)
- carbon dioxide CO_2 (% of gas)
- hydrocarbons HC (ppm)
- nitrogen oxides NO_x (ppm)

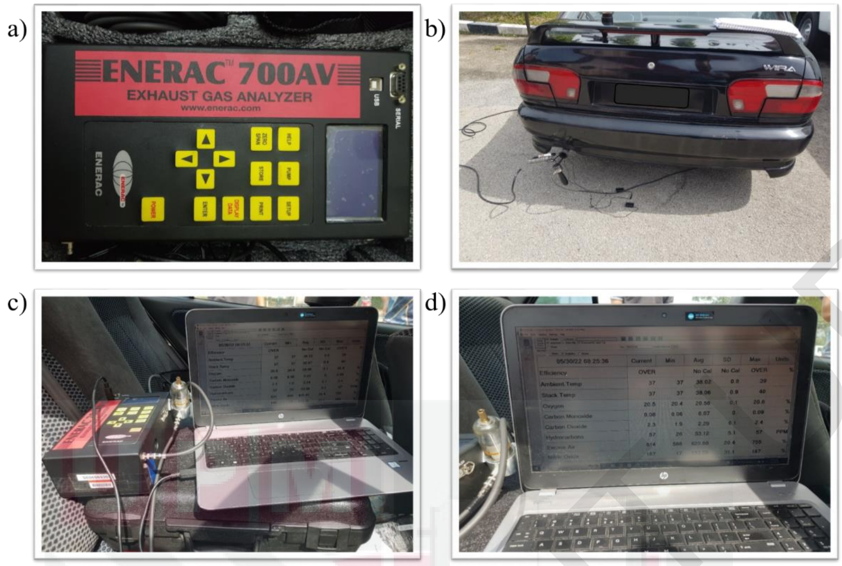

Figure 3.38: Emissions gas analyzer, a) model (ENERAC 700AV), b) probe insertation into exhaust tailpipe, c) attachment of gas analyzer with ENERCOM software, and d) interface of ENERCOM software

A. Vehicle running position

As the vehicle starts moving, the amplitude of emission factor increases with the increase in acceleration. Therefore, for a comparison point of view between each stage, the overall average value of each toxic gas retrieved from all stage tests was presented in the result section.

B. Vehicle parking position

This was measured at every 1 min interval for each stage, along with the overall average value for 11 min for each stage test was also presented in the result section for assessment purposes.

3.11.4 Intake and exhaust temperature

The temperature at the inlet and outlet of LHE was measured to check the temperature drop of the air intake. This was achieved with the help of a temperature sensor, as shown in Figure 3.39, located at the inlet and outlet of LHE for airflow. The temperature at the outlet of LHE is basically the temperature of air entering into engine.

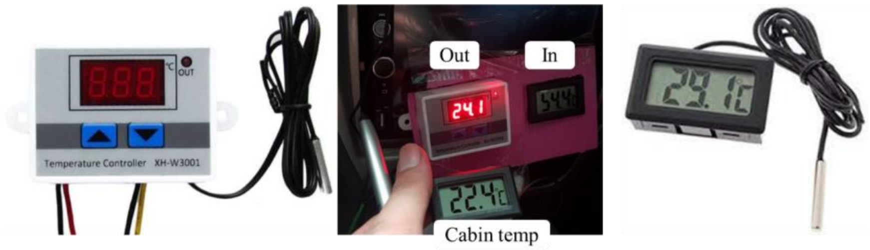

Figure 3.39: Temperature sensors used to monitor the temperature of intake air and cabin

A. Vehicle running position

Intake temperature to the engine is recorded using thermocouples for all the stages, to compare the temperature variations for each stage. The average intake temperature is presented in result section.

B. Vehicle parking position

Intake temperature to the engine is measured at every 1-minute interval for the whole test duration for each stage. The overall average value of respective stages was also presented to express the temperature difference created due to LHE on intake air.

Exhaust temperature at the tailpipe was also measured with the help of a temperature sensor at every 1-minute interval for the whole test duration for each stage to find the effect of cold intake air on combustion conditions. The difference between exhaust temperatures with and without using LHE will define the combustion temperature circumstances.

CHAPTER 4

RESULTS AND DISCUSSION

4.1 Introduction

In this chapter, the results of the study are presented and discussed with reference to the aim of the study, which was to determine the influence of EICAC on engine performance. For that purpose, an intercooler named LHE was designed and fabricated based on the available space in the test vehicle engine bay. The performance of LHE as a cold intake air system is predicted numerically through CFD simulations, and its effect on engine performance is demonstrated experimentally through chassis dynamometer tests. First, numerical simulations were performed and reported to find the best geometry of the LHE for maximum cooling and minimum pressure drop among the initially proposed design geometries (mentioned in Table 3.1). The simulations were presented against different engine speed and selected intake temperature for heat transfer, temperature drop, pressure drop, temperature contours, NTU, and LMTD. Results from simulations helped not only to select the best geometry of LHE but also to compare with the reference model adopted, for performance comparison.

Second, again numerical investigation was conducted and presented, as the best geometry of LHE from initial simulations was reformed according to the exact available space in the test vehicle engine bay to install it at a later stage. The results of the final adopted geometry size were stated using the same parameters as they were for the initial simulations to judge its performance against different intake air temperatures and RPMs, mentioned in Table 3.4. Third, the performance of fabricated LHE is presented using the experimental test bench (described in the section 3.8) to validate with numerical simulations. Last, the effect of the EICAC technique using LHE on a test vehicle engine is presented for two different positions of the car: in the moving position and vehicle parking/static position. The effect of the cold intake air on the engine power-torque curve, exhaust emissions, and fuel consumption were reported for each vehicle position.

4.2 Numerical results of initially proposed LHE models

As described earlier in section 3.4.2, initially, four models based on the minimum inside opening of the lamella were selected to check the performance behavior of LHE before the final selection of the model for the test vehicle. The outer dimensions of all the models were kept similar to the design available in the literature and acquired as a reference model. The only difference between all these models was the number of lamellas (10, 12, 15, 17) incorporated in a confined shell box space. Moreover, the reason for adopting the reference model was to compare the performance of LHE with respect to the already available design for cooling intake operating on a vehicle refrigeration unit for a 1.5L naturally aspirated SI-engine. The physical description of the simulations carried out is presented in Figure 4.1.

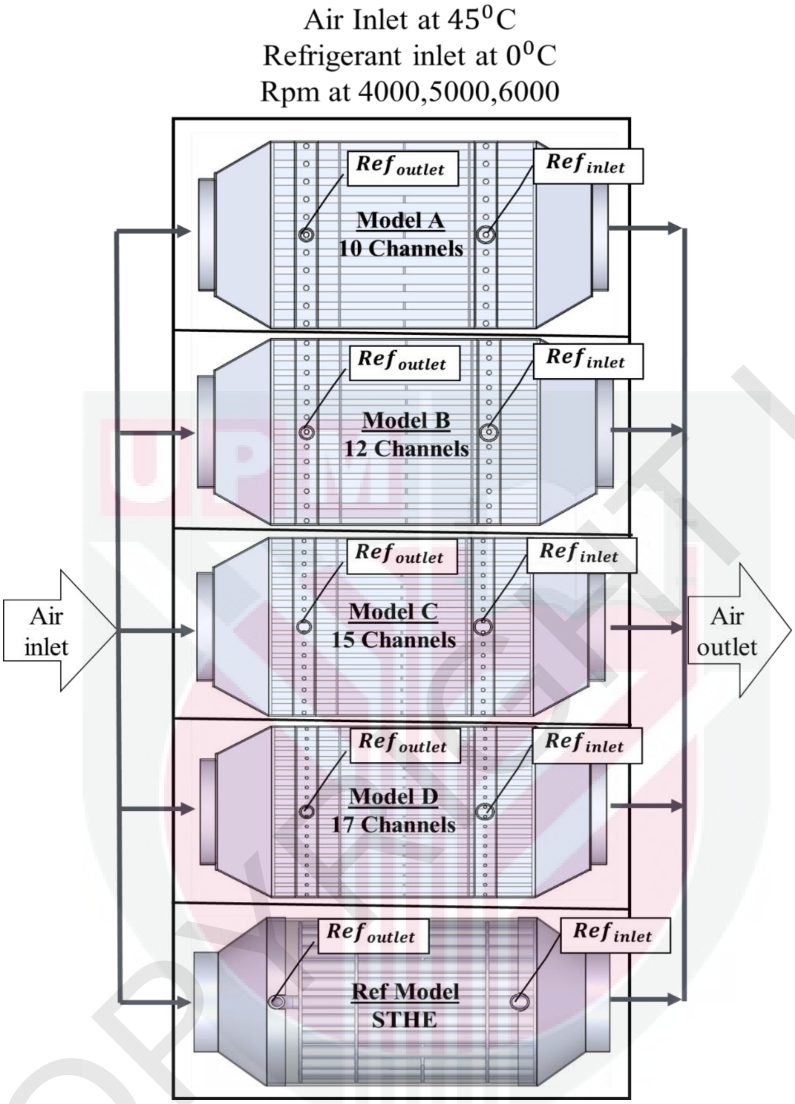

Figure 4.1: Parameters of simulations for initial proposed models (A, B, C, D) and reference model
(Pshtiwan M. Sharif et al., 2019)

4.2.1 Verification of numerical results

Nusselt number and fanning friction factor results are adopted to examine the accuracy of the CFD simulations performed for this study with the experimental correlations available in literature (described in section 3.4.7). The relation utilized to find the nusselt number and fanning friction factor was mentioned in equation (3-13) and (3-14), respectively. Figure 4.2 (bar chart) compares the CFD and experimental results for the

Nusselt number and fanning friction factor, indicating good agreement between numerical and experimental relations at 6000 rpm. In the case of the Nusselt number, a maximum difference of 6.14% is observed for model A, and a maximum difference of 5.89% is observed for model D in the case of the friction factor.

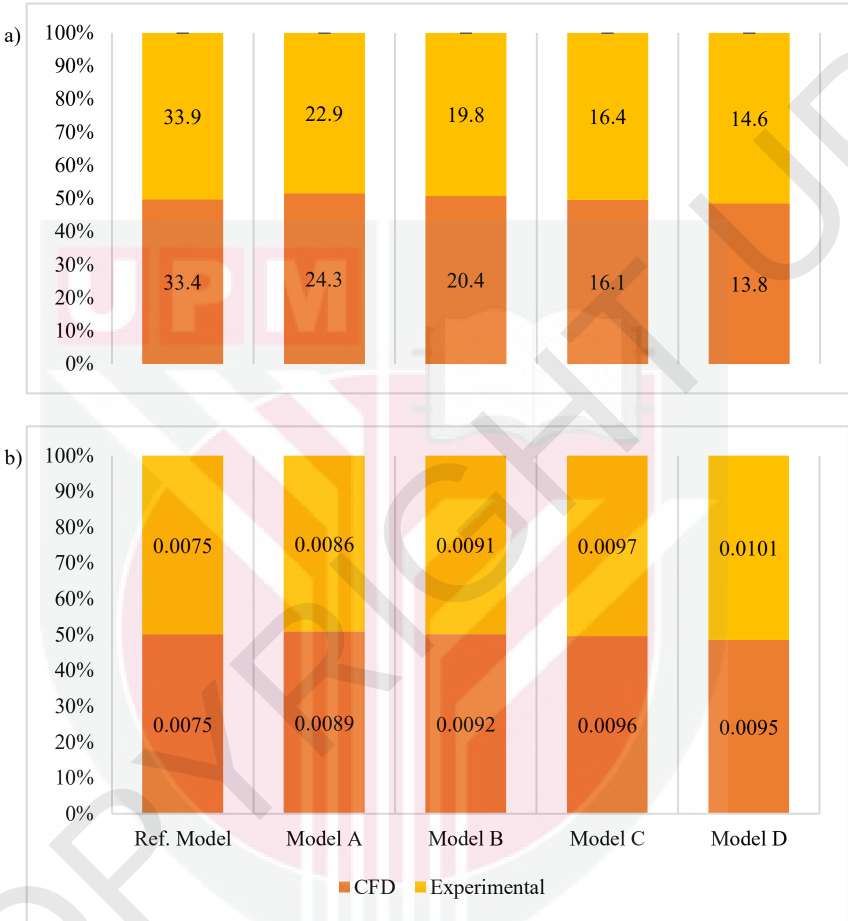

Figure 4.2: Comparison between the results of CFD and experimental correlations at 6000 rpm for a) Nusselt number and b) fanning friction factor

4.2.2 Temperature drop

The evaluation of the temperature drop is the most important key parameter in the present study, as the thermal efficiency of the Otto cycle engine depends on inlet and combustion temperatures (Akasyah et al., 2015). Inlet temperature depends on ambient or IHE conditions, whereas combustion temperature depends on burning combustion and heat release, which vary with the fuel/air ratio. Theoretically, the engine's thermal efficiency increases as the inlet temperature decrease (Z. Zhang et al., 2022). Figure 4.3

exhibits the temperature drop value for each model as a column chart for selected engine speeds. The highest temperature drop of 21.11°C is recorded for model D, followed by model C, model B, and model A, with 18.78°C, 14.98°C, and 12.48°C values, respectively, at 6000 rpm. The same trend is observed for each model at different engine speeds. The temperature drop is almost double for model D compared to the reference geometry, which has a temperature drop of 11.44°C. The air temperature results indicate a reduction from 45°C to 23.8°C at 6000 rpm. Further, a decrease in engine rpm causes a reduction in airflow velocity and a rise in the time of contact surface between the air and lamella surfaces, due to which a higher temperature drop is observed for 4000 rpm, i.e., 45°C to 20.9°C. On the other hand, at higher rpm ranges, owing to an increase in flow rate and air velocity, decreases the time of contact between the air and a cooling surface. As a result, a decrement in cooling impact and a lower temperature differential is observed for 5000 & 6000 rpm. In other words, the air temperature drop is inversely proportional to engine speed. On the shell side, theoretically, the phase change phenomenon is assumed to occur at a constant temperature.

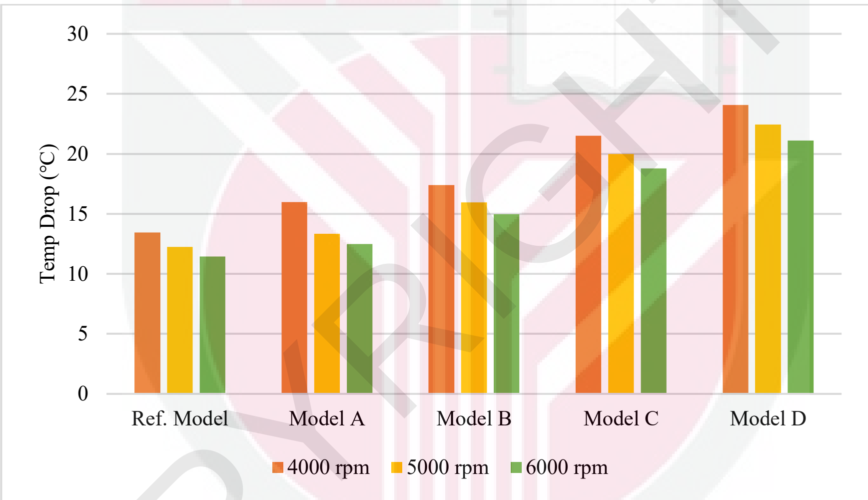

Figure 4.3: Comparison of temperature drop for each model at different rpm

4.2.3 Heat transfer

The heat transfer amount derived from the Ansys Fluent software analysis is measured using the air inlet and outlet temperatures. High heat transfer is observed for all the models under discussion, comparable to the reference model (Pshtiwan M. Sharif et al., 2019) , as presented in Figure 4.4. The maximum heat transfer amount of 1.55 kW is observed for model D, followed by model C, model B, and model A, with heat transfer of 1.38 kW, 1.07 kW, and 0.89 kW, respectively, for 6000 rpm. The same trend is observed for 4000 rpm and 5000 rpm. The heat transfer in the column chart clearly depicts that heat transfer increases with the increase in engine speed and vice versa (Song et al., 2021; Mei et al., 2022). Lower heat transfer is realized at lower engine speed due to the lower airflow rate requested by the engine itself. It is known that heat transfer is proportioned to the surface area of geometry, and the highest surface area is observed for model D. Heat transfer coefficients for the plate heat exchangers are superior to those for Shell and tube heat exchanger (reference model). The lamella configuration reveals more heat transfer surface per unit volume than the tube. Consequently, LHEs are likely to be more compact than shell and tube heat exchangers even when of the same surface area or give more surface area for heat transfer for the same geometry size.

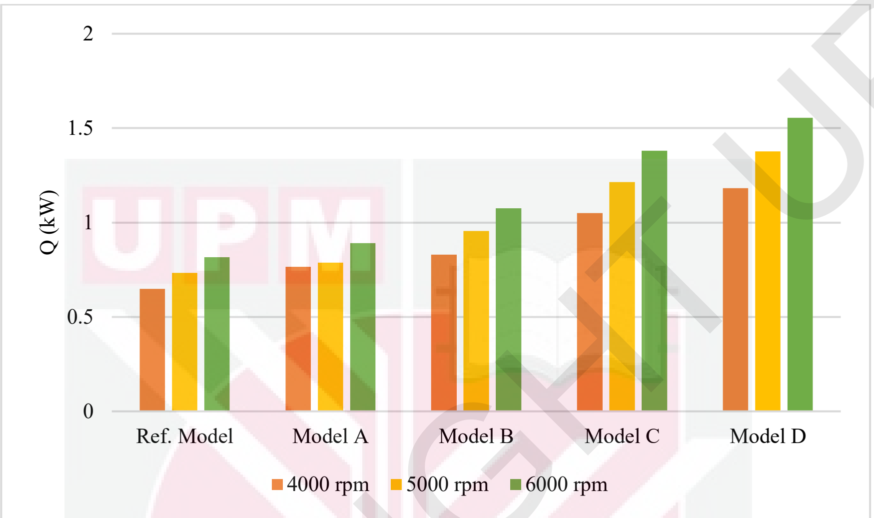

Figure 4.4: Comparison of heat transfer amount for each model at various engine speeds

4.2.4 Temperature contours

Figure 4.5 shows the instantaneous temperature contours at the outlet of the air section for all models at 6000 rpm. The forced convection heat transfer from lamellas is primarily affected by the inside opening of the lamellas. The hotter section of the stream is present at the center of the lamella. The temperature profile looks like a blunt parabolic profile in a thermally fully developed region (Barnoon et al., 2021).

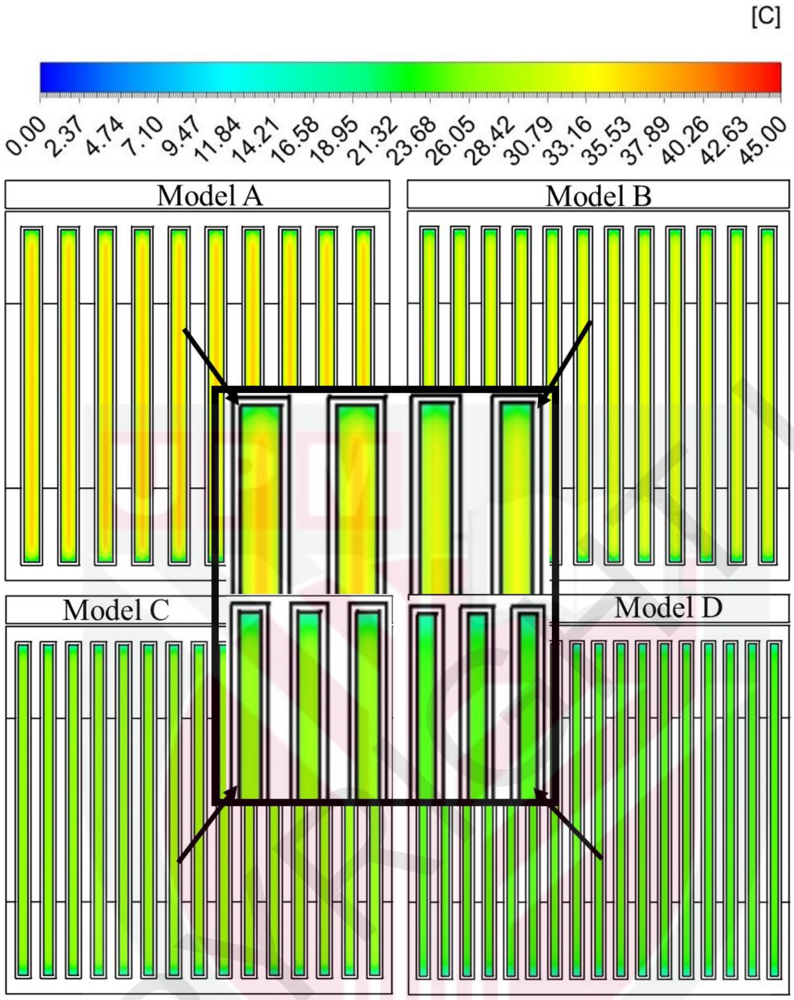

Figure 4.5: Temperature contours at the outlet of the air section for all models at 6000 rpm

For model A, the distance from the center of the lamella to the side of the lamella is high, which means that the cold surface is not close to the hot medium by virtue of less temperature drop observed. For model B, model C and model D, the distance from the center of the lamella to the side of the lamella is decreasing, respectively, and the cold side is getting closer to the hotter medium present in the center of the lamella; therefore, more temperature drop is witnessed. In other words, it can be explained as the greater inside opening of the lamella causing less temperature drop at the outlet section. In all models, the portion at corners has less temperature compared to other lamella portions. This is due to refrigerant gas surrounding the lamella surface from three sides compared to the remaining portions, where heat is only transferred from two adjacent sides only. The temperature profile distribution in the middle section of a single lamella plate has been presented in Figure 4.6 for each case, and the temperature forms in the middle section along the length of the complete LHE (model A) are shown in Figure 4.7.

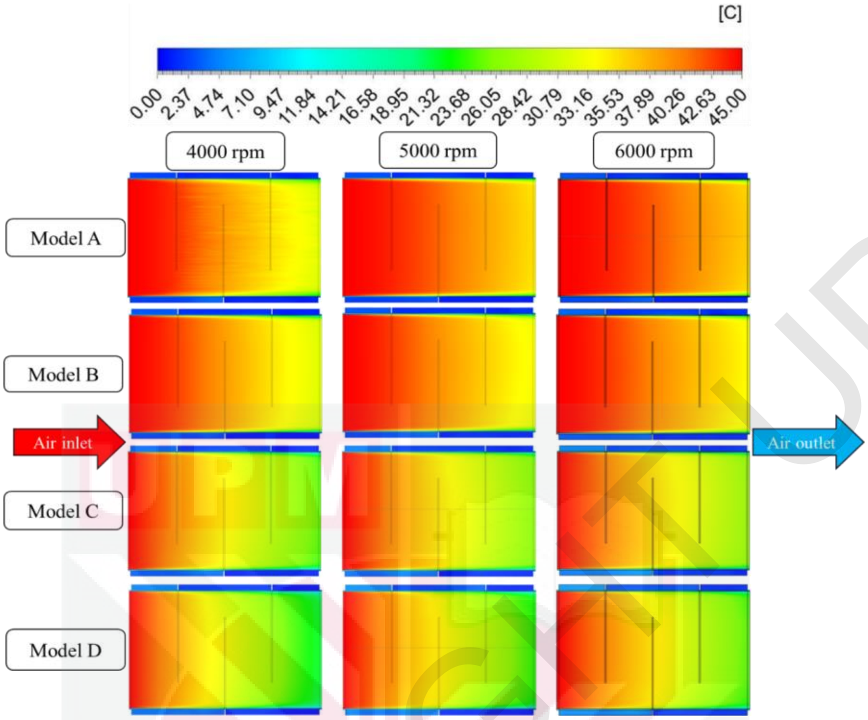

Figure 4.6: The temperature profile distribution in the middle section of a single lamella plate

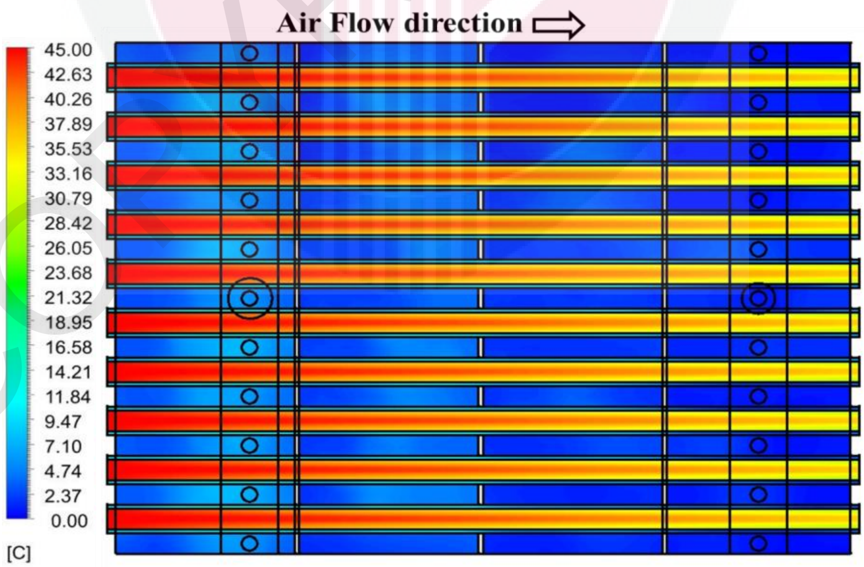

Figure 4.7: Temperature forms in the middle section (top view) along the length of the complete LHE (model A) at 6000 rpm.

4.2.5 Pressure drop

Assessing the pressure drop is an important aspect in the design of intercooler heat exchangers, especially for the naturally aspirated engine, where no pressure devices like turbo and supercharger are installed to increase the engine's power. The engine draws the atmospheric air during the intake process, determining the inlet boundary conditions at the intake manifold. The pressure drop analysis is carried out at the inlet and outlet faces of the lamella. Figure 4.8 demonstrates the pressure drop for the air side for all models under consideration and the reference model. The highest pressure drop of 69.23, 100.45 & 137.9Pa is recorded for model D at 4000, 5000 & 6000 rpm, respectively. This is because model D has the highest aspect ratio. Similarly, for other models, the pressure drop is decreased with the decrement of the aspect ratio of the lamella. However, the maximum pressure drop for model D at 6000 rpm is even less than the reference case (shell and tube exchanger) by 28% and well below the allowable pressure drop percentage, which is 5% of atmospheric pressure. The pressure drop inside lamellas is tightly associated with the mass flow rate of air required by the engine. In response to that, the rpm of an engine is directly proportioned to the pressure drop inside the lamella. In other words, high rpm yields a high-pressure drop, and low rpm yields a low-pressure drop.

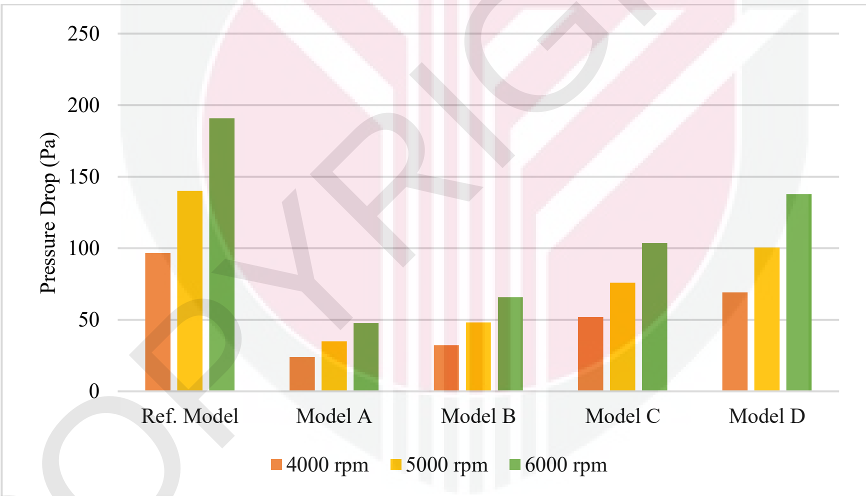

Figure 4.8: Comparison of pressure drop for each model at different rpm

4.2.6 Number of transfer units-NTU

In heat exchanger design, a number of transfer units (NTU) have a significant role. The performance of a heat exchanger can be easily assessed if the number of transfer units is known. The number of transfer units amalgamates overall heat transfer coefficients, transfer area, fluid flow rate, and heat capability. It combines all of these dimensional variables into a single dimensionless parameter. NTUs for each model are presented in

Figure 4.9. Model D has the highest number of transfer units, 0.592 at 6000 rpm, comparable to all other models, followed by model C, model B, model A, and the reference model. NTU of model D is 91.2% greater than the reference model at 6000 rpm. The highest number of transfer units for model D advocates that model D is the most effective model compared to all other models. The trend of NTU obtained from the column chart is directly proportional to the aspect ratio of lamellas and inversely proportional to engine speed. Normally for NTU > 5, the exit temperature of the fluid becomes almost equal to the surface temperature. A small value of NTU indicates more heat transfer opportunities, which can be obtained by adding more surface area. As for this study, the availability of space in engine bays is the controlled parameter; consequently, increasing the shell box's dimensions is not feasible.

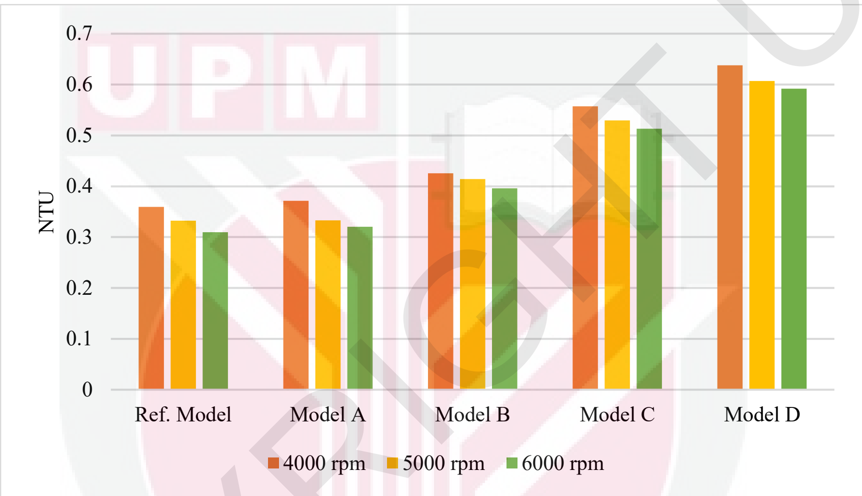

Figure 4.9: Comparison of number of transfer units (NTU) for each model at different rpm

4.2.7 Logarithmic mean temperature difference (LMTD)

The logarithmic mean temperature difference ΔT_{ln} is usually obtained by locating the actual temperature profile of the fluid along the channel and a precise demonstration of the average temperature difference between the fluid and the surface. It truly reflects the exponential decay of the local temperature difference. Figure 4.10 display the LMTD's of each model under consideration. A negative sign, along with the values, represents the heat released from hot air due to the cooling process. At 6000 rpm, model D has the lowest value of LMTD, i.e., -33.34°C, comparable to all other models, clearly depicting that the average air temperature difference is close to surface temperature, which is the temperature of the refrigerant. The reference model (shell and tube) has the highest LMTD value, i.e. -39°C at 6000 rpm. The trend of the LMTD chart is also influenced by the aspect ratio of the lamella. As the aspect ratio increases, the logarithmic mean temperature difference decreases.

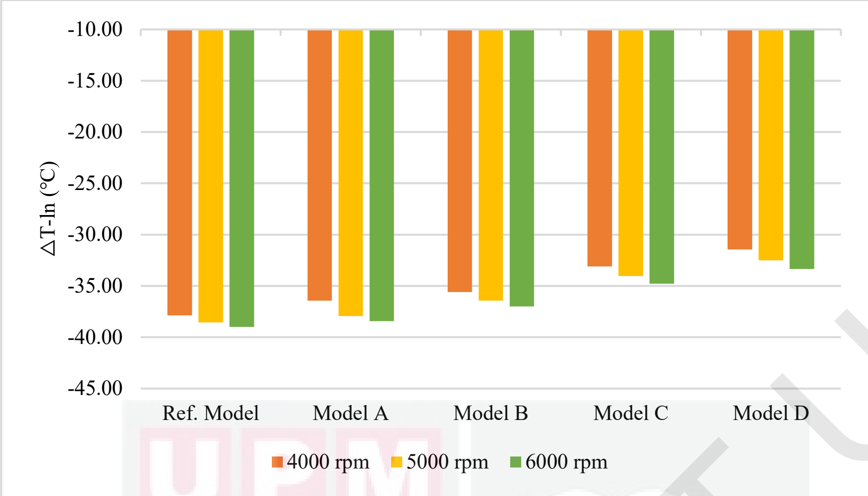

Figure 4.10: Comparison of LMTD's for each model at different rpm

4.2.8 Conclusion from numerical results

Results clearly express that all the parameters, except LMTD, are inversely proportional to the inside opening of the lamella and directly proportional to the aspect ratio of the lamella. The less inside opening of the lamella results in more heat transfer, temperature drop, number of transfer units, and pressure drop. Based on the parameters under consideration, all models are ranked from high to low: model D, model C, model B, and model A. All four models have high heat transfer, NTU, temperature drop, and less pressure drop compared to the reference model. Although model D has the highest temperature drop and pressure drop is also within the maximum allowable limit. However, the pressure drop will further rise at higher rpm ranges. Moreover, there are some other considerations that need to be considered for the final selection of the geometry. For that, a multi-weigh scoring model is used to finalize the geometry, given in Table 4.1. Criteria is established according to the requirement and restrictions of the intercooler heat exchanger. Each selection criterion is assigned a weight, and the total weight is 11. The highest weight is given to temperature drop (5), followed by pressure drop (3), ease of fabrication (1), low fabrication cost (1), and low fabrication time (1). Scores are assigned to each criterion for all models (0 to 10) based on their performance and importance. The weights and scores are multiplied to get a total weighted score for the project. Using these multiple screening criteria, proposed models are compared, and the model with the higher weighted score is considered better, which is model C.

Table 4.1: Multi-weigh scoring model

Criteria particulars	Weight	Model A	Model A Weighted	Model B	Model B Weighted	Model C	Model C Weighted	Model D	Model D Weighted
Temperature drop	5	5	25	7	35	9	45	10	50
Pressure drop	3	10	30	9	27	7	21	5	15
Ease of fabrication	1	10	10	9	9	8	8	7	7
Low fabrication cost	1	10	10	9	9	8	8	7	7
Low fabrication time	1	10	10	9	9	8	8	7	7
SUM			**85**		**89**		**90**		**86**

4.3 Numerical results of the final selected LHE design

As the final size or outer dimensions of the model depends on the available space in the test vehicle engine bay, i.e., 1.5L Proton Wira SE, a detailed description was provided in section 3.4.4. The maximum available space measured in the engine bay was 0.007 m^3, as shown in Figure 3.16. The available space is directly related to shell box size. However, the inner geometry dimensions are selected from the analysis of the above numerical study in which model C is found better. The final dimensions of the model are already given in Figure 3.17.

4.3.1 Air flow characteristics inside lamella and intake duct

Before proceeding to the numerical results, it is important to apprehend the airflow characteristics inside lamellas and intake duct. In this regard, the volume and mass flow rate of air induced by the engine is calculated theoretically to evaluate the airflow characteristics. The volume flow rate in equation (3-12) was used to calculate theoretical airflow for the engine at different engine speeds. Figure 4.11 demonstrates the trend of volume and mass flow rate of air against engine speed. The volume and mass flow rate of air increases with the increment in engine speed. This means that a higher amount of air is required to burn fuel properly at higher engine speed. Figure 4.12 demonstrates the velocities and corresponding Reynolds number of airflow at different engine speeds, both for the intake duct and inside lamellas. The velocity and corresponding Reynolds number increase with the increase in engine speed. However, the velocity and corresponding Reynolds number for airflow inside lamellas are small. The reason behind this is that the cross-sectional area of the intake duct is smaller than the cross-sectional area of total lamella channels.

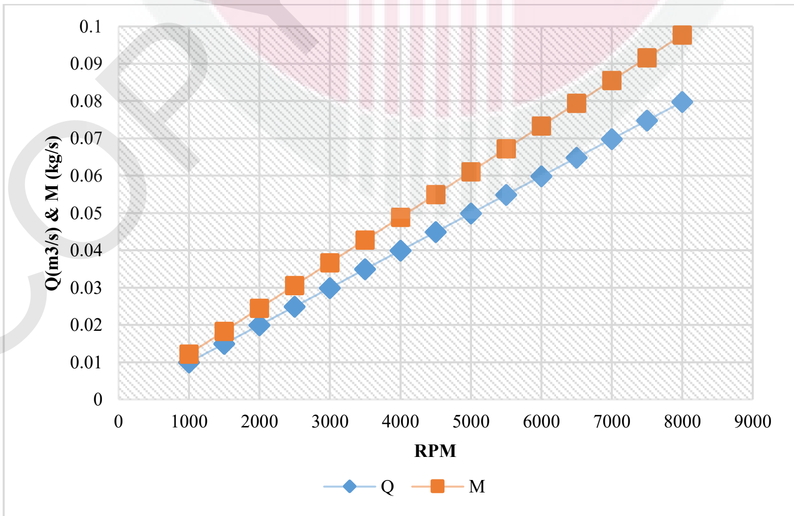

Figure 4.11: Volume and mass flow rate of air required by the engine at different engine speeds

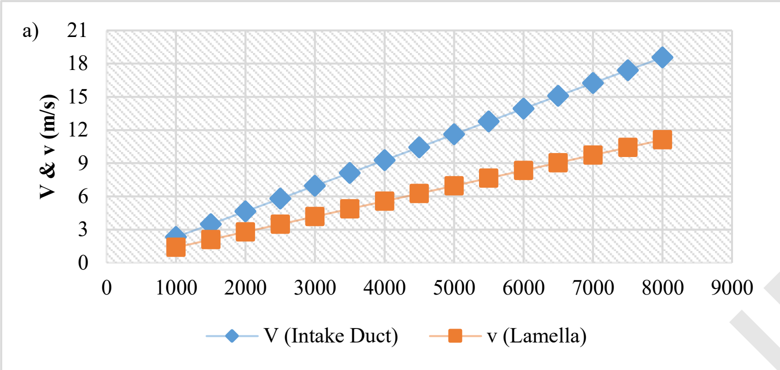

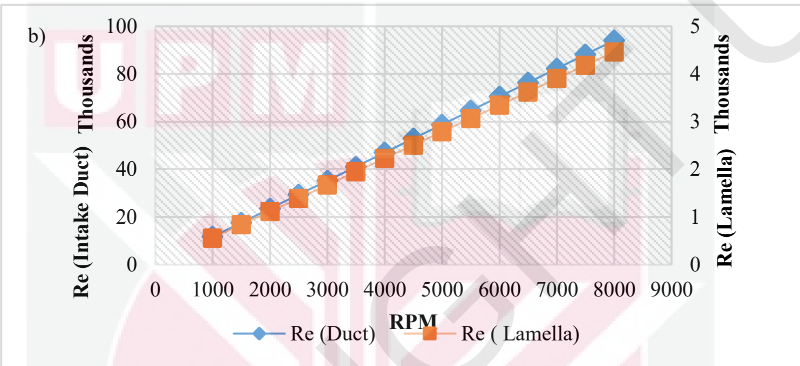

Figure 4.12: a) velocities and their corresponding, b) Reynolds number inside intake duct and lamellas

4.3.2 Verification of numerical results

The credibility of simulations is achieved through verification to estimate the degree of accuracy to which the model represents the real phenomenon, and it involves extensive comparisons with experiments. For the present study, the experimental correlation of the nusselt number and pressure drop available in the literature is utilized for comparison to verify the CFD simulations, to build confidence that the governing equations are solved with certain accuracy, and that the results are obtained by solving the right model equations. Details of the correlations already provided in section 3.4.7.

4.3.2.1 Nusselt number

For the hot intake air entering at 45℃ into LHE, Figure 4.13 shows the nusselt number against different rpm ranges, is validated through Dittus Boelter and Gnielinski equation. The results show good agreement between CFD and experimental correlations. The CFD results fall in the middle of both the experimental correlations. The CFD results coincided more with the Gnielinski equation at higher rpm and more coincided with the Dittus Boelter equation at a lower rpm range. Both the experimental correlations are valid and have high precision for a particular range of Reynolds number, due to which their results are presented for the available limits of Reynolds numbers in this study.

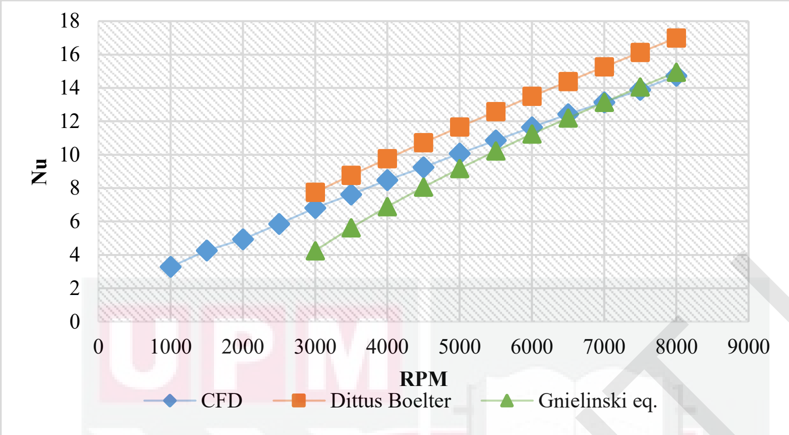

Figure 4.13: Comparison of CFD result for nusselt number with Dittus Boelter and Gnielinski equation at 45℃ intake temperature

4.3.2.2 Pressure drop

For the hot intake air entering at 40℃ into LHE, Figure 4.14 shows the pressure drop against different rpm ranges, is validated through the pressure equation. The bar chart shows the equal distribution of percentages between CFD and experimental correlations. The maximum difference of 11.74% is observed at 1000 rpm. Hence, the results clearly show that CFD simulations are performed correctly.

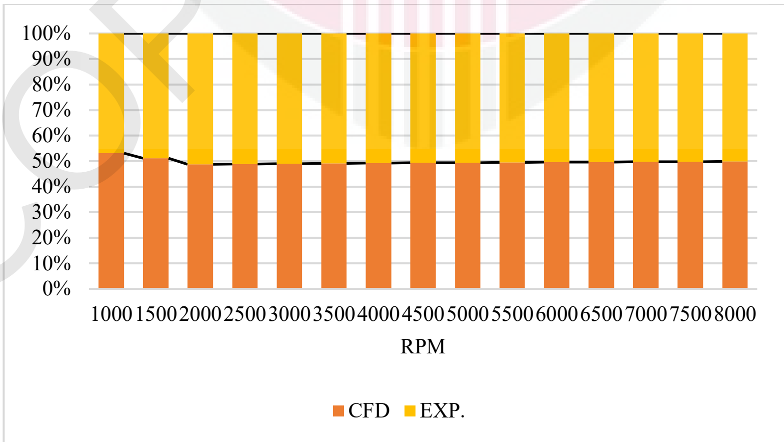

Figure 4.14: Pressure drop comparison between CFD and experimental correlations, at 40℃ intake temperature

4.3.3 Heat transfer

Heat transfer refers to the flow of heat due to temperature differences. Figure 4.15 shows the heat transfer amount from hot air to cold refrigerant. Higher heat transfer is observed for 55°C. This is due to the higher temperature difference between the hot and cold sides than the other temperature ranges, and that temperature difference is the driving force for heat transfer. The rise in the heat transfer amount is observed with the increment in rpm for all temperature ranges. The reason behind this is the intensification of the velocity gradients of air, which ultimately increase the convective heat transfer coefficient. The maximum heat transfer of 2.14 kW is observed at engine speed of 8000 rpm for 55°C intake air. Likewise, the minimum heat transfer of 0.42 kW is recorded at 1000 rpm for 40°C intake air. Further, the gap between the heat transfer amount for all temperature ranges rises with the engine speed.

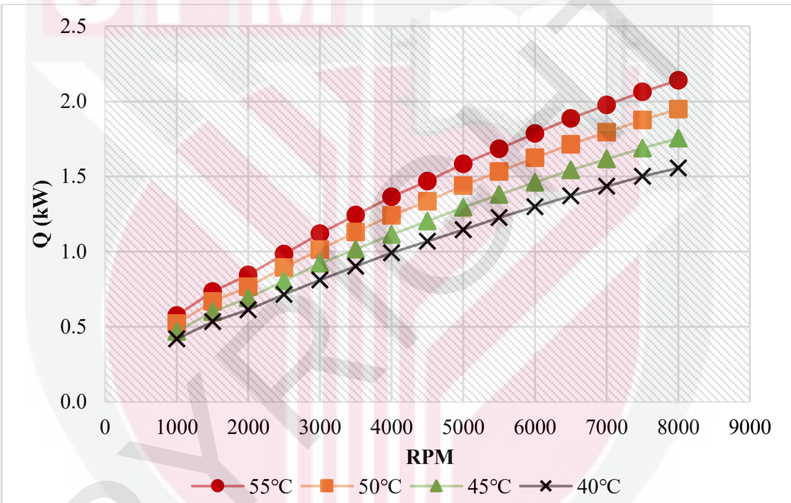

Figure 4.15: Heat transfer from hot air to cold refrigerant at different engine speeds and intake temperatures

4.3.4 Temperature drop

The temperature drop is a direct indication of energy extracted from hot air by the LHE. Figure 4.16 indicates the temperature drop at various engine speeds. As the engine speed increases, the temperature drop decrease. The higher temperature drop is observed for low engine speed. This is because, at low engine speed, the velocity of airflow inside lamella is too low, and it has sufficient time to be in contact with the cold walls of lamellas to lose its temperature. On the other hand, at higher engine speed, the time of contact between the air and a cooling surface is reduced due to an increase in flow rate and air velocity. As a result, it leads to a decrease in cooling impact, and a smaller temperature drop is observed. In other words, the air temperature drop is inversely proportional to engine speed. The maximum temperature drop of 46°C is observed at

1000 rpm for 55°C hot intake air. Likewise, the minimum temperature drop of 15.89°C is recorded at 8000 rpm for 40°C hot intake air. The temperature drop for 55°C hot intake air is higher at all engine speeds compared to the other intake temperatures. This is due to the maximum temperature difference between the hot air and the cold refrigerant.

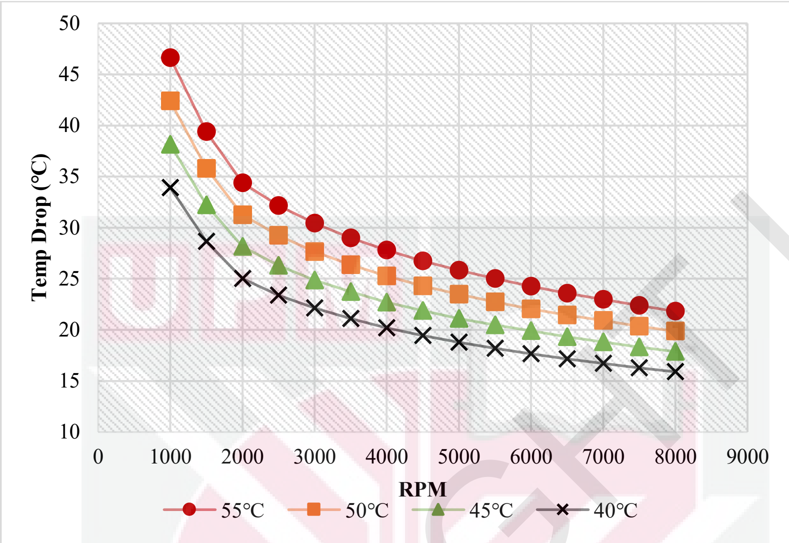

Figure 4.16: Temperature drop of air at different engine speeds and intake temperatures

4.3.5 Log Mean Temperature Difference (LMTD)

The LMTD is perhaps the most commonly known method to analyze heat transfer in heat exchangers. The LMTD for this study is a logarithmic average of the temperature difference between the hot intake air and cold refrigerant at each end of the LHE. The log mean temperature difference is recorded at various engines speed and presented in Figure 4.17 to determine the temperature driving force for heat transfer in LHE. The LMTD of the exchanger increases with the increase in engine speed. Generally, the larger the LMTD, the more heat is transferred. From the results, a higher value of LMTD is observed for the hottest air, i.e., 55°C, followed by 50°C, 45°C and 40°C, which endorsed the heat transfer result section. The lowest values for 40°C intake air means that the average temperature of this intake air inside LHE is close to refrigerant temperature.

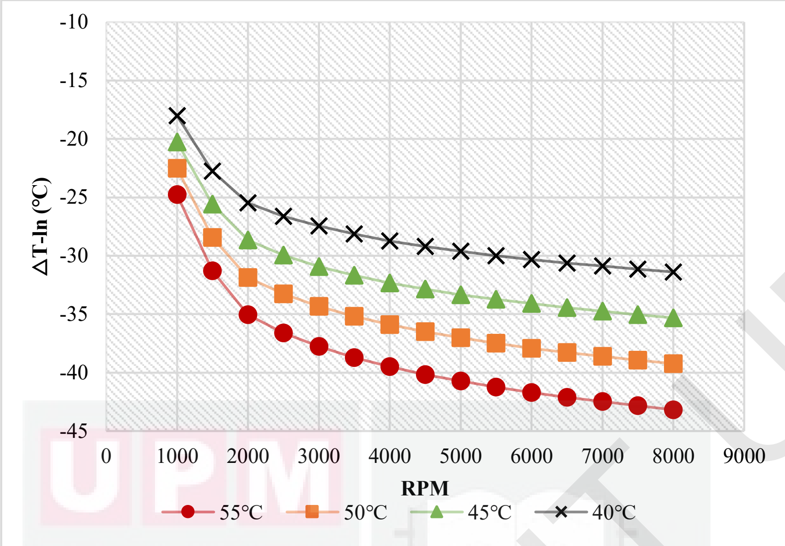

Figure 4.17: LMTDs at various engine speeds and intake temperatures

4.3.6 Number of Transfer Units (NTU)

The Number of Transfer Units (NTU) is the ratio of the heat exchanger's ability to transfer heat to the fluid's minimum ability to absorb heat. In other words, it measures the effectiveness of heat transfer systems. The number of transfer units at different engine speeds is plotted as a radar chart in Figure 4.18 for intake air at 55°C. The NTU decreases with the increase in engine speed. This clearly indicates that LHE is performing very well at low engine speed compared to higher engine speed. The effectiveness of the LHE decreases with the increase in engine speed. The trend of NTU endorsed the temperature drop result section.

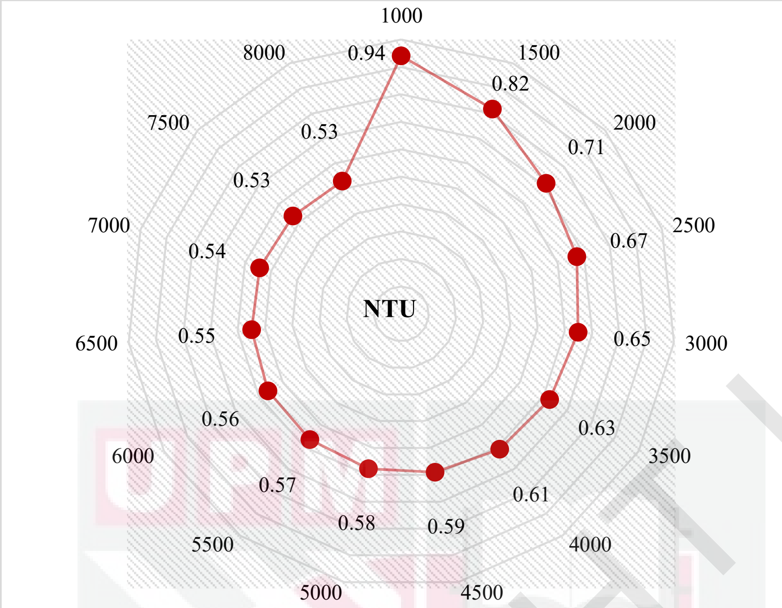

Figure 4.18: NTUs at various engine speeds for 55°C intake temperature

4.3.7 Temperature Contours

To observe the temperature distribution inside lamellas, temperature contours are presented in the middle section of the whole LHE (on left side) and for the lamella alone along the length (on right side) in Figure 4.19, for the case of 45°C intake air temperature.

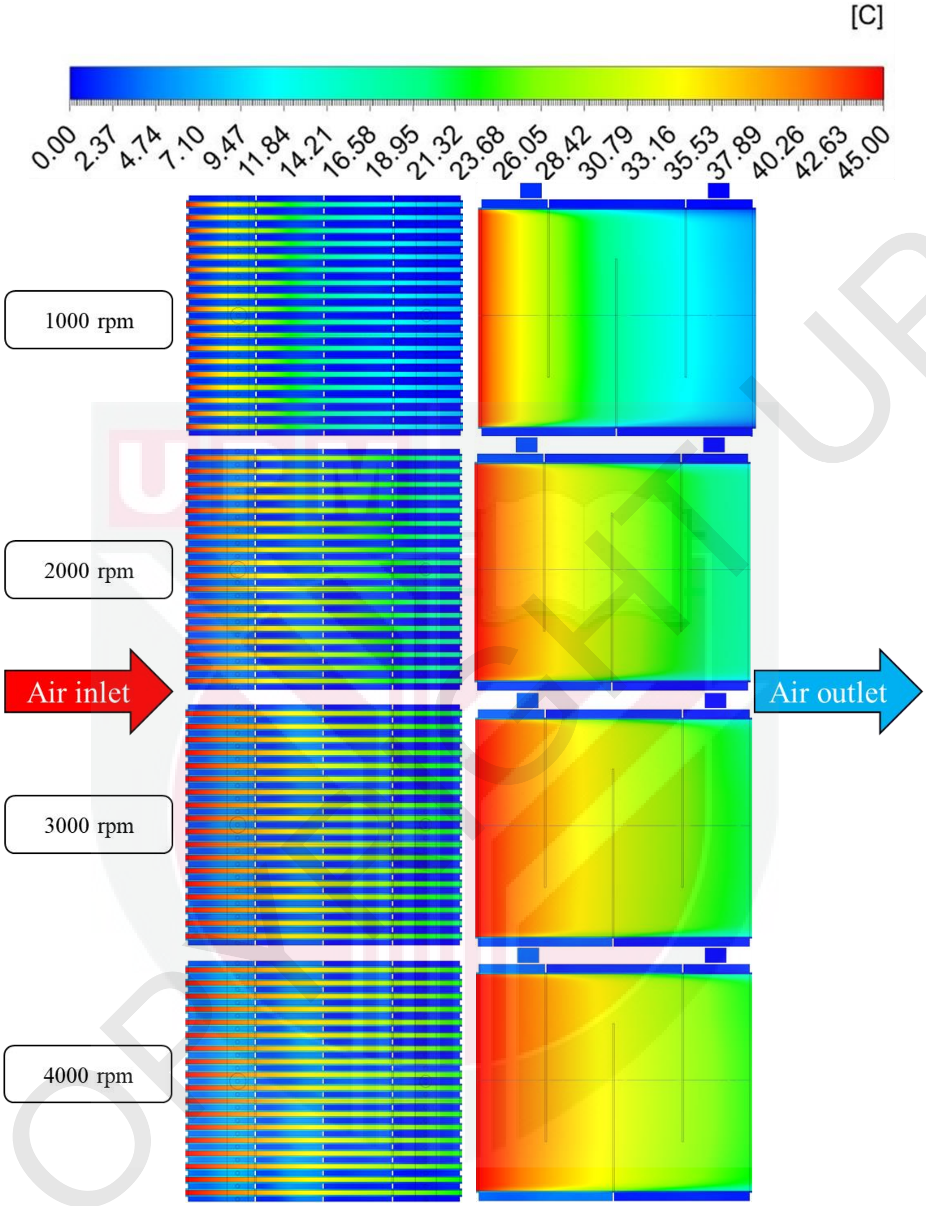

Figure 4.19: Temperature contours at various engine speeds for 45℃ intake temperature

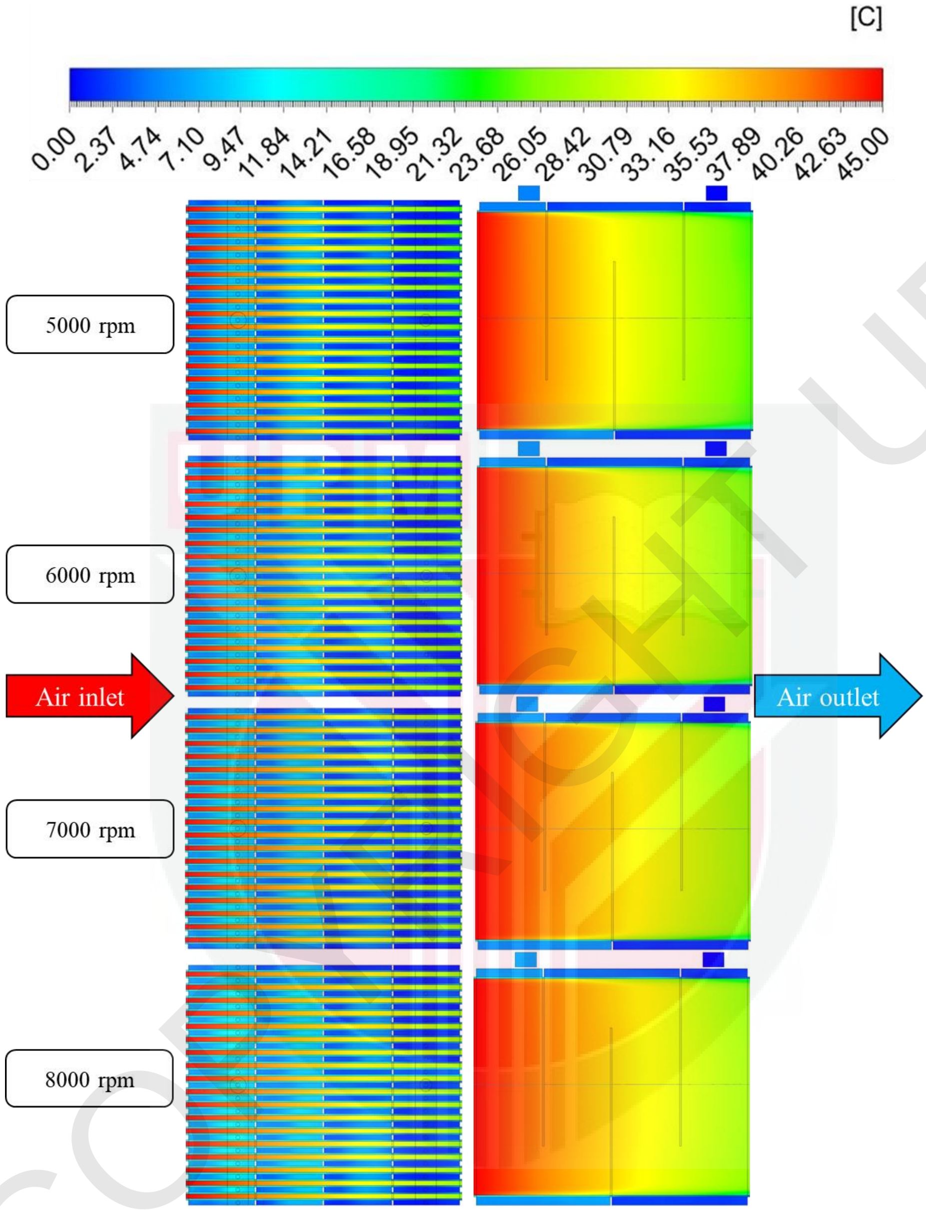

Figure 4.19: Temperature contours at various engine speeds for 45°C intake temperature (continued)

The temperature contours demonstrate the effect of various engine speeds (airflow velocity) on heat transfer distribution inside the LHE; the lower airflow speed shows better heat transfer, and the outlet air is reduced to a lower temperature. While at higher airflow velocity, the heat transfer is reduced, and higher outlet air temperature is observed. The temperature contours of the inner side of the lamella indicate that the hot air enters the lamella from one end and releases heat to the cold refrigerant circulating in the narrow channels of the shell box side, and thus air exits the lamella at a lower temperature. Further, the contours also display that the temperature of the cold refrigerant at the exit point gets higher and higher with the increment of engine speed, which indicates high heat transfer at higher engine speed. The temperature contours at the lamella interface body in 3D view are shown in Figure 4.20 for a better understanding of heat transfer between the two fluids. The thermal conductivity of the used material and its thickness has its own importance in heat transfer (Tran and Wang, 2019).

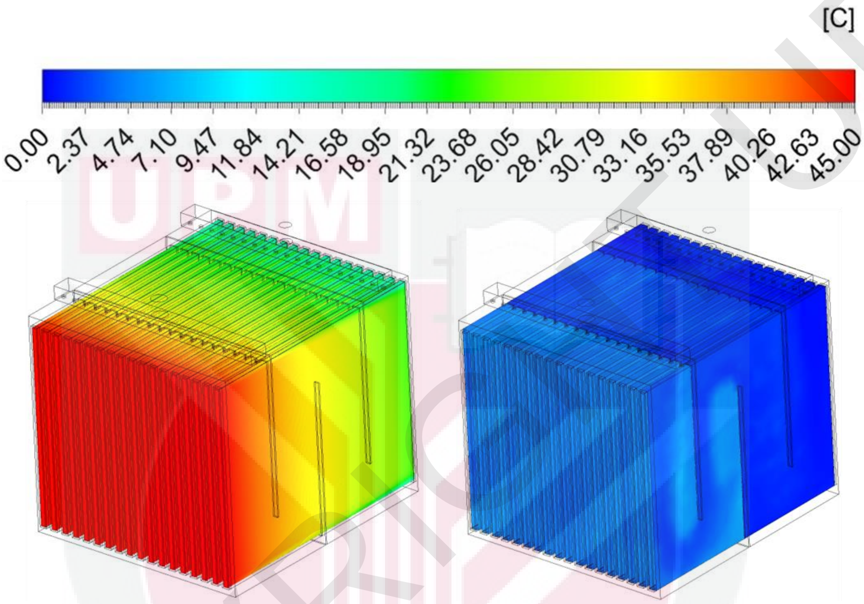

Figure 4.20: Temperature contours at lamellas wall interface for 45℃ intake air

4.4 Lab tests results

The experimental study shows to what extent the ideal conditions assumed in analytical and numerical studies can be realized in laboratory research. For the experimental laboratory measurement, there is some accuracy level of the sensors involved in it. Table 4.2 illustrates the uncertainty of each measurement and sensor used in the lab test.

Table 4.2: Summary table with the characteristics of the instrumentation and sensors used in the experimental set-up

Parameters	Measuring apparatus	Variable measured	Range	Accuracy
Temperature	Thermocouple	T1 T2 T3 T4	0--55℃	±0.7%
Pressure	Differential pressure manometers	P1 P2	0--100Pa	±0.5%
Speed	Anemometer	RPM	1000--8000	-2.5%

4.4.1 Validation of fabricated LHE

The validation of the fabricated LHE model with the numerical results will be the green signal to the next stage of the applied real-world vehicle test. The fabricated model of LHE is validated through experimentation in the laboratory with the numerical study under the same boundary conditions. For the said purpose, the temperature drops and the corresponding heat transfer results are reported.

4.4.1.1 Temperature drop

The temperature drops in Figure 4.21 is presented for both numerical and experimental results. Through experiments, the same trend and behavior of temperature drop are observed as for numerical study, showing good agreement between numerical and experimental results. The percentage error is shown in Figure 4.22. The column chart of percentage error shows higher errors at higher engine speeds but within the acceptable range. The maximum error of 15.7% is recorded for 55°C intake air at 8000 rpm, and the minimum amount of percentage error is 0.66% for 40°C intake air at 1500 rpm.

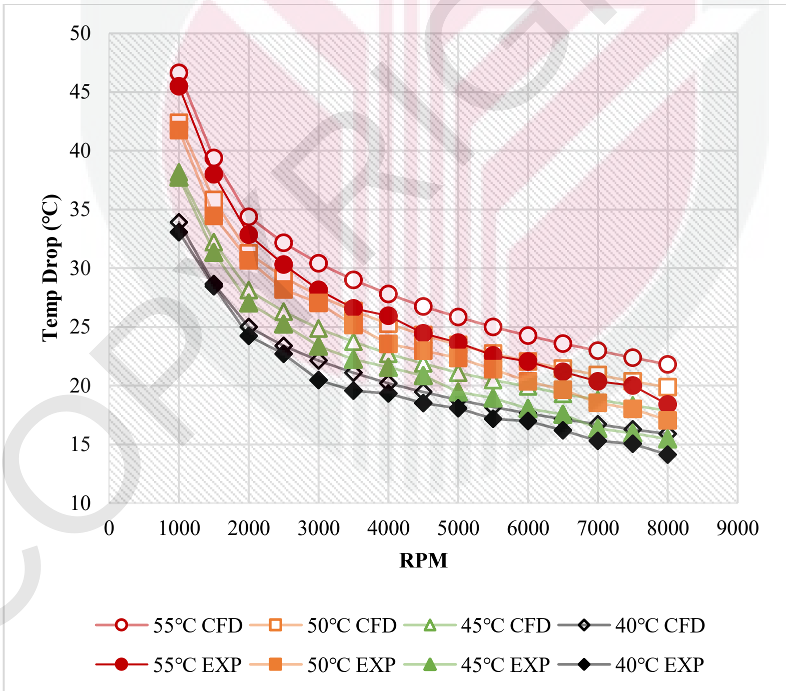

Figure 4.21: Comparison of temperature drop between experimental and numerical outcomes at various engine speeds and intake temperatures

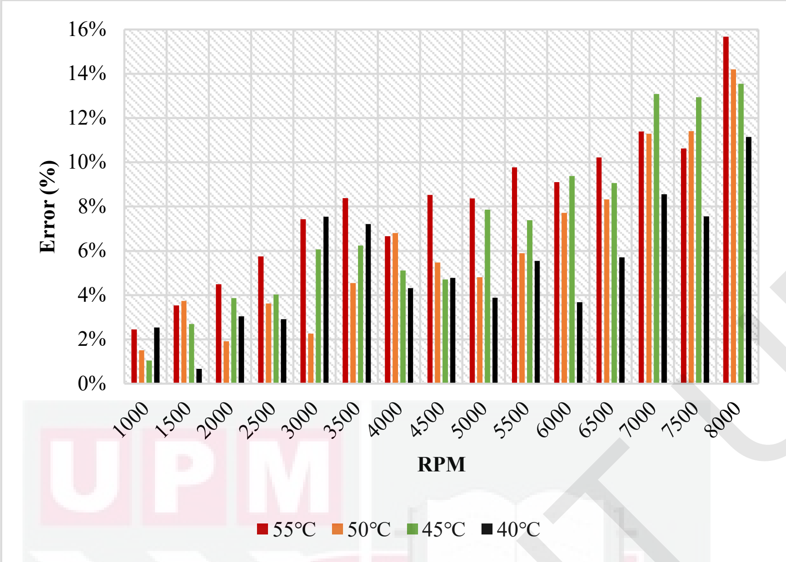

Figure 4.22: Percentage error of temperature drop between numerical and experimental outcomes

4.4.1.2 Heat transfer

The corresponding heat transfer of the temperature drop result is shown in Figure 4.23, and the percentage error of the results is presented in Figure 4.24. Likewise, the temperature drops, same trend, and behavior of heat transfer through experimentation are observed compared to numerical results. The maximum error of 15.68% is recorded for 55°C intake air at 8000 rpm, and the minimum amount of percentage error is 1.07% for 40°C intake air at 1000 rpm. The percentage error for 55°C intake air is high for most of the engine speeds for temperature drop and heat transfer. The reason behind this is disclosed in the refrigerant performance section because the inlet temperature of refrigerant plays an important role here.

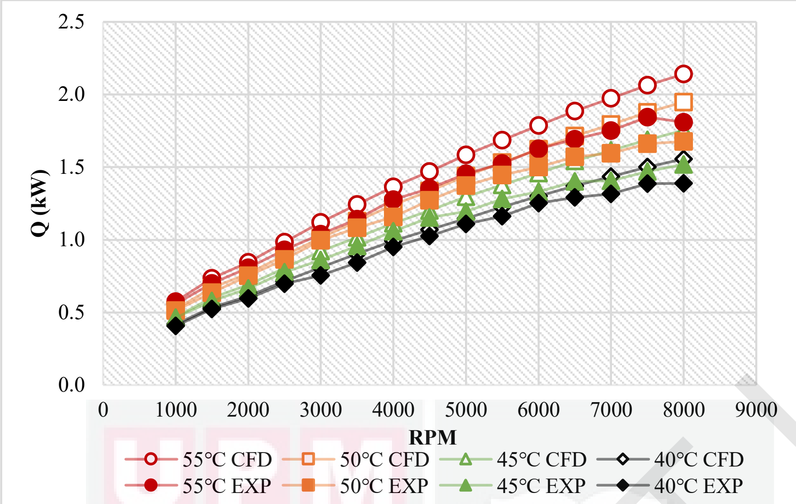

Figure 4.23: Comparison of heat transfer between experimental and numerical outcomes at various engine speeds and intake temperatures

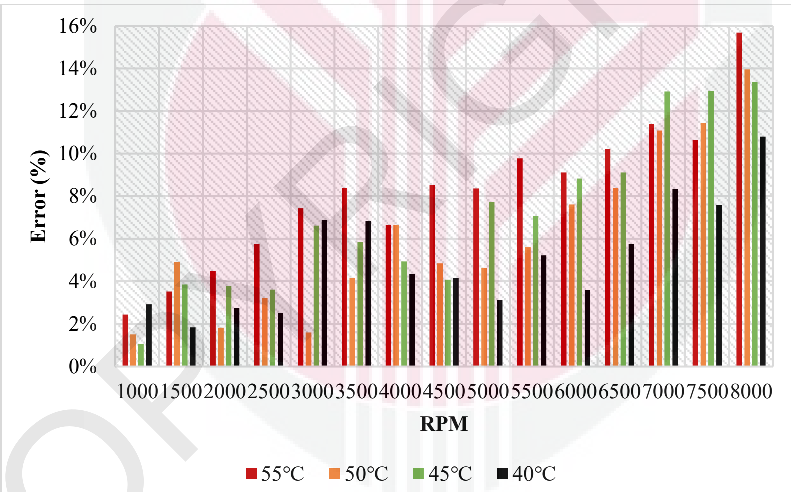

Figure 4.24: Percentage error of temperature drop between numerical and experimental outcomes

4.4.1.3 Uncertainties in temperature and heat transfer results

The rising trend of uncertainties for both parameters i.e. temperature drop and heat transfer, is observed at high engine speed. The maximum error of 15.7% is recorded for 55°C intake air at 8000 rpm. The reason behind this high difference between numerical and experimental results is due to the application of boundary condition i.e. refrigerant inlet temperature. For numerical study, the inlet temperature of refrigerant was set to

0℃, which couldn't be changed during the simulation process due to isentropic process. However, in laboratory conditions, the refrigerant inlet temperature couldn't be fixed and eventually there is no ideal process. Basically, the temperature of air that surrounds the refrigerant has an effect on its pressure. When the air temperature rises, the refrigerant absorbs that heat and causes an increment both in its temperature and pressure. If the system contained R-22, the vapor pressure would range from 58 to 85 Psig, but these pressures would also rely on the temperature of the wet bulb within the building and the outside ambient air temperature. The indoor wet bulb temperature displays the heat load within the building because it takes into account both temperature and humidity. The pressure on the vapor line will increase proportionally to the building's internal heat load. Subsequently, the higher the outdoor air temperature is, the less heat the system can reject outside. This also results in a higher vapor pressure (William C. Whitman et al., 2012). Assuming the LHE acting as an evaporator in VAC cycle, therefore for laboratory testing, indoor unit of the normal home split type air conditioning unit is replaced by LHE for testing purpose. R22 is the refrigerant gas used for laboratory testing. The evaporative suction pressure is set to 70 psi and the corresponding temperature of the refrigerant is 0°C, which can vary due to above-cited reasons in laboratory conditions. The refrigerant inlet and outlet temperature during the laboratory tests are presented in Figure 4.25. The highest increase in refrigerant inlet temperature is recorded for 55℃ intake air at a particular engine speed. This refers to the increase in the vapor pressure of refrigerant in the evaporator, which ultimately increases the temperature of the refrigerant. Likewise, the outlet temperature of the refrigerant is highest for the same intake air, i.e., 55℃. Therefore the only reason behind the dissimilarity between numerical and experimental results is the difference of the refrigerant inlet temperature, which should be 0℃, instead of 4.2℃ for laboratory conditions at 8000 rpm and accordingly for other various engine speeds and intake temperatures.

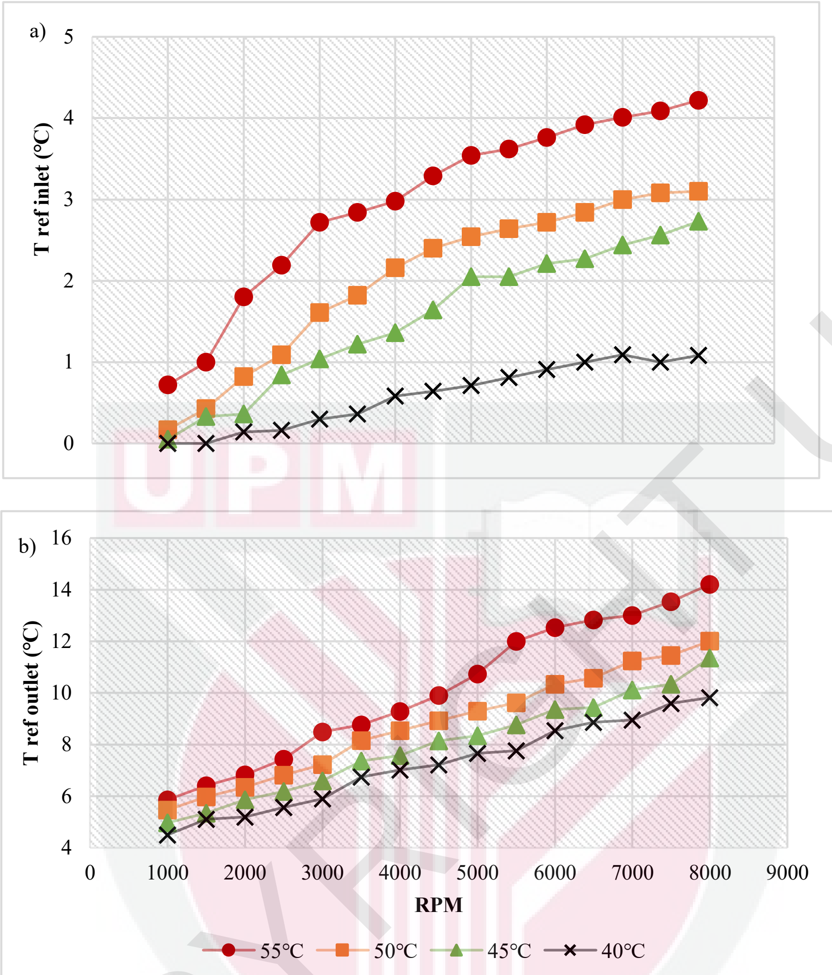

Figure 4.25: Refrigerant temperatures at various engine speeds and intake temperatures, a) inlet, b) outlet

4.4.2 Pressure drop test

The fabricated LHE model is tested for pressure drop at various engine speeds and intake air temperatures, presented in Figure 4.26. As expected, the increase in pressure drop is observed with the increase in engine speed for all the intake temperatures. Generally, the pressure drop inside lamellas or any tube depends on friction factor, length and hydraulic diameter of the lamella, density of air, and velocity of air. The said factors are directly proportional to the pressure drop. As air velocity inside lamella increases with the increase in engine speed, the collision between molecules increases resulting in greater loss of kinetic energy, subsequently, greater pressure drop. The pressure drop is different for different intake air temperatures. The highest pressure drop is observed for 40℃ intake air temperature. To understand the reason behind this, density variations are given in Figure 4.27 against the outlet temperature of the air at various engine speeds.

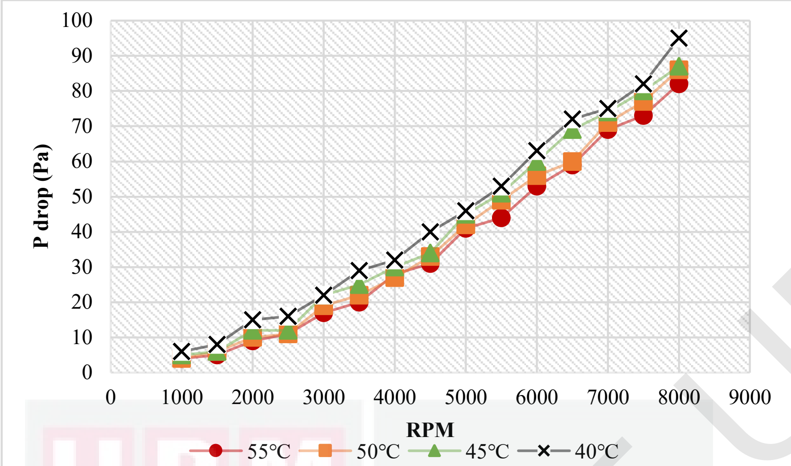

Figure 4.26: Pressure drop inside lamellas at various engine speeds and intake temperatures

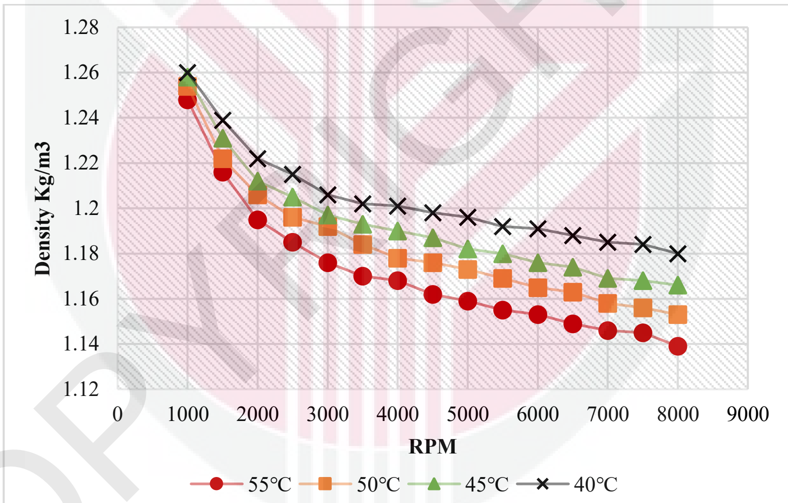

Figure 4.27: Density of air at the outlet section of lamellas (cold side) at various engine speeds and intake temperatures

As known, the density of air increase with the decrease in temperature. The lowest outlet temperature is recorded for 40°C intake air for all engine speeds. Therefore, the density of this intake air is higher as compared to other cases. As the density is directly proportional to pressure drop, resultantly, the highest pressure drop is recorded for 40°C intake air. The density of outlet air decreases with the increase in engine speed, referring towards the decrease in outlet temperature of air with the increase in engine speed.

4.4.3 Refrigerant performance

The average inlet and outlet temperature of refrigerant for all engine speeds at a particular intake air temperature is shown in Figure 4.28. The difference between the average inlet and outlet temperature of refrigerant refers to the real operation of the refrigerant cycle. Theoretically, the output refrigerant temperature and pressure should be isentropically equal, but in real applied operation, there is no ideal process in the refrigerant cycle. Also, the inlet and outlet temperature shows a gradual increase with the increase in intake temperature. Through the average inlet and outlet temperature of the refrigerant, the coefficient of performance is calculated and reported in Figure 4.29. The maximum COP is achieved for 40℃ intake air, and then a gradual decrement is observed with the increased intake temperature of the air. That means the refrigeration effect becomes less with the increase in intake temperature, and the compressor is required to work more.

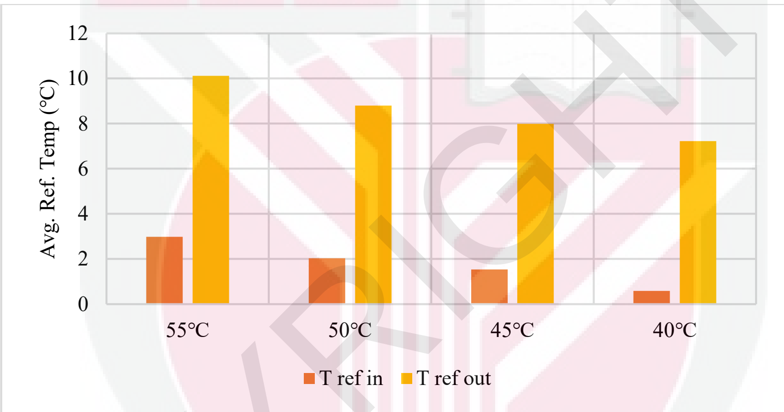

Figure 4.28: Average inlet and outlet refrigerant temperature for different intake air temperatures

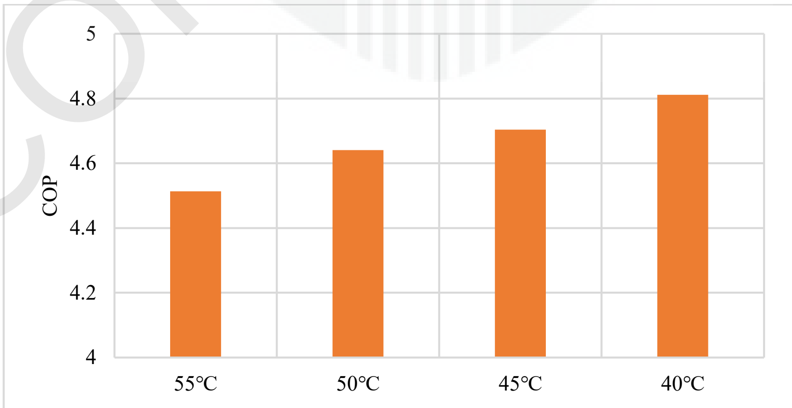

Figure 4.29: COP of LHE for different intake temperatures

4.5 Engine Performance during Vehicle running position

After the validation of the fabricated geometry through detailed testing in the laboratory, LHE was now installed in the test vehicle in order to check its performance on a real time basis and can perceive the actual effects of cold intake air on engine performance using a chassis dynamometer. The details of testing were already briefed in the methodology section. In short, the test was conducted in three stages; Stage one (Normal: neither air-conditioning nor LHE), Stage two (AC: use of vehicle air-conditioning), and Stage three (LHE+AC: use of vehicle air-conditioning along with LHE). Three tests of each stage are performed to ensure accurate data reading. The average temperature of the intake air during tests is presented in Table 4.3. The increase in the intake temperature of air for the AC test and decrease in intake temperature of air through LHE is recorded compared to the normal test during the dyno chassis test. Almost 30℃ decrement is observed through the use of LHE compared to AC stage test, which is 64.31% reduction in intake temperature. The minimum temperature attained (16.7℃) through LHE is dependent on the setting of the thermostat for cabin cooling temperature. No less than that temperature could be achieved from LHE and most of the vehicles cabin have lowest temperature limit up to 16℃ through AC. Moreover, when it comes to the comparison with the already existing intercoolers operating on VAC system, Pshtiwan Mohammad Sharif (2021) and Johnson, (2010) claimed 40.8% and 25.5% reduction in intake air temperature from their developed intercoolers, respectively. Further, Roberto Cipollone et al. (2017b), recorded a maximum 20℃ reduction in intake temperature through his designed intercooler. By keeping above, LHE shows admirable performance, when it comes to temperature drop of intake air and kept his supremacy among others existing intercoolers.

Table 4.3: Average intake air temperature during vehicle running test

Tests	Test Stages		
	Normal (℃)	AC (℃)	LHE+AC (℃)
1	40.7	46.8	16.7
2	40.9	47.1	17.6
3	41.5	48.6	18.8

4.5.1 Engine power

The maximum power obtained at wheels from the chassis dynamometer for each stage test and their associated average value of all tests for each stage is presented in Figure 4.30.

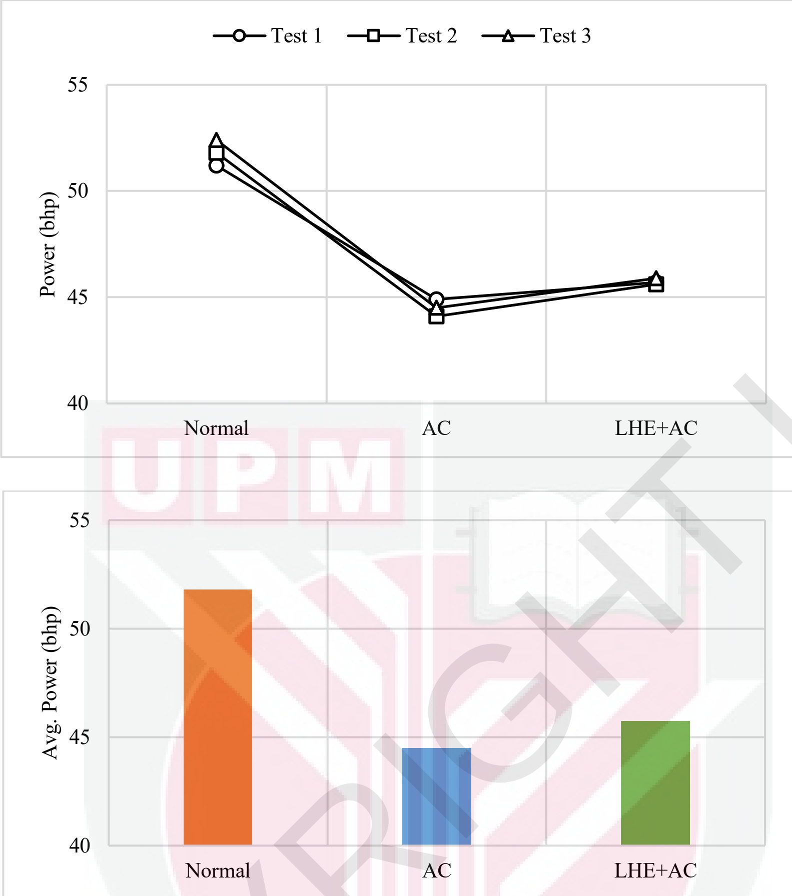

Figure 4.30: Maximum vehicle power comparison between different stage tests

As expected, the results clearly show the loss in power of the engine for the AC test, which consumed 7.3 bhp from the engine due to extra load on the engine, compared to the normal operation of the engine without air conditioning. On the other hand, cold intake air recovered some of the amount of lost power consumed by AC. The amount of 1.23 bhp is recorded for such loss recovered. The reason behind this gain in engine power is because of early center of heat release (COHR), due to cold intake air (Kadunic et al., 2014). This also evade the tendency of engine knock, as it requires late COHR (Virt et al., 2021). The COHR has a vital role in correlating engine performances especially related to combustion process and oxygen enrichment through reducing the intake air temperature is known to improve the overall combustion process and subsequently increasing heat release rate. The time available for the mixing of fuel and air before the onset of combustion is determined by the engine speed and the ignition delay. The ignition delay itself is mainly governed by the charge temperature and pressure (Heywood, 1988).

$$Chemical\ ignition\ delay = AP^{-n} exp \frac{E_a}{R_u x T} \qquad 4.1$$

Where; P: Cylinder pressure at injection timing

E_a: Apparent activation energy for the fuel auto ignition process
R_u: The universal gas constant (8.3143 J/mol·K)
A, n: Constants, dependent on the fuel

Therefore, EICAC technique prolongs the delay period (combustion duration) and tries to gain maximum output (power) from combustion. Conversely, high intake air temperatures increase the in-cylinder gas temperature at the end of the compression stroke and accelerate the chemical reactions, which is undesirable (Cinar et al., 2015). Further, the effect of intake temperature on power of an engine can also be elaborated with engine thermal efficiency (Al-Shemmeri, 2011). By keeping in mind the Equation 2.22, the influence of intake air temperature (-20℃ to 50℃) on engine thermal efficiency has been presented in figure 4.31 at constant engine speed of 2800 rpm with fuel ratio of 15:1. The results shows a significant impact of charge air cooling on engine performance. With the decrease in intake air temperature, the engine thermal efficiency increases, endorsing the increase in engine power due to cold intake air.

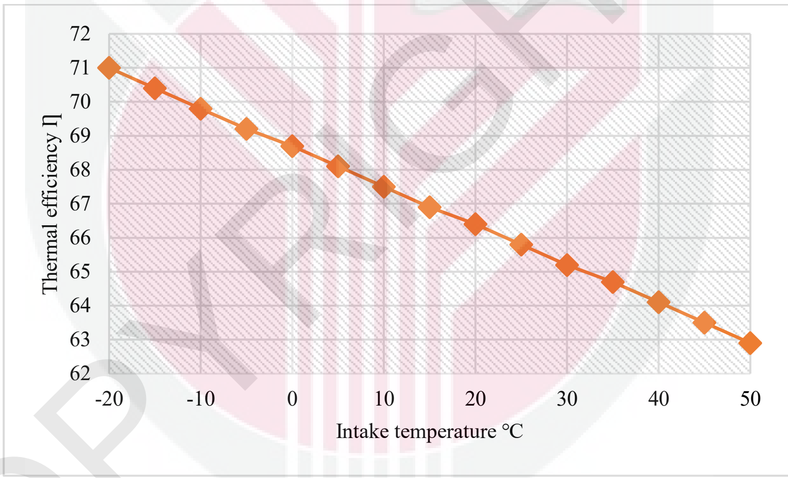

Figure 4.31: EICAC influence on engine thermal efficiency

4.5.1.1 Normal test (stage one)

The findings of three tests conducted for normal operation of engine power without air conditioning are presented in Figure 4.32. The maximum engine speed for all the tests and different stages is limited to 6500 rpm, which is the maximum allowable speed to reach by the test vehicle manufacturer. As shown in the figure, the maximum power of 52.3 bhp is recorded at wheels for test 3 at 5250 rpm. After the maximum power is achieved by the engine, the decline in power is observed at higher rpm till it reaches 6500 rpm.

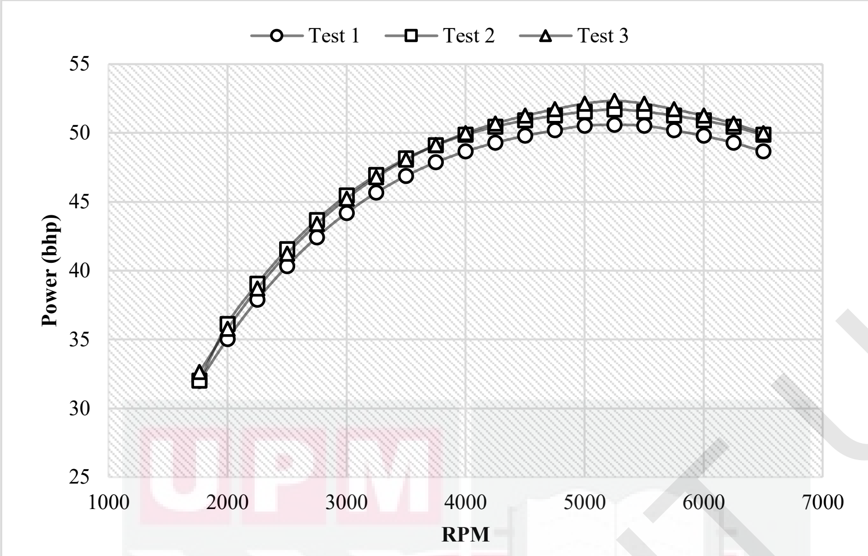

Figure 4.32: Power curves for three tests of normal stage

4.5.1.2 AC test (stage two)

The normal test helps to understand the vehicle output without any additional load on the engine to set a benchmark for comparison purposes with other stage tests. The power curves for AC tests and an average of normal test for comparison is presented in Figure 4.33. The AC test shows a reduction in engine power by 14% (7.3 bhp) compared to the normal test due to the additional load on the engine. The compressor of the air conditioning system is known to be the main reason for that power loss. As the compressor of the air conditioning system can add up to 5-6 kW peak power draw on a vehicle's engine, which is about the same load as air conditioning of a small single family home (Rugh et al., 2004). By converting the lost power due to AC for the current stage tests into kW, it falls within the range prescribed above, endorsing the AC test result.

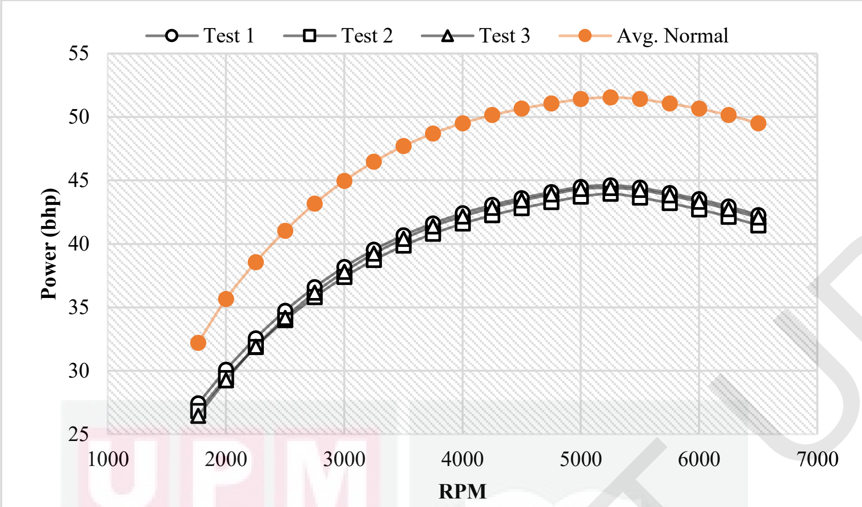

Figure 4.33: Power curves for three tests of AC stage, along with average of normal stage tests

4.5.1.3 LHE+AC (stage three)

The earlier tests determined how the test vehicle performed with and without the air conditioning. The third stage test is conducted using the LHE along with air-conditioning in a way that the intake air is first cooled to the lowest temperature obtained through LHE and then run the test vehicle on a chassis dynamometer to examine the effect of the cold intake air on engine power. The three test results from stage three, along with an average of normal and AC test, are shown in Figure 4.34, in order to provide better rationalization. A slightly high engine power curve is observed for cold intake air compared to the average of the AC tests. The highest power output is recorded at rpm 5250, with an extra power of 1.23 bhp compared to AC test. Out of the power loss from air conditioning (7.3 bhp), cold intake air recovered 17% (1.23 bhp) of it. Thus EICAC technique helps to recover the lost power due to air conditioning (Herbert Joyner, 1963). Treeamnuk et al. (2018), endorsed the present result and recorded a 3.2% increment in power due to cold intake air at 22°C, comparable to 50°C ambient intake air.

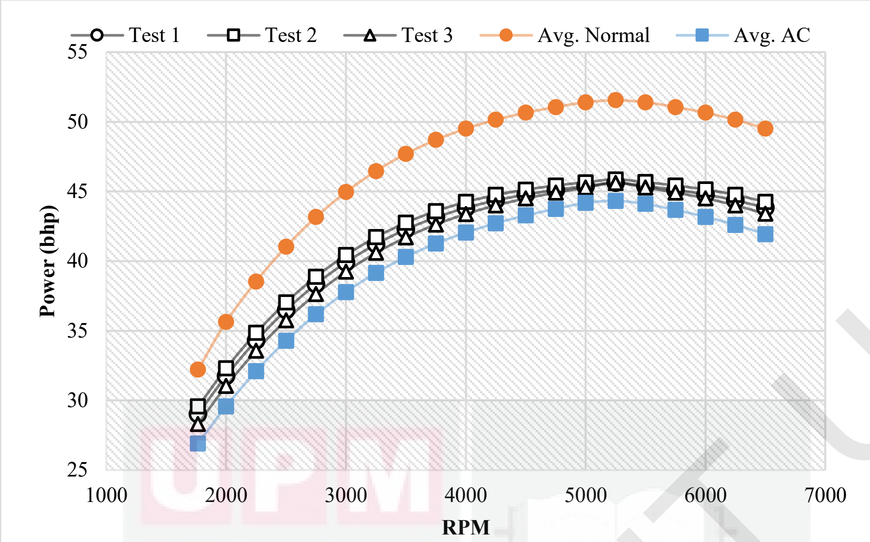

Figure 4.34: Power curves for three tests of LHE+AC stage, along with average curves of normal and AC stages

4.5.1.4 Conclusion of all stage tests

Figure 4.35 presented the average results of all the tests of different stages in one picture, which helped to understand the effect of air conditioning and of cold intake air on the engine power curve, compared to the normal test, neither with air conditioning nor with LHE. The trend of each power curve for all stage tests are same. However, the difference in their magnitude is observed. The primary reason for the lost power in the AC test, compared to the normal test, is the extra load on the engine, which the vehicular air conditioning system indulged on the engine and the compressor of the AC system is the main source. The amount of lost power due to air conditioning is recovered by 17% by bringing the cold intake air into the engine, in contrast to hot intake air. On the other side of the story, it is also observed that although cold intake air has a positive effect on engine power, but the impact of AC on engine power is higher than the output of cold intake air.

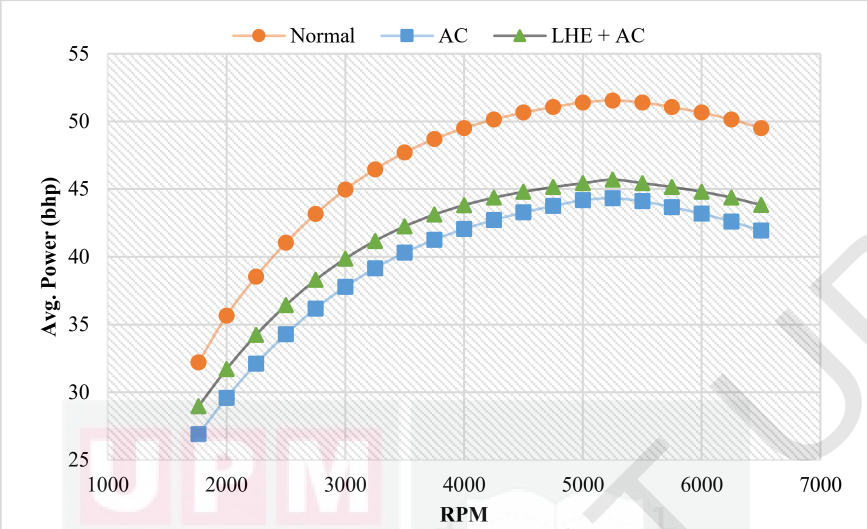

Figure 4.35: Comparison of average power curves for all stages

4.5.2 Engine torque

Generally, torque is the ability of an engine to perform work. The more torque an engine produces, the greater its ability to perform work. Both the torque and power of an engine are proportional to each other and measured to give learners a sense of the performance they might expect from the vehicle. The torque related to all stage tests and their overall associated average is shown in Figure 4.36 to provide an idea of how the engine performs under different situations. The torque for normal test provides a benchmark to compare with AC and LHE stage tests. The maximum torque recorded for the normal stage tests is 120.83 Nm. By turning the air conditioning ON, the amount of torque is decreased by 15.8 Nm, compared to the torque obtained for normal stage tests. The effect of cold intake air on engines torque is positive, adding 3.8 Nm of torque to the value obtained from the AC test. The trend of the recorded result agrees with Treeamnuk et al. (2018), that reducing the intake temperature increases the mass of air and pressure induced into engine. Therefore, the maximum pressure in cylinder after power stroke raises and creates the higher torque. The torque curves for each stage and tests are presented for further discussion.

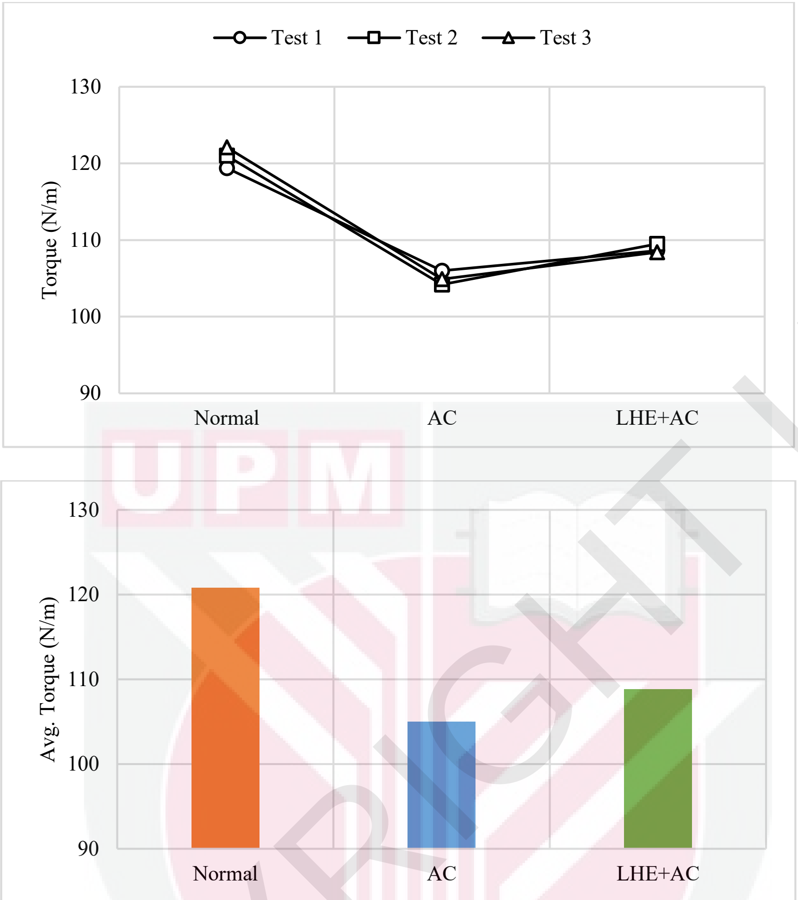

Figure 4.36: Maximum vehicle torque comparison between different stage tests

4.5.2.1 Normal test (stage one)

The torque curves related to three tests for the normal stage are presented in Figure 4.37. The lowest value of torque (107.05 Nm) is observed at minimum rpm; 1765. From this point with the increase in engine speed, the torque value increases significantly and found maximum value of torque (122.174 Nm) at rpm 3250. Further increase in engine speed from this point, the torque curve starts gradual decrement till the highest allowable engine speed.

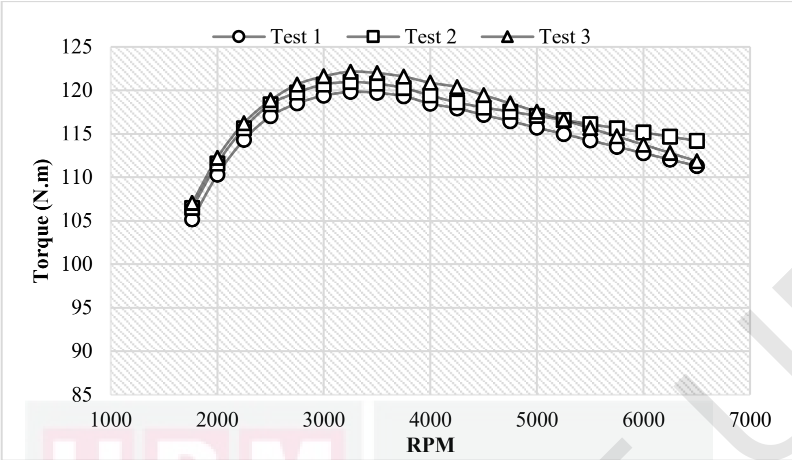

Figure 4.37: Engine torque curves for three tests of Normal stage

4.5.2.2 AC test (stage two)

After the completion of benchmark (normal test), the three tests for the second stage with the vehicle air conditioner were performed and reported in Figure 4.38. The trend of the engine torque curve for the AC test is similar to the normal test but with a difference in magnitude due to the AC load. The maximum torque of 107.5 Nm is recorded for test 2 at 3250 rpm, with a decrement of 13.5 Nm compared to the average normal test at the same rpm. Thus air conditioner puts inevitable pressure on the car's engine, affecting car performance by 13.07 %.

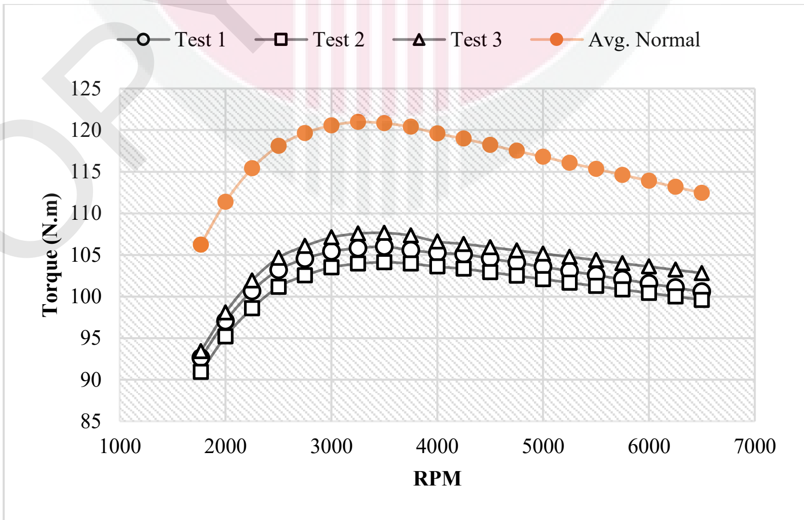

Figure 4.38: Engine torque curves for three tests of AC stage, along with average of Normal stage tests

4.5.2.3 LHE+AC (stage three)

The effect of cold intake air and the performance of LHE is shown through this stage tests. All three tests for stage three along with the average of normal and AC tests are shown in Figure 4.39. A slight increment in the engine torque curve is observed for cold intake air. The maximum torque of 109.47 Nm is recorded at the same rpm to which AC and Normal test provided their highest output, i.e., 3250, with an addition of 3.8 Nm compared to an average of AC test and decrement of 12 Nm compared to an average of normal tests. The amount of lost torque due to AC load is partially recovered by 24.06% by applying the EICAC technique.

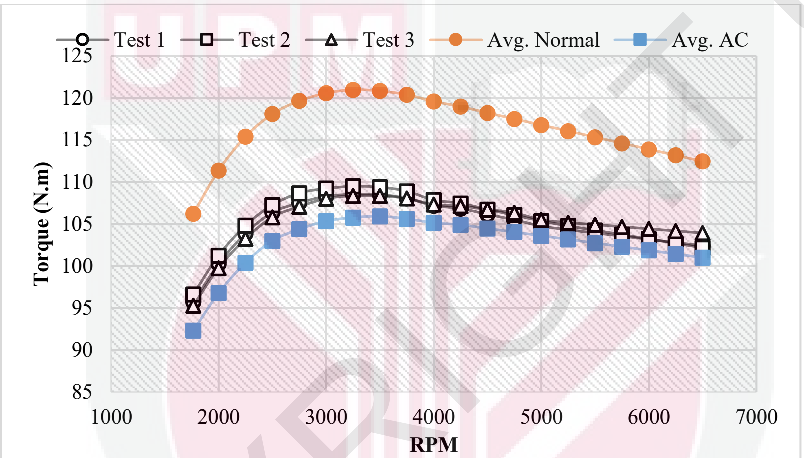

Figure 4.39: Engine torque curves for three test of LHE+AC stage, along with average curves of Normal and AC stages

4.5.2.4 Conclusion of all stage tests

Figure 4.40 shows the averages of all tests conducted for various stages in one image, making it easier to understand the impact of both cold intake air and air conditioning on engine torque curves. The trend of all curves is similar to each other with a difference in magnitude. The AC of a test vehicle consumed 13.07% of engine torque compared to a normal test. LHE, along with the air conditioner, introduced cold air into the engine and recovered the amount of lost torque in the AC test by 24.06 %. The gap at the initial rpm stages is higher between AC and LHE+AC curves till rpm 4250. Afterward, the gap between curves becomes decreased. The reason for this decrement in the gap at higher rpm is that, the suction of air increases to meet the engine demand, due to which more mass of air passes through LHE at higher speed, which decreases the time of contact of hot air and lamella cold surface, results in less temperature drop of intake air at high rpm. Kadunic et al. (2014) presented a maximum torque increment by 12% with the 30K reduction in intake temperature for 1.4L turbocharged SI engine, through AC driven intercooler.

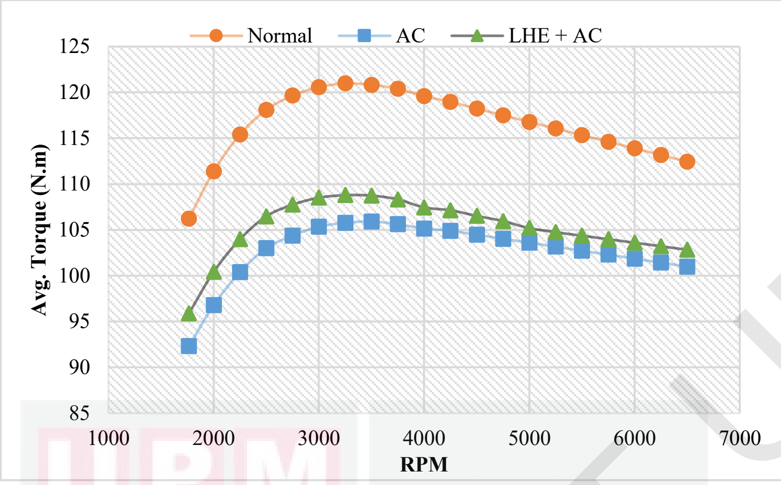

Figure 4.40: Comparison of average engine torque curves for all stages

4.5.3 Comparison with the reference model

Pshtiwan Mohammad Sharif (2021) claimed in his study during testing on same vehicle model and size which was used for this study, that the cold intake air recovered almost all the lost power and torque caused by VAC systems through his proposed EIHE; it was the same model that the present study adopted for initial numerical simulations, termed as “reference model” taken from (Pshtiwan M. Sharif et al., 2019). That triggered the attention of the author by keeping in view the power and torque results for the present study. Even though the initial numerical results proved the better performance of LHE than the EIHE in all result sections. Further, by investigating the problem, a difference in the method of attachment of the intercooler with the VAC system was witnessed. The only difference between the present and reference method of attachment of intercoolers was the number of electric solenoid valves which separate the intercooler from the standard AC system, presented in Figure 4.41.

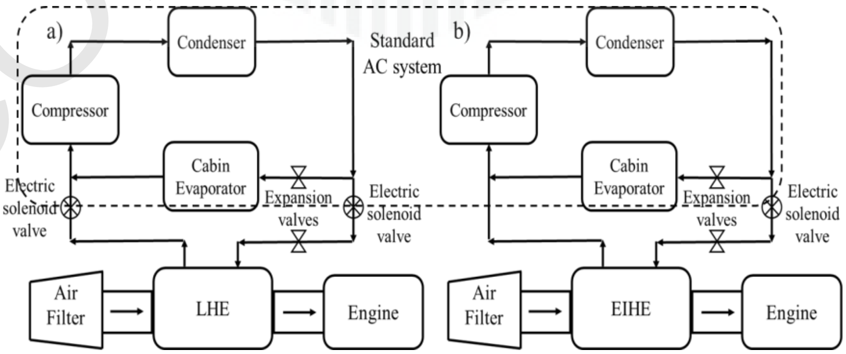

Figure 4.41: Method of attachment of intercooler with standard AC system separated with solenoid valves, a) present method, and b) reference method

The basic purpose of the electric solenoid valve was to allow and cut the supply of refrigerant to the intercooler on demand. Two electric solenoid valve for the present study completely separated the additional loop added to install the LHE with standard VAC system. However, in figure 4.41b for reference method, only one electric solenoid valve was available to control the refrigerant. To examine the impact of solenoid valves on AC system, it's better to elucidate the working parameters of standard VAC system. To attain adequate cooling in vehicle cabin, the vapor compression cycle of VAC system containing R134a as refrigerant must have to maintain the exact amount of refrigerant charge that system requires. This can be achieved either through maintaining the operating pressures (high and low side) given in Table 4.4 or by filling the refrigerant in terms of weight. For any VAC system, there is some minimum and maximum weight of refrigerant that can be inserted, usually mentioned in the engine bay through sticker. Other than the mentioned weight value, it causes problems in the VAC system in terms of damaging products and inadequate cooling. For the present test vehicle and also for a normal size car, it was 0.500 grams to 0.580 grams for the standard AC system. By inserting that much weight, the VAC system ultimately operates with the same pressure ranges as mentioned in Table 4.4.

Table 4.4: Operating temperature and pressure of the refrigerant R134a

Particulars	Values	Reference
Low side temperature and pressure (Evaporator)	0 - 4℃	(Harris & Hughes, 2011)
	2.8 - 3.25 bar	(X. Chen et al., 2020)
High side temperature and pressure (Condenser)	47 – 57℃	
	12 – 15 bar	(Shana, 2021)

As for the present study, an additional component (LHE) installed in the standard AC cycle, therefore, extra amount of refrigerant was added compared to the standard AC cycle. The vehicle AC system was charged by running both the evaporators for cabin cooling and cold intake air for the engine. The refrigerant continued to charge until the operating pressures were achieved, which helped to maintain the best cabin cooling as well as intake air. The role of two electric solenoid valves was important in the sense that it regulates the additional loop of refrigerant added to the standard AC system. To operate the LHE, both electric solenoid valves opened to circulate the additional refrigerant in the loop, and closed when only standard AC system requires by the vehicle passenger. In the closing position, the extra amount of refrigerant added will remain in LHE, and the standard AC system will run with its original amount of refrigerant and maintain its operating pressures. Subsequently, the cooling and other components of the AC system will not affect. The same was observed in the present study. On the other side, the method introduced by Pshtiwan Mohammad Sharif (2021) contained only one electric solenoid valve on the inlet side of the refrigerant. To compare the results, the same method was also applied for the present study to test LHE by keeping the electric solenoid valve "ON" to the compressor side at all times, through which the present system resembles the reference method. The performance of LHE was checked against that setup. The testing was divided into two categories, A and B.

Category A

The category A test was for the extra amount of refrigerant added in the additional or bypass loop as for the present study method.

i. For the LHE+AC stage test, the vehicle performance was the same as it was with the present study method with two electric solenoid valves, and cabin cooling was also admirable.

ii. For the standard AC stage test, the vehicle shows a problem with the AC system. The compressor was tripping on and off again and again, loud noises started from the AC system, and no cooling in the cabin was observed. The reason behind this problem was that the extra refrigerant on the LHE side moved towards the standard AC system due to the suction of the compressor, as the electric solenoid valve of the compressor side was opened, while the electric solenoid valve of the other side remained closed to protect the refrigerant moved towards LHE. This caused the overcharging of refrigerant in the standard AC system, resulting in warm air and loud noises from the AC system. Generally, overcharged system operated with very high temperature and pressure. The condenser may have a surplus of liquid refrigerant (Yuqing et al., 2018), and ultimately compressor may start to have liquid refrigerant get inside of it from the strain of the pressure. This will lower the lubrication in the compressor and allow oil to pool up and damaging it.

Category B

The category B test was conducted by eliminating the overcharged refrigerant from the Standard AC system to overcome the problems faced in the category A test.

i. For the AC stage test, the vehicle performance was the same as for the present study method for the AC stage test. Cooling inside the cabin was observed to be perfect in that case.

ii. For the LHE+AC stage test, the engine power curve obtained was near to the claim made by Pshtiwan Mohammad Sharif (2021). The lost power due to the air conditioning of the system seems to be recovered for this stage test by almost 70%, as presented in Figure 4.42. However, the cooling inside the cabin was poor and warm air was sensed.

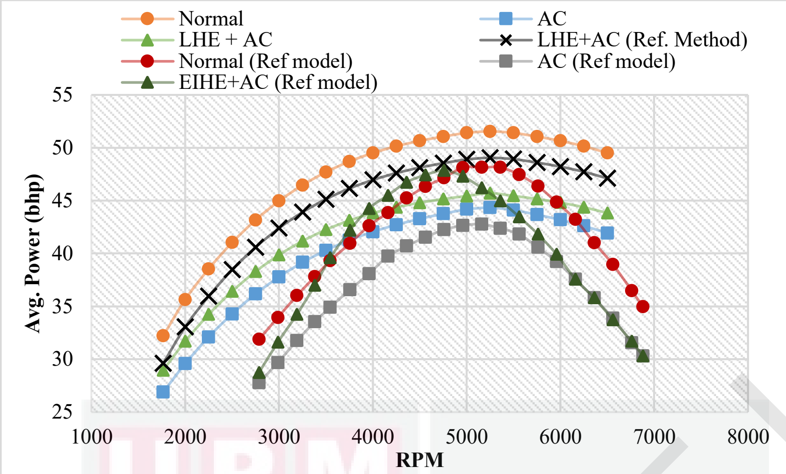

Figure 4.42: Comparison of average power curve obtained from reference method, along with other stage tests and the power curves derived from Pshtiwan Mohammad Sharif's (2021) study

The power curve from the reference method shows the better recovery of lost power. However, in reality the case is different. The reason behind this power curve is the lack of refrigerant in the AC system when operated with an additional loop of LHE. As a matter of fact, the refrigerant charge in the standard AC system is divided into two parts (cabin evaporator and LHE). Due to this reason the operating pressures of the VAC system could not be maintained. Consequently, neither cabin cooling nor intake air cooling was observed. Further low charge level of refrigerant for reference method, compressor requires less input power compared to a fully charged system, as for the present study method (Goswami et al., 2001). Therefore, it can be concluded that the improvement shown in power curve for the reference method is not due to the cold intake air but owing to the less power consumption by the compressor. The same trend and magnitude difference for torque curves is also observed and presented in Figure 4.43.

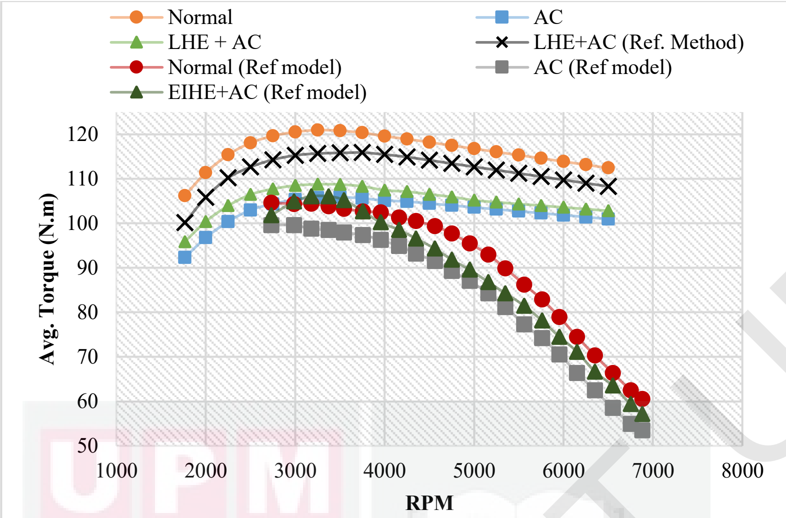

Figure 4.43: Comparison of average torque curve obtained from reference method, along with other stage tests and the torque curves derived from Pshtiwan Mohammad Sharif's (2021) study

The refrigerant charge amount is one of the main parameters affecting the refrigeration's system cooling performance and energy consumption (Yun & Chang, 2021). Both undercharged and overcharged reduced cooling equipment longevity, capacity, and efficiency (W. Kim & Braun, 2012). If the charge quantity of refrigerant is too small, only part of the evaporator will be infiltrated. The heat transfer area of the evaporator will not be fully utilized. The total evaporation capacity in the unit time will also be less, so the system cannot meet the suction requirements of the compressor. The evaporation pressure drops, the flow velocity decreases, the heat transfer coefficient of the evaporator decreases, the superheat of the evaporator outlet and the suction specific volume of the compressor increases, and the circulating flow and cooling capacity decreases. Moreover, the difference in the magnitude of the power and torque curves for the LHE model and EIHE (reference) model can be seen in Figure 4.42 and 4.43, especially for the normal and AC stage, where no cooling is involved. That particular difference is due to the amount of pressure drop in air flow engendered by the intercooler device. LHE model shows better engine power and torque curves compared to EIHE model, due to very minimal pressure drop caused by LHE in air flow (similar to stock system).

4.5.4 Vehicle emission performance

The gas analyzer was used to analyze the exhaust emission at the chassis dynamometer test, the final instrument report for all stage tests shown in Table 4.5.

Table 4.5: Vehicle emissions recorded during chassis dynamometer test

Stage	Test	Emissions				AFR
		CO (%)	CO_2 (%)	HC (PPM)	NO_x (PPM)	
Normal	1	0.682	11.52	277	702	17.354
	2	0.728	11.31	312	753	17.554
	3	0.691	11.33	286	731	17.865
	Average	0.700	11.38	291.66	728.66	17.601
AC	1	1.213	12.36	365	778	15.441
	2	1.146	12.31	347	780	15.534
	3	1.154	12.33	351	769	15.112
	Average	1.171	12.33	354.33	775.66	15.36
LHE+AC	1	0.921	11.96	321	746	15.987
	2	0.999	11.99	328	736	16.321
	3	0.977	11.91	325	754	16.569
	Average	0.965	11.95	324.66	745.33	16.292

4.5.4.1 Carbon Monoxide (CO)

The gas analyzer measures the CO in percentage (%) of the gas. The selected emission parameter (CO) measured for each stage and tests to evaluate the change response to the EICAC technique. The percentage of CO in the exhaust tailpipe of the vehicle for each test and its total average are presented in Figure 4.44. With the usage of AC in the vehicle, the CO is increased by 67.19% than normal operation of vehicle without air conditioning. By adding LHE with the aid of AC of the vehicle, a 17.6% reduction in CO is recorded compared to the emissions emitted during AC operation with ambient intake air temperature. It might also be concluded that the quantity of CO increased due to AC is lowered by 43.6% due to EICAC technique. CO is undesirable in emissions and represents the loss of chemical energy, as CO is a fuel that can be combusted to supply additional thermal energy (V. Ganesan, 2012). According to previous studies, incomplete combustion is the reason for generation of CO, due to improper mixing i.e. when some particle of fuel does not find molecule of oxygen to burn, according to the following reaction (Raman & Bahari, 2021).

$$4CH_4 + 7O_2 \rightarrow 2CO + 2CO_2 + 8H_2O \qquad 4.2$$

To avoid improper mixing, EICAC technique helped to attain more oxygen molecules per unit volume due to augmentation in the density of air (oxygen) according to equation 2-6 and lead to a significant reduction of CO emission (Abdullah et al., 2015) compared to engine operation with air-conditioning with normal intake air (AC stage). In other words, EICAC technique also aids thermal energy during the combustion process.

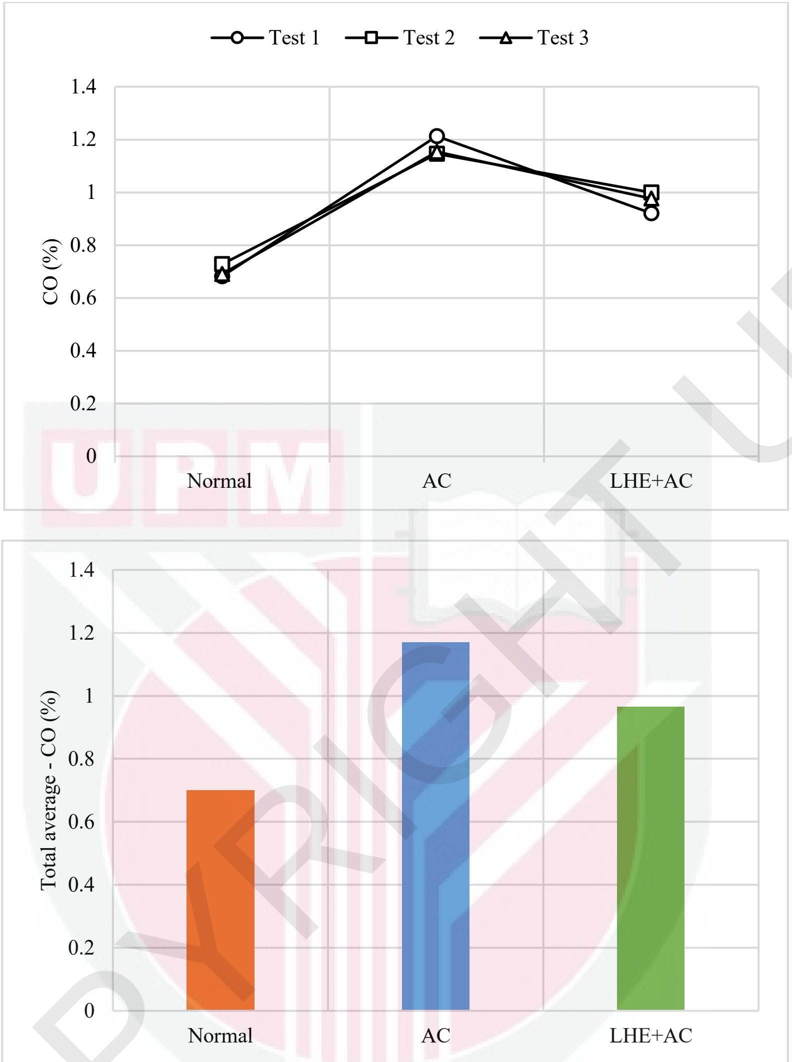

Figure 4.44: Comparison of CO in exhaust tailpipe for different stage tests

4.5.4.2 Carbon dioxide (CO_2)

Figure 4.45 shows the CO_2 exhaust emissions for each stage test and their corresponding total average of tests. The selected emissions parameter CO_2 was measured by a gas analyzer in percentage (%) of gas to evaluate the effect of the EICAC technique using the LHE. An increase in emissions is observed for the AC test by 8.35 % compared to the normal test without AC. The same observation is reported by (Costa & Valle, 2018) during a study on CO_2 emissions. Reduction in the temperature of the intake air after utilizing the LHE causes a decrement in CO_2 emissions by 3.08 % compared to the AC test. Another way to state that the amount of CO_2 increased by AC use is reduced by 39.5%.

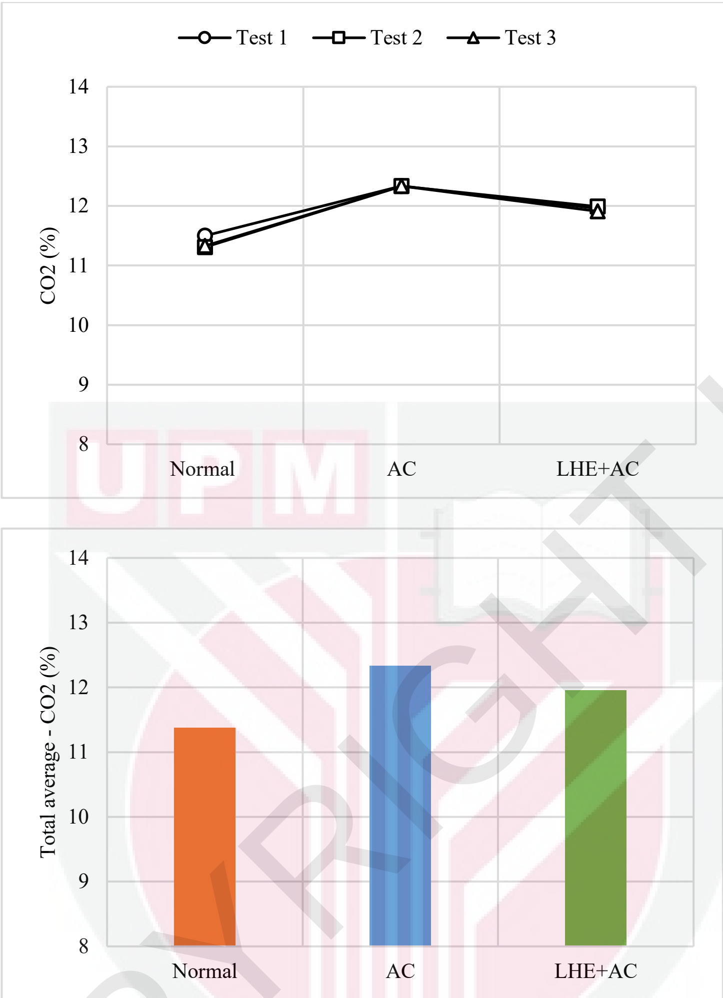

Figure 4.45: Comparison of CO_2 in exhaust tailpipe for different stage tests

4.5.4.3 Hydrocarbons (HC)

HCs, or more appropriately organic emissions, are the consequence of incomplete combustion of the hydrocarbon fuel. Typically, the level of unburned HC in the exhaust gases of gasoline fueled spark-ignition engines is typically 1 to 2% of the fuel. For the present study, the level of unburnt HC in the exhaust gas is expressed in PPM for each test and stage, presented in Figure 4.46. The total average of HC showed an increase in HC by 21.50 % with AC compared to the normal running of the vehicle without AC. However, with the introduction of cold air with the help of LHE, the amount of HC is reduced by 8.37 % compared to the AC stage tests. Another way to summarize it that the proportion of HC raised specifically through AC operation is reduced by 62.66% due to EICAC technique. On the other hand, it is still higher by 11.31 % than the normal stage tests. Unburnt hydrocarbons are typically an output of incomplete combustion, and in addition to the effects of burned HC, they are even more harmful when they escape in their unburned form (Tavakoli et al., 2021). Even when the fuel and air entering an engine are at the ideal stoichiometric condition, perfect combustion does not occur and some HC ends up in the exhaust. There are several reasons for this. Complete and homogeneous mixing of fuel and air is almost impossible. The incomplete combustion is due to improper mixing of the air and fuel in such a way that, some fuel particles do not find oxygen to react with. Another common reason of incomplete combustion is the flame quenching. As the flame goes very close to the walls it gets quenched at the walls leaving a small volume of unreacted air-fuel mixture. However, it may be noted that some of this mixture near the wall that does not originally get burned as the flame front passes will burn later in the combustion process due to additional mixing, swirl and turbulence. Oxidation of the HCs which escape the primary combustion process by any of the above processes can occur during expansion and exhaust. The amount of oxidation depends on the temperature and oxygen-concentration time histories of these HC as they mix with the bulk gases (Heywood, 2018). Therefore, LHE emerged out as a solution towards the reduction of incomplete combustion through the enrichment of oxygen molecules for mixture.

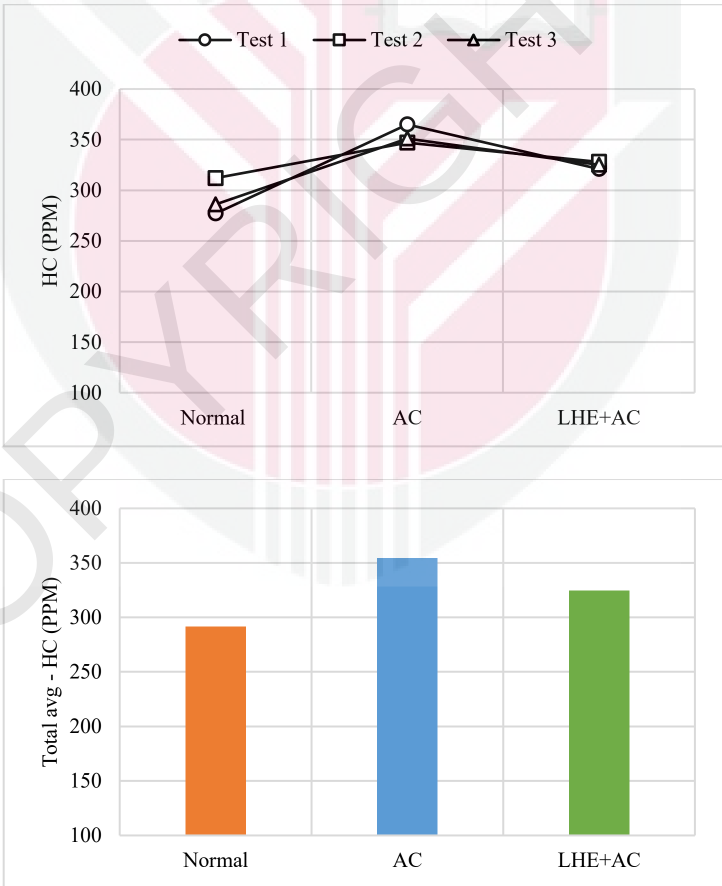

Figure 4.46: Comparison of HC in exhaust tailpipe for different stage tests

4.5.4.4 Nitrogen oxides (NO_x)

The level of nitrogen oxides in the exhaust gas is expressed in part per million PPM for each test and stage, presented in Figure 4.47. The total average of NO_x showed an increment in its amount by 6.45% while using the air conditioning system of the vehicle, as compared to the normal tests. That increment in NO_x is controlled by applying the cold air with the help of LHE. A reduction of 3.91 % in the amount of NO_x is recorded compared to the AC stage tests with ambient intake air temperature. It could also be concluded that the quantity of NO_x increased due to AC is lowered by 64.5% due to EICAC technique. It was due to the established fact that NO_x emissions are a function of in-cylinder temperature and atmospheric nitrogen, which was 78% during the intake (Semakula & Inambao, 2020). The higher the combustion reaction temperature, the more diatomic nitrogen, N_2, will dissociate with monatomic nitrogen, N, and the more NO_x will be formed. NO_x reduction using LHE is due to lower combustion temperature (Misztal et al., 2009), because higher combustion temperature tends to promote a thermal pathway that eases the production of Zeldovich NO_x (Brakora & Reitz, 2010).

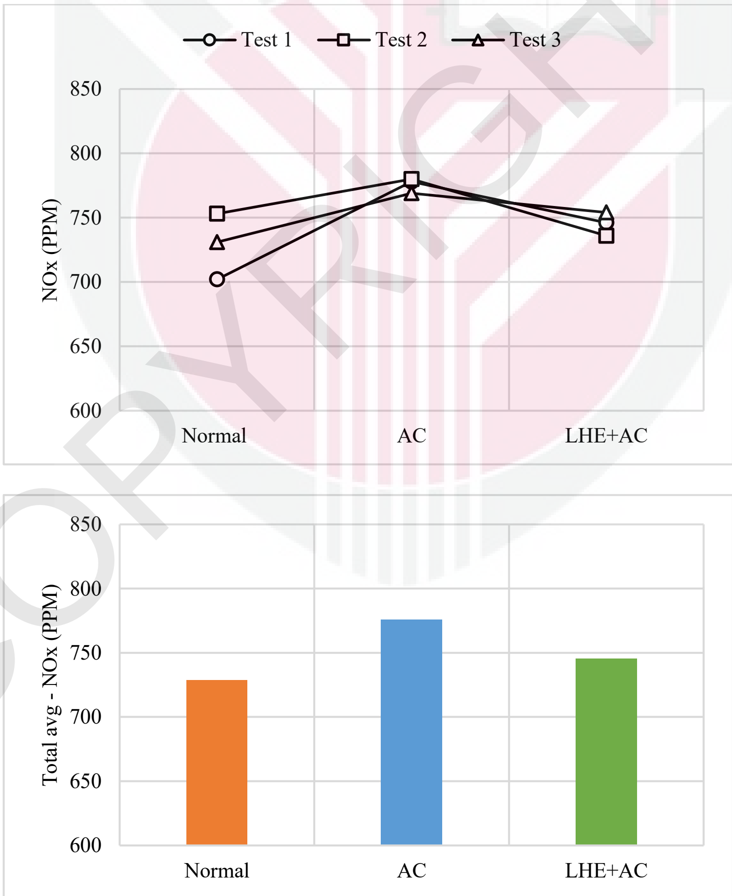

Figure 4.47: Comparison of NO_x in exhaust tailpipe for different stage tests

4.5.4.5 Air-fuel ratio (AFR)

AFR, the important parameter related to engine performance and exhaust emissions, is recorded by a gas analyzer for each stage and test, presented in Figure 4.48. According to the results of normal stage tests, it is observed that the test vehicle is normally operating with a high AFR ratio, which means that vehicle operates with a lean mixture. The use of air conditioning causes the reduction of the air-fuel ratio by 13%, which means more fuel is taken by vehicle during AC operation. However, with the introduction of cold air to the engine, a gain in AFR is observed by 6.05% compared to the AC test, which means denser air containing high oxygen molecules entered into the combustion chamber.

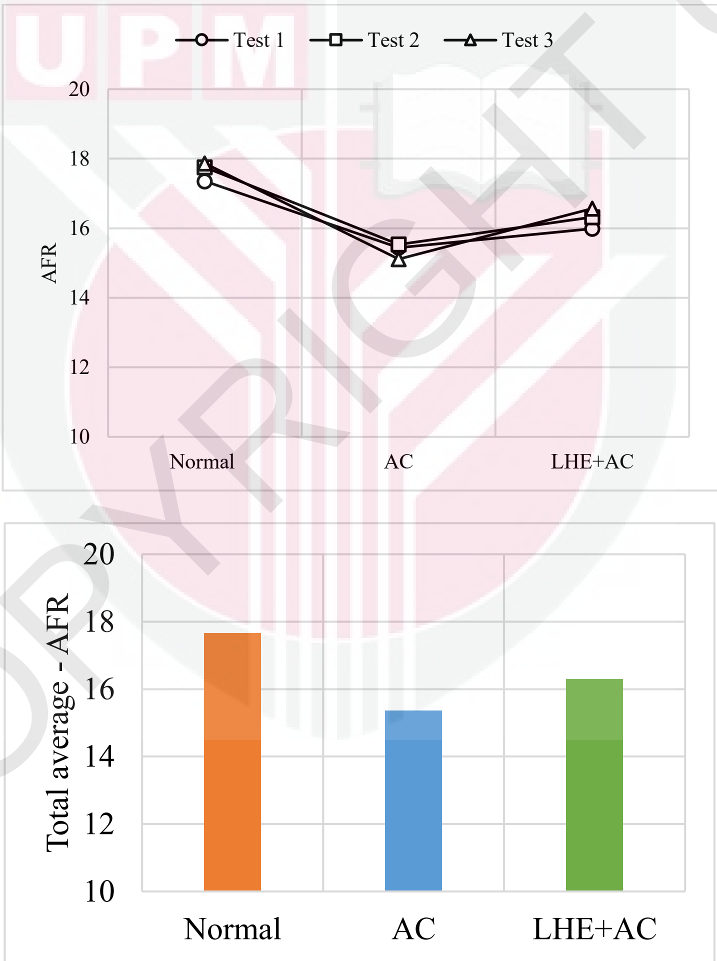

Figure 4.48: Comparison of AFR in exhaust tailpipe for different stage tests

As the engine combustion process is very sensitive to AFR, slight variations of AFR can already alter the engine behavior among the highest power, lowest emissions, and best fuel economy. For example, as shown in Figure 4.49, the amount of engine emissions for gasoline is minimum when AFR is at 14.7, which is the stoichiometric ratio of gasoline, indicating that the correct amount of air and fuel is supplied to produce complete combustion (Wong et al., 2018). The minimum air–fuel ratio is around or near 6:1, and the maximum can get around 20:1 for the combustion of gasoline-fueled engines (Al-Arkawazi, 2019). The figure shows qualitatively how HC, CO and NO_x vary with this parameter. A leaner mixture gives lower emissions until the combustion quality becomes poor (and eventually, misfire occurs) when HC emissions rise sharply, and engine operations become erratic. The shape of these curves indicates the complexities of emission control. Maximum NO_x emissions occur at slightly lean conditions, where the combustion temperature is high, and there is an excess of oxygen to react with the nitrogen.

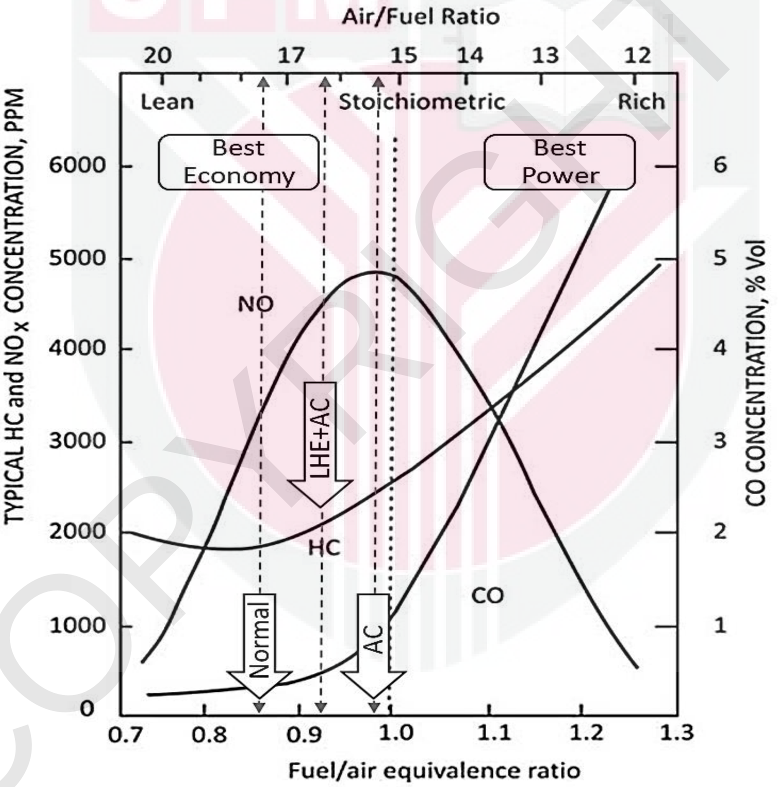

Figure 4.49: AFR and emission chart for SI engine

4.5.5 Fuel consumption

Fuel consumed by the vehicle to perform the tests are recorded in liters and presented in Figure 4.50. Total average fuel consumption for the AC test is higher by 32.3%

compared to the normal test. The reason behind this is the extra load on the engine due to the attachment of the AC compressor with the engine through the belt. AC is known to be the largest auxiliary engine load and contributes more to fuel consumption than other auxiliary units (Khan & Frey, 2019). On the other hand, the EICAC technique shows a minute improvement in fuel reduction upto 0.77%. Nevertheless, this is attributed to better combustion at lower air intake temperature (higher oxygen concentration) compared to a higher air intake temperature. It can also be concluded that a lower air intake temperature would improve the fuel economy by hosting a leaner air-fuel mixture, as the cold air is denser and contains a large amount of oxygen that showed rich combustion. Up to this point, it is also clear that there is a significant and direct correlation between fuel consumption and air-fuel ratio (Saranya et al., 2022).

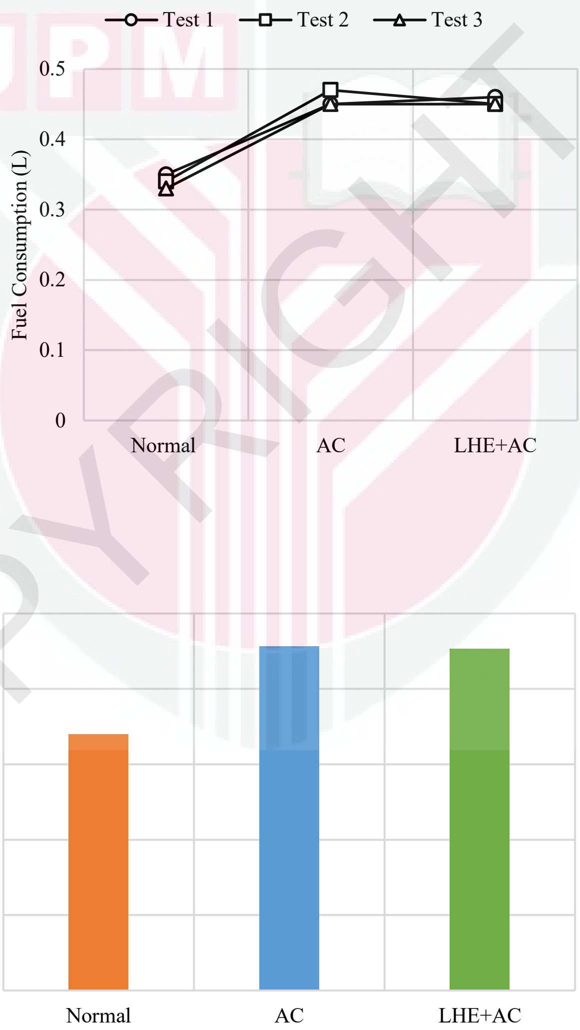

Figure 4.50: Comparison of vehicle fuel consumption for different stage tests

4.6 Engine performance during Vehicle parking position

The vehicle parking test refers to a vehicle state when the engine runs at low power but the vehicle is not moving. Every day, thousands of drivers idle needlessly, unavoidably or purposely on roads. It may include while the vehicle is parked for a few minutes, stuck in a traffic jam or at a red light, in the drive-through line, or waiting for school pick-up. Idling wastes fuel and gives rise to greenhouse gas emissions as well as local air pollutants, which harm public health. Therefore, this test was conducted to measure the effectiveness of the EICAC technique on engine emissions and fuel consumption performance. The test authenticates the working performance of LHE at zero vehicle velocity, as it was the challenge of design, as described in the literature.

4.6.1 Intake temperature

The intake temperature of the air is recorded for the time duration of 11 minutes (for better accuracy and stable result) against each stage test. This helped to understand the variation in intake temperature of air during different vehicle states/conditions. The total data of EICA temperature during the tests against every minute are presented in Table 4.6. At normal test, a gradual increase in intake temperature is observed, starting from 56.6℃ to a maximum of 61℃. Further increase in intake temperature is recorded for the test vehicle at idle state with the use of air conditioning starting from 64.1℃ to a maximum of 67.8℃. Roughly 6℃ intake temperature is raised with the use of the vehicle AC system compared to the normal test stage, without air conditioning. Several factors come into play for the rise in intake temperature due to air conditioning. First, higher load on the engine due to AC auxiliaries, for which the engine is burning more fuel and creates a bit more heat (Marshall et al., 2019). Secondly, the fan just started spinning electrically, means the alternator is now needing more power from the engine. A bit more fuel, a bit more heat created for the engine's cooling system. Thirdly, all that energy (heat) that the AC has removed from the car's interior goes to its radiator, properly called a condenser coil, that's located right in front of the radiator and engine. In short, running the air conditioning in the summer will make the engine run hotter. Thus more heat created in the engine compartment.

Table 4.6: EICA temperature record for each stage test

Time (Minutes)	EICA temperature (℃)		
	Normal	AC	LHE+AC
1	56.6	64.1	64.7
2	57.5	64.7	53.4
3	58.4	64.2	45.5
4	58.9	64.7	41.6
5	59.9	65.5	35.8
6	59.3	65.9	34.7
7	60.3	65.7	30.7
8	60.8	66.9	29.4
9	61	67.4	27.2
10	61.1	67.8	27.1
11	61	67.8	27
Average	59.527	65.881	37.918

The LHE helps to reduce the intake temperature raised by AC or also below the temperature of the normal test stage and ambient temperature as well. The temperature of intake air after 11 min of working of LHE is recorded to 27℃ . Thus a temperature drop of 40℃ is recorded for the vehicle standing at parking position. That high temperature drop by LHE makes it different with the available intercoolers in the market. The graphical presentation of Table 4.6 is shown in Figure 4.51a, illustrating the comparison of intake air temperature between the three-stage tests. The decrease in EICA temperature from higher temperatures to lower cooling temperature, actually represents the effectiveness of the LHE. Figure 4.51b contains the comparison of the total average of intake temperature calculated from 11-minute data for each stage test, depicting the decrease in intake temperature by 42% and 36.3% compared to AC and normal tests respectively.

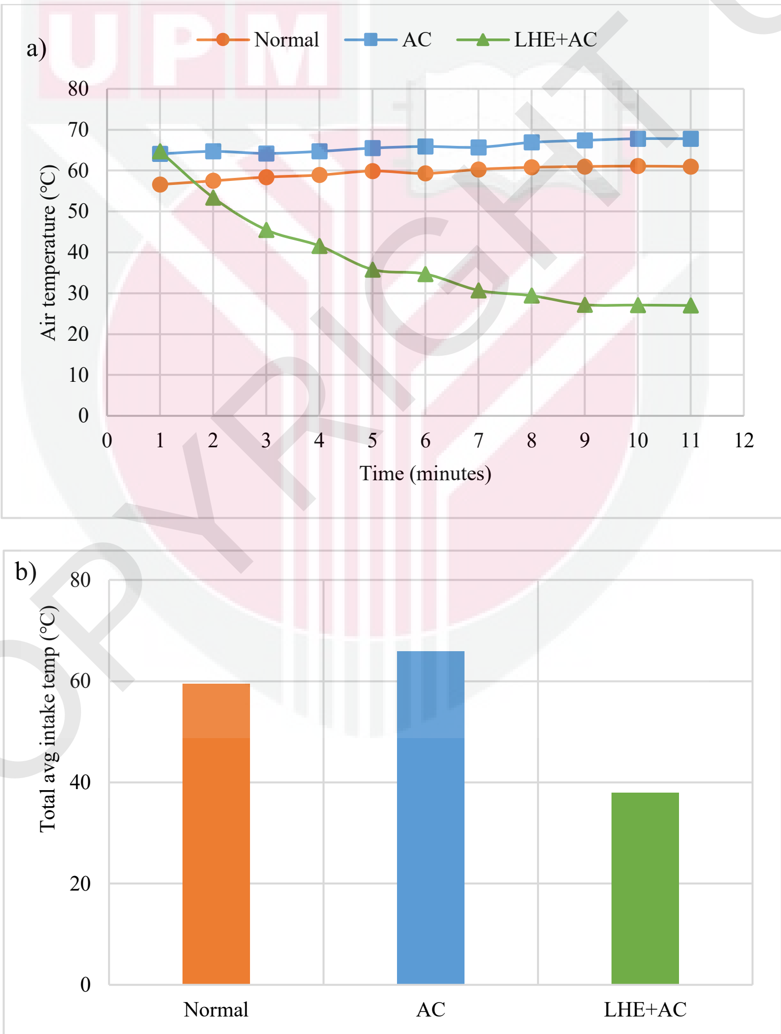

Figure 4.51: Engine intake temperature record for each stage, a) at 1 min interval, and b) total average of 11minute duration

4.6.2 Exhaust temperature

The exhaust temperature at the tailpipe of the vehicle is recorded at every 1 minute for all three stages. The temperature sensor is located exactly with the gas emission analyzer, from where the exhaust gases just ready to leave the tailpipe and enter the atmosphere. Figure 4.52 displayed the exhaust temperature at every minute, along with the total average of 11 min exhaust temperature to give a better understanding of the overall effect.

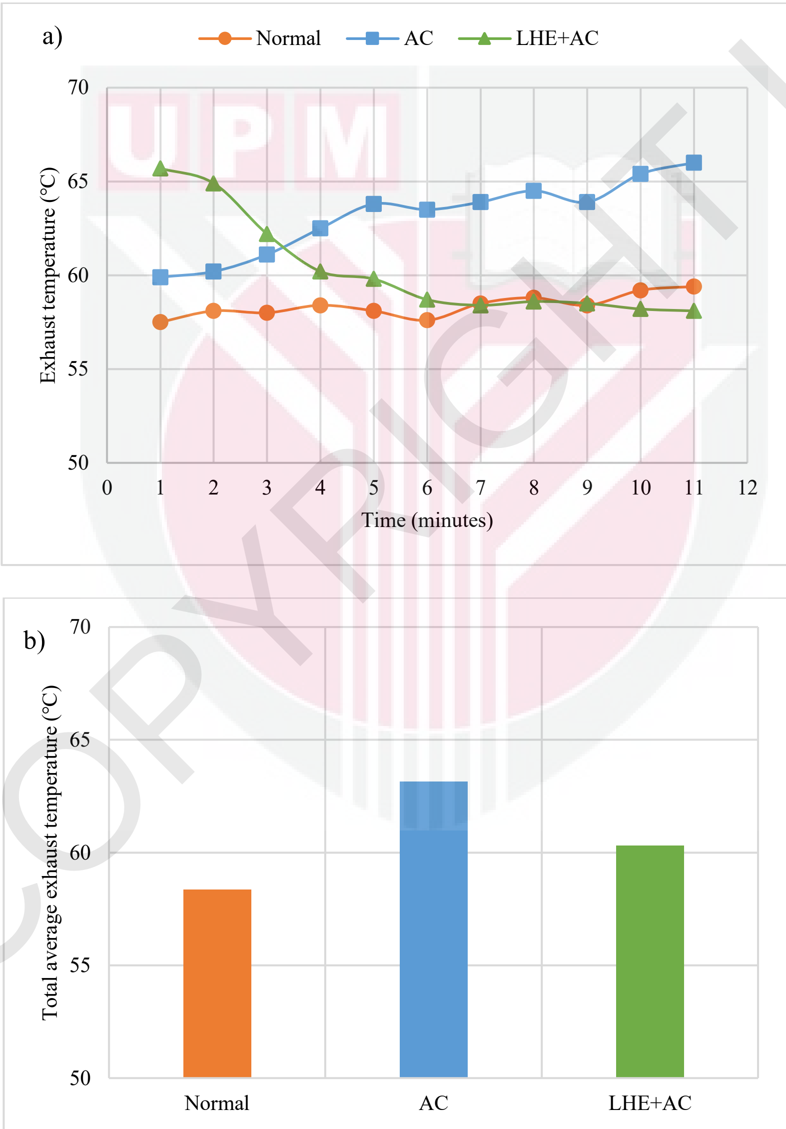

Figure 4.52: Exhaust temperature record for each stage, a) at 1 min intervals, and b) total average of 11min duration

The average exhaust temperature for AC shows an increment of 4.8℃ compared to the normal stage test. However, for cold intake air, the average exhaust temperature is decreased by 2.85℃, demonstrating colder combustion inside the cylinder. Battista et al. (2018) also reported a reduction in exhaust emission temperature due to cold intake air, during his experiment on 3L turbocharged diesel engine. Basically, the exhaust gas temperature indicates the effective use of the heat energy of a fuel. The heat loss in the exhaust pipe or an increase in the exhaust temperature reduces the conversion of heat energy of the fuel to work. Therefore, it can be concluded that, reducing the intake air temperature reduces the loss of heat energy of the fuel. The low value of engine exhaust gas temperature indicates that the mixture (fuel and air) is burned well in the cylinders. Further, the lower value of exhaust temperature due to EICAC technique may also suggest that the engine was not thermally overloaded, which is a positive outcome (Enweremadu & Rutto, 2010).

4.6.3 Vehicle emission performance

The emission gas analyzer monitors the exhaust emissions of each stage test for the whole test duration with an interval of 1 minute. The final instrument report for each stage test is shown in Table 4.7. Vehicle exhaust emission may be affected by many factors, including the features of vehicles (such as vehicle type, technical level, emission control devices, and operation condition), maintenance frequency, fuel type, the levels and effect of maintenance, and the characteristics of roads (altitude, temperature and humidity, road conditions, and traffic conditions) (Xue et al., 2013).

Table 4.7: Exhaust emissions recorded during the vehicle static position test for each stage at every 1-minute interval

Stage	Time (minutes)	Emissions			
		CO (%)	CO_2 (%)	HC (PPM)	NO_x (PPM)
Normal	1	0.395	10.84	194	28
	2	0.392	10.72	201	23
	3	0.387	10.66	197	27
	4	0.372	10.6	204	28
	5	0.382	10.59	209	28
	6	0.387	10.52	200	22
	7	0.376	10.57	208	30
	8	0.378	10.55	213	29
	9	0.397	10.55	203	22
	10	0.373	10.59	212	31
	11	0.383	10.56	215	29
AC	1	0.543	13.38	235	216
	2	0.526	13.4	236	212
	3	0.521	13.4	239	213
	4	0.532	13.42	242	240
	5	0.537	13.37	241	245
	6	0.515	13.48	235	232
	7	0.523	13.49	228	218
	8	0.538	13.4	227	234
	9	0.529	13.52	230	244
	10	0.529	13.58	234	244
	11	0.515	13.49	230	217

Table 4.7: Continued

	1	0.517	12.94	229	225
	2	0.503	12.58	224	206
	3	0.49	12.44	223	179
	4	0.495	12.31	221	173
	5	0.467	12.37	224	177
LHE+AC	6	0.474	12.33	220	182
	7	0.451	12.21	218	174
	8	0.458	12.09	216	175
	9	0.455	12.15	215	163
	10	0.459	12.17	214	169
	11	0.449	12.08	216	159

4.6.3.1 Carbon monoxide

The formation and destruction of CO is a principal reaction pathway in hydrocarbon combustion, which essentially consists of breakdown of the hydrocarbon fuel to carbon monoxide. The selected emission parameter for analysis is measured in percentage of gas by the gas analyzer. Findings related to each stage test for each minute and their corresponding total average is presented in Figure 4.53. The percentage of CO increased by 37.83% during the use of AC at an idle position compared to the normal test without AC of the test vehicle. The reason behind this increment is that, to operate the AC of vehicle requires energy, that comes from engine. To power the AC compressor, the engine burns more fuel, leading to an increase in CO emissions. Further, the most important engine parameter influencing carbon monoxide levels is the fuel–air equivalence ratio. During the AC operation, the equivalence ratio increased, which means that the fuel quantity is greater and the oxygen quantity is decreased more than the required amount for the complete burning of fuel. Due to the non-availability of oxygen in the rich mixture, part of the air-fuel mixture that must be converted to CO_2 comes out as CO. On the other hand, the EICAC technique reduces the amount of CO by 10.22% compared to the AC test and might also be concluded that the quantity of CO increased due to AC is lowered by 37.2%. The prime logic behind this decrement in emission level is that lowering the intake air temperature increases its density, means more number of oxygen molecules per unit volume are available for fuel to attain complete combustion and balance the equivalence ratio. The same decreasing trend in the level of CO emissions through EICAC technique has been reported by Pshtiwan Mohammad Sharif (2021) upto 4.4%, using his designed intercooler for naturally aspirated engine.

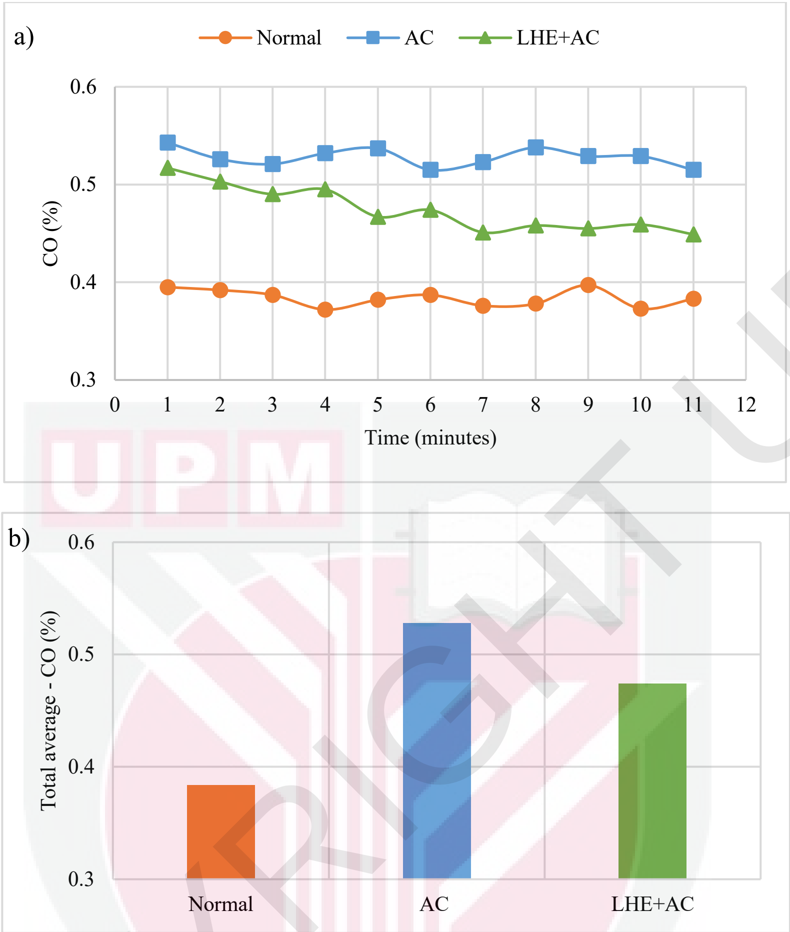

Figure 4.53: CO at exhaust tailpipe for each stage during vehicle static position, a) at every 1-minute interval, and b) total average of 11 minutes

4.6.3.2 Carbon dioxide (CO_2)

The transportation industry releases a massive amount of CO_2 into the atmosphere every year and found to be a major contributor to greenhouse gas emissions. The more greenhouse gases that industry release into the atmosphere, the stronger the effects of climate change will be. CO_2 is released as a hot gas in the gas engine exhaust. The gas analyzer used in this study measures the CO_2 in the percentage of gas. Figure 4.54 depicts the results of each stage test for each minute and their associated overall average. The overall average reading of CO_2 recorded for the AC test is 26.6% higher than the normal test. The high emission of carbon dioxide produced by test vehicle during AC stage test can be determined by fuel consumption. The greater the fuel consumption, the greater the carbon dioxide emissions released by vehicle (Sari & Sofwan, 2021). Therefore, as stated earlier in section 4.6.3.1, AC of the vehicle utilizes high fuel to power the compressor and subsequently releases high emission levels of CO_2 compared to normal stage. Conversely, a reduction is observed in the overall average of CO_2 by 8.29% with the induction of cold air into the engine compared to AC stage tests. Another way to state that the volume of CO_2 increased by AC usage is reduced by 39.5%.

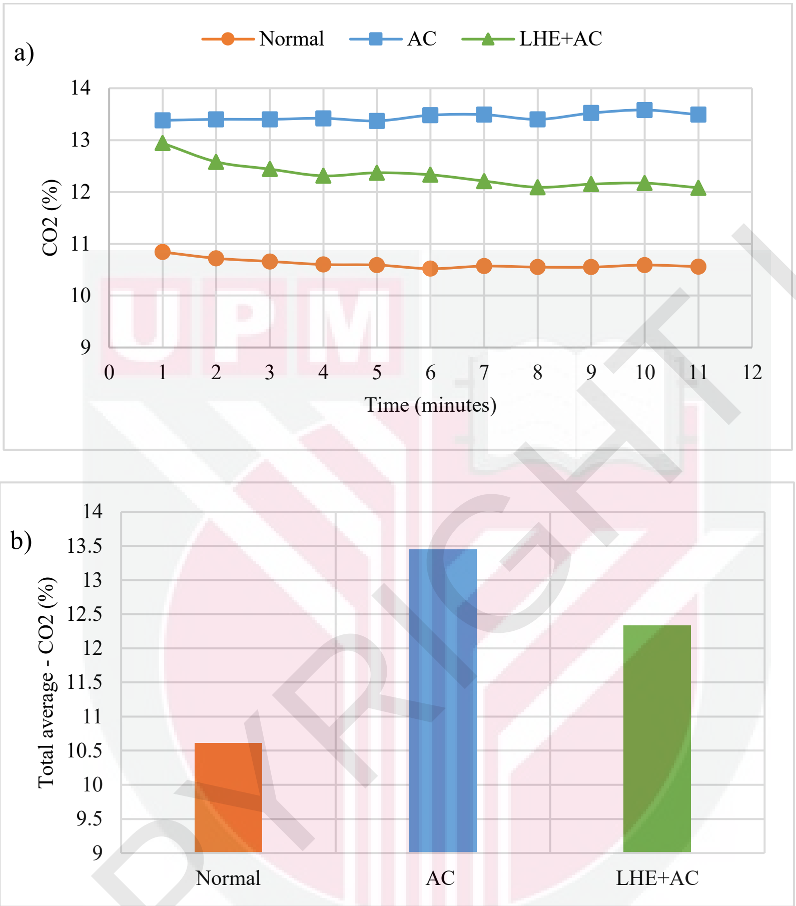

Figure 4.54: CO_2 at exhaust tailpipe for each stage during vehicle static position, a) at every 1-minute interval, and b) total average of 11 minutes

4.6.3.3 Hydrocarbons (HC)

Hydrocarbon emissions result as part of the fuel inducted into the engine escapes combustion. In other words, the fuel avoids flame zone. Most of hydrocarbons in exhaust HC are the same compounds as in the fuel and dependent on many mechanisms such as adsorption and desorption of fuel in oil layer, flame quenching, fuel escaping into crevices and accumulation of fuel in engine deposits. The findings regarding the HC emission from the test vehicle are presented in Figure 4.55, against each stage test and their associated overall average, to check the response of cold intake air on its behavior. The total average of HC emissions for the AC test is 14.22% higher than a normal test.

Reducing the temperature of air along with air conditioning causes a reduction in the count of HC emissions by 6.09% compared to the AC test; however, it is still higher by 6.78% compared to the normal test. Almost 49% reduction is observed in the amount of HC raised by AC stage tests. Unburnt HCs emissions are generally produced due to incomplete combustion of a carbon containing fuel. Lower excess oxygen concentration results in rich air– fuel mixtures at different locations inside the combustion chamber (Birtok-Băneasă et al., 2017). This heterogeneous mixture does not combust completely and results in higher unburnt HCs emissions. In addition, the longer ignition delay due to the oxygen deficiency caused by increased air intake temperature during AC stage test as reported in section 4.6.1, lead to poor unburnt HCs oxidation process. Conversely, LHE helped to enrich oxygen content in the air fuel mixture resulting in lower levels of unburned hydrocarbons (HC). Therefore, it can be concluded that HC can be reduced by providing excess air (fuel lean mixtures) until the reduced flammability of the mixtures causes a net increase in HC emissions. The same decreasing trend in unburnt HC is also reported by Abdullah et al., (2015) through the induction of cold intake air in naturally aspirated engine.

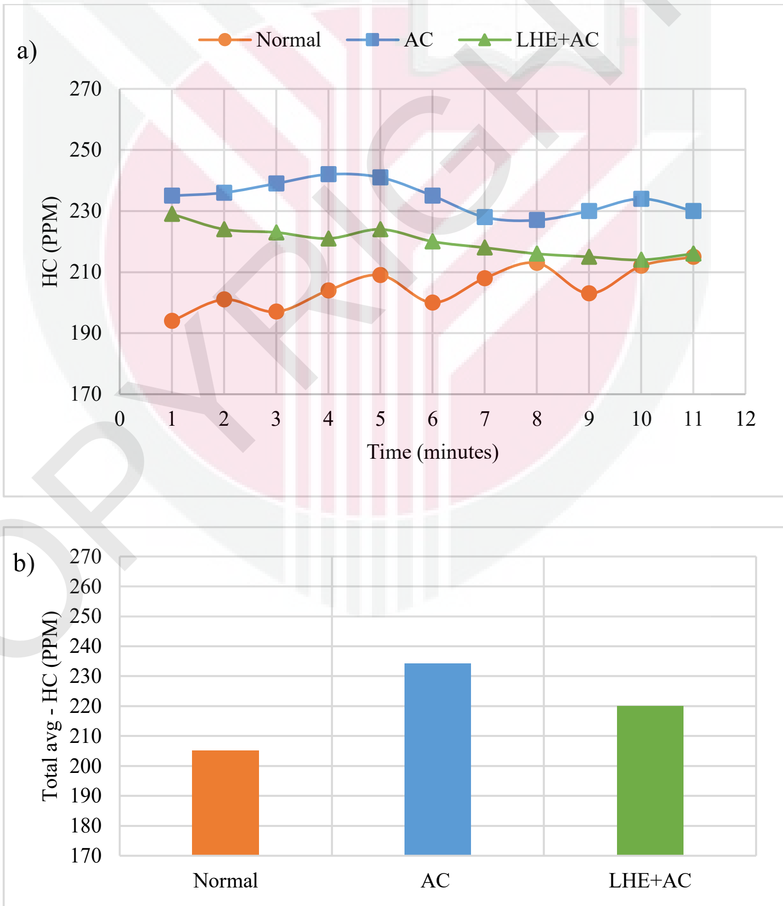

Figure 4.55: HC at exhaust tailpipe for each stage during vehicle static position, a) at every 1-minute interval, and b) total average of 11 minutes

4.6.3.4 Nitrogen oxide (NO_x)

The gas analyzer measures the chosen emission quantity in part per million (PPM). Figure 4.56 depicts the results of each stage test for each minute and their associated overall average. When compared to a normal test without air conditioning, the proportion of NO_x increased by 744.1% when using air conditioning at an idle position. However, when compared to the AC test, the EICAC approach reduces NO_x by 21.19%. It could also be summarized that the quantity of NO_x increased due to AC is lowered by 24% due to EICAC technique. The formation of NO_x is a strong function of in-cylinder temperature. In rich mixture conditions during the AC stage test, higher NO_x formed due to high temperatures developed inside the engine cylinder. This is because at high temperatures, the nitrogen present in the diatomic state gets dissociated into monoatomic nitrogen, which is an unstable and highly reactive compound. This monoatomic nitrogen reacts with oxygen present in the air to form NO and NO_2, according to the following reactions (Kirkpatrick, 2021):

$$N_2 \rightarrow 2N \tag{4.3}$$

$$O + N_2 \rightarrow NO + N \tag{4.4}$$

$$N + O_2 \rightarrow NO + O \tag{4.5}$$

$$N + OH \rightarrow NO + H \tag{4.6}$$

The equation 4-4, is a nitrogen dissociation reaction triggered by an oxygen atom. This reaction is slow and therefore rate limiting, as it is endothermic with activation energy of 313.8 kJ/mol. The equation 4-5, is very fast, as a nitrogen atom reacts exothermically with an oxygen molecule to form nitrogen oxide and an oxygen atom. The equation 4-6, is an exothermic reaction between a nitrogen atom and a hydroxide radical, which forms nitrogen oxide and a hydrogen atom. When the temperatures during combustion are less due to cold intake air using LHE, the nitrogen entered into the engine cylinder does not react with oxygen and is emitted from the engine as diatomic nitrogen, which is stable and resulting in less emission of NO_x. (Roberto Cipollone et al., 2017a) reported a decrement in NO_x emission upto 4.5% through EICAC technique. Moreover, during low temperature combustion, there is no distinct flame or wave front that propagates across the chamber, but low temperature combustion simultaneous ignition at a number of sites throughout the cylinder. With this cylinder-wide distribution of ignition sites, the energy release is volumetric. The combustion duration is shorter, and the peak pressures and energy release rates are greater relative to conventional combustion.

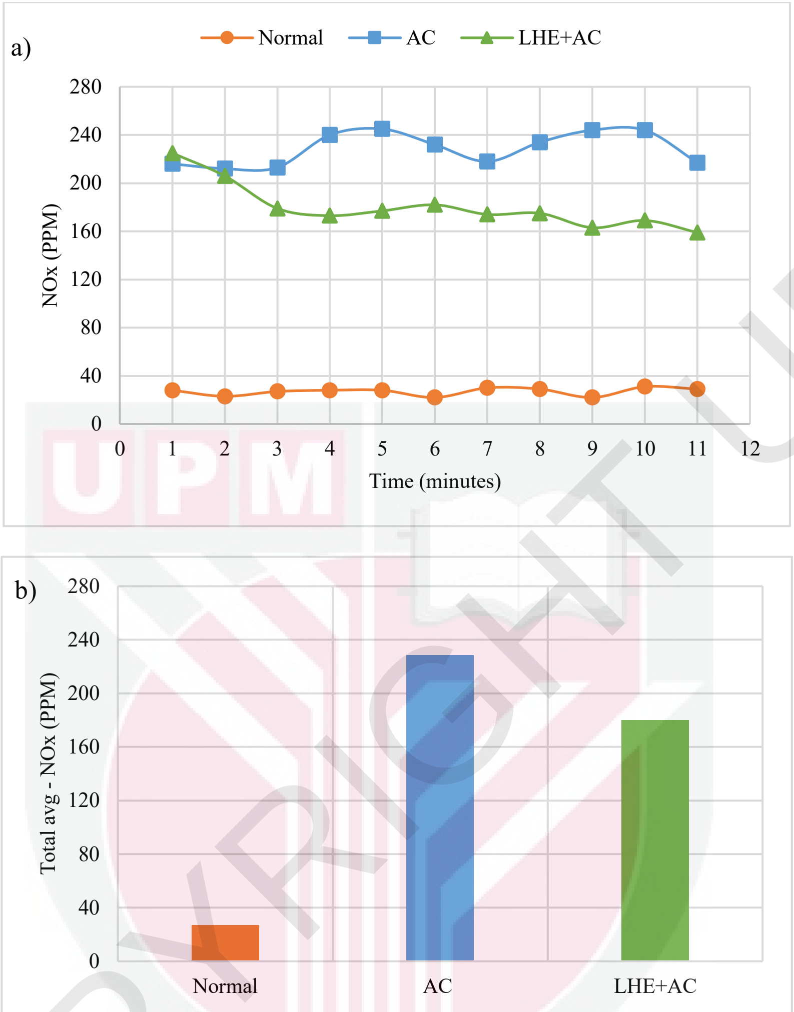

Figure 4.56: NO_x at exhaust tailpipe for each stage during vehicle static position, a) at every 1-minute interval, and b) total average of 11 minutes

4.6.4 Fuel consumption (L)

The fuel consumption for the tests under consideration is measured to check and compare the amount of fuel consumed by each stage test, presented in Figure 4.57a. The fuel consumed for the AC test is higher by 64.4% compared to the normal test. The same has been claimed by J. Lee et al. (2013) up to 90% at idle position. The prime logic behind this increment is that, operation of the conventional automotive A/C compressor produces a parasitic load on the engine (due to its connection through belt to engine crank shaft), thereby increasing fuel consumption. Further, there are many inter-related factors that can affect the parasitic load induced by the A/C compressor, such as ambient temperature and humidity (both inside and outside the vehicle), system charge level, solar load, vehicle exterior and interior color, use of window glazing, etc (Huff et al., 2013). On the other hand, the amount of fuel for the EICAC technique is almost the same as for the AC test. Only 0.9% fuel saving is shown for cold intake air compared to the AC test, which is negligible. It can also be concluded that, cold intake air permits slightly advanced ignition timing, therefore there is a great chance for any thermodynamic improvements to be overcompensated by power consumption of the AC compressor. At the same time, the air density increase from temperature reduction lowers the required boost pressure to achieve nominal full load at all engine speeds. This can also be a particular advantage of getting cold intake air in regards to a slight decrease in fuel consumption. The overall engine speed range for each stage test is also shown in Figure 4.57b. The higher rpm for AC and cold air tests draws more fuel to balance the load due to air conditioning, which justifies the increased fuel consumption compared to normal tests.

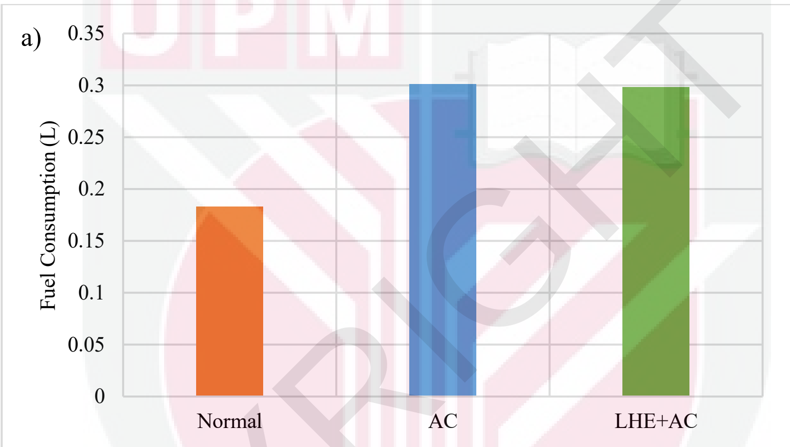

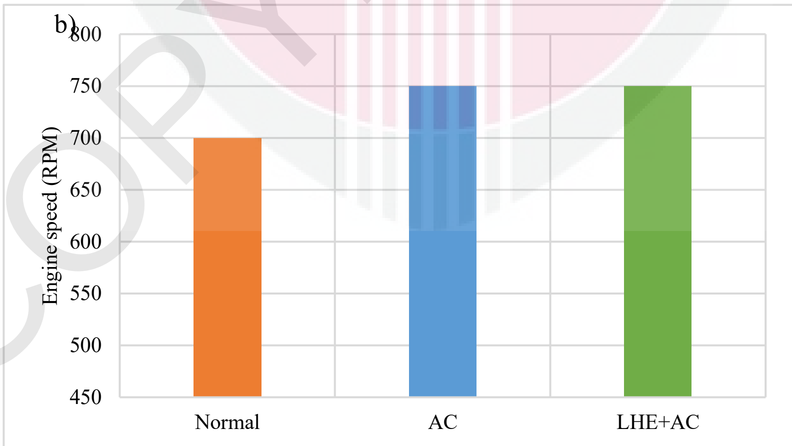

Figure 4.57: a) Fuel consumed, and b) engine rpm, for each stage during the vehicle static test

4.7 Potential benefits of upgraded LHE

The potential benefits of upgraded LHE are listed for future research endeavors.

1. The developed LHE shows minimal pressure drop (less than 5%) for the selected naturally aspirated engine, which surely could also be very useful for charged engines, where high pressure is involved and can offer substantial improvements in engine power and torque.

2. The size of the LHE presented in this study is particular for the selected test vehicle (1.5L Proton Wira), due to its dependence on the available space in engine bay. However, the design structure of LHE is so flexible, that it can be made/altered for any existing vehicle engine bays by increasing or decreasing the number of lamellas inside shell box.

3. The developed LHE shows high thermal cooling capability when compared to the design sizes of other available intercoolers in the market. This would also help to offer its services where space is limited in engine bays.

4. The attachment of LHE with VAC system also allows it to be used as heat pump during winter seasons.

5. The developed LHE could also be utilized for electric and hybrid vehicles, where cooling is required to cool the battery bank or electric motors.

CHAPTER 5

CONCLUSION AND RECOMMENDATION

5.1 Conclusions

In this study, a novel heat exchanger named Lamella heat exchanger was developed as a vehicle engine intercooler for lowering the intake air temperature to improve engine performance by utilizing the vehicle refrigeration system as a coolant source, the same used for cabin cooling. The conclusions from present study is arranged in chronological order according to the objectives of the study.

i. Numerical investigation concluded that the selected geometry of LHE exposes more surface area per unit volume by 55% (on same design scale), compared to mostly used intercoolers in literature i.e., shell and tube configuration (reference model), resultantly offers a high heat transfer by 41%. Simulation results also reveals that the amount of heat transfer from hot air to the cold refrigerant, the temperature drop of the hot air, the pressure drop inside LHE, and the number of transfer units, all were inversely proportional to the inside opening of the lamella geometry and directly proportional to the aspect ratio of the lamella. The less inside opening of the lamella results in more heat transfer, temperature drop, number of transfer units, and pressure drop. On the contrary, LMTD shows inverse relation to the aspect ratio.

ii. Laboratory experiments revealed that with the increase in engine speed (mass flow rate of air), the pressure drop inside LHE increases, while a temperature drop decreases. Thus, pressure and temperature drop are inversely proportional to each other, for the present study. The maximum pressure drop of 95 Pa is recorded for maximum engine speed (8000 rpm) at 40℃ intake air temperature, due to higher collision of air molecules resulting in greater loss of kinetic energy, subsequently, higher pressure drop. In addition to that, the pressure drop inside lamella plates are found to be directly proportional to the friction factor, length and hydraulic diameter of the lamella, density of air, and velocity of air. On the other hand, the maximum temperature drop of 45.48℃ is witnessed for minimum engine speed (1000 rpm) at 55℃ intake air temperature due to rise in the time of contact surface between the air and lamella surfaces. Moreover, the developed LHE presented the outstanding heat transfer range between 0.42kW to 2.14kW, at various engine speed limit (1000 to 8000 rpm), due to the intensification of the velocity gradients of air inside lamellas, which causes high convective heat transfer coefficient and made LHE superior among the available intercoolers in the market.

iii. Real-time performance of the intercooler in the test vehicle using chassis dyno test shows a substantial improvement in engine performance in terms of power, torque, and emissions. The loss in engine power (7.3bhp) due to the extra load applied by the AC compressor is partly recovered by 17%, by introducing the cold intake air through LHE. Likewise, the lost torque (15.8Nm) is also recuperated by 24% through EICAC technique. Moreover, the increased quantities of exhaust tailpipe emissions due to AC operation is reduced by 43.6%, 39.5%, 47.3%, 64.5% for CO, CO_2, HC and NO_x respectively by having cold intake air. On the contrary during vehicle static test, a remarkable drop of 38.8℃ in intake temperature is recorded, by operating LHE, which resulted in the reduction of the elevated levels of exhaust tailpipe emissions produced during AC operation by 37.2%, 39.3%, 48.9%, 24% for CO, CO_2, HC and NO_x respectively. However, no noteworthy improvement in fuel consumption is observed, only 0.9% saving is observed.

The overall benefits of having cold intake air outlined in the literature are achieved magnificently through developed LHE and are significantly ahead of currently available intercoolers and cooling techniques, as discussed in results section. The substantial reduction of exhaust pollutants, and admirable increase in engine power, and torque are the main benefits achieved through LHE, operating on VAC system. The adverse effects generated on engine performance by using the VAC system with ambient intake air are partially recovered through the presented EICAC technique in this study, which definitely has a meaningful impact or application in real world. Moreover, that particular technique does not need any expensive replacement parts or the need to make any kind of physical changes in engine bays, instead it simply involves the addition/installation of developed intercooler on the engine intake line with existing VAC system.

5.2 Recommendations

i. This study investigated the EICAC technique for SI-engine vehicles; hence, it could be utilized for diesel and charged engines as well.

ii. One of the key feature to improve heat transfer is to enhance surface area. Thus, modifications could be employed and tested to lamella inner geometry by adding grooving patterns and extended surfaces, to enhance thermal capability.

iii. The LHE shared refrigerant coolant from vehicle air-conditioning cycle; hence, an independent refrigerant cycle using an electric motorized compressor could be employ which may help to gain more cooling.

iv. The use of lightweight and heat-resistant materials, such as advanced alloys or composite materials, can further contribute to improved intercooler performance.

v. The use of advanced thermal coatings on intercooler surfaces to enhance heat resistance and reduce heat transfer to surrounding components.

REFERENCES

Aaron. (2011). *Liquid CO_2 cooled intercooler | 3D CAD Model library | GrabCAD*. https://grabcad.com/library/liquid-co2-cooled-intercooler

Abbod, M. H., Kurjib, H. J., & Imran, M. S. (2019). The effect of intake air temperature on spark ignition engine performance. *Journal of Engineering and Applied Sciences*, *14*(10).

Abdelaal, M. M., Rabee, B. A., & Hegab, A. H. (2013). Effect of adding oxygen to the intake air on a dual-fuel engine performance, emissions, and knock tendency. *Energy*, *61*, 612–620. https://doi.org/10.1016/j.energy.2013.09.022

Abdullah, N. R., Ismail, H., Michael, Z., Rahim, A. A., & Sharudin, H. (2015). Effects of air intake temperature on the fuel consumption and exhaust emissions of natural aspirated gasoline engine. *Jurnal Teknologi*, *76*(9), 25–29. https://doi.org/10.11113/jt.v76.5639

Aboul Khail, A., & Erişen, A. (2021). Improvement of plate heat exchanger performance using a new plate geometry. *Arabian Journal for Science and Engineering*, *46*(3), 2877–2889. https://doi.org/10.1007/s13369-020-05287-8

Aboul Khail, A., & Erişen, A. (2022). Heat transfer and performance enhancement investigation of novel plate heat exchanger. *Thermal Science and Engineering Progress*, *34*, 101368. https://doi.org/https://doi.org/10.1016/j.tsep.2022.101368

Adair, D., Bakenov, Z., & Jaeger, M. (2014). Building on a traditional chemical engineering curriculum using computational fluid dynamics. *Education for Chemical Engineers*. https://doi.org/10.1016/j.ece.2014.06.001

Adithya, K., Ahmed, F., Padmanathan, P., Mohan, C. G., & Prakash, R. (2021). Design optimization of intake manifold of dual fuel engine. *Materials Today: Proceedings*, *45*, 646–651. https://doi.org/10.1016/j.matpr.2020.02.726

Akasyah, M. K., Mamat, R., Abdullah, A., Aziz, A., & Yassin, H. M. (2015). Effect of ambient temperature on diesel-engine combustion characteristics operating with alcohol fuel. *International Journal of Automotive and Mechanical Engineering*, *11*(1), 2373–2382. https://doi.org/10.15282/ijame.11.2015.18.0199

Al-Arkawazi, S. A. F. (2019). Analyzing and predicting the relation between air–fuel ratio (AFR), lambda (λ) and the exhaust emissions percentages and values of gasoline-fueled vehicles using versatile and portable emissions measurement system tool. *SN Applied Sciences*, *1*(11), 1–12. https://doi.org/10.1007/s42452-019-1392-5

Al-Ibrahim, A. M., & Varnham, A. (2010). A review of inlet air-cooling technologies for enhancing the performance of combustion turbines in Saudi Arabia. *Applied Thermal Engineering*, *30*(14–15), 1879–1888. https://doi.org/10.1016/j.applthermaleng.2010.04.025

Al-Shemmeri, T. T. (2011). Thermodynamics, performance analysis and computational modelling of small and micro combined heat and power (CHP) systems. In *Woodhead Publishing Series in Energy* (pp. 42–69). Woodhead Publishing. https://doi.org/https://doi.org/10.1533/9780857092755.1.42

Al zahrani, S., Islam, M. S., Xu, F., & Saha, S. C. (2020). Thermal performance investigation in a novel corrugated plate heat exchanger. *International Journal of Heat and Mass Transfer*, *148*, 119095. https://doi.org/https://doi.org/10.1016/j.ijheatmasstransfer.2019.119095

Alam, M., Song, K. H., & Boehman, A. (2005). Effects of inlet air temperature on performance and emissions of a direct injection diesel engine operated with ultra low sulfur diesel fuel. *Proceedings of the International Conference on Mechanical Engineering 2005*, *December*, 1–6.

Alam, T., & Kim, M. (2018). A comprehensive review on single phase heat transfer enhancement techniques in heat exchanger applications. *Renewable and Sustainable Energy Reviews*, *81*(June 2017), 813–839. https://doi.org/10.1016/j.rser.2017.08.060

Alao, F. I., & Babatunde, S. (2020). On some basics of compressible fluid flows. In *Woodhead Publishing Series in Energy* (pp. 55–66). Woodhead Publishing. https://doi.org/https://doi.org/10.1016/B978-0-12-817949-9.00011-6

Alcan, G., Unel, M., Aran, V., Yilmaz, M., Gurel, C., & Koprubasi, K. (2019). Predicting NO_x emissions in diesel engines via sigmoid NARX models using a new experiment design for combustion identification. *Measurement*, *137*, 71–81. https://doi.org/10.1016/j.measurement.2019.01.037

Alexander H. King. (1951). *Refrigerant Cooled Intercooler.* (Patent No. 2571256). https://patents.google.com/patent/US25%0A71256

Alfa-Laval. (2022). *Reasons to use plate-and-frame heat exchangers instead of shell-and-tube.* https://www.alfalaval.com/microsites/gphe/tools/gphe-vs-shell-and-tube/

Alkidas, A. C. (2007). Combustion advancements in gasoline engines. *Energy Conversion and Management*, *48*, 2751–2761. https://doi.org/10.1016/j.enconman.2007.07.027

Alves, C. A., Lopes, D. J., Calvo, A. I., Evtyugina, M., Rocha, S., & Nunes, T. (2015). Emissions from light-duty diesel and gasoline in-use vehicles measured on chassis dynamometer test cycles. *Aerosol and Air Quality Research*, *15*(1), 99–116. https://doi.org/10.4209/aaqr.2014.01.0006

Andrews, G. E., Ounzain, A. M., Li, H., Bell, M., Tate, J., & Ropkins, K. (2007). The use of a water/lube oil heat exchanger and enhanced cooling water heating to increase water and lube oil heating rates in passenger cars for reduced fuel consumption and CO_2 emissions during cold start. *SAE Technical Papers*, *1*. https://doi.org/10.4271/2007-01-2067

Andrews, G. E., Zhu, G., Li, H., Simpson, A., Wylie, J. A., Bell, M., & Tate, J. (2004). The effect of ambient temperature on cold start urban traffic emissions for a real world SI car. *SAE Technical Papers Series*, *1*. https://doi.org/10.1016/S1366-5545(02)00012-1

Anenberg, S. C., Miller, J., Minjares, R., Du, L., Henze, D. K., Lacey, F., Malley, C. S., Emberson, L., Franco, V., Klimont, Z., & Heyes, C. (2017). Impacts and mitigation of excess diesel-related NO x emissions in 11 major vehicle markets. *Nature*, *545*(7655), 467–471. https://doi.org/10.1038/nature22086

Ansys, I. (2009). *ANSYS FLUENT 12.0 Theory Guide-1.6.1 When to use the compressible flow-model*. https://www.afs.enea.it/project/neptunius/docs/fluent/html/th/node23.htm

Anuj Bhatia. (2018). HVAC system for cars and automotive vehicles. In *CED Engineering*.

Arani, A. A. A., & Moradi, R. (2019). Shell and tube heat exchanger optimization using new baffle and tube configuration. *Applied Thermal Engineering*, *157*, 113736. https://doi.org/10.1016/j.applthermaleng.2019.113736

Arif, S., Muhammad, S., Naqvi, A., Gill, F. T., Qadeer, A., Taweekun, J., Noranai, Z., & Kalvin, R. (2021). Effect of refrigeration assisted intercooler turbocharging on engine's horse power. *Journal of Advanced Research in Fluid Mechanics and Thermal Sciences*, *2*(2), 95–111.

Atkins, R. D. (2009). *An Introduction to Engine Testing and Development*. SAE International.

Atzler, F., Wiedensohler, A., Roß, T., Weinhold, K., & Dobberkau, M. (2021). Roller dynamometer particle emmission measurement. *Automotive and Engine Technology*. https://doi.org/10.1007/s41104-021-00094-1

Aun, S. H. A., Abdullah, M. L., & Al-Zuhairy, R. C. (2020). The influence of ambient conditions on compression ignition engine performance: (experimental study). *Journal of Mechanical Engineering Research and Developments*, *43*(7), 317–325.

Baakeem, S. S., Orfi, J., Alaqel, S., & Al-Ansary, H. (2017). Impact of ambient conditions of arab Gulf countries on the performance of gas turbines using energy and exergy analysis. *Entropy*, *19*(1). https://doi.org/10.3390/e19010032

Bagheri, M., Ghafourian, H., Kashefiolasl, M., Pour, M. T. S., & Rabbani, M. (2020). Travel management optimization based on air pollution condition using markov decision process and genetic algorithm (case study: Shiraz city). *Archives of Transport*, *53*(1), 89–102. https://doi.org/10.5604/01.3001.0014.1746

Balmer, R. T. (2011). Vapor and gas power cycles. In *Modern Engineering Thermodynamics*. https://doi.org/10.1016/b978-0-12-374996-3.00013-0

Barnoon, P., Ashkiyan, M., & Toghraie, D. (2021). Embedding multiple conical vanes inside a circular porous channel filled by two-phase nanofluid to improve thermal performance considering entropy generation. *International Communications in Heat and Mass Transfer*, *124*. https://doi.org/10.1016/j.icheatmasstransfer.2021.105209

Becker, B. (2019). *Cold-air intakes: How and why they work - NASA Speed News Magazine*. https://nasaspeed.news/tech/engine/cold-air-intakes-how-and-why-they-work/

Bentrcia, M., Alshatewi, M., & Omar, H. (2017). Developments of vapor-compression systems for vehicle air-conditioning : A review. *Advances in Mechanical Engineering*, *9*(8), 1–15. https://doi.org/10.1177/1687814017717186

Berger, M., & Cristie, V. (2015). CFD post-processing in Unity3D. *ICCS 2015 International Conference On Computational Science*, *51*, 2913–2922. https://doi.org/10.1016/j.procs.2015.05.476

Bhatt, A. N., & Shrivastava, N. (2022). Application of artificial neural network for internal combustion engines: a state of the art review. *Archives of Computational Methods in Engineering*, *29*(2), 897–919. https://doi.org/10.1007/s11831-021-09596-5

Bhatti, M. M., Marin, M., Zeeshan, A., & Abdelsalam, S. I. (2020). Editorial: recent trends in computational fluid dynamics. *Frontiers in Physics*, *8*(October), 1–4. https://doi.org/10.3389/fphy.2020.593111

Bhatti, S. S., Tyagi, S. K., & Verma, A. (2021). Energy and exergy analysis of vapour absorption cooling system driven by exhaust heat of ic engine. *Lecture Notes in Mechanical Engineering*, 269–276. https://doi.org/10.1007/978-981-15-6360-7_24

Bhavsar, J. J., Matawala, V. K., & Dixit, S. B. (2013). Performance analysis of spiral tube heat exchanger. *International Journal of Engineering and Advanced Technology (IJEAT)*, *2*(4), 684–687.

Bhutta, M. M. A., Hayat, N., Bashir, M. H., Khan, A. R., Ahmad, K. N., & Khan, S. (2012). CFD applications in various heat exchangers design: A review. *Applied Thermal Engineering*, *32*, 1–12.

Biçer, N., Engin, T., Yaşar, H., Büyükkaya, E., & Aydın, A. (2020). Design optimization of a shell-and-tube heat exchanger with novel three-zonal baffle by using CFD and taguchi method. *International Journal of Thermal Sciences*, *155*(April). https://doi.org/10.1016/j.ijthermalsci.2020.106417

Birtok-Băneasă, C., Raţiu, S., & Hepuţ, T. (2017). Influence of intake air temperature on internal combustion engine operation. *IOP Conference Series: Materials Science and Engineering*, *163*, 1–7. https://doi.org/10.1088/1757-899X/163/1/012039

Blazek, J. (2015). Turbulence modeling. In *Computational fluid dynamics: Principles and applications (third edition)* (pp. 213–252). Butterworth-Heinemann. https://doi.org/https://doi.org/10.1016/B978-0-08-099995-1.00007-5

Bonnick, A. (2008). *Automotive science and mathematics*. Routledge.

Borucka, A., Wiśniowski, P., Mazurkiewicz, D., & Świderski, A. (2021). Laboratory measurements of vehicle exhaust emissions in conditions reproducing real traffic. *Measurement*, *174*. https://doi.org/10.1016/j.measurement.2021.108998

Bozza, F., De Bellis, V., & Teodosio, L. (2016). Potentials of cooled EGR and water injection for knock resistance and fuel consumption improvements of gasoline engines. *Applied Energy*, *169*, 112–125. https://doi.org/10.1016/j.apenergy.2016.01.129

Brakora, J. L., & Reitz, R. D. (2010). Investigation of NO_x predictions from biodiesel-fueled HCCI engine simulations using a reduced kinetic mechanism. *SAE International*. https://doi.org/10.4271/2010-01-0577

Brusseau, M. L., Matthias, A. D., Comrie, A. C., & Musil, S. A. (2019). Atmospheric pollution. In *Environmental and Pollution Science (Third Edition)* (3rd ed., Vol. 43). Elsevier Inc. https://doi.org/10.1021/i650501a715

Bucknell, J. R., & Marc Musial. (2004). *Charge air intercooler having a fluid loop integrated with the vehicle air conditioning system* (Patent No. US6796134B1). https://patents.google.com/patent/US6796134B1/en?oq=US+6%2C796%2C134+B

Burke, F. (2018). *Refrigerant allocation between automotive HVAC and engine air/fuel cooling* (Patent No. US9987903B2).

Burke, R. D., Burke, K. A., Chappell, E. C., Gee, M., & Williams, R. (2018). A novel use of multivariate statistics to diagnose test-to-test variation in complex measurement systems. *Measurement*, *130*(June), 467–481. https://doi.org/10.1016/j.measurement.2018.07.059

Buruiana, D. L., Sachelarie, A., Butnaru, C., & Ghisman, V. (2021). Important contributions to reducing nitrogen oxide emissions from internal combustion engines. *International Journal of Environmental Research and Public Health*.

Byard, R. W. (2019). Carbon monoxide – the silent killer. *Forensic Science, Medicine, and Pathology*, *15*(1), 1–2. https://doi.org/10.1007/s12024-018-0040-5

Caillat, S., & Vakkilainen, E. (2013). Large-scale biomass combustion plants: An overview. In *Biomass Combustion Science, Technology and Engineering*. Woodhead Publishing Limited. https://doi.org/10.1533/9780857097439.3.189

Can, G., Saylll, U., Aksu Sayman, Ö., Kuyumcu, Ö. F., Yllmaz, D., Esen, E., Yurtseven, E., & Erginöz, E. (2019). Mapping of carbon monoxide related death risk in

Turkey: A ten-year analysis based on news agency records. *BMC Public Health*, *19*(1), 1–7. https://doi.org/10.1186/s12889-018-6342-4

Casadei, S., & Maggioni, A. (2016). Performance testing of a locomotive engine aftertreatment pre-prototype in a passenger cars chassis dynamometer laboratory. *Transportation Research Procedia*, *14*, 605–614. https://doi.org/10.1016/j.trpro.2016.05.305

Cash, R. Y., Lumsdaine, E., Talekar, A., & AbdulNour, B. (2016). An experimental and computational investigation of water condensation inside the tubes of an automotive compact charge air cooler. *SAE International*, *April*. https://doi.org/10.4271/2016-01-0224

Cesur, I., Gonca, G., Parlak, A., Boru, B., & Ayhan, V. (2013). The effects of electronic controlled steam injection on spark ignition engine. *Applied Thermal Engineering*, *55*, 61–68. https://doi.org/10.1016/j.applthermaleng.2013.02.020

Chan, T. W., Meloche, E., Kubsh, J., Brezny, R., Rosenblatt, D., & Rideout, G. (2013). Impact of ambient temperature on gaseous and particle emissions from a direct injection gasoline vehicle and its implications on particle filtration. *SAE International*, *6*(2). https://doi.org/10.4271/2013-01-0527

Chang, Y., Mendrea, B., Sterniak, J., & Bohac, S. V. (2017). Effect of ambient temperature and humidity on combustion and emissions of a spark-assisted compression ignition engine. *Journal of Engineering for Gas Turbines and Power*, *139*(5), 1–7. https://doi.org/10.1115/1.4034966

Chen, L.-Y., Adi, V. S. K., & Laxmidewi, R. (2022). Shell and tube heat exchanger flexible design strategy for process operability. *Case Studies in Thermal Engineering*, *37*, 102163. https://doi.org/https://doi.org/10.1016/j.csite.2022.102163

Chen, X., Liang, K., Li, Z., Zhao, Y., Xu, J., & Jiang, H. (2020). Experimental assessment of alternative low global warming potential refrigerants for automotive air conditioners application. *Case Studies in Thermal Engineering*, *22*(November). https://doi.org/10.1016/j.csite.2020.100800

Chen, Z., Xiao, F., Shi, J., & Li, A. (2022). Dynamic model development for vehicle air conditioners based on physics-guided deep learning. *International Journal of Refrigeration*, *134*, 126–138. https://doi.org/https://doi.org/10.1016/j.ijrefrig.2021.11.021

Chhalotre, S., Baredar, P., & Soni, S. (2018). Experimental investigation of the effects of insulated air intake system on the performance of naturally aspirated MPSEFI spark ignition engine. *International Conference on Sustainable Engineering and Technology (IConset 2018) AIP Conf. Proc. 2039*, *020001*. https://doi.org/10.1063/1.5078960

Chiba, K., Nozaki, T., Kamiya, Y., & Tanaka, H. (2011). Reduction of pressure loss in suction flow passage of oil flooded screw compressors. *7th International*

Conference on Compressors and Their Systems 2011, 429–439. https://doi.org/10.1533/9780857095350.8.429

Childs, P. R. N., Greenwood, J. R., & Long, C. A. (2000). Review of temperature measurement. *Review of Scientific Instruments*, *71*(8), 2959–2978. https://doi.org/10.1063/1.1305516

Chit, S. P., MA, P. K., & Khaing, C. (2019). Thermal design of a shell and tube heat exchanger. *Iconic Research and Engineering Journals*, *3*(1), 313–318. https://doi.org/10.3303/CET1976044

Choo, R. (2005). *Cryo2-Cryogenic Intake System-Chill2 Win*. https://www.motortrend.com/reviews/turp-0510-cryogenics-intake-system-cryo2/

Christian, C., Christophe, M., & Fariz, M. (2019). How CFD can help to understand corrosion in heat exchanger. *Abu Dhabi International Petroleum Exhibition & Conference*, *November*, 1–16.

Cinar, C., Uyumaz, A., Solmaz, H., Sahin, F., & Yilmaz, E. (2015). Effects of intake air temperature on combustion , performance and emission characteristics of a HCCI engine fueled with the blends of 20 % n-heptane and 80 % isooctane fuels. *Fuel Processing Technology*, *130*, 275–281. https://doi.org/10.1016/j.fuproc.2014.10.026

Cipollone, R., Di Battista, D., & Gualtieri, A. (2013). A novel engine cooling system with two circuits operating at different temperatures. *Energy Conversion and Management*, *75*, 581–592. https://doi.org/10.1016/j.enconman.2013.07.010

Cipollone, Roberto, Di Battista, D., & Gualtieri, A. (2012). Head and block split cooling in ICE. *Workshop on Engine and Powertrain Control, Simulation and Modeling: The International Federation of Automatic Control Rueil-Malmaison, France*, *45*(30), 400–407. https://doi.org/10.3182/20121023-3-FR-4025.00056

Cipollone, Roberto, Di Battista, D., Gualtieri, A., & Massimi, M. (2013). Development of thermal modeling in support of engine cooling design. *SAE International*, 1–11. https://doi.org/10.4271/2013-24-0090

Cipollone, Roberto, Di Battista, D., & Vittorini, D. (2017a). Experimental assessment of engine charge air cooling by a refrigeration unit. *Energy Procedia*, *126*, 1067–1074. https://doi.org/10.1016/j.egypro.2017.08.226

Cipollone, Roberto, Di Battista, D., & Vittorini, D. (2017b). Experimental assessment of engine charge air cooling by a refrigeration unit. *Energy Procedia*, *126*, 1067–1074. https://doi.org/10.1016/j.egypro.2017.08.226

Coker, A. K. (2015). Refrigeration Systems. In *Ludwigs applied process design for chemical and petrochemical plants (fourth edition)* (pp. 623–727). Gulf Professional Publishing. https://doi.org/https://doi.org/10.1016/B978-0-08-094242-1.00017-6

Costa, T. D. O., & Valle, R. M. (2018). Carbon dioxide emissions by tetrafuel technology vehicles (gasoline-ethanol-NGV) with air conditioning on and off. *Energy Efficiency*, *11*, 1009–1021.

Couper, J. R., Penney, W. R., Fair, J. R., & Walas, S. M. (2005). Heat transfer and heat exchangers. In *Chemical Process Equipment (Second Edition)* (pp. 165–224).

Crooks, W. R. (1964). *Method and apparatus for refrigerating combustion air for internal combustion engines* (Patent No. 3141293). https://patents.google.com/patent/US3141293A/en?oq=US3141293

Cruz, P. A. D., Yamat, E.-J. E., Nuqui, J. P. E., & Soriano, A. N. (2022). Computational Fluid Dynamics (CFD) analysis of the heat transfer and fluid flow of copper (II) oxide-water nanofluid in a shell and tube heat exchanger. *Digital Chemical Engineering*, *3*, 100014. https://doi.org/https://doi.org/10.1016/j.dche.2022.100014

Cuce, E., Guclu, T., & Cuce, P. M. (2020). Improving thermal performance of thermoelectric coolers (TECs) through a nano fl uid driven water to air heat exchanger design : An experimental research. *Energy Conversion and Management*, *214*(February), 112893. https://doi.org/10.1016/j.enconman.2020.112893

Cui, G., Dong, Z., Xie, K., Wang, S., Guo, T., Liu, J., Xing, X., & Li, Z. (2021). Effects of gas content and ambient temperature on combustion characteristics of methane hydrate spheres. *Journal of Natural Gas Science and Engineering*, *88*(October 2020), 103842. https://doi.org/10.1016/j.jngse.2021.103842

Cui, X., Chua, K. J., Islam, M. R., & Yang, W. M. (2014). Fundamental formulation of a modified LMTD method to study indirect evaporative heat exchangers. *Energy Conversion and Management*, *88*, 372–381. https://doi.org/10.1016/j.enconman.2014.08.056

Curran, S. J., & Irick, D. K. (2009). On-road emissions evaluation of student-produced biodiesel. *SAE International*, *1*.

Cushman-Roisin, B., & Beckers, J.-M. (2011). Equations of fluid motion. In *Introduction to Geophysical Fluid Dynamics* (Vol. 101, pp. 77–97). Academic Press. https://doi.org/https://doi.org/10.1016/B978-0-12-088759-0.00003-1

Czaban, J., & Szpica, D. (2013). Drive test system to be used on roller dynamometer. *Mechanika*, *19*(5), 600–605. https://doi.org/10.5755/j01.mech.19.5.5542

Dagnachew, A., Hof, A., Van Soest, H., & Van Vuuren, D. (2021). Climate change measures and sustainable development goals. In *PBL Netherlands Environmental Assessment Agency* (Issue June). www.pbl.nl/en.

Dahlan, A. A., Zulkifli, A. H., Nasution, H., Aziz, A. A., Perang, M. R. M., Jamil, H. M., & Zulkifli, A. A. (2014). Efficient and "green" vehicle air conditioning system using electric compressor. *Energy Procedia*, *61*, 270–273. https://doi.org/10.1016/j.egypro.2014.11.1105

Degraeuwe, B., & Weiss, M. (2017). Does the new european driving cycle (NEDC) really fail to capture the NO_X emissions of diesel cars in Europe? *Environmental Pollution*, *222*(X), 234–241. https://doi.org/10.1016/j.envpol.2016.12.050

Dey, S., & Mehta, N. S. (2020). Automobile pollution control using catalysis. *Resources, Environment and Sustainability*, *2*(November), 100006. https://doi.org/10.1016/j.resenv.2020.100006

Di Battista, D., Mauriello, M., & Cipollone, R. (2015). Waste heat recovery of an ORC-based power unit in a turbocharged diesel engine propelling a light duty vehicle. *Applied Energy*, *152*, 109–120. https://doi.org/10.1016/j.apenergy.2015.04.088

Di Battista, Davide, & Cipollone, R. (2016). High efficiency air conditioning model based analysis for the automotive sector. *International Journal of Refrigeration*, 1–44. https://doi.org/10.1016/j.ijrefrig.2015.12.014

Di Battista, Davide, Vittorini, D., Di Bartolomeo, M., & Cipollone, R. (2018). Optimization of the engine intake air temperature through the air conditioning unit. *SAE Technical Papers*, *2018-April*, 1–10. https://doi.org/10.4271/2018-01-0973

Dincer, I. (2017). *Refrigeration systems and applications*. John Wiley & Sons.

Doo, J. H., Ha, M. Y., Min, J. K., Stieger, R., Rolt, A., & Son, C. (2012). Theoretical prediction of longitudinal heat conduction effect in cross-corrugated heat exchanger. *International Journal of Heat and Mass Transfer*, *55*(15), 4129–4138. https://doi.org/https://doi.org/10.1016/j.ijheatmasstransfer.2012.03.054

Dora, N., Mendu, S. S., & Lakshmipati Raju, B. (2020). Comparative study of conjugate heat transfer characteristics in chevron corrugated plate heat exchanger using CuO nanocoolant. *Arabian Journal for Science and Engineering*, *45*(11), 8955–8967. https://doi.org/10.1007/s13369-020-04631-2

Douaud, A. M., & Eyzat, P. (1978). Four-octane-number method for predicting the anti-knock behavior of fuels and engines. *SAE Technical Papers*, 294–308. https://doi.org/10.4271/780080

Elrentisy, M. H., Abdellatif, Y. M., Elbashir, A. M., & Ahmed, S. F. (2022). Development of an air-cooled induction manifold for diesel engines in hot and humid climate. *Journal of Energy Resources Technology*, *144*(7).

Engkuah, S., Nasution, H., & Aziz, A. A. (2016). Performance characteristic study on air to water intercooler. *Applied Mechanics and Materials*, *819*(1), 42–45. https://doi.org/10.4028/www.scientific.net/AMM.819.42

Enweremadu, C. C., & Rutto, H. L. (2010). Combustion, emission and engine performance characteristics of used cooking oil biodiesel—A review. *Renewable* *and Sustainable Energy Reviews*, *14*(9), 2863–2873. https://doi.org/https://doi.org/10.1016/j.rser.2010.07.036

Epstein, Y., & Moran, D. S. (2019). Extremes of temperature and hydration. In *Travel Medicine* (Fourth Edi, pp. 407–415). Elsevier Inc. https://doi.org/10.1016/B978-0-323-54696-6.00044-6

Espinel-Blanco, E. E., Flores-Solano, E., & Arévalo-Ruedas, J. H. (2020). Energy evaluation of a refrigeration system by calculating the coefficient of performance. *Journal of Physics: Conference Series*, *1708*(1). https://doi.org/10.1088/1742-6596/1708/1/012010

Fathi, M., Ganji, D. D., & Jahanian, O. (2020). Intake charge temperature effect on performance characteristics of direct injection low-temperature combustion engines. *Journal of Thermal Analysis and Calorimetry*, *139*(4), 2447–2454. https://doi.org/10.1007/s10973-019-08515-y

Fayazbakhsh, M. A., & Bahrami, M. (2013). Comprehensive modeling of vehicle air conditioning loads using heat balance method. *SAE International*, *1*. https://doi.org/10.4271/2013-01-1507

Ferrari, G., Onorati, A., & D'Errico, G. (2022). *Internal combustion engines*. Società Editrice Esculapio.

Focke, W. W., Zachariades, J., & Olivier, I. (1985). The effect of the corrugation inclination angle on the thermohydraulic performance of plate heat exchangers. *International Journal of Heat and Mass Transfer*, *28*(8), 1469–1479. https://doi.org/https://doi.org/10.1016/0017-9310(85)90249-2

Forde, C. J., Meaney, M., Carrigan, J. B., Mills, C., Boland, S., & Hernon, A. (2014). Biobased Fats (Lipids) and Oils from Biomass as a Source of Bioenergy. In *Bioenergy Research: Advances and Applications*. https://doi.org/10.1016/B978-0-444-59561-4.00012-7

Fredrico Burke. (2018). *Refrigerant allocation between automotive hvac and engine air / fuel cooling.* (Patent No. US9987903B2).

G.Speight, J. (2020). *Handbook of Industrial Hydrocarbon Processes (Second Edition)* (Vol. 130, Issue 3281). https://doi.org/10.1016/B978-0-12-809923-0.00010-2

Gado, A., Hwang, Y., & Radermacher, R. (2008). Dynamic behavior of mobile Air-Conditioning systems. *HVAC and R Research*, *14*(2), 307–321. https://doi.org/10.1080/10789669.2008.10391010

Galindo, J., Dolz, V., Tiseira, A., & Ponce-Mora, A. (2019). Thermodynamic analysis and optimization of a jet ejector refrigeration cycle used to cool down the intake air in an IC engine. *International Journal of Refrigeration*, *103*, 253–263. https://doi.org/10.1016/j.ijrefrig.2019.04.019

Galindo, José, Climent, H., Varnier, O., & Patil, C. (2018). Effect of boosting system architecture and thermomechanical limits on diesel engine performance: Part-I—Steady-state operation. *International Journal of Engine Research*, *19*(8), 854–872. https://doi.org/10.1177/1468087417731654

Gan, G., Riffat, S. B., & Shao, L. (2000). CFD modelling of pressure loss across tube bundles of a heat exchanger for closed-wet cooling towers. *International Journal of Ambient Energy*, *21*(2), 77–84. https://doi.org/10.1080/01430750.2000.9675358

Ge, H., & Zhao, P. (2019). Numerical Investigation of the Spark Plug Orientation Effects on Flame Kernel Growth. *SAE Technical Papers*, *2019-Janua*(January). https://doi.org/10.4271/2019-01-0005

Geeks, L. (2023). *The impact of ambient temperature on four-stroke engine performance: a comprehensive analysis*. https://lambdageeks.com/the-impact-of-ambient-temperature-on-four-stroke-engine-performance/

George D Thurston. (2017). Outdoor air pollution: sources, atmospheric transport, and human health effects. In *International Encyclopedia of Public Health* (Second Edi, Vol. 5, Issue 69). Elsevier. https://doi.org/10.1016/B978-0-12-803678-5.00320-9

Ghasemzadeh, K., Sadati Tilebon, S. M., Nasirinezhad, M., & Basile, A. (2018). Economic assessment of methanol production. In *Methanol: Science and Engineering*. Elsevier B.V. https://doi.org/10.1016/B978-0-444-63903-5.00023-6

Gherasim, I., Galanis, N., & Nguyen, C. T. (2011). Heat transfer and fluid flow in a plate heat exchanger. Part II: Assessment of laminar and two-equation turbulent models. *International Journal of Thermal Sciences*, *50*(8), 1499–1511. https://doi.org/https://doi.org/10.1016/j.ijthermalsci.2011.03.017

Gis, W., & Taubert, S. (2021). The issues of the air-fuel ratio in exhaust emissions tests carried out on a chassis dynamometer. *Energies*, *14*(9). https://doi.org/10.3390/en14092360

Gnielinski, V. (1976). New equations for heat and mass transfer in turbulent pipe and channel flow. *Int. Chem. Eng.*, *16*(2), 359–368.

Gocmen, K., & Soyhan, H. S. (2020). An intake manifold geometry for enhancement of pressure drop in a diesel engine. *Fuel*, *261*(March 2019). https://doi.org/10.1016/j.fuel.2019.116193

Goswami, D. Y., Ek, G., Leung, M., Jotshi, C. K., Sherif, S. A., & Colacino, F. (2001). Effect of refrigerant charge on the performance of air conditioning systems. *International Journal of Energy Research*, *25*(8), 741–750. https://doi.org/10.1002/er.719

Gürel, B., Akkaya, V. R., Göltaş, M., Şen, Ç. N., Güler, O. V., Koşar, M. İ., & Keçebaş, A. (2020). Investigation on flow and heat transfer of compact brazed plate heat exchanger with lung pattern. *Applied Thermal Engineering*, *175*, 115309. https://doi.org/https://doi.org/10.1016/j.applthermaleng.2020.115309

H.Forsberg, C. (2021a). Heat exchangers. In *Heat Transfer Principles and Applications* (pp. 305–341). Elsevier Inc. https://doi.org/10.1016/B978-0-12-802296-2.00008-1

H.Forsberg, C. (2021b). Introduction to heat transfer. In *Heat Transfer Principles and Applications* (pp. 1–21). Elsevier Inc. https://doi.org/10.1016/B978-0-12-802296-2.00001-9

Hall, D. O., Barnard, G. W., & Moss, P. A. (1982). Future biomass energy options. *Biomass for Energy in the Developing Countries*, 29–106. https://doi.org/10.1016/B978-0-08-028689-1.50014-7

Hamrock, B. J., Schmid, S. R., & Jacobson, B. O. (2004). *Fundamental of Fluid Film Lubrication Second edition*.

Han, W., Saleh, K., Aute, V., Ding, G., Hwang, Y., & Radermacher, R. (2011). Numerical simulation and optimization of single-phase turbulent flow in chevron-type plate heat exchanger with sinusoidal corrugations. *HVAC and R Research*, *17*(2), 186–197. https://doi.org/10.1080/10789669.2011.558167

Handibag, R., Potdar, D. U., & Jadhav, A. (2020). *Thermal Design of Tube and Shell Heat Exchanger and Verification by HTRI Software*. *9*(12), 525–530.

Harada, M., Yasuda, T., Terachi, S., Pujols, S., & Spenny, J. R. (2016). Water cooled charge air cooler development. *SAE Technical Papers*, 1–5. https://doi.org/10.4271/2016-01-0651

Haraldsson, G., Tunestål, P., Johansson, B., & Hyvonen, J. (2004). HCCI closed-loop combustion control using fast thermal management. *SAE Technical Papers Series*, *1*.

Harris, A., & Hughes, C. A. V. (2011). Development of a thermal management control system for electric vehicles. In *Institution of Mechanical Engineers - VTMS 10, Vehicle Thermal Management Systems Conference and Exhibition* (pp. 363–372). Woodhead Publishing Limited. https://doi.org/10.1533/9780857095053.4.363

Heard, S. (2018). *Can a bad compressor stop the car from moving? - Quora*. https://www.quora.com/Can-a-bad-compressor-stop-the-car-from-moving

Herbert Joyner. (1963). *Utilizing vehicle air-conditioning system for internal combustion engine.* (Patent No. 3071934). https://patents.google.com/patent/US30%0A71934A/en

Hewitt, G. F., Shires, G. L., & Bott, T. R. (1994). *T. Reg Bott G. F. Hewitt, G. L. Shires , George L. Shires, T. R. Bott - Process Heat Transfer,* CRC Press.

Heywood, J. B. (1988). *Internal combustion engine fundamentals. N. York: McGraw-Hill*.

Heywood, J. B. (2018). *Internal combustion engine fundamentals* (Second). McGraw Hill Education.

Hiereth, H., & Prenninger, P. (2007). *Charging the Internal Combustion Engine*. SpringerWienNewYork.

Hinch, E. J. (2020). Think before you compute, a prelude to computational fluid dynamics. In *Cambridge University Press*. https://doi.org/10.1017/9781108855297

Hu, T., Wei, Y., Liu, S., & Zhou, L. (2007). Improvement of spark-ignition (SI) engine combustion and emission during cold start, fueled with methanol/gasoline blends. *Energy and Fuels*, *21*(1), 171–175. https://doi.org/10.1021/ef0603479

Hu, Z., & Ladommatos, N. (1996). Reduction of unburnt hydrocarbon emissions from spark ignition engines using in-cylinder catalysts. *Proceedings of the Institution of Mechanical Engineers, Part D: Journal of Automobile Engineering*, *210*(2), 123–129. https://doi.org/10.1243/PIME_PROC_1996_210_253_02

Huang, Y., Hong, G., & Huang, R. (2015). Investigation to charge cooling effect and combustion characteristics of ethanol direct injection in a gasoline port injection engine. *Applied Energy*, *160*, 244–254. https://doi.org/10.1016/j.apenergy.2015.09.059

Hudelson, D. L. (2002). Engine charge air cooler (Patent No. US6394076B1). In *United States Patent* (US6394076B1). https://patents.google.com/patent/US6394076B1/en?oq=US+6%2C394%2C076+B1

Huff, S., West, B., & Thomas, J. (2013). Effects of air conditioner use on real-world fuel economy. *SAE Technical Papers*, *2*. https://doi.org/10.4271/2013-01-0551

Huilgol, R. R. (2021). Serrin's accumulation function, the First and the Second Laws of Thermodynamics. *Applications in Engineering Science*, *7*, 100057. https://doi.org/10.1016/j.apples.2021.100057

Hundy, G. F., Trott, A. R., & Welch, T. C. (2008). *Refrigeration and Air conditioning* (Fourth). Butterworth-Heinemann.

Hundy, G. F., Trott, A. R., & Welch, T. C. (2016). Air conditioning methods and applications. In *Refrigeration, Air Conditioning and Heat Pumps*. https://doi.org/10.1016/b978-0-08-100647-4.00024-3

Huo, X. Q., Xu, Y., Zhang, T., Wang, J. H., & Wang, H. X. (2019). Research on the pressure drop characteristics of spiral flow in horizontal straight pipe. *2019 IEEE International Instrumentation and Measurement Technology Conference (I2MTC)*. https://doi.org/10.1109/I2MTC.2019.8826932

Ikhtiar, U., Manzoor, S., Sheikh, N. A., & Ali, M. (2016). Free stream flow and forced convection heat transfer around a rotating circular cylinder subjected to a single gust impulse. *International Journal of Heat and Mass Transfer*, *99*, 851–861. https://doi.org/10.1016/j.ijheatmasstransfer.2016.04.045

Ilnicki, A., & Rzasa, M. (2018). Problems of mesh generation in numerical modeling of the combustion engine with variable compression ratio. *2018 International Interdisciplinary PhD Workshop (IIPhDW)*, 248–253.

Ino, M., Sato, O., & Yamamoto, Y. (2015). *Air intake device* (Patent No. US8955497B2). https://patents.google.com/patent/US89%0A55497B2/en

Irimescu, A., Merola, S. S., Tornatore, C., & Valentino, G. (2017a). Effect of coolant temperature on air–fuel mixture formation and combustion in an optical direct injection spark ignition engine fueled with gasoline and butanol. *Journal of the Energy Institute*, *90*(3), 452–465. https://doi.org/https://doi.org/10.1016/j.joei.2016.03.004

Irimescu, A., Merola, S. S., Tornatore, C., & Valentino, G. (2017b). Effect of coolant temperature on air e fuel mixture formation and combustion in an optical direct injection spark ignition engine fueled with gasoline and butanol. *Journal of the Energy Institute*, *90*(3), 452–465. https://doi.org/10.1016/j.joei.2016.03.004

Jadhav, A. D., & Koli, T. A. (2014). CFD analysis of shell and tube heat exchanger to study the effect of baffle cut on the pressure drop. *International Journal of Research in Aeronautical and Mechanical Engineering*, *2*(7), 1–7.

Jain, R., Pal, S. K., & Singh, S. B. (2017). Numerical modeling methodologies for friction stir welding process. In J. B. T.-C. M. and P. E. Paulo Davim (Ed.), *Woodhead Publishing Reviews: Mechanical Engineering Series* (pp. 125–169). Woodhead Publishing. https://doi.org/https://doi.org/10.1016/B978-0-85709-481-0.00005-7

Jaiprakash, & Habib, G. (2018). On-road assessment of light duty vehicles in Delhi city: Emission factors of CO, CO2 and NOX. *Atmospheric Environment*, *174*(July 2017), 132–139. https://doi.org/10.1016/j.atmosenv.2017.11.039

Jayakumar, J. S., Mahajani, S. M., Mandal, J. C., Vijayan, P. K., & Bhoi, R. (2008). Experimental and CFD estimation of heat transfer in helically coiled heat exchangers. *Chemical Engineering Research and Design*, *86*(3), 221–232. https://doi.org/https://doi.org/10.1016/j.cherd.2007.10.021

Jayanti, S. (2018). Computational fluid dynamics for engineers and scientists. In *Computational Fluid Dynamics for Engineers and Scientists*. https://doi.org/10.1007/978-94-024-1217-8

Jemni, M. A., HadjKacem, S., Ammar, M., Saaidia, R., Brayek, M., & Abid, M. S. (2021). Variable intake manifold geometry influence on volumetric efficiency enhancement at gaseous engine starting speeds. *Proceedings of the Institution of Mechanical Engineers, Part E: Journal of Process Mechanical Engineering*, *235*(2), 548–559. https://doi.org/10.1177/0954408920973129

Jeter, S. M. S. (2006). Effectiveness and LMTD correction factor of the cross flow exchanger: a simplified and unified treatment. *2006 ASEE Southeast Section Conference*, 1–10. http://icee.usm.edu/ICEE/conferences/ASEE-SE-2010/Conference Files/ASEE2006/P2006092JET.pdf

Jia-Wei, W., & Hsueh, M.-H. (2013). The analysis of engine intake air cooling device by using thermoelectric module. In *Intelligent Technologies and Engineering Systems, Lecture Notes in Electrical Engineering 234* (pp. 773–782). Springer. https://doi.org/10.1007/978-1-4614-6747-2_89

Jianbo Li, S. X. (2013). The performance of absorption-compression hybrid refrigeration driven by waste heat and power from coach engine. *Applied Thermal Engineering*, *61*(2), 747–757. https://doi.org/10.1016/j.applthermaleng.2013.08.048

Jo, S., Park, S., Jun, H., & Lee, J. (2019). Combustion improvement and emission reduction through control of ethanol ratio and intake air temperature in reactivity controlled compression ignition combustion engine. *Applied Energy*, *250*, 1418–1431. https://doi.org/10.1016/j.apenergy.2019.05.012

Joel H. Ferziger, Perić, M., & -, R. L. S. (2020). *Computational Methods for Fluid Dynamics-(Fourth Edition)* (Fourth). Springer. https://doi.org/https://doi.org/10.1007/978-3-319-99693-6

Johnson, T. (2010). *Engine air intake and fuel chilling system and method.* (Patent No. US7658183B1). https://patents.google.com/patent/US7658183B1/en

Jonathan Michael Stearns Mattson. (2019). *Modeling of compression ignition engines for advanced engine operation and alternative fuels by the second law of thermodynamics*. University of Kansas.

Kadunic, S., Scherer, F., Baar, R., & Friedrich, I. (2014). Cool2Power - Increased petrol engine power and efficiency through an AC driven intercooling system. In *Institution of Mechanical Engineers - 11th International Conference on Turbochargers and Turbocharging*. Woodhead Publishing Limited. https://doi.org/10.1533/978081000342.3

Kakaç, S., Liu, H., & Pramuanjaroenkij, A. (2020). *Heat exchangers; Selection, Rating and Thermal Design 4th edition*. CRC Press Taylor and Francis Group.

Kalghatgi, G. (2018). Is it really the end of internal combustion engines and petroleum in transport? *Applied Energy*, *225*(April), 965–974. https://doi.org/10.1016/j.apenergy.2018.05.076

Kalkan, O. O. (2014). *Implementation of k-epsilon turbulence models in a two dimensional parallel navier-stokes solver on hybrid grids* (Issue September). The Graduate School Of Natural And Applied Sciences Of Middle East Technical University.

Kamal, S., Eqqab, I., & Raphael, R. (2022). Influence of intake air temperature on the performance of gasoline engines using a different type of fuel. *Al-Qadisiyah Journal for Engineering Sciences*, *15*, 229–237.

Kamaruddin, R. B. (2010). *Design of a small heat exchaner (Shell and tube type)* (Issue November). Universiti Malaysia Pahang.

Kaul, S., Joshi, T., & Varshney, L. (2021). Analysis of hot air duct between turbocharger and intercooler. *Materials Today: Proceedings*, *43*, 719–725. https://doi.org/10.1016/j.matpr.2020.12.846

Kaviany, M. (2014). *Heat transfer physics*. Cambridge University Press.

Ketwong, W., Deethayat, T., & Kiatsiriroat, T. (2021). Performance enhancement of air conditioner in hot climate by condenser cooling with cool air generated by direct evaporative cooling. *Case Studies in Thermal Engineering*, *26*(January), 101127. https://doi.org/10.1016/j.csite.2021.101127

Khairul, M. A., Alim, M. A., Mahbubul, I. M., Saidur, R., Hepbasli, A., & Hossain, A. (2014). Heat transfer performance and exergy analyses of a corrugated plate heat exchanger using metal oxide nanofluids. *International Communications in Heat and Mass Transfer*, *50*, 8–14. https://doi.org/https://doi.org/10.1016/j.icheatmasstransfer.2013.11.006

Khan, T., & Frey, H. C. (2019). Effect of air-conditioning on light duty gasoline vehicles fuel economy. *Transportation Research Record*, 1–11. https://doi.org/10.1177/0361198119838507

Khayyam, H., Nahavandi, S., Hu, E., Kouzani, A., Chonka, A., Abawajy, J., Marano, V., & Davis, S. (2011). Intelligent energy management control of vehicle air conditioning via look-ahead system. *Applied Thermal Engineering*, *31*(16), 3147–3160. https://doi.org/10.1016/j.applthermaleng.2011.05.023

Kim, S., & Kim, H. (2016). A new metric of absolute percentage error for intermittent demand forecasts. *International Journal of Forecasting*, *32*(3), 669–679. https://doi.org/10.1016/j.ijforecast.2015.12.003

Kim, W., & Braun, J. E. (2012). Evaluation of the impacts of refrigerant charge on air conditioner and heat pump performance Evaluation. *International Journal of Refrigeration*, *35*(7), 1805–1814. https://doi.org/10.1016/j.ijrefrig.2012.06.007

Kirkpatrick, A. T. (2021). *Internal combustion engines* (Fourth). Wiley.

Klem, R. H. (2002). *Intercooler system for internal combustion engine.* (Patent No. US2002/0116927A1).

https://patents.google.com/patent/US6347618?oq=Intercooler+system+for+internal+combustion+engine.

Kolakoti, A., Kumar, A. V., Metta, R., Setiyo, M., & Rochman, M. L. (2022). Experimental studies on in-cylinder combustion, exergy performance, and exhaust emission in a Compression Ignition engine fuelled with neat biodiesels. *Indonesian Journal of Science and Technology*, *7*(2), 219–236. https://doi.org/10.17509/ijost.v7i2.49680

Koltsakis, G. C., & Stamatelos, A. M. (1997). Catalytic automotive exhaust aftertreatment. *Progress in Energy and Combustion Science*, *23*(1), 1–39. https://doi.org/10.1016/s0360-1285(97)00003-8

Konar, D. (2015). Applications of jet ejectors for efficient refrigeration and modelling of multi phase multi fluid flow in ejectors. *IOP Conference Series: Materials Science and Engineering*, *88*(1). https://doi.org/10.1088/1757-899X/88/1/012060

Kula, S., Bulut, E., Altay, E., Sümer, O., & Öztürk, F. (2022). Smart cooling design using dual loop cooling to increase engine efficiency and decrease fuel emissions with artificial intelligence. *Case Studies in Thermal Engineering*, *40*. https://doi.org/10.1016/j.csite.2022.102351

Kumar, V., Saini, S., Sharma, M., & Nigam, K. D. P. (2006). Pressure drop and heat transfer study in tube-in-tube helical heat exchanger. *Chemical Engineering Science*, *61*(13), 4403–4416. https://doi.org/https://doi.org/10.1016/j.ces.2006.01.039

Kumareswaran, S. (2014). *Design of a shell and tube heat exchangers* [University of Moratuwa]. https://doi.org/10.13140/RG.2.1.2721.6720/1

Larowski, A., & Taylor, M. A. (1983). Systematic procedure for selection of heat exchangers. *Proceedings of the Institution of Mechanical Engineers, Part A: Journal of Power and Energy*, *197*(1), 51–69. https://doi.org/10.1243/PIME_PROC_1983_197_006_02

Laskowski, P., Zasina, D., Zimakowska-Laskowska, M., Zawadzki, J., & Warchałowski, A. (2019). Vehicle hydrocarbons' emission characteristics determined using the monte carlo method. *Environmental Modeling and Assessment*, *24*(3), 311–318. https://doi.org/10.1007/s10666-018-9640-4

Lauren Forth. (2021). *316 Stainless Steel - Special Piping Materials*. https://specialpipingmaterials.com/316-stainless-steel/

Lee, Jonghyeok, & Lee, K.-S. (2015). Friction and Colburn factor correlations and shape optimization of chevron-type plate heat exchangers. *Applied Thermal Engineering*, *89*, 62–69. https://doi.org/https://doi.org/10.1016/j.applthermaleng.2015.05.080

Lee, Jungwoo, Kim, J., Park, J., & Bae, C. (2013). Effect of the air-conditioning system on the fuel economy in a gasoline engine vehicle. *Proceedings of the Institution of Mechanical Engineers, Part D: Journal of Automobile Engineering*, *227*(1), 66–77. https://doi.org/10.1177/0954407012455973

Lee, M. Y. (2017). Design and cooling performances of an air conditioning system with two parallel refrigeration cycles for a special purpose vehicle. *Applied Sciences*, *7*(2). https://doi.org/10.3390/app7020190

Lee, T., Shin, K., Kim, J., Jung, D., & Kim, J. (2021). Design optimization of external variable displacement compressor with R1234yf for vehicle air conditioning system. *Applied Thermal Engineering*, *198*(September), 117493. https://doi.org/10.1016/j.applthermaleng.2021.117493

Li, A., Kosonen, R., & Hagström, K. (2020). Industrial ventilation design method. In *Industrial Ventilation Design Guidebook (Second edition)* (pp. 19–37). https://doi.org/10.1016/b978-0-12-816780-9.00003-4

Lim, J. W., Narendran, N., Chai, C. E., & Ma'Arof, M. I. N. (2020). A review on the air flow behaviour in the intake pipe. *IOP Conference Series: Materials Science and Engineering*, *854*, 1–12. https://doi.org/10.1088/1757-899X/854/1/012010

Lima, A. A. S., Leite, G. de N. P., Ochoa, A. A. V., Dos Santos, C. A. C., da Costa, J. A. P., Michima, P. S. A., & Caldas, A. M. A. (2021). Absorption refrigeration systems based on ammonia as refrigerant using different absorbents: Review and applications. *Energies*, *14*(1). https://doi.org/10.3390/en14010048

Lindhjem, C., Chan, L., Pollack, A., Corporation, E. I., Way, R., & Kite, C. (2004). Applying humidity and temperature corrections to on and off-road mobile source emissions. *EPA 13th International Emission Inventory Conference: Working for Clean Air in Clearwater,FL*.

Liu, Z., Karimi, I. A., & He, T. (2019). A novel inlet air cooling system based on liquefied natural gas cold energy utilization for improving power plant performance. *Energy Conversion and Management*, *187*(November 2018), 41–52. https://doi.org/10.1016/j.enconman.2019.03.015

Ma'arof, M. I. N., Asmara, Y. P., Suresh, S., Suresh, S., & Chala, G. T. (2019). The development of an aftermarket intercooler spray for turbocharged vehicles using water. *INTI Journal*, *017*. https://doi.org/10.1088/1757-899X/863/1/012066

Ma'Arof, M. I. N., Chala, G. T., Suresh, S., & Suresh, S. (2020). The development of an aftermarket intercooler spray for turbocharged vehicles using ethylene glycol and hyaluronic acid. *IOP Conference Series: Materials Science and Engineering*, *863*(1). https://doi.org/10.1088/1757-899X/863/1/012066

Mader, C. A., Kenway, G. K. W., Yildirim, A., & Martins, J. R. R. A. (2020). ADflow: An open-source computational fluid dynamics solver for aerodynamic and multidisciplinary optimization. *Journal of Aerospace Information Systems*, *17*(9), 508–527. https://doi.org/10.2514/1.I010796

Malaquias, A. C. T., Netto, N. A. D., Filho, F. A. R., da Costa, R. B. R., Langeani, M., & Baêta, J. G. C. (2019). The misleading total replacement of internal combustion engines by electric motors and a study of the Brazilian ethanol importance for the sustainable future of mobility: a review. *Journal of the Brazilian Society of Mechanical Sciences and Engineering*, *41*(12), 1–23. https://doi.org/10.1007/s40430-019-2076-1

Mamat, R., Abdullah, N. R., Xu, H., Wyszynski, M. L., & Tsolakis, A. (2009). Effect of air intake pressure drop on performance and emissions of a diesel engine operating with biodiesel and ultra low sulphur diesel (ULSD). *Renewable Energy and Power Quality Journal*, *1*(7), 787–794. https://doi.org/10.24084/repqj07.504

Mamat, R., Yusop, A. F., Abdullah, A. A., Aziz, A., & Abdullah, N. R. (2013). Effect of exhaust gas recirculation system and air temperature on exhaust emission of a diesel engine operating with biodiesel. *Journal of Biobased Materials and Bioenergy*, *7*(4), 461–463. https://doi.org/10.1166/jbmb.2013.1346

Manmadhachary, A., Santosh Kumar, M., & Ravi Kumar, Y. (2017). Design & manufacturing of spiral intake manifold to improve volument efficiency of injection diesel engine by AM process. *Materials Today: Proceedings*, *4*, 1084–1090. https://doi.org/https://doi.org/10.1016/j.matpr.2017.01.123

Manzela, A. A., Hanriot, S. M., Cabezas-Gómez, L., & Sodré, J. R. (2010). Using engine exhaust gas as energy source for an absorption refrigeration system. *Applied Energy*, *87*(4), 1141–1148. https://doi.org/10.1016/j.apenergy.2009.07.018

Marshall, G. J., Mahony, C. P., Rhodes, M. J., Daniewicz, S. R., Tsolas, N., & Thompson, S. M. (2019). Thermal management of vehicle cabins, external surfaces, and onboard electronics: an overview. *Engineering*, *5*(5), 954–969. https://doi.org/10.1016/j.eng.2019.02.009

Martyr, A. J., & Plint, M. A. (2007). *Engine Testing Theory and Practice* (Vol. 53, Issue 9). Elsevier Butterworth-Heinemann.

Martyr, A. J., & Plint, M. A. (2012). Engine testing. In *Engine Testing* (Fourth). Elsevier BH. https://doi.org/10.1016/C2010-0-66322-X

Martyr, Anthony J., & Rogers, D. R. (2021). Measurement of liquid fuel, oil, and combustion air consumption. *Engine Testing*, 511–535. https://doi.org/10.1016/B978-0-12-821226-4.00015-2

Masson-Delmotte, Zhai, P., Pirani, A., Connors, S. L., Péan, C., Berger, S., Caud, N., Chen, Y., Goldfarb, L., Gomis, M. I., Huang, M., Leitzell, Lonnoy, K. E., Matthews, J. B. R., Maycock, T. K., Waterfield, T., & Yelekçi, O. (2021). IPCC, 2021: Summary for policymakers in climate change; the physical science basis. In *Working Group I Contribution to the Sixth Assessment Report of the Intergovernmental Panel on Climate Change*. https://www.ipcc.ch/report/ar6/wg1/

Matti Maricq, M. (2007). Chemical characterization of particulate emissions from diesel engines: A review. *Journal of Aerosol Science*, *38*(11), 1079–1118. https://doi.org/10.1016/j.jaerosci.2007.08.001

Mebarki, B., Draoui, B., Allaou, B., Rahmani, L., & Benachour, E. (2013). Impact of the air-conditioning system on the power consumption of an electric vehicle powered by lithium-ion battery. *Modelling and Simulation in Engineering*. https://doi.org/10.1155/2013/935784

Mei, B., Barnoon, P., Toghraie, D., Su, C. H., Nguyen, H. C., & Khan, A. (2022). Energy, exergy, environmental and economic analyzes (4E) and multi-objective optimization of a PEM fuel cell equipped with coolant channels. *Renewable and Sustainable Energy Reviews*, *157*. https://doi.org/10.1016/j.rser.2021.112021

Melo, C., da Silva, L. W., & Pereira, R. H. (2000). Experimental evaluation of the heat transfer through the walls of household refrigerators. *International Refrigeration and Air Conditioning Conference*, 353–360. http://docs.lib.purdue.edu/iracc/502

Merdan, S. A., & Kadhim, Z. khalefa. (2021). Study the flow direction and number of tubes in cross-flow heat exchanger to improve the heat transfer coefficient. *IOP Conference Series: Materials Science and Engineering*, *1076*(1), 012075. https://doi.org/10.1088/1757-899x/1076/1/012075

Mezher, H., Migaud, J., Raimbault, V., Lelong, J. G., Chalet, D., Perrot, N., Hunault, A., Chesse, P., & Huurdeman, B. (2013). Optimized air intake for a turbocharged engine taking into account water-cooled charge air cooler reflective properties for acoustic tuning. *SAE Technical Papers*, *2*. https://doi.org/10.4271/2013-01-0575

Miansari, M., Ali, M., Hossein, V., & Davood, A. (2020). Energy and exergy analysis and optimization of helically grooved shell and tube heat exchangers by using Taguchi experimental design. *Journal of Thermal Analysis and Calorimetry*, *139*(5), 3151–3164. https://doi.org/10.1007/s10973-019-08653-3

Mifdal, M. Y. A., Nuraida, M. H., Norzalina, O., & Shamil, A. H. (2015). Turbo intercooler cooling system. *International Journal of Engineering Science Invention*, *4*(1), 49–56.

Mingrui, W., Thanh Sa, N., Turkson, R. F., Jinping, L., & Guanlun, G. (2017). Water injection for higher engine performance and lower emissions. *Journal of the Energy Institute*, *90*(2), 285–299. https://doi.org/10.1016/j.joei.2015.12.003

Misztal, J., Xu, H., Tsolakis, A., Wyszynski, M. L., Constandinides, G., Price, P., & Qiao, J. (2009). Influence of inlet air temperature on gasoline HCCI particulate emissions. *Combustion Science and Technology*, *181*(5), 695–709. https://doi.org/10.1080/00102200902851610

Mnati, H., Almayyahi, A., & Al-obaidi, M. (2022). Sensitivity analysis of air-intake temperature on the performance of a gasoline engine of Daewoo prince. *IMDC-IST*, 1–9. https://doi.org/10.4108/eai.7-9-2021.2314435

Mokhtari, M., Gharehpetian, G. B., & Mousavi Agah, S. M. (2017). Distributed energy resources. In *Distributed Generation Systems: Design, Operation and Grid Integration*. Elsevier Inc. https://doi.org/10.1016/B978-0-12-804208-3.00001-7

Morad, M. M. A., & Alrajhi, J. (2014). The effect of high temperature on engine performance in kuwait conditions. *Journal of Mechanical Engineering and Automation*, *4*(2), 55–62. https://doi.org/10.5923/j.jmea.20140402.02

Moskalik, A., Dekraker, P., Kargul, J., & Barba, D. (2015). Vehicle component benchmarking using a chassis dynamometer. *SAE International Journal of Materials and Manufacturing*, *8*(3), 869–879. https://doi.org/10.4271/2015-01-0589

Murad, S. H. B. M. (2009). *Study of a new air intake system for a single cylinder, fuel injection, 4 stroke Go-Kart engine*. Universiti Teknologi PETRONAS.

Musgrove, G., Bauer, B., Hall, K., Hinchliff, M., Meher-Homji, C., Kurz, R., Pettinato, B., Ristanovic, D., & Taher, M. (2018). Drivers. In *Compression Machinery for Oil and Gas*. Elsevier Inc. https://doi.org/10.1016/B978-0-12-814683-5.00007-9

N. N. Trushin, V. Y. Antsev, & A. A. Obozov. (2019). Improving automotive torque converter quality. *Proceedings of the 5th International Conference on Industrial Engineering (ICIE 2019)*, *II*, 727–735.

Nader, W. B., Breque, F., Mazloum, Y., Dumand, C., & Nemer, M. (2019). Dynamic modeling and fuel consumption potential of an intercooled regenerative reheat gas turbine auxiliary power unit on series hybrid electric vehicle. *Journal of Energy Resources Technology*, *7*. https://doi.org/10.1115/1.4044366

Nakasone, Y., Yoshimoto, S., & Stolarski, T. A. (2006). *Engineering Analysis with Ansys Software*. Elsevier Butterworth-Heinemann.

Nandanwar, Y. N., Walke, P. V, Kalbande, V. P., & Mohan, M. (2023). Performance improvement of vapour compression refrigeration system using phase change material and thermoelectric generator. *International Journal of Thermofluids*, *18*, 100352. https://doi.org/https://doi.org/10.1016/j.ijft.2023.100352

Narendhiran, B., Selvakumar, M., Surulivelrajan, T., Kathiresan, S., & Sathi, G. (2022). Performance enhancement in SI engine by air-fuel mixture recirculating system. *AIP Conference Proceedings*, *2393*(1).

Nasution, H., Aziz, A. A., Latiff, Z. A., & Engkuah, S. (2015). Comparison of air to air and air to water intercoolers in the cooling process of a turbocharger engine. *Jurnal Teknologi*, *10*, 45–51.

Nasution, M. K. M., Elveny, M., Syah, R., Behroyan, I., & Babanezhad, M. (2022). Numerical investigation of water forced convection inside a copper metal foam tube: Genetic algorithm (GA) based fuzzy inference system (GAFIS) contribution with CFD modeling. *International Journal of Heat and Mass Transfer*, *182*, 122016. https://doi.org/10.1016/j.ijheatmasstransfer.2021.122016

Nathaniel, S. P., & Adeleye, N. (2021). Environmental preservation amidst carbon emissions, energy consumption, and urbanization in selected African countries: implication for sustainability. *Journal of Cleaner Production*, *285*, 125409.

Nazmi, M., Khaifullizan, N., Jaat, N., Fadzil, S., Abidin, Z., Darlis, N., & Zahari, I. (2021). Effect of intake air temperature on engine performance and fuel consumption of passenger car. *Fuel, Mixture Formation and Combustion Process*, *3*(2), 1–7. www.fazpublishing.com/fmc

Ni, P., Wang, X., & Wei, S. (2014). Effects of intake air temperature on SI engine emissions during a cold start. *International Journal of Sustainable Energy*, *33*(2), 243–250. https://doi.org/10.1080/14786451.2011.622764

Nikam, A. N., & Hole, J. A. (2014). A review on use of peltier effects. *International Journal of Science, Spirituality, Business And Technology*, *2*(2), 6–12.

Nimkar, D. M. P., Shivankar, S., Sharma, N., Mudliar, V., Gaidhani, P., Borkar, P., Sheskar, P., & Mate, M. (2021). Design and fabrication of turbo operated car (A . C) Compressor – A Review. *International Journal of Engineering and Creative Science*, *4*(1), 17–21.

Nishikawa, H. (2019). A face-area-weighted 'centroid' formula for finite-volume method that improves skewness and convergence on triangular grids. *Journal of Computational Physics*, 1–30. https://doi.org/10.1016/j.jcp.2019.109001

Nithya, G. P., & Miniyadan, A. C. (2021). Priority based intelligent traffic control for emergency vehicles at intersections using IoT. *International Research Journal of Engineering and Technology*, *8*(3), 1415–1417.

Nitsche, M., & Gbadamosi, R. O. (2016). Heat exchanger design guide: A Practical Guide for Planning, Selecting and Designing of Shell and Tube Exchangers. In *Heat Exchanger Design Guide*. Elsevier. https://doi.org/10.1016/b978-0-12-803764-5.01001-4

Novella, R., Dolz, V., Martín, J., & Royo-Pascual, L. (2017). Thermodynamic analysis of an absorption refrigeration system used to cool down the intake air in an Internal Combustion Engine. *Applied Thermal Engineering*, *111*, 257–270. https://doi.org/10.1016/j.applthermaleng.2016.09.084

Noyama, H., Hayashi, T., & Kodama, A. (2010). *Intake-air cooling device for internal combustion engine and automobile using the same.* (Patent No. US7779821B2). https://patents.google.com/patent/US77%0A79821B2/en

Nullis, C. (2023). *Global temperatures set to reach new records in next five years*. World Meteorological Organization. https://public.wmo.int/en/media/press-release/global-temperatures-set-reach-new-records-next-five-years

Ola, U. E. (2011). *Plate heat exchanger design mathodology* (Issue February). Central Ostrobothnia University of Applied Sciences.

Pan, W., Yao, C., Han, G., Wei, H., & Wang, Q. (2015). The impact of intake air temperature on performance and exhaust emissions of a diesel methanol dual fuel engine. *Fuel*, 101–110. https://doi.org/10.1016/j.fuel.2015.08.073

Pandey, A., & Dubey, K. K. (2021). Heat transfer analysis of recuperator for waste heat recovery purpose using LMTD & NTU method. *IOP Conference Series: Materials Science and Engineering*, *1149*(1), 1–7. https://doi.org/10.1088/1757-899x/1149/1/012022

Pant, H., Shukla, D., Rathor, S., & Senthur Prabu, S. (2021). Heat transfer analysis on different pin fin types using solid works. *IOP Conference Series: Earth and Environmental Science*, *850*(1). https://doi.org/10.1088/1755-1315/850/1/012028

Patil, V., H, M., & Kusammanavar, B. (2013). Validation of plate heat exchanger design using CFD. *International Journal of Mechanical Engineering and Robotics Research*, *2*(4).

Pavlovic, J., Fontaras, G., Broekaert, S., Ciuffo, B., Ktistakis, M. A., & Grigoratos, T. (2021). How accurately can we measure vehicle fuel consumption in real world operation ? *Transportation Research Part D*, *90*, 102666. https://doi.org/10.1016/j.trd.2020.102666

Pawar, N. (2016). Thermal design and development of intercooler. *International Conference on Global Trends in Engineering, Technology and Management (ICGTETM-2016) Thermal*, 9–17.

Pelkmans, L., & Debal, P. (2006). Comparison of on-road emissions with emissions measured on chassis dynamometer test cycles. *Transportation Research Part D*, *11*, 233–241. https://doi.org/10.1016/j.trd.2006.04.001

Piao, C., Wang, W., Liu, Z., Wu, C., & Yuan, R. (2021). Research on vehicle cabin temperature and thermal comfort optimal control based on fuzzy PID. *Journal of Physics: Conference Series*, *1865*(3). https://doi.org/10.1088/1742-6596/1865/3/032039

Pinilla Fernandez, D. A., Foliaco, B., Padilla, R. V., Bula, A., & Gonzalez-Quiroga, A. (2021). High ambient temperature effects on the performance of a gas turbine-based cogeneration system with supplementary fire in a tropical climate. *Case Studies in Thermal Engineering*, *26*(June), 101206. https://doi.org/10.1016/j.csite.2021.101206

Prabhu, C. S. S. (2015). Improved efficiency in engine cooling system by repositioning of turbo intercooler. *Applied Mechanics and Materials*, *787*, 792–796. https://doi.org/10.4028/www.scientific.net/AMM.787.792

Pradeep Varma, G. V., & Srinivas, T. (2015). Design and analysis of a cogeneration plant using heat recovery of a cement factory. *Case Studies in Thermal Engineering*, *5*, 24–31. https://doi.org/10.1016/j.csite.2014.12.002

Premkartikkumar, S. R., Annamalai, K., & Pradeepkumar, A. R. (2014). Significance of inlet air temperature on reducing engine-out emissions of di diesel engine operating under the influence of oxygen enriched hydrogen gas. *IJST, Transactions of Mechanical Engineering*, *38*(M1), 57–68.

Pronobis, M. (2020). Reduction of nitrogen oxide emissions. In *Environmentally Oriented Modernization of Power Boilers* (Issue 2). https://doi.org/10.1016/b978-0-12-819921-3.00004-2

Puetzer, J.P. (2015). *Evaporative intercooler* (Patent No. US2015/0101782A1). https://patents.google.com/patent/US20150101782A1/en?oq=US20150101782A1

Qi, C., Helian, Y., Liu, J., & Zhang, L. (2017). Experiment study on the thermal comfort inside a car passenger compartment. *Procedia Engineering*, *205*, 3607–3614. https://doi.org/10.1016/j.proeng.2017.10.211

Qiao, H. (2018). Correction of log mean temperature difference method and effectiveness-NTU relations for two-phase heat transfer with pressure drop and temperature glide. *International Refrigeration and Air Conditioning Conference at Purdue*, 1–10.

R M Harrison. (2005). Outdoor air. *Revision of the Previous-Edition Article by R M Harrison and J D Peak, Pp. 55–59, & 1995, Elsevier Ltd.*, 43–48. http://www.who.int/phe/health_topics/outdoorair/databases/en/

Raman, P. K. N., & Bahari, A. (2021). Effect of changing in air intake temperature on engine performance using thermocouple. *Journal of Advanced Industrial Technology and Application*, *02*(01), 43–50. https://doi.org/10.30880/jaita.2021.02.01.006

Rapp, B. E. (2017). Fluids. In *Microfluidics: Modeling, Mechanics and Mathematics* (pp. 243–263). Elsevier. https://doi.org/https://doi.org/10.1016/B978-1-4557-3141-1.50009-5

Rapp, V., Killingsworth, N., Therkelsen, P., & Evans, R. (2016). Lean-burn internal combustion engines. In *Lean Combustion: Technology and Control: Second Edition*. Elsevier Inc. https://doi.org/10.1016/B978-0-12-804557-2.00004-3

Ravindra Kapse, & Dr. R. R. Arakerimath. (2017). Study and comparison of charge air cooling techniques their effects on efficiency of automobile engine. *International Journal of Engineering Research and Technology*, *V6*(07), 196–201. https://doi.org/10.17577/ijertv6is070152

Refrigeration, I. of. (2011). *Guide to Good Leak Testing* (pp. 1–9). www.realzero.org.uk

Rêgo, A. T., Hanriot, S. M., Oliveira, A. F., Brito, P., & Rêgo, T. F. U. (2014). Automotive exhaust gas flow control for an ammonia-water absorption refrigeration system. *Applied Thermal Engineering*, *64*, 101–107. https://doi.org/10.1016/j.applthermaleng.2013.12.018

Reitz, R. D., Ogawa, H., Payri, R., Fansler, T., Kokjohn, S., Moriyoshi, Y., Agarwal, A. K., Arcoumanis, D., Assanis, D., Bae, C., Boulouchos, K., Canakci, M., Curran, S., Denbratt, I., Gavaises, M., Guenthner, M., Hasse, C., Huang, Z., Ishiyama, T., Zhao, H. (2019). The future of the internal combustion engine. *International Journal of Engine Research*, 1–8. https://doi.org/10.1177/1468087419877990

Reitz, R. D., Ogawa, H., Payri, R., Fansler, T., Kokjohn, S., Moriyoshi, Y., Agarwal, A. K., Arcoumanis, D., Assanis, D., Bae, C., Boulouchos, K., Canakci, M., Curran, S., Denbratt, I., Gavaises, M., Guenthner, M., Hasse, C., Huang, Z., Ishiyama, T., Zhao, H. (2020). IJER editorial: The future of the internal combustion engine. *International Journal of Engine Research*, *21*(1), 3–10. https://doi.org/10.1177/1468087419877990/FORMAT/EPUB

Riffat, S. B., & Ma, X. (2003). Thermoelectrics: A review of present and potential applications. *Applied Thermal Engineering*, *23*(8), 913–935. https://doi.org/10.1016/S1359-4311(03)00012-7

Ross, S. M. (2010). *Linear Regression* pp. (537–604). Academic Press. https://doi.org/https://doi.org/10.1016/B978-0-12-374388-6.00012-0

Rossouw, D. J. (2016). Chapter 6 - Point temperature measurements. In *Application of Thermo-Fluidic Measurement Techniques*. Elsevier Inc. https://doi.org/10.1016/B978-0-12-809731-1/00006-X

Roychowdhury, D. G. (2020). *Computational Fluid Dynamics for Incompressible Flow*. CRC Press Taylor and Francis Group.

Rugh, J. P., Hendricks, T. J., & Koram, K. (2001). Effect of solar reflective glazing on ford explorer climate control, fuel economy, and emissions. *SAE Technical Papers*, *724*. https://doi.org/10.4271/2001-01-3077

Rugh, J. P., Hovland, V., & Andersen, S. O. (2004). Significant fuel savings and emission reductions by improving vehicle air conditioning. *15th Annual Earth Technologies Forum and Mobile Air Conditioning Summit. NREL/CP-5400-62232*.

Sadavarte, P., & Venkataraman, C. (2014). Trends in multi-pollutant emissions from a technology-linked inventory for India: Industry and transport sectors. *Atmospheric Environment*, *99*(2014), 353–364. https://doi.org/10.1016/j.atmosenv.2014.09.081

Safakish, G. R. (2012). Temperature estimation in the combustion chamber of an internal combustion engine. *Advances in Mechanical Engineering*, *2012*, 1–6. https://doi.org/10.1155/2012/931584

Sahu, M. K., Singh, A. K., & Choudhary, T. (2022). Experimental investigation of thermal potential at diesel engine exhaust and numerical simulation of heat recovery in heat exchangers. *Materials Today: Proceedings*, *56*, 220–225. https://doi.org/https://doi.org/10.1016/j.matpr.2022.01.076

Salimi, M., & Al-Ghamdi, S. G. (2020). Climate change impacts on critical urban infrastructure and urban resiliency strategies for the middle east. *Sustainable Cities and Society*, *54*, 101948. https://doi.org/https://doi.org/10.1016/j.scs.2019.101948

Sankar, J. N. D., & Kishore, P. . (2016). Thermal analysis of water cooled charge air cooler in turbo charged diesel engine. *International Journal of Research in Engineering and Technology*, *05*(02), 193–197. https://doi.org/10.15623/ijret.2016.0502033

Saranya, P., Anantharaj, R., Gnana Prakash, D., & Vichitra, M. (2022). Experimental investigation of performance of bio diesel with different blends in diesel engine. In B. Gurunathan & R. B. T.-B. and B. Sahadevan (Eds.), *Biofuels and bioenergy, a techno-economic approach* (pp. 553–567). Elsevier. https://doi.org/https://doi.org/10.1016/B978-0-323-90040-9.00026-6

Sari, E. G., & Sofwan, M. (2021). Carbon Dioxide (CO_2) emissions due to motor vehicle movements in Pekanbaru city , Indonesia. *Journal of Geoscience, Engineering , Environment , and Technology*, *6*(4). https://doi.org/10.25299/jgeet.2021.6.4.7692

Sarjovaara, T., Larmi, M., & Vuorinen, V. (2015). Effect of charge air temperature on E85 dual-fuel diesel combustion. *FUEL*, *153*, 6–12. https://doi.org/10.1016/j.fuel.2015.02.096

Sarkar, D. K. (2017). Air-tightness/leakage test of the furnace, air, and flue gas ducts of a steam generator. In *Thermal Power Plant* (pp. 211–223). Elsevier. https://doi.org/10.1016/b978-0-08-101112-6.00010-1

Schenk, A., & Clausen, U. (2021). Future developments in the transportation area and their impact on vehicle distribution logistics. *Interdisciplinary Conference on Production, Logistics and Traffic*, 1–5.

Sealy, B. E., Feit, J., Vaught, A. T., & Beaber, W. E. (2003). *Charge air management system for automotive engine* (Patent No. US6561169B2). https://patents.google.com/patent/US6561169B2/en?oq=US6561169B2

Sedef, A. Y., & Bilen, K. (2018). The effect of plate-fin types on the thermal-hydraulic and second law performances of a vehicle intercooler. *International Journal of Exergy*, *27*(3), 287–310.

Semakula, M., & Inambao, F. L. (2020). Assessing the effects of engine load on compression ignition engines using biodiesel blends. In *Internal Combustion Engine Technology and Applications of Biodiesel Fuel* (pp. 83–98). Intech open. https://doi.org/10.2139/ssrn.3659252

Şen, G., Nil, M., Mamur, H., Doğan, H., Karamolla, M., Karaçor, M., Kuyucuoğlu, F., Yörükeren, N., & Bhuiyan, M. R. A. (2018). The effect of ambient temperature on electric power generation in natural gas combined cycle power plant—A case study. *Energy Reports*, *4*, 682–690. https://doi.org/10.1016/j.egyr.2018.10.009

Seo, J., Park, J., Park, J., & Park, S. (2020). Emission factor development for light-duty vehicles based on real-world emissions using emission map-based simulation. *Environmental Pollution*, *270*. https://doi.org/10.1016/j.envpol.2020.116081

Sergienko, S. N., Mikhailov, A. D., Poslavsky, A. P., & Kletsova, O. A. (2021). Assessment of the technical condition of intercoolers for turbocharged internal combustion engines. *Journal of Physics: Conference Series*, *1926*(1). https://doi.org/10.1088/1742-6596/1926/1/012034

Seyam, S. (2019). Energy and exergy analysis of refrigeration systems. In *Low temperature technologies* (pp. 1–20). https://doi.org/10.1108/IJESM-04-2013-0012

Shah, R. K., & Sekulic, D. P. (2003). *Fundamentals of Heat Exchanger Design*.

Shahridzuan, I., Khalid, A., Jaat, N., & Saputra, R. (2021). A study of ignition delay , combustion process and emissions in a high ambient temperature of diesel combustion. *Fuel*, *297*(January), 120706. https://doi.org/10.1016/j.fuel.2021.120706

Shaik, S. V., Babu, T. P. A., Mahapatra, D., Shaik, S., Gorantla, K. K., & Subramanyam, V. S. S. (2021). Analytical computation of thermodynamic performance of various new eco-friendly alternative refrigerants applicable for air conditioners. *Advances in AirConditioning and Refrigeration, Lecture Notes in Mechanical Engineering*, 317–328. https://doi.org/https://doi.org/10.1007/978-981-15-6360-7_29

Shana, B. (2021). *134a Operating Pressures in a Refrigerator Explained - Love Cuppa*. https://lovecuppa.com/134a-operating-pressures-in-a-refrigerator-explained/

Sharif, Pshtiwan M., Hairuddin, A. A., As'arry, A., Rezali, K. A. M., Noor, M. M., & Shareef, S. M. (2019). Development of evaporative intercooler heat exchanger for vehicle charge air enhancement using CFD simulation. *Journal of Mechanical Engineering and Sciences*, *53*(9), 1689–1699. https://doi.org/10.1017/CBO9781107415324.004

Sharif, Pshtiwan Mohammad. (2021). Novel heat exchanger for cold air intake on spark ignition engine performance. In *University Putra Malaysia*.

Sharma, A. (2021). *Introduction to Computational Fluid Dynamics*. Springer.

Simanjuntak, J. P., Daryanto, E., Tambunan, B. H., & Eswanto. (2022). An operating parameter study of the biomass solid feedstock incinerator of fixed-bed type with two stage air supply. *Journal of Physics: Conference Series*, *2193*(1). https://doi.org/10.1088/1742-6596/2193/1/012077

Sinaga, N., khorasani, S., Sooppy Nisar, K., & Kaood, A. (2021). Second law efficiency analysis of air injection into inner tube of double tube heat exchanger. *Alexandria Engineering Journal*, *60*(1), 1465–1476. https://doi.org/10.1016/j.aej.2020.10.064

Sinigaglia, T., Eduardo Santos Martins, M., & Cezar Mairesse Siluk, J. (2022). Technological evolution of internal combustion engine vehicle: A patent data analysis. *Applied Energy*, *306*. https://doi.org/https://doi.org/10.1016/j.apenergy.2021.118003

Skočilas, J., & Palaziuk, I. (2015). CFD simulation of the heat transfer process in a chevron plate heat exchanger using the SST turbulence model. *Acta Polytechnica*, *55*(4).

Song, Y., Kaviyani, O., Barnoon, P., Xia, W., & Toghraie, D. (2021). Numerical analysis of heat transfer in peripheral air vaporizers used in cryogenic storage tanks. *Journal of Energy Storage*, *40*. https://doi.org/10.1016/j.est.2021.102774

Soo, G., Raza, W., & Cheol, Y. (2021). Capacity control of a vehicle air-conditioning system using pulse width modulated duty cycle compressor. *Case Studies in Thermal Engineering*, *26*(March), 100986. https://doi.org/10.1016/j.csite.2021.100986

Soysal, D., Şahin, Z., & Durgun, O. (2022). Experimental investigation of the effects of water adding to the intake air on the engine performance and exhaust emissions in a spark ignition engine. *J. of Thermal Science and Technology*, *42*, 75–90. https://doi.org/10.1016/j.fuel.2012.10.080

Stubblefield, M., & Haynes, J. H. (2000). *The Haynes Automotive Heating & Air Conditioning Systems Manual*. Haynes.

Su, S., Lv, T., Lai, Y., Mu, J., Ge, Y., & Giechaskiel, B. (2021). Particulate emissions of heavy duty diesel engines measured from the tailpipe and the dilution tunnel. *Journal of Aerosol Science*, *156*(March), 105799. https://doi.org/10.1016/j.jaerosci.2021.105799

Subiantoro, A., Ooi, K. T., & Stimming, U. (2014). Energy saving measures for automotive air conditioning (AC) system in the tropics. *15th International Refrigeration and Air Conditioning Conference at Purdue, July 14-17*.

Sugiura, H. (1987). *Air Conditioner for automotive vehicles capable of cooling intake air supplied to an internal combustion engine* (Patent No. 4683725). https://patents.google.com/patent/US4683725?oq=Sugiura+1987+Air+Conditioner+for+automotive+vehicles+capable+of+cooling+intakeair+supplied+to+an+internal+combustion+engine

Sukri, M. F., Musa, M. N., Senawi, M. Y., & Nasution, H. (2016). Experimental investigation of an automobile air-conditioning system using integrated brushless direct current motor rotary compressor. *MATEC Web of Conferences*, *74*(January). https://doi.org/10.1051/matecconf/20167400013

Sun, X., Liu, H., Duan, X., Guo, H., Li, Y., Qiao, J., Liu, Q., & Liu, J. (2022). Effect of hydrogen enrichment on the flame propagation, emissions formation and energy balance of the natural gas spark ignition engine. *Fuel*, *307*. https://doi.org/10.1016/j.fuel.2021.121843

Sundén, B., & Fu, J. (2017). Computational methods for the investigations of heat transfer phenomena in aerospace applications. In *Heat Transfer in Aerospace Applications* (pp. 179–196). https://doi.org/10.1016/b978-0-12-809760-1.00010-7

Sutton, I. (2010). Chapter 6 - Asset integrity. In *Process Risk and Reliability Management*. Ian Sutton. https://doi.org/10.1016/B978-1-4377-7805-2.10006-7

Taggart, J. (2017). Ambient temperature impacts on real-world electric vehicle efficiency & range. *2017 IEEE Transportation and Electrification Conference and Expo, ITEC 2017*, 186–190. https://doi.org/10.1109/ITEC.2017.7993269

Tavakoli, S., Jensen, M. V., Pedersen, E., & Schramm, J. (2021). Unburned hydrocarbon formation in a natural gas engine under sea wave load conditions. *Journal of Marine Science and Technology (Japan)*, *26*(1), 128–140. https://doi.org/10.1007/s00773-020-00726-5

Taylor, P., & Sundén, B. (2011). Computational fluid dynamics in research and design of heat exchangers. *Heat Transfer Engineering*, *August 2013*, 37–41. https://doi.org/10.1080/01457630701421679

Teoh, Y. H., Huspi, H. A., How, H. G., Sher, F., & Din, Z. U. (2021). Effect of intake air temperature and premixed ratio on combustion and exhaust emissions in a partial hcci-di diesel engine. *Sustainability*, *13*.

Thirumalai Kumaran, S., Baranidharan, K., Uthayakumar, M., & Parameswaran, P. (2021). Corrosion studies on stainless steel 316 and their prevention – A Review. *Incas Bulletin*, *13*(3), 245–251. https://doi.org/10.13111/2066-8201.2021.13.3.21

Thomaz, F., Teixeira Malaquias, A. C., Resende de Paula, G. A., & Baêta, J. G. C. (2021). Thermal management of an internal combustion engine focused on vehicle performance maximization: A numerical assessment. *Proceedings of the Institution of Mechanical Engineers, Part D: Journal of Automobile Engineering*, *235*(8), 2296–2310. https://doi.org/10.1177/0954407020982825

Thulukkanam, K. (2013). Heat exchanger design handbook second edition. In *Heat Exchanger Design Handbook*. CRC Press Taylor and Francis Group. https://doi.org/10.1201/9781420026870

Tiwari, A. K., Ghosh, P., Sarkar, J., Dahiya, H., & Parekh, J. (2014). Numerical investigation of heat transfer and fluid flow in plate heat exchanger using nanofluids. *International Journal of Thermal Sciences*, *85*, 93–103. https://doi.org/https://doi.org/10.1016/j.ijthermalsci.2014.06.015

Torabi, F. (2022). Numerical simulation of a wind turbine. In *Wind Energy Engineering* (pp. 187–214). Academic Press. https://doi.org/https://doi.org/10.1016/B978-0-12-823016-9.00012-7

Torregrosa, A. J., Broatch, A., Olmeda, P., & Romero, C. (2008). Assessment of the influence of different cooling system configurations on engine warm-up, emissions and fuel consumption. *International Journal of Automative Technology*, *9*(4), 447–458. https://doi.org/10.1007/s12239

Tosun, I. (2007). Molecular and convective transport. In *Modelling in transport phenomenon (Second edition)* (pp. 13–34). Elsevier Science B.V. https://doi.org/https://doi.org/10.1016/B978-044453021-9/50003-8

Treeamnuk, T., Treeamnuk, K., & Papakae, S. (2018). Influence of intake air temperature on performance of small gasoline engine. *The Asian Conference on Sustainability, Energy & the Environment 2018, Official Conference Proceedings*.

V. Ganesan. (2012). *IC Engines* (4th ed.). Tata McGraw Hill Education Private Limited.

Vakkilainen, E. K. (2017). Solid biofuels and combustion. In *Steam Generation from Biomass*. https://doi.org/10.1016/b978-0-12-804389-9.00002-2

Vankov, Y. V., Gaponenko, S. O., Arendateleva, S. I., Politova, T. O., & Khvorystkina, A. M. (2016). Numerical simulation of a heat exchanger with improved plate shape. *12th International Conference on Heat Transfer, Fluid Mechanics and Thermodynamics*, 1737–1742. https://doi.org/10.1063/5.0105607

Virt, M., Granovitter, G., Zöldy, M., & Nyerges, Á. B. and Á. (2021). Multipulse ballistic injection : a novel method for improving low temperature combustion with early injection timings. *Energies*.

Walker, G. (1983). *Cryocoolers Part 2: Applications*. Plenum Press New York. https://doi.org/0.1007/978-1-4684-4430-8

Wang, P., Li, Y., Duan, X., Liu, J., Wang, S., Zou, P., & Fang, Y. (2020). Experimental investigation of the effects of CR, hydrogen addition strategies on performance, energy and exergy characteristics of a heavy-duty NGSI engine fueled with 99% methane content. *Fuel*, *259*(August 2019), 116212. https://doi.org/10.1016/j.fuel.2019.116212

Wang, Z., Liu, H., & Reitz, R. D. (2017). Knocking combustion in spark-ignition engines. *Progress in Energy and Combustion Science*, *61*, 78–112. https://doi.org/10.1016/j.pecs.2017.03.004

Weinrebe, G., Bergermann, R., & Schlaich, J. (2022). Solar updraft towers. In *Solar thermal energy . Encyclopedia of Sustainability Science and Technology Series. Springer, New York, NY* (pp. 135–166). Springer US. https://doi.org/10.1007/978-1-0716-1422-8_682

Welch, L. W., & Fish, G. E. (1979). *Reciprocating machine with refrigerated cooling of intake air.* (Patent No. 4169436). https://patents.google.com/patent/US41%0A69436A/en

William C. Whitman, Johnson, W. M., Tomcztk, J. A., & Silberstein, E. (2012). *Refrigeration and air conditioning technology* (7th ed.). Delmar Cengage Learning.

Wimmer, A., & Schnessl, E. (2006). Effects of humidity and ambient temperature on engine performance of lean burn natural gas engines. *ASME Internal Combustion Engine Division, Sacramento, California, USA*, 1–9.

Wiriyasart, S., Hommalee, C., & Naphon, P. (2019). Thermal cooling enhancement of dual processors computer with thermoelectric air cooler module. *Case Studies in Thermal Engineering*, *14*(February), 100445. https://doi.org/10.1016/j.csite.2019.100445

Wong, P. K., Gao, X. H., Wong, K. I., Vong, C. M., & Yang, Z. X. (2018). Initial-training-free online sequential extreme learning machine based adaptive engine air–fuel ratio control. *International Journal of Machine Learning and Cybernetics*, *10*(9), 2245–2256. https://doi.org/10.1007/s13042-018-0863-0

Wu, C. H., Morris, E. D., & Niki, H. (1973). The reaction of nitrogen dioxide with ozone. *The Journalof Physical Chemistry*, *77*(21).

Wu, H., Chen, T., Kelana, N., & Huang, D. (2020). Influence of dimple height on turbulent heat transfer of fin array with alternate convex / concave dimples. *Inventions*, *33*(5).

Xu, L., & Grönstedt, T. (2010). Design and analysis of an intercooled turbofan engine. *Journal of Engineering for Gas Turbines and Power*, *132*(11), 1–4. https://doi.org/10.1115/1.4000857

Xue, H., Jiang, S., & Liang, B. (2013). A study on the model of traffic flow and vehicle exhaust emission. *Mathematical Problems in Engineering*, *2013*. https://doi.org/10.1155/2013/736285

Yang, S.-J., Park, D.-H., & Han, J.W. (2019). *Water cooled intercooler system using air conditioning system and control method thereof.* (Patent No. US10240514B2). https://patents.google.com/patent/US10%0A240514B2/en

Yang, X., Dong, C., & Qu, Z. (2017). Design and dynamic analysis of a novel double-swing vane compressor for electric vehicle air conditioning systems. *International Journal of Refrigeration*. https://doi.org/10.1016/j.ijrefrig.2017.01.028

Yang, Z., Deng, B., Deng, M., & Huang, S. (2018). An overview of chassis dynamometer in the testing of vehicle emission. *MATEC Web of Conferences 175*, 1–4.

Yeh, T. J., Chen, Y. J., Hwang, W. Y., & Lin, J. L. (2009). Incorporating fan control into air-conditioning systems to improve energy efficiency and transient response. *Applied Thermal Engineering*, *29*(10), 1955–1964. https://doi.org/10.1016/j.applthermaleng.2008.09.017

Yi, J. T. (2008). *Charge air cooler having refrigerant coils and method for cooling charge air* (Patent No. US7341050B2). https://patents.google.com/patent/US7341050?oq=US+7%2C341%2C050+B2

Yu, C., Qin, S., Chai, B., Huang, S., & Liu, Y. (2019). The effect of compressible flow on heat transfer performance of heat exchanger by computational fluid dynamics (CFD) simulation. *Entropy*, *21*(9), 1–12. https://doi.org/10.3390/e21090829

Yue, Z., & Liu, H. (2023). Advanced research on internal combustion engines and engine fuels. *Energies*, *16*(5940). https://doi.org/10.3390/en16165940

Yue, Z., & Som, S. (2021). Fuel property effects on knock propensity and thermal efficiency in a direct-injection spark-ignition engine. *Applied Energy*, *281*(November). https://doi.org/10.1016/j.apenergy.2019.114221

Yum, K. K., Lefebvre, N., & Pedersen, E. (2017). An experimental investigation of the effects of cyclic transient loads on a turbocharged diesel engine. *Applied Energy*, *185*, 472–481. https://doi.org/10.1016/j.apenergy.2016.10.138

Yun, Y., & Chang, Y. S. (2021). Refrigerant charge prediction of vapor compression air conditioner based on start-up characteristics. *Applied Sciences (Switzerland)*, *11*(4), 1–16. https://doi.org/10.3390/app11041780

Yunus A. Cengel. (2002). *Heat transfer*.

Yuqing, Z., Yun, D., Jianling, G., & Qingqing, L. (2018). Study on the influence of refrigerant charge on performance of heat pump units. *IOP Conf. Series: Earth and Environmental Science 199 (2018) 022058*, 1–7. https://doi.org/10.1088/1755-1315/199/2/022058

zahrani, S. Al, Islam, M. S., & Saha, S. C. (2019). A thermo-hydraulic characteristics investigation in corrugated plate heat exchanger. *Energy Procedia*, *160*, 597–605. https://doi.org/https://doi.org/10.1016/j.egypro.2019.02.211

Zakaria, M. S., Ismail, F., Tamagawa, M., Abdul Azi, A. F., Wiriadidjaya, S., Basri, A. A., & Ahmad, K. A. (2018). Computational fluid dynamics study of blood flow in aorta using OpenFOAM. *Journal of Advanced Research in Fluid Mechanics and Thermal Sciences*, *43*(1), 81–89.

Zegenhagen, M. T., & Ziegler, F. (2015a). Experimental investigation of the characteristics of a jet-ejector and a jet-ejector cooling system operating with R134a as a refrigerant. *International Journal of Refrigeration*, *56*, 173–185. https://doi.org/10.1016/j.ijrefrig.2015.01.001

Zegenhagen, M. T., & Ziegler, F. (2015b). Feasibility analysis of an exhaust gas waste heat driven jet-ejector cooling system for charge air cooling of turbocharged gasoline engines. *Applied Energy*, *160*, 221–230. https://doi.org/10.1016/j.apenergy.2015.09.057

Zhang, C., Wang, D., Han, Y., Zhu, Y., & Peng, X. (2017). Experimental and numerical investigation on the exergy and entransy performance of a novel plate heat exchanger. *Experimental Heat Transfer*, *30*(2), 162–177. https://doi.org/10.1080/08916152.2016.1179358

Zhang, Q., Stockar, S., & Canova, M. (2015). Energy-optimal control of an automotive air conditioning system for ancillary load reduction. *IEEE Transactions On Control Systems Technology*.

Zhang, X., & Zhou, Z. (2020). Research on development of vehicle chassis dynamometer. *Journal of Physics: Conference Series*, *1626*(1). https://doi.org/10.1088/1742-6596/1626/1/012150

Zhang, Y., Jiang, C., Yang, Z., Zhang, Y., & Bai, B. (2016). Numerical study on heat transfer enhancement in capsule-type plate heat exchangers. *Applied Thermal Engineering*, *108*, 1237–1242. https://doi.org/https://doi.org/10.1016/j.applthermaleng.2016.08.033

Zhang, Z., Liu, H., Yue, Z., Li, Y., Liang, H., Kong, X., Zheng, Z., & Yao, M. (2022). Effects of intake high-pressure compressed air on thermal-work conversion in a stationary diesel engine. *International Journal of Green Energy*, 1–14. https://doi.org/10.1080/15435075.2022.2040509

Zhao, F., Chen, K., Hao, H., & Liu, Z. (2020). Challenges, potential and opportunities for internal combustion engines in China. *Sustainability*, *12*(12), 1–15. https://doi.org/10.3390/su12124955

Zhuang, Y., Sun, Y., Huang, Y., Teng, Q., He, B., Chen, W., & Qian, Y. (2020). Investigation of water injection benefits on downsized boosted direct injection spark ignition engine. In *Fuel* (Vol. 264, Issue November 2019). https://doi.org/10.1016/j.fuel.2019.116765

APPENDICES

Appendix A

Uncertainty in instruments and sensors

Experimental instruments and sensors used in this study were calibrated in the UPM thermodynamics laboratory, to prevent uncertainties in measurements and provide accuracy. In order to accomplish this, it is important to know the absolute and relative errors associated with the measurements in order to understand the possible consequences of inaccuracies, limitations of the data and the most accurate measurement possible. Absolute error may be called approximation error and it is the difference between a measurement and a true value (Chai & Draxler, 2014).

$$E = |X_o - X|$$

Where E is absolute error, X_o is the measured value and X is the true or actual value.

Further, relative error/uncertainty is also important to consider, because it puts the error into a realistic perspective given the actual size of the measurement and can be described as the ratio of absolute error to the measured value (Chai & Draxler, 2014).

$$RE = \frac{E}{X_o}$$

A.1 Temperature sensors

The temperature sensor utilized in tests was the (DS18B20 Waterproof Digital Thermal Sensor Temperature Probe), coupled with the XH-W3001 digital thermostat. Purchased items were pre-calibrated under the company testing process with ISO9001 standard, and all the products passed certifications of CE, FCC, and ROHS.

A.1.1 Sensor's calibration

For more reliability about the quality of the sensors, a lab test was conducted to calibrate and measure the sensors uncertainty error measuring using a comparison with existing calibrated sensors owned by the (UPM) thermodynamics laboratory. Figure A1: demonstrate the test schematic and connection diagram, whereas Figure A2 shows the actual depiction of the temperature calibration setup. A total of 8 temperature sensors were calibrated.

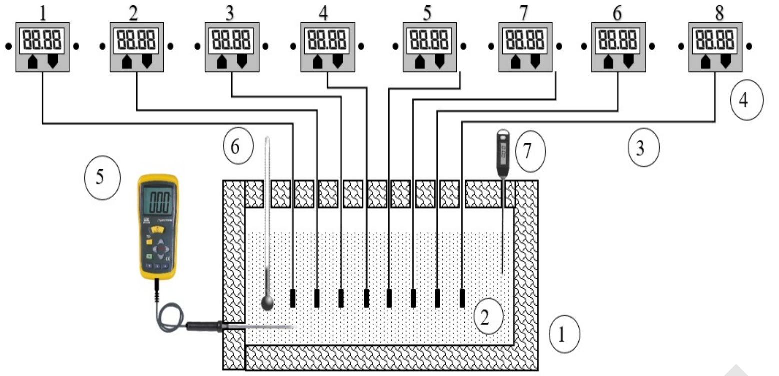

1) Thermal enclosure box
2) Water medium
3) Temperature sensors
4) Digital meter
5) Calibrated thermometer
6) Mercury Thermometer
7) Digital Thermometer

Figure A1: Schematic of temperature sensors calibration

Figure A2: Testbed of temperature calibration process components

A.1.2 Data and Calculation of uncertainty

The calibration process was conducted within a selected temperature range of (0°C – 50°C) in two (2) stages upstream and downstream temperature grade using the liquid water as a controlled parameter. The sensor's test results are shown in (Table A1) used to investigate the accuracy of the sensors and measure the uncertainty of each sensor used. Table A2 and A3 depicts the absolute error and relative uncertainty, respectively.

Table A1: Experimental test reading.

Controlled Temperature	Sensors reading ℃							
	T_1	T_2	T_3	T_4	T_5	T_6	T_7	T_8
0	0	0	0	0	0	0	0	0
10	10	10.1	10	10	10	10	10	10
20	20	20	20	19.9	20	20	20	20
30	30	30	30.1	30	30	30	30.1	29.8
40	40.1	40.1	40	40	39.9	40.1	40	40
50	50.2	50	50	49.8	50	50.2	49.9	50
40	40	40	40.1	40	40.1	40	40.1	39.9
30	30	30	30	39.9	30.2	30	30	30
20	20	20.1	20	20	20	20.1	2	20
10	10	10	10	10	10	10	9.9	10
0	0	0	0	0	0	0	0	0

Table A2: Absolute errors in test reading.

Absolute error ℃							
T_1	T_2	T_3	T_4	T_5	T_6	T_7	T_8
0	0	0	0	0	0	0	0
0	0.1	0	0	0	0	0	0
0	0	0	-0.1	0	0	0	0
0	0	0.1	0	0	0	0.1	-0.2
0.1	0.1	0	0	-0.1	0.1	0	0
0.2	0	0	-0.2	0	0.2	-0.1	0
0	0	0.1	0	0.1	0	0.1	-0.1
0	0	0	-0.1	0.2	0	0	0
0	0.1	0	0	0	0.1	0	0
0	0	0	0	0	0	-0.1	0
0	0	0	0	0	0	0	0

Table A3: Relative uncertainty in sensors

Relative uncertainty							
T_1	T_2	T_3	T_4	T_5	T_6	T_7	T_8
--	--	--	--	--	--	--	--
0	0.01	0	0	0	0	0	0
0	0	0	-0.005	0	0	0	0
0	0	0.0033	0	0	0	0.0033	-0.007
0.0025	0.0025	0	0	-0.003	0.0025	0	0
0.004	0	0	-0.004	0	0.004	-0.002	0
0	0	0.0025	0	0.0025	0	0.0025	-0.003
0	0	0	-0.003	0.0067	0	0	0
0	0.005	0	0	0	0.005	0	0
0	0	0	0	0	0	-0.01	0
--	--	--	--	--	--	--	--

The absolute error in sensors readings shows the range of (±0.2℃) and percentage uncertainty from Table A3 shows the range of (±0.7%).

A.2 Portable Anemometer

The portable anemometer was used to measure the EICA flow rate velocity for the designed testbed in the UPM laboratory, which provided good accurate readings. The anemometer model used was (VICTOR 816B) with digital readability and the convenience of a separate (USB) connector remote sensor.

A.2.1 Sensors calibration

The quality of the selected instrument was investigated through laboratory tests conducted to calibrate and measure the uncertainty error measuring using comparison with existing calibrated anemometer in laboratories at the UPM facility. Figure A3 demonstrates the test schematic and connection diagram.

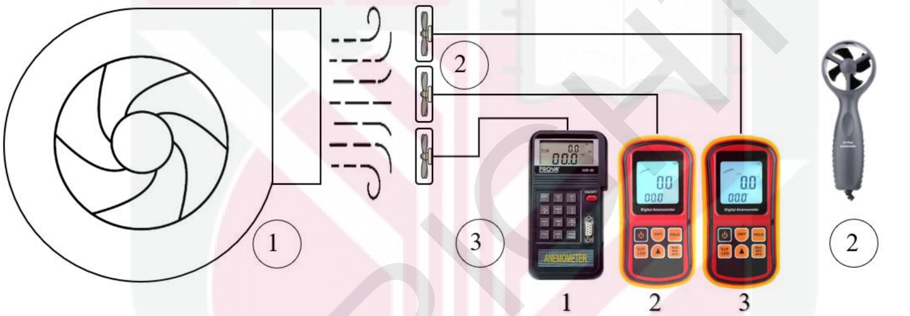

1) Air blower fan 2) Anemometer sensor fan 3) Anemometer device

Figure A3: Schematics of anemometer calibration.

The calibration process was conducted within a selected airflow velocity range controlled by the air blower speed controller (4 speed). Figure A4 illustrates the actual calibration process conducted.

Figure A4: Laboratory calibration test comparison of the portable anemometer with two calibrated Anemometer

A.2.2 Data and Calculation of uncertainty

Table A4 shows the test readings gained during the calibration process and Table A5 shows the errors obtained in readings.

Table A4: Anemometer test results

Air blower speed	Anemometer reading (m/s)		
	Anemo-UPM	Anemo-1	Anemo-2
Speed 1	1.71	1.72	1.7
Speed 2	1.83	1.82	1.83
Speed 3	2.08	2.09	2.08
Speed 4	2.20	2.21	2.22

Table A5: Anemometer error outcomes

Absolute error (m/s)		Relative uncertainty	
Anemo-1	Anemo-2	Anemo-1	Anemo-2
0.01	-0.01	0.005	-0.005
-0.01	0.00	-0.005	0.00
0.01	0.00	0.004	0.00
0.01	0.02	0.004	0.008

The findings show a percentage of relative uncertainty upto (±0.8%) from the calibrated anemometer of UPM.

A.3 Digital Manometer

Digital manometer model (XINSITE LCD) was used to measure the pressure drop.

A.3.1 Instrument uncertainty

The uncertainty in the instrument was assessed through comparison with the existing calibrated manometer available at the UPM thermodynamics lab. Figure A5 demonstrates the test schematic connection diagram and a certified calibrated manometer belonging to UPM. The instrument was connected directly to the outlet and inlet of the LHE to measure the simulated EICA pressure.

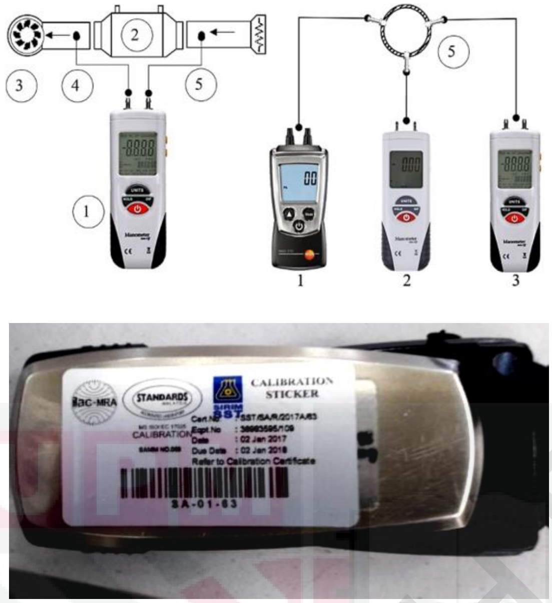

1) Digital Manometer 2) LHE 3) Vacuum fan
4) Outlet airflow duct 5) Inlet airflow duct

Figure A5: Manometer Differential Gauge, calibration test schematic compared to UPM laboratory calibrated instrument.

A.3.2 Data and Calculation of uncertainty

The calibration process was conducted within a selected airflow velocity range simulated by engine RPM (1000 – 8000 RPM for each step of (500 RPM). Air velocity controlled by the vacuum fan speed through the voltage regulator controller in the control panel.

Table A6: Manometer experimental test reading

Controlled engine speed	Manometers reading (kpa)		
	Mano-1(UPM)	Mano-2	Mano-3
1000	0.005	0.005	0.005
1500	0.007	0.007	0.007
2000	0.013	0.013	0.013
2500	0.014	0.014	0.014
3000	0.021	0.021	0.021
3500	0.029	0.029	0.028
4000	0.031	0.032	0.030
4500	0.038	0.040	0.039
5000	0.045	0.046	0.043
5500	0.050	0.052	0.051
6000	0.062	0.063	0.061
6500	0.072	0.072	0.070
7000	0.074	0.075	0.074
7500	0.081	0.082	0.083
8000	0.094	0.095	0.093

Table A7: Absolute and relative error from test readings

Controlled engine speed	Absolute error(kpa)		Relative error	
	Mano-2	Mano-3	Mano-2	Mano-3
1000	0.00	0.00	0.00	0.00
1500	0.00	0.00	0.00	0.00
2000	0.00	0.00	0.00	0.00
2500	0.00	0.00	0.00	0.00
3000	0.00	0.00	0.00	0.00
3500	0.00	0.00	0.00	0.00
4000	0.001	-0.001	0.031	-0.031
4500	0.002	0.001	0.040	0.025
5000	0.001	-0.002	0.021	-0.042
5500	0.002	0.001	0.038	0.019
6000	0.001	-0.001	0.015	-0.016
6500	0.00	-0.002	0.00	-0.028
7000	0.001	0.000	0.013	0.00
7500	0.001	0.002	0.012	0.024
8000	0.001	-0.001	0.010	-0.010

The experimental results show absolute uncertainty ranges of (-0.002 to 0.002) Kpa, along with percentage of relative uncertainty upto ±4%.

A3. Fuel flow meter

The digital flow meter (13mm Liquid Fuel Oil Flow Meter Counter Diesel Gasoline Gear Flow Sensor / Model- OF05ZAT) was used to measure consumed fuel. The sensor was connected to a digital meter (ZJ-LCD-17) for visual reading and data saving. The sensors were connected on both sides of the vehicle fuel line (inlet and outlet) to measure the consumed fuel.

A.3.1 Instrument calibration

The process calibration was conducted within a controlled volume of water. The water was pumped by a pump at a constant flowing speed and allowed to pass through fuel sensors and end up in the calibrated cylinder. The difference between readings (measured water) helped to check uncertainty. Repeated tests ensure better reading quality and better accuracy. Figure A6 illustrates the schematic diagram of the calibration test, whereas Figure A7 depicts the actual laboratory setup to calculate uncertainty.

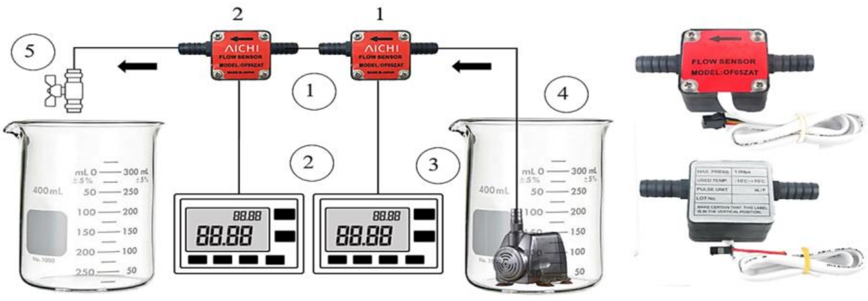

1) Flowmeter sensor
2) LCD meter
3) Water pump
4) Calibrated cylinder
5) Control valve

Figure A6: Flowmeter sensor calibration test schematic compared to laboratory calibrated instrument

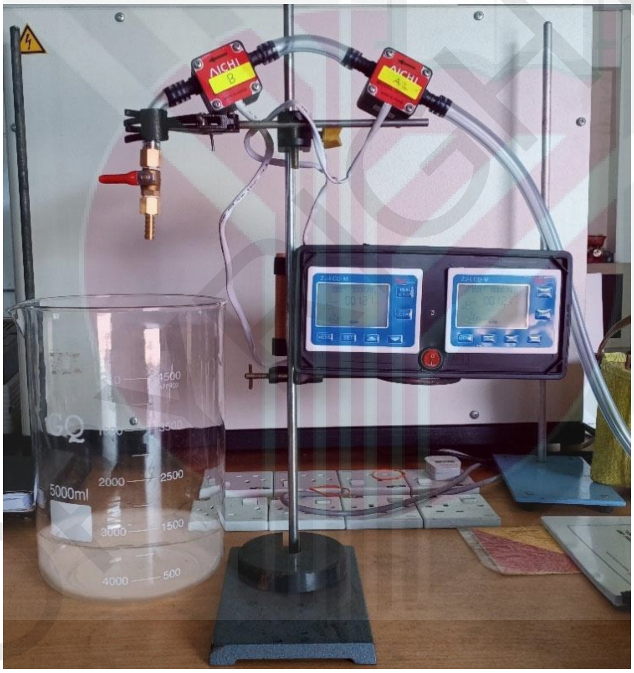

Figure A7: Fuel meter calibration test conducted in the laboratory

A.3.2 Uncertainty in the fuel meter sensor

The calibrated cylinder was used to check the uncertainty errors in the fuel sensor. The target was to fill the calibrated cylinder with 0.5L of water after passing through fuel sensors. In the end, readings were recorded from digital fuel meters of fuel sensors. Multiple readings were taken into account for finer results. Table A8 shows the recorded values and Table A9 shows the error in recorded readings.

Table A8: Flowmeter sensor experimental test reading

Data reading	Fuel flowmeter reading (L)	
	Sensor-1	Sensor-2
1	0.49	0.49
2	0.51	0.49
3	0.49	0.50
4	0.49	0.49
5	0.5	0.51
6	0.49	0.51

Table A9: Errors in fuel flowmeter outputs

Absolute error (L)		Relative uncertainty	
Sensor-1	Sensor-2	Sensor-1	Sensor-2
-0.01	-0.01	-0.02	-0.02
0.01	-0.01	0.02	-0.02
-0.01	0	-0.02	0
-0.01	-0.01	-0.02	-0.02
0	0.01	0	0.02
-0.01	0.01	-0.02	0.02

The findings show a percentage uncertainty of (±2%) for fuel sensors from the calibrated cylinder values.

A.4 Emission gas analyzer

The gas analyzer used in the emission analyzing records while testing, the device model size, and shape is a portable type, which has the ability of mobility due to its small size. The device model was (ENERAC 700AV) and belonged to the University of Putra Malaysia-UPM mechanical laboratory. The device was purchased by the university from (LEE HUNG SCIENTIFIC SDN BHD – Selangor – Malaysia) with (serial number 700583). An advanced technology device with the ability options of self-calibration and sensor reset. Furthermore, the device was already calibrated by the manufacturer shown in Figure A8.

Figure A8: The (ENERAC 700AV) component of emission testing gas analyzer

Appendix B

Fabrication of LHE

The LHE was fabricated using stainless steel 316L, commonly available in any part of the world. Figure A9 shows the detailed fabricated parts of the LHE, comprised of header plates, baffle plates, lamellas, fitting covers, and shell box bearing inlet and outlet fittings of refrigerant.

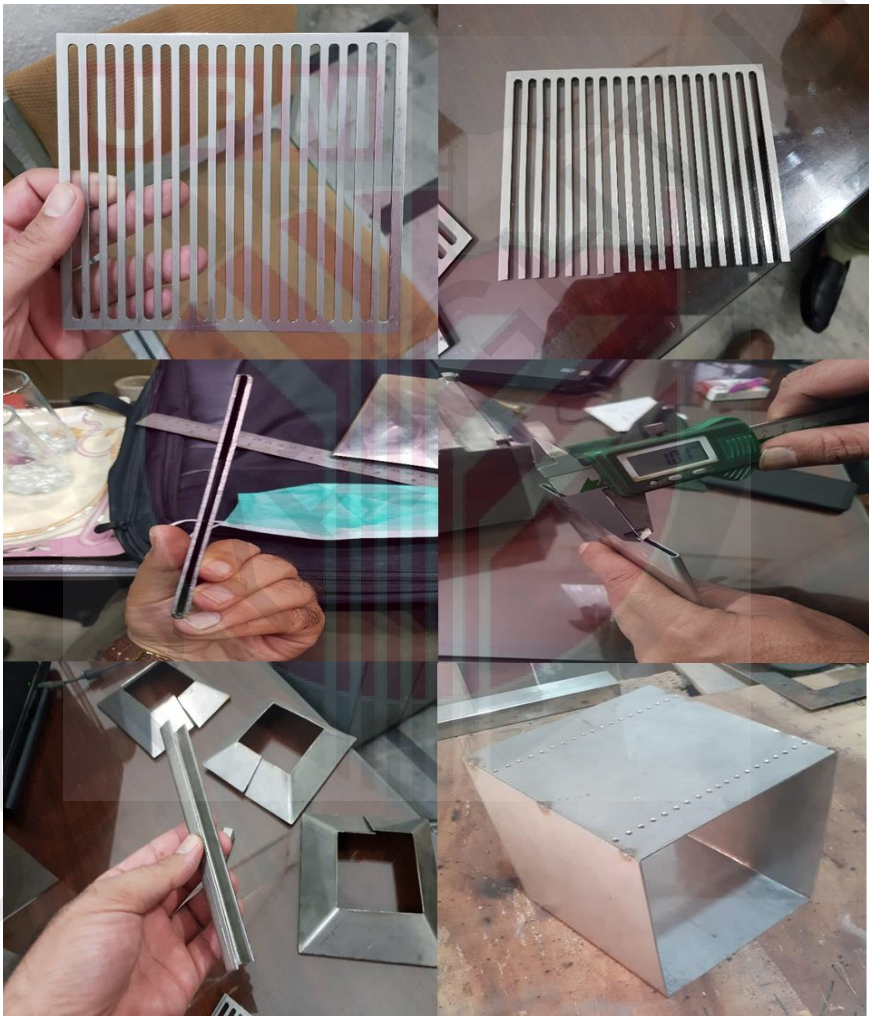

Figure A9: Fabrication of LHE

Figure A9: Fabrication of LHE (continued)

Appendix C

Testbed design and component

C.1 The Testbed components

After fabricating the physical model of the LHE, a model was installed on an experimental testbed for experimental investigation and design validation with numerical analysis. The testbed was designed to be suitable in fitting with the selected LHE. The experimental testbed was fabricated and designed from available local materials, and it consists of four major parts; The EICA simulator, ambient simulator, vehicle air-conditioning simulator, and the control panel. Other parts consist of measurement tools and sensors mentioned in appendixes (A) and the PVC ducting tubes. Figure A10 illustrates the component schematic of the Testbed. The testbed was installed inside the thermodynamics laboratory (UPM) campus for the availability of measurements and power source facilities by the university.

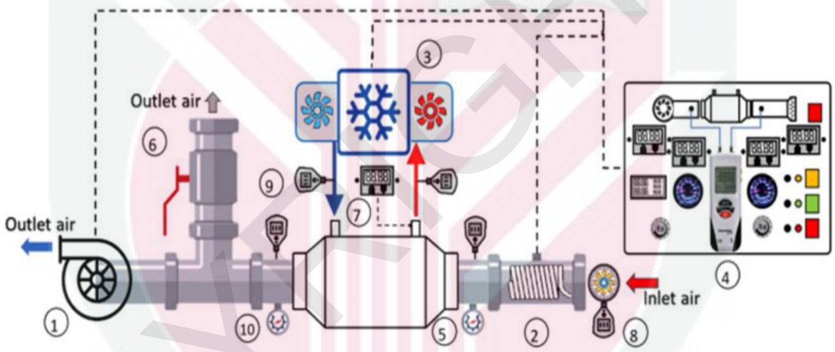

1	Vacuum fan	2	Heater	3	Air Conditioner
4	Control Panel	5	LHE	6	Airflow neutralizer
7	Temperature control	8	Anemometer gauge		

Figure A10: Testbed diagram schematic shows the component

Besides, the (Testbed) was used to measure the LHE cooling and air pressure performance inside the air domain and simulate the tests required for LHE analysis parameters of temperature and pressure. Figure A11 shows the fabricated testbed at the UPM laboratory.

Figure A11: Fabricated testbed in laboratory

C.2 The EICA simulator part

The EICA simulator part represents the engine induced air manifold in vacuum status, simulating the airflow induced by the engine. This part consists of an electrical motor vacuum fan. The flow level was controlled by an electrical voltage regulator model (AC 220V 4000W SCR Voltage Regulator), controlling the motor speed by governing the supply power (Figure A12). The vacuum fan was adopted from an electric vacuum cleaner purchased from an electric spear part shop. The vacuum body size was fit into the (PVC) duct for installation. The airflow velocity was controlled by the anemometer device reading, which was installed on the inlet (PVC) duct, and the (SCR) regulator controlled the vacuum motor supply voltage till reaching the desired velocity.

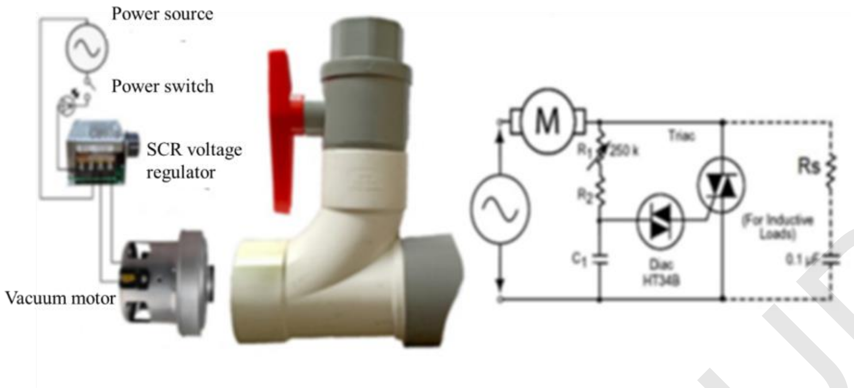

Figure A12: The EICA simulator vacuum connection and electric circuit connection

C.3 Ambient temperature simulator part

The ambient air temperature simulator part simulates the airflow induced by the engine at various temperatures, stimulating the environment temperature of the air. This part consists of an electrical heater controlled by an electrical voltage regulator model (AC 220V 4000W SCR Voltage Regulator) controlling the heat applied by controlling the supply power (Figure A13). The heat capacity applied was measured by the digital power meter (Digital AC 20A 100A Voltage Energy Meter Voltmeter Ammeter Power Current Panel), which measures the electric power consumed by the heater to convert to heat. The heater was adopted from an electric hair drier, purchased from an electric shop. The heater was modified and fabricated to fit into the (PVC) duct for installation.

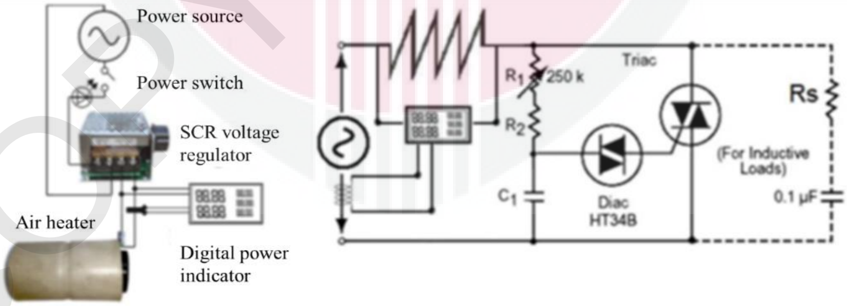

Figure A13: The ambient temperature simulator heater part

C.4 Vehicle air-conditioning simulator part

The vehicle air-conditioning simulator part simulates the refrigerant supply by the vehicle, stimulating the air-conditioning cycle. This part consists of a modified split air conditioning cooler with one horsepower cooling capacity, using the high-pressure outdoor part, which includes the (Compressor, Condenser, and expansion valve) to supply the refrigerant to the LHE. The split operation was controlled by a (Digital thermostat controller model XH-W3001), a digital electrical thermostat with an adjustable range of temperature desired. The thermostat controls the supply power feeding of the Air-conditioning (Figure A14), the temperature sensor of the thermostat was placed on the LHE refrigerant exit side, and the compressor low-pressure return line to prevent overcooling of the refrigerant, returning to the compressor.

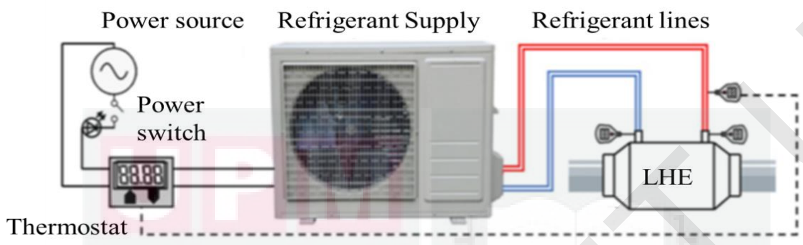

Figure A14: The Vehicle air-conditioning simulator circuit connection and parts

C.5 The Control panel

The control panel was an enclosed flat unit used to control the system unit's part or to monitor the instrument's and sensor's data to be displayed visually. The control panel enclosed all electrical parts used to supply power to the units and was controlled by the main switch with a control switch for each unit. Indicated light was used to identify the operational units and protect the system from any electric short circuits or prevent damage to the system by using a fuse conductor melt in case of short or any electric failure. The flat board contains the digital meters and the (SCR) voltage regulators with other units required for the (Testbed) Figure A15. The technician can easily control the test operation and monitor the test data directly from the control panel, an option of modification can be added to the controlling system and data reading for any digital device acquisition if needed by direct connections available inside the encloser.

Figure A15: The Testbed control panel

Appendix D

Technical installation of LHE

Figure A16 shows the details of the parts employed to install the LHE with the air conditioning system of the test vehicle, which includes the t-joint of the VAC pipe, electric solenoid valve, fuel sensors, temperature sensor, expansion valve.

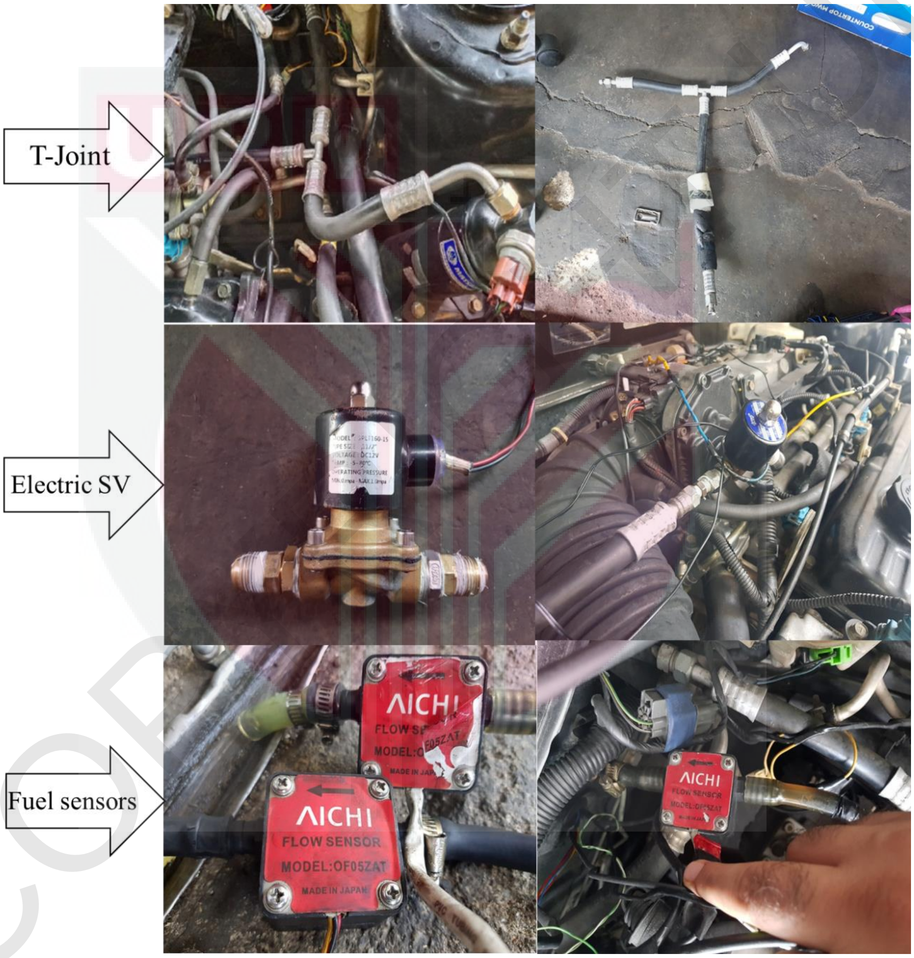

Figure A16: Technical installation of LHE in the test vehicle

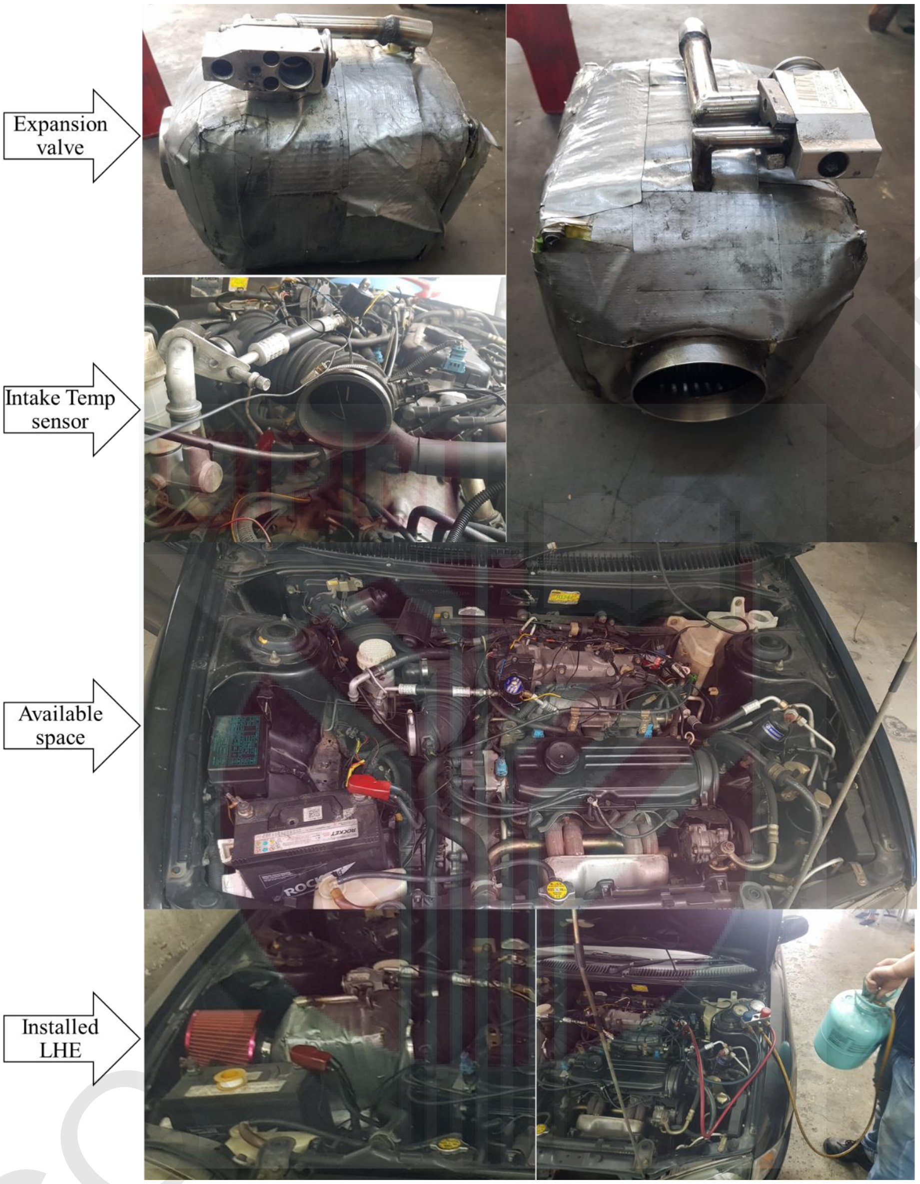

Figure A16: Technical installation of LHE in the test vehicle (continued)

Appendix E

Dyno chassis Program Structure

The Dyno operation program was menu-oriented. The data or instructions can be entered via the PC keyboard. The remote control was used for the setup operation, e.g., wheelbase setting, starting and stopping of the pre-selected driving cycle. The Dyno menu can be illustrated as shown in Figure A17:

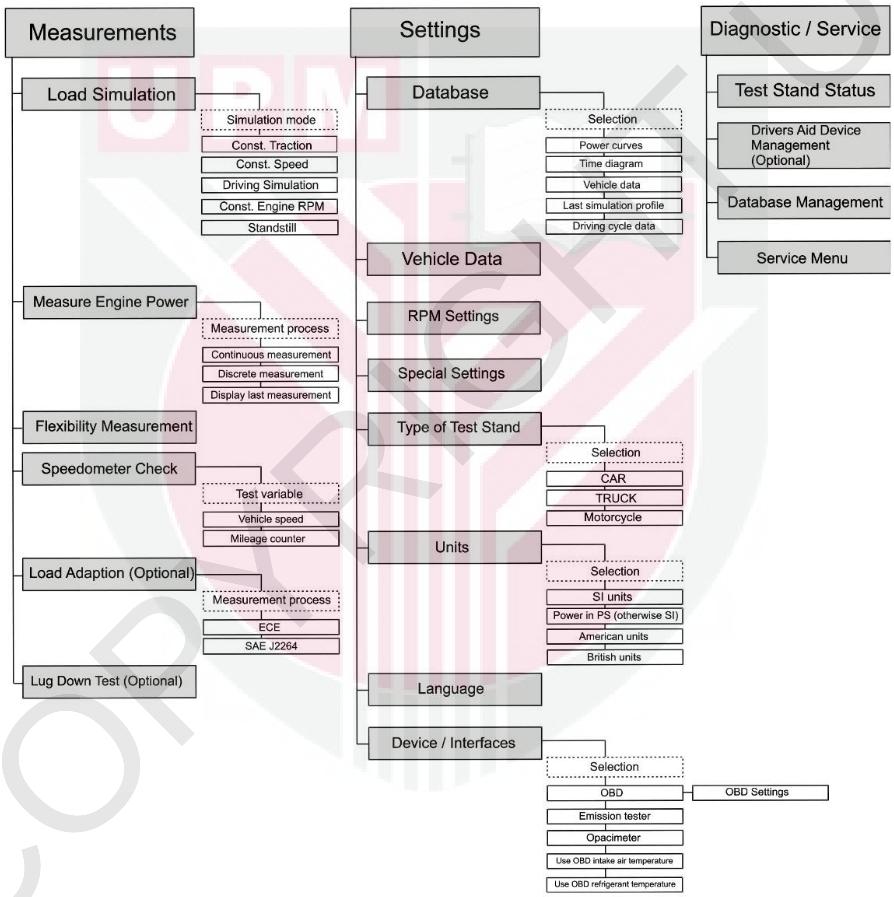

Figure A17: The Chassis Dynamometer Software Tree Model menu

The selection of commands or data entry was made through visual software designed by the (MAHA) with the (LPS3000) software interface.

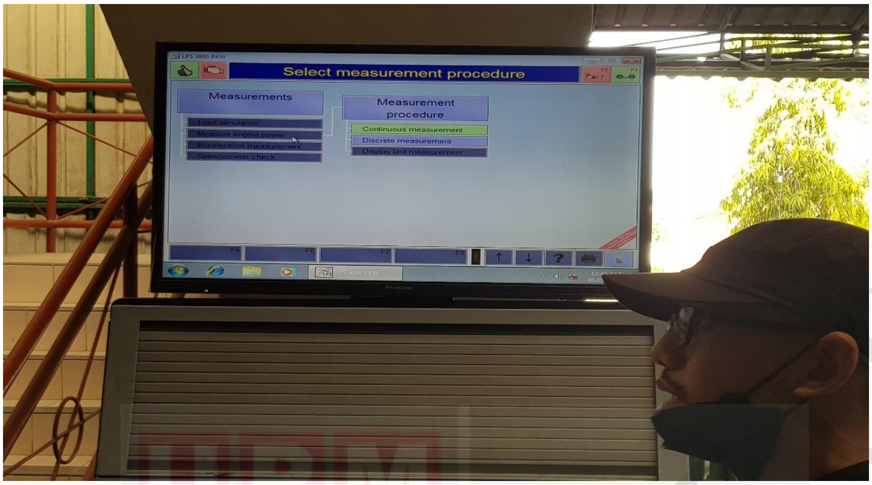

Figure A18: MAHA Chassis dynamometer monitor view for select measurement procedure test

The Dyno determined the maximum power during a continuous measurement, and the engine power was calculated by software according to (DIN 70020, EWG 80/1269, ISO 1585, and SAE J1349) depending on the menu selection setting in the category (Power Correction).

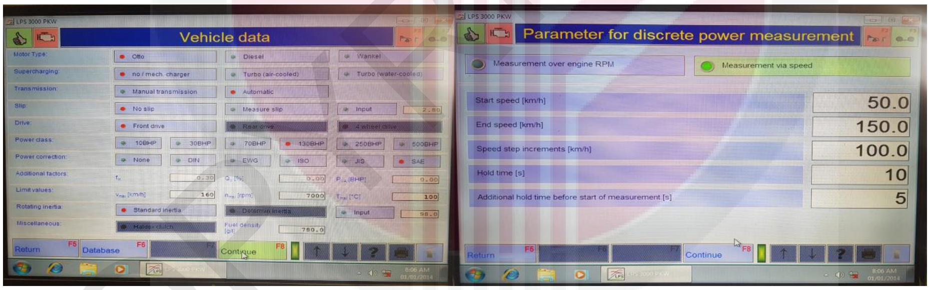

Figure A19: MAHA Chassis dynamometer discrete power measurement test input control parameter menu

The wheel, drag, and engine performance results were illustrated on the computer screen, as shown in Figure A20. A discrete power measurement test makes it possible to approach pre-defined data points and hold them for a specified duration of time input as a function of engine speed or RPM. In this test, pre-controlled input data was intended to control the test parameters depending on Start- and End speeds or (RPM) in the range of (1765-6500 RPM). Hold time represents the length of time pre-set test approached (RPM) in a held constant speed selected to be (10 seconds). The holding time required at stable test point duration to measure the fuel consumption, it is the eases of regulation procedure for better accurate test results.

Figure A20: MAHA Chassis dynamometer discrete power result illustrating test results

E.1 Calculation Basis of the chassis dynamometer

The system utilizes equation calculation fundamentals to measure the following parameters:

a) Road Load

$$F_x = \frac{P_{Air}.3.6v}{v_{ref}^3} + \frac{P_{Flex}.3.6v}{v_{ref}^2} + \frac{P_{Roll}.3.6}{v_{ref}} + a.m$$

Where:

v_{ref} Reference speed for resistance performance values-normally 90 km/h
V Driving speed
P_{Air} Air resistance performance [KW]
P_{Flex} Flex performance [KW]
P_{Roll} Roll resistance performance [KW]
$a.m$ Vehicle mass

b) Flex power P-Flex [KW]

Flex power or resistance is defined as the power loss which occurs due to the flexing o fthe tire on the road surface and/or roller.

$$P_{Flex} = \mu_w.m.g.v$$

c) Roller resistance power P-Roll [KW]

The rolling resistance power arises from tire and road surface deformation as a function of speed.

$$P_{Roll} = \mu_r.m.g.v$$

Where:

μ_r	Roll resistance coefficient of the tires = 0.012
m	Vehicle mass
g	Gravitation constant [m^2/s]
v	Driving speed [Km/h]

d) Torque [Nm]

$$M = \frac{P[KW].9549}{n[U_{min}]}$$

e) Extrapolation of drag power by 2nd coast down the trial

From the dyno manual, " Traction is loaded with the second coast down trial so that there is a shorter coast downtime. The traction loaded for the coast down trial is calculated from the following equation:

$$F = \frac{P_{wheel-max}}{v(withP_{wheel-max})}.Factor$$

The factor normally has a value of 650.

Appendix F

(Enerac 700AV) device Interface connection and manual

The presented information refers to the manufacture manual book information (CHAPTER 10) of how to install the device connection and software manual use:

F.1 Getting started

In order to be able to communicate between the analyzer and a computer, a connection must be established in one of three ways:

a) RS-232 connection

For RS-232 connections, use a standard 9-pin serial cable. (This is not included) Connections up to 100 ft long are possible. The analyzer‟s RS-232 port is a DTE type. Three wires are necessary for communications: TxD (pin 2), RxD (pin 3) and ground (pin 5).

b) USB connection

For USB connections, use the A-to-B type USB cable supplied with the instrument. To establish a USB connection, the FTDI USB driver must first be installed on your computer. The USB drivers for Windows computers are located on the ENERAC CD and are also available from the ENERAC website: www.enerac.com.

c) Bluetooth connection

For Bluetooth connections, the connection process varies with different Bluetooth devices. Follow your manufacturer's instructions for adding a device. The ENERAC‟S Bluetooth modem is a Class 1 device, with a maximum range of 100m. Obstacles such as walls and equipment will reduce the effective range.

F.2 ENERCOM Software

You can enhance the performance and versatility of the ENERAC Model 700 by using the Enercom software program. Enercom is available for most Windows operating systems Figure A21.

The Enercom software is a robust package that allows you to:

1. Monitor all emissions parameters.

2. Record maximum, minimum, average, and standard deviation for all emissions parameters.

3. Select a variety of saving and printing options.

4. Retrieve stored data.

5. Enter custom fuel information.

6. Open a terminal window to communicate directly using serial commands.

The Enercom software can be downloaded from the website at: www.enerac.com. Consult the Enercom manual for details on installing and operating the program.

F.3 STARTING ENERCOM

1. Before starting Enercom, have your analyzer turned on and connected via RS-232, USB, or Bluetooth.

2. Start Enercom. If you have connected before, the analyzer icon will appear. If this is the first time you are connecting, you will need to add a new port.

3. On the Enercom window, click on "Connections," then click on "Add Port."

4. Enter the COM port number, which appeared in the Device Manager, and click "OK."

5. The COM port with its number should appear on the left side of the Enercom window. Enercom will look for an analyzer on this port. After a moment, the ENERAC analyzer icon should appear. You are now connected to your analyzer.

Click on the ENERAC icon. A menu will appear. Choose "Monitor" from the menu. (Follow the ENERCOM manual for further instructions).

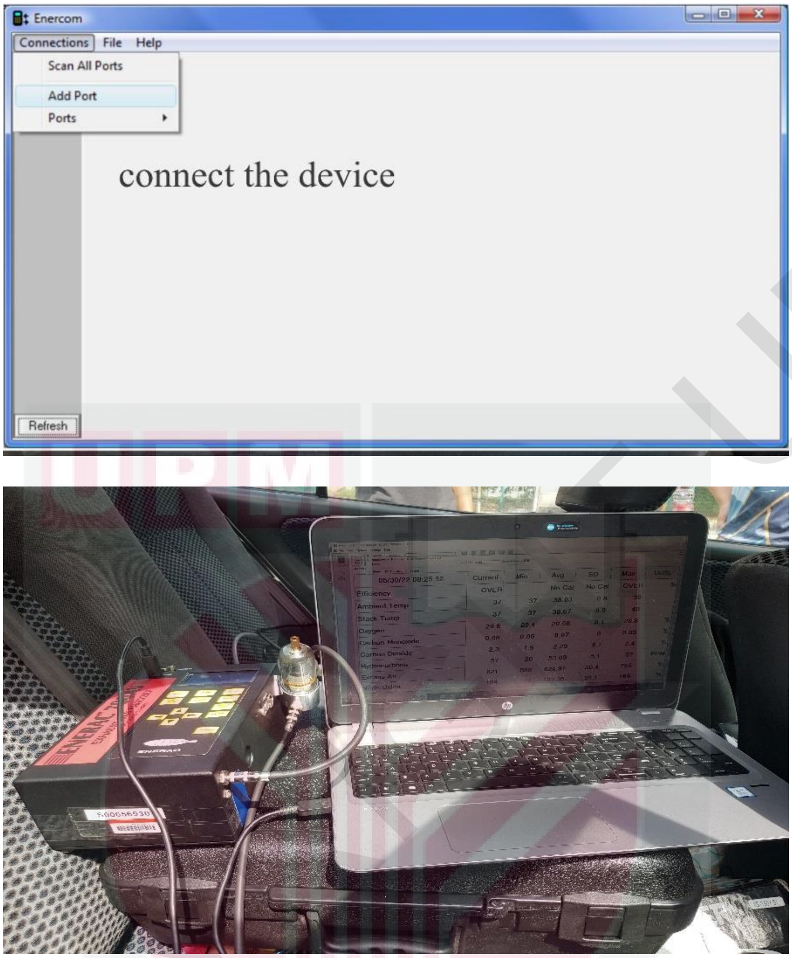

Figure A21: (Enrack700AV) device Interface connected to a computer for data logging and visual control

LIST OF PUBLICATIONS

Journal Articles

Ikhtiar, U., Hairuddin, A. A. B., Asarry, A. B., Rezali, K. A. B. M., & Ali, H. M. (2023). Numerical investigation of lamella heat exchanger for engine intake charge air cooling utilizing refrigerant as coolant medium. *Alexandria Engineering Journal*, *65*, 661-673.
Impact factor: 6.8; Quartile: Q1

Ikhtiar, U., Hairuddin, A. A. B., Asarry, A. B., Rezali, K. A. B. M., Ali, H. M., & Jalal, R. I. A. (2023). Experimental assessment of lamella heat exchanger as cold intake air system for spark ignition engine by utilizing vehicle air conditioning system. *International Communications in Heat and Mass Transfer*, *148*, 106989.
Impact factor: 7.0; Quartile: Q1

Intellectual Property Patent

Ikhtiar, U., Hairuddin, A. A. B., Asarry, A. B., Rezali, K. A. B. M. Intake air cooling device (PI2021007236).

Course work publication

Singh, B., Ikhtiar, U., Firzan, M., Huizhen, D., & Ahmad, K. A. (2021). Numerical Analysis of a Mobile Leakage-Detection System for a Water Pipeline Network. *Journal of Advanced Research in Fluid Mechanics and Thermal Sciences, 87(*1*),* 134-150.